



**HAL**  
open science

# Modeling techniques for building design considering soil-structure interaction

Reine Fares

► **To cite this version:**

Reine Fares. Modeling techniques for building design considering soil-structure interaction. Structures. Université Côte d'Azur, 2018. English. NNT : 2018AZUR4103 . tel-02366973v2

**HAL Id: tel-02366973**

**<https://theses.hal.science/tel-02366973v2>**

Submitted on 29 Nov 2019

**HAL** is a multi-disciplinary open access archive for the deposit and dissemination of scientific research documents, whether they are published or not. The documents may come from teaching and research institutions in France or abroad, or from public or private research centers.

L'archive ouverte pluridisciplinaire **HAL**, est destinée au dépôt et à la diffusion de documents scientifiques de niveau recherche, publiés ou non, émanant des établissements d'enseignement et de recherche français ou étrangers, des laboratoires publics ou privés.



$$\rho \left( \frac{\partial v}{\partial t} + v \cdot \nabla v \right) = -\nabla p + \nabla \cdot T + f$$

$$e^{i\pi} + 1 = 0$$

# THÈSE DE DOCTORAT

Techniques de modélisation pour la conception des  
bâtiments parasismiques en tenant compte de  
l'interaction sol-structure

Modeling techniques for building design considering  
soil-structure interaction

**Reine FARES**

Laboratoire Géoazur – Laboratoire Jean Alexandre Dieudonné

**Présentée en vue de l'obtention du grade  
de docteur en sciences** pour l'ingénieur de  
l'Université Côte d'Azur

**Dirigée par :** Anne Deschamps  
**Co-encadrée par :** Maria Paola Santisi d'Avila  
**Soutenue le :** 16/11/2018

**Devant le jury, composé de :**

Pierfrancesco Cacciola  
Jean-François Semblat  
Etienne Bertrand  
Luca Lenti

Principal lecturer  
Professeur  
Directeur de recherche  
Chargé de recherche

University of Brighton  
ENSTA ParisTech  
CEREMA Méditerranée  
IFSTTAR Champs-sur-Marne



Région  
Provence  
Alpes  
Côte d'Azur



## Techniques de modélisation pour la conception des bâtiments parasismiques en tenant compte de l'interaction sol-structure

---

### Résumé

La conception des bâtiments selon le code sismique européen ne prend pas en compte les effets de l'interaction sol-structure (ISS). L'objectif de cette recherche est de proposer une technique de modélisation pour prendre en compte l'ISS et l'interaction structure-sol-structure (ISSS).

L'approche de propagation unidirectionnelle d'une onde à trois composantes (1D-3C) est adoptée pour résoudre la réponse dynamique du sol. La technique de modélisation de propagation unidirectionnelle d'une onde à trois composantes est étendue pour des analyses d'ISS et ISSS. Un sol tridimensionnel (3-D) est modélisé jusqu'à une profondeur fixée, où la réponse du sol est influencée par l'ISS et l'ISSS, et un modèle de sol 1-D est adopté pour les couches de sol plus profondes, jusqu'à l'interface sol-substrat. Le profil de sol en T est assemblé avec une ou plusieurs structures 3-D de type poteaux-poutres, à l'aide d'un modèle par éléments finis, pour prendre en compte, respectivement, l'ISS et l'ISSS dans la conception de bâtiments.

La technique de modélisation 1DT-3C proposée est utilisée pour étudier les effets d'ISS et analyser l'influence d'un bâtiment proche (l'analyse d'ISSS), dans la réponse sismique des structures poteaux-poutres. Une analyse paramétrique de la réponse sismique des bâtiments en béton armé est développée et discutée pour identifier les paramètres clé du phénomène d'ISS, influençant la réponse structurelle, à introduire dans la conception de bâtiments résistants aux séismes.

La variation de l'accélération maximale en haut du bâtiment avec le rapport de fréquence bâtiment / sol est tracée pour plusieurs bâtiments, chargés par un mouvement à bande étroite, excitant leur fréquence fondamentale. Dans le cas de sols et de structures à comportement linéaire, une tendance similaire est obtenue pour différents bâtiments. Cela suggère l'introduction d'un coefficient correcteur du spectre de réponse de dimensionnement pour prendre en compte l'ISS. L'analyse paramétrique est répétée en introduisant l'effet de la non-linéarité du sol et du béton armé.

La réponse sismique d'un bâtiment en béton armé est estimée en tenant compte de l'effet d'un bâtiment voisin, pour un sol et des structures à comportement linéaire, dans les deux cas de charge sismique à bande étroite excitant la fréquence fondamentale du bâtiment cible et du bâtiment voisin. Cette approche permet une analyse efficace de l'interaction structure-sol-structure pour la pratique de l'ingénierie afin d'inspirer la conception d'outils pour la réduction du risque sismique et l'organisation urbaine.

---

**Mots clés** : Interaction Structure-Sol-Structure ; interaction Sol-Structure ; méthode d'éléments finis ; propagation d'onde ; chargement sismique à trois composantes ; béton armé ; comportement non-linéaire.



### Abstract

Building design according to European seismic code does not consider the effects of soil-structure interaction (SSI). The objective of this research is to propose a modeling technique for SSI and Structure-Soil-Structure Interaction (SSSI) analysis.

The one-directional three-component (1D-3C) wave propagation approach is adopted to solve the dynamic soil response. The one-directional three-component wave propagation model is extended for SSI and SSSI analysis. A three-dimensional (3-D) soil is modeled until a fixed depth, where the soil response is influenced by SSI and SSSI, and a 1-D soil model is adopted for deeper soil layers until the soil-bedrock interface. The T-soil profile is assembled with one or more 3-D frame structures, in a finite element scheme, to consider, respectively, SSI and SSSI in building design.

The proposed 1DT-3C modeling technique is used to investigate SSI effects and to analyze the influence of a nearby building (SSSI analysis), in the seismic response of frame structures.

A parametric analysis of the seismic response of reinforced concrete (RC) buildings is developed and discussed to identify the key parameters of SSI phenomenon, influencing the structural response, to be introduced in earthquake resistant building design.

The variation of peak acceleration at the building top with the building to soil frequency ratio is plotted for several buildings, loaded by a narrow-band motion exciting their fundamental frequency. In the case of linear behaving soil and structure, a similar trend is obtained for different buildings. This suggests the introduction of a corrective coefficient of the design response spectrum to take into account SSI. The parametric analysis is repeated introducing the effect of nonlinear behaving soil and RC.

The seismic response of a RC building is estimated taking into account the effect of a nearby building, for linear behaving soil and structures, in both cases of narrow-band seismic loading exciting the fundamental frequency of the target and nearby building. This approach allows an easy analysis of structure-soil-structure interaction for engineering practice to inspire the design of seismic risk mitigation tools and urban organization.

---

**Keywords:** Structure-Soil-Structure Interaction; Soil-Structure interaction; finite element method; wave propagation; three-component seismic motion; reinforced concrete; nonlinear behavior.



# Table of Contents

Résumé.....	3
Abstract.....	5
Table of Contents.....	7
List of Acronyms .....	11
List of Figures.....	13
List of Tables .....	21
Acknowledgements.....	23
Introduction.....	27
Chapter 1 - Overview on soil and structural dynamics.....	39
1.1 Introduction to structural dynamic problem.....	40
1.1.1. Single degree of freedom (SDOF).....	40
1.1.2. Numerical solution of the dynamic equilibrium equation for SDOF oscillators	42
1.1.3. Dynamic study of a MDOF system in the frequency domain .....	42
1.1.4. Dynamic equilibrium for MDOF structures .....	44
1.2 Numerical methods.....	46
1.2.1 Finite difference method.....	46
1.2.2 Finite element method.....	47
1.2.3 Spectral element method.....	48
1.2.4 Boundary element method.....	48
1.3 Site effect.....	49
1.3.1. Impact of soil characterization.....	49
1.3.2. Impact of the soil constitutive model.....	51
1.4 Soil structure interaction .....	52
1.4.1. Observations on existing building and prototype experiments.....	53
1.4.2. Analytical study .....	54
1.4.3. Numerical study.....	55
1.5 Structure-soil-structure interaction.....	58
1.5.1. Analytical study .....	58
1.5.2. Experimental study .....	59

1.5.3.	Numerical study .....	60
1.6	Conclusion.....	62
Chapter 2 - One-dimensional three-component wave propagation model for soil-structure interaction .....		
2.1.	1D-3C wave propagation model.....	64
2.1.1.	Spatial discretization of soil domain and boundary conditions .....	64
2.1.2.	Soil constitutive relationship: Iwan's model.....	67
2.1.3.	Elasto-plastic model in Abaqus .....	69
2.1.4.	Building model.....	72
2.1.5.	Time discretization.....	73
2.1.6.	Soil domain area concerned by the SSI .....	73
2.2.	Input data.....	74
2.2.1.	Soil data .....	74
2.2.1.	Building data.....	75
2.2.2.	Input motion.....	76
2.2.3.	Signal processing of the output motion .....	78
2.3.	Verification of the proposed model.....	78
2.3.1.	Comparison with other codes.....	79
2.4.	1D-3C vs 3D-3C wave propagation model for vertical propagation .....	82
2.5.	SSI analysis .....	86
2.6.	Conclusion.....	89
Chapter 3 - One-directional three-component wave propagation in a T-shaped soil domain for SSI and SSSI.....		
3.1.	1DT-3C wave propagation model for SSI and SSSI analyses .....	92
3.2.	Verification of the proposed model.....	94
3.2.1.	Input data .....	94
3.2.1.	Verification .....	95
3.3.	SSI analysis .....	98
3.3.1.	Impact of the excitation frequency on the structural response .....	98
3.3.2.	SSI estimation .....	99
3.3.3.	1st vs 2nd natural frequency .....	100
3.4.	Conclusion.....	102
Chapter 4 - Response spectrum for structural design considering soil-structure interaction		
4.1.	1DT-3C wave propagation model .....	106

4.2.	Input data for the parametric analysis .....	108
4.2.1.	Soil profiles.....	108
4.2.2.	RC buildings .....	109
4.2.3.	Input motion.....	111
4.3.	SSI analysis .....	111
4.3.1.	Linear elastic analyses .....	112
4.3.2.	Effect on SSI of soil and structure nonlinear behavior .....	115
4.4.	Conclusion.....	120
Chapter 5 - Structure-soil-structure interaction analysis .....		123
5.1.	1DT-3C wave propagation model for SSSI analysis.....	124
5.2.	Input data for the parametric analysis .....	124
5.2.1.	Soil profiles.....	124
5.2.2.	Buildings characteristics .....	125
5.2.3.	Input motion.....	126
5.3.	SSSI analysis .....	126
5.3.1.	SSSI versus SSI.....	126
5.3.2.	SSSI parametric analysis.....	131
5.4.	Semi-infinite elements and dashpot boundary conditions.....	134
5.4.1.	Semi-infinite elements vs dashpots.....	137
5.4.2.	Domain truncation definition.....	138
5.5.	Conclusion.....	139
Chapter 6 - Conclusions and perspectives .....		141
References.....		147
Appendix A - Nonlinear behavior of RC .....		157
Appendix B - 1D-3C model for SSI analysis.....		171
Appendix C - Soil behavior calibration .....		210
Appendix D - Guide for 1DT-3C model for SSI and SSSI in Abaqus .....		219
Author's publications.....		267



## List of Acronyms

SDOF	: Single Degree of freedom
FB	: Fixed Base
SSI	: Soil-Structure Interaction
SSSI	: Structure-Soil-Structure Interaction
iD	: i direction
i-D	: i dimension
PGA	: Peak Ground Acceleration
FF	: Free Field
FE	: Finite Element
RC	: Reinforced Concrete
1D-3C	: One-directional three-component
GoF	: Goodness of Fit



## List of Figures

Figure 1-1 Single degree of freedom oscillator (SDOF) subjected to earthquake ground motion $u_g(t)$ . .....	40
Figure 1-2 Free vibration of a SDOF system with different levels of damping: $\zeta = 2, 5, 10,$ and $20\%$ . (Chopra 2001).....	41
Figure 1-3 Multiple degree of freedom oscillator (MDOF) subjected to an earthquake ground motion $u_g(t)$ .....	43
Figure 1-4 Time histories of the May 13, 1995 earthquake ( $M_s$ 6.6, distance 130 km) recorded on north-south components of stations of the EUROSEISTEST network. ( <a href="http://euroseisdb.civil.auth.gr">http://euroseisdb.civil.auth.gr</a> ).....	50
Figure 1-5 (a) Geotechnical model of the Mygdonia basin: complete model (top) and simplified model (bottom), (b) Amplification/frequency curves for various locations along the basin surface for simplified (continuous) and complete models (dashed). (Semblat et al. 2005) .....	50
Figure 1-6 Reduction of the borehole site responses at IWTH23 with respect to the input-motion PGA ( $\text{cm/s}^2$ ). (Régnier et al. 2013).....	51
Figure 1-7 Two-step analyses; step one (left) Free Field analyses and step two (right) Fixed Base analyses. ....	53
Figure 1-8 Photograph of a prototype model for the shaking table test. (Lu et al. 2004).....	54
Figure 1-9 One-step analysis for SSI problems. ....	57
Figure 1-10 Prototype of a shaking table model scaled to the 1/15, SSI test model (left) and SSSI test model (right). (Li et al. 2012).....	59
Figure 1-11 Overview of experiment: (a) single building; (b) two identical buildings; (c) three identical buildings; (d) experimental system mounted on the shaking table. (Aldaikh et al. 2016) .....	60
Figure 1-12 (a) Prototype and (b) Finite Element Model of two different structures protected by the ViBa. (Tombari et al. 2018).....	60

Figure 2-1 Assembly of a frame structure and a multilayer soil domain shaken by a three-component seismic motion, for SSI analysis: (a) 1D-3C wave propagation model, where the assembly is done in only one node; (b) 3D-3C wave propagation model, with connection node-to-node between building and soil; (c) 3D-3C model, where the foundation is modeled and embedded in the soil domain.....	64
Figure 2-2 Unit area quadratic solid FE with 20 nodes, where $h_e$ is the element height. ....	65
Figure 2-3 One dimensional series-parallel rheological model proposed by Iwan in 1967. ...	68
Figure 2-4 (a) Shear modulus decay curve and (b) shear strain time history. ....	68
Figure 2-5 Schematic behavior of yield surfaces of Iwan model, in plane.....	70
Figure 2-6 Yield surface transformation after kinematic hardening (left) or isotropic hardening (right). ....	70
Figure 2-7 Ratchetting (Abaqus User Manual 2014, Figure 23.2.2–5) .....	70
Figure 2-8 Hysteresis loop in a unit cube of soil obtained with the Fortran implementation of Iwan’s model (UMAT/SWAP_3C) .....	71
Figure 2-9 Hysteresis loops in a unit cube of soil loaded by a 1-, 2- and 3-Component strain, for a different number of backstresses in the kinematic hardening model. ....	72
Figure 2-10 Floor plan of the two analyzed three-story buildings that have same (a) and different (b) inertia to horizontal motion in the two orthogonal directions x and y. The dimensions of the two buildings are the same; the difference is in the rectangular column orientation. ....	75
Figure 2-11 Building base to bedrock Transfer Function, evaluated for different soil areas, and free-field to bedrock Transfer Function. ....	76
Figure 2-12 NS component of the synthetic seismic signal at the outcropping bedrock, in terms of normalized acceleration $\hat{a}_q$ , for the predominant frequencies $f_q = 2.8$ Hz . ....	77
Figure 2-13 Velocity time history (a) and Fourier spectrum (b) for the NS, EW and UP components of the 2009 Mw 6.3 L’Aquila earthquake at recorded ANT station. Dashed lines show the predominant frequency in NS, EW and UP directions. ....	78
Figure 2-14 Acceleration time history at the soil surface, in the case of free-field solution and linear soil behavior, for one- (a) and three-component (b) motion.....	79

Figure 2-15 Acceleration time history at the soil surface (top) and at the building top (bottom), in the case of linear soil behavior, for one- (a) and three-component (b) motion. ....	80
Figure 2-16 Parameters associated to lowest GoF scores: (top-left) Response spectrum for the 1C motion in x-direction at the free-field, (top-right) Response spectrum for the 1C motion in x-direction at the building bottom, (bottom-left) Fourier spectrum for the 3C motion in z-direction at the building bottom (bottom-right) Fourier spectrum for the 3C motion in z- direction at the building top. ....	81
Figure 2-17 Acceleration time history at the soil surface, in the case of free-field solution and nonlinear soil behavior, for one- (a) and three-component (b) motion.....	82
Figure 2-18 Acceleration time history at the building base (top) and top (bottom), in the case of nonlinear soil behavior, for one- (a) and three-component (b) motion. ....	82
Figure 2-19 Simulated acceleration time history at the building bottom in the case of resonance ( $f_b = f_s = 3.8$ Hz) during the input signal duration (top) and in a 10 s time window over the largest amplitudes (bottom). ....	83
Figure 2-20 Simulated acceleration time history at the building top in the case of resonance ( $f_b = f_s = 3.8$ Hz ) during the input signal duration (top) and in a 10 s time window over the largest amplitudes (bottom). ....	84
Figure 2-21 Simulated acceleration time history at the building bottom in the case of SSI ( $f_b = 3.8 > f_s = 2.8$ Hz) during the input signal duration (top) and in a 10 s time window over the largest amplitudes (bottom). ....	87
Figure 2-22 Simulated acceleration time history at the building top in the case of SSI ( $f_b = 3.8 > f_s = 2.8$ Hz) during the input signal duration (top) and in a 10 s time window over the largest amplitudes (bottom). ....	87
Figure 2-23 Horizontal acceleration time history in the cases of soil profile with fundamental frequency $f_s = f_b = f_q = 3.8$ Hz , at building bottom (top) and at building top (bottom). .....	88
Figure 2-24 Horizontal acceleration time history in the cases of soil profile with fundamental frequency $f_s = 2.8$ Hz, and $f_b = f_q = 3.8$ Hz, at building bottom (top) and at building top (bottom). ....	89

Figure 3-1 Assembly of a multilayer soil domain and a frame structure shaken by a three-component seismic motion: 1D-3C (a) and 3D-3C (b) model for SSI analysis. ....	92
Figure 3-2 Section of the 1DT-3C model for SSI analysis where h is the thickness of the 3-D soil domain and H is the Thickness of the considered soil until bedrock interface. ....	93
Figure 3-3 1DT-3C model for soil-structure interaction (a) and for structure-soil-structure (b) analysis.....	93
Figure 3-4 Maximum shear strain (a) and stress (b) profile with depth obtained using de 1D-3C wave propagation model for the SSI analysis in a linear elastic regime.....	95
Figure 3-5 Comparison of 1DT-3C and 3D-3C wave propagation approaches for SSI analysis: acceleration time history at the building bottom (top) and roof drift time history at the building top (bottom). ....	96
Figure 3-6 Comparison of T and 3-D soil models for 1D-3C wave propagation approach for SSI analysis: energy integral (IE), response spectrum acceleration ( $S_{pa}$ ) and Fourier spectrum (FS) for the horizontal x-component of motion at the building bottom (top) and top (bottom). ....	97
Figure 3-7 Comparison of T and 3-D soil models for 1D-3C wave propagation approach for SSI analysis: correlation coefficient of accelerations for the horizontal x-component of motion at the building bottom (a) and top (b).....	97
Figure 3-8 Acceleration time history at the building bottom (left) and roof drift at the building top (right), for the building-soil system composed by a T-shaped horizontally layered soil having frequency $f_s = 1.9$ Hz and a building having fundamental frequency $f_b = 3.8$ Hz , in the case of earthquake predominant frequency equal to $f_q = f_s = 3.8$ Hz and $f_q = f_s = 1.9$ Hz .....	98
Figure 3-9 Building top to bottom transfer function estimated for a fixed-base building and for SSI analysis in the cases of building-soil resonance ( $f_b = f_s = 3.8$ Hz ) and softer soil ( $f_q = 3.8$ Hz $>$ $f_s = 1.9$ Hz).....	99
Figure 3-10 Acceleration time history at the building bottom and roof drift at the building top, for the building-soil system composed by a building having fundamental frequency $f_b = 3.8$ Hz and a T-shaped horizontally layered soil having frequency $f_s = f_b = 3.8$ Hz	

(a) and  $f_s = 1.9 \text{ Hz} < f_b = 3.8 \text{ Hz}$ (b), in the case of earthquake predominant frequency equal to  $f_q = f_b = 3.8 \text{ Hz}$  ..... 100

Figure 3-11 Acceleration time history at the building bottom and roof drift at the building top, for the building-soil system composed by a building having fundamental frequencies  $f_{b1} = 2.8 \text{ Hz}$  and  $f_{b2} = 4.7 \text{ Hz}$  and a T-shaped horizontally layered soil having frequency  $f_s = 1.9 \text{ Hz}$ , in the case of earthquake predominant frequency equal to  $f_q = f_{b1} = 2.8 \text{ Hz}$  ..... 101

Figure 3-12 Acceleration time history at the building bottom and roof drift at the building top, for the building-soil system composed by a building having fundamental frequencies  $f_{b1} = 2.8 \text{ Hz}$  and  $f_{b2} = 4.7 \text{ Hz}$  and a T-shaped horizontally layered soil having frequency  $f_s = 1.9 \text{ Hz}$ , in the case of earthquake predominant frequency equal to  $f_q = f_{b2} = 4.7 \text{ Hz}$  ..... 102

Figure 4-1 2-D section of the 1DT-3C model for SSI analysis where h is the thickness of the 3-D soil domain and H is the Thickness of the considered soil until bedrock interface. .... 106

Figure 4-2 Variation of the peak acceleration at the top of five different buildings, normalized with respect to the maximum amplitude of the seismic load  $a_q$ , with the soil fundamental frequency: synthetic signal having predominant frequency close to the building fundamental frequency (left) and 2009 Mw 6.3 L'Aquila earthquake (right) as seismic loading. A vertical dashed line indicates the building fundamental frequency ..... 113

Figure 4-3 Variation with the building to soil fundamental frequency ratio of the peak acceleration at the top of five different buildings, normalized with respect to its maximum: synthetic signal having predominant frequency close to the building fundamental frequency (left) and 2009 Mw 6.3 L'Aquila earthquake (right) as seismic loading..... 114

Figure 4-4 Variation of the peak acceleration at the top of the building in a one-step analysis over that in a two-step analysis with the building to soil fundamental frequency ratio, for five different buildings: synthetic signal having predominant frequency close to the building fundamental frequency (left) and 2009 Mw 6.3 L'Aquila earthquake (right) as seismic loading..... 115

Figure 4-5 Variation of the peak acceleration at the top of the building in a one-step analysis over that in a two-step analysis with the soil fundamental frequency, for five different

buildings and a synthetic signal having predominant frequency close to the building fundamental frequency as seismic loading. The ground type range is indicated by vertical boundaries ..... 116

Figure 4-6 Variation with the soil fundamental frequency of the peak acceleration at the top of two buildings having fundamental frequency  $f_b = 1.5$  Hz (left) and  $f_b = 3.8$  Hz (right), in the case of nonlinear behaving soil and nonlinear behaving building-soil system. The synthetic input signal has predominant frequency close to the building fundamental frequency..... 117

Figure 4-7 Variation with the soil fundamental frequency of the peak acceleration, normalized with respect to the maximum amplitude of the seismic load  $a_q$ , at the top of two buildings having fundamental frequency  $f_b = 1.5$  Hz (left) and  $f_b = 3.8$  Hz (right), for the cases of linear behaving building-soil system, nonlinear behaving soil and nonlinear behaving building-soil system. The synthetic input signal has predominant frequency close to the building fundamental frequency ..... 118

Figure 4-8 Variation with the building to soil fundamental frequency ratio of the peak acceleration, normalized with respect to the maximum amplitude of the seismic load  $a_q$ , at the top of two buildings having fundamental frequency  $f_b = 1.5$  Hz (left) and  $f_b = 3.8$  Hz (right), for the cases of linear behaving building-soil system, nonlinear behaving soil and nonlinear behaving building-soil system. The synthetic input signal has predominant frequency close to the building fundamental frequency..... 118

Figure 4-9 Variation with the building to soil fundamental frequency ratio of the peak acceleration at the top of two analyzed buildings, normalized with respect to its maximum, for the cases of linear behaving building-soil system (left), nonlinear behaving soil (middle) and nonlinear behaving building-soil system (right). The synthetic input signal has predominant frequency close to the building fundamental frequency..... 119

Figure 4-10 Variation with the building to soil fundamental frequency ratio of the peak acceleration at the top of the building in a one-step analysis over that in a two-step analysis, for the two analyzed buildings, in the cases of linear behaving building-soil system (left), nonlinear behaving soil (middle) and nonlinear behaving building-soil system (right). The synthetic input signal has predominant frequency close to the building fundamental frequency..... 120

Figure 5-1 2-D section of the 1DT-3C model for SSI analysis where  $h$  is the thickness of the 3-D soil domain and  $H$  is the Thickness of the considered soil until bedrock interface. .... 124

Figure 5-2 Simulated acceleration time history of the building with  $f_{b1} = f_{b2} = 3.8$  Hz at the building bottom, in the case of a nearby building with  $f_{b1} = f_{b2} = 3.8$  Hz, during the input signal duration (top) and in a 10 s time window over the largest amplitudes (bottom). .... 128

Figure 5-3 Simulated acceleration time history of the building with  $f_{b1} = f_{b2} = 3.8$  Hz at the building bottom, in the case of a nearby building with  $f_{b1} = 2.8$  Hz different than  $f_{b2} = 4.7$  Hz, during the input signal duration (top) and in a 10 s time window over the largest amplitudes (bottom). .... 128

Figure 5-4 Simulated acceleration time history of the building with  $f_{b1} = 2.8$  Hz different than  $f_{b2} = 4.7$  Hz at the building bottom, in the case of a nearby building with  $f_{b1} = 2.8$  Hz different than  $f_{b2} = 4.7$  Hz, during the input signal duration (top) and in a 10 s time window over the largest amplitudes (bottom). .... 129

Figure 5-5 Simulated acceleration time history of the building with  $f_{b1} = 2.8$  Hz different than  $f_{b2} = 4.7$  Hz at the building bottom, in the case of a nearby building with  $f_{b1} = f_{b2} = 3.8$  Hz, during the input signal duration (top) and in a 10 s time window over the largest amplitudes (bottom). .... 129

Figure 5-6 Comparison of results obtained using the 1DT-3C wave propagation model for isolated building and SSSI, in terms of Arias integral (AI), energy integral (IE), pseudo-acceleration response spectrum ( $S_{pa}$ ) and Fourier spectrum (FS) for the vertical component ( $z$ ) of motion and  $f_s = 2.8$  Hz: (a) building with  $f_{b1} = f_{b2} = 3.8$  Hz at the building bottom, in the case of a nearby building with  $f_{b1} = f_{b2} = 3.8$  Hz; (b) building with  $f_{b1} = f_{b2} = 3.8$  Hz at the building bottom, in the case of a nearby building with  $f_{b1} = 2.8$  Hz different than  $f_{b2} = 4.7$  Hz; (c) building with  $f_{b1} = 2.8$  Hz different than  $f_{b2} = 4.7$  Hz at the building bottom, in the case of a nearby building with  $f_{b1} = 2.8$  Hz different than  $f_{b2} = 4.7$  Hz; (d) building with  $f_{b1} = 2.8$  Hz different than  $f_{b2} = 4.7$  Hz at the building bottom, in the case of a nearby building with  $f_{b1} = f_{b2} = 3.8$  Hz..... 130

Figure 5-7 1DT-3C for SSSI analysis..... 131

Figure 5-8 Variation of the peak acceleration at the top of the excited building with the natural frequency of the nearby building, for the cases of soil profile having natural frequency $f_s = 1.5$ Hz (left) and $f_s = 2$ Hz (right).....	132
Figure 5-9 Variation of the peak acceleration at the top of the target building in a SSSI analysis over that in a SSI analysis (single excited building) with the natural frequency of the nearby building, for the cases of soil profile having natural frequency $f_s = 1.5$ Hz (left) and $f_s = 2$ Hz (right): excited target building (top); excited nearby building (bottom)	133
Figure 5-10 Variation of the peak acceleration at the top of the target building in a SSSI analysis over that in a SSI analysis (single excited building) with the target to nearby building fundamental frequency ratio, for the cases of soil profile having natural frequency $f_s = 1.5$ Hz (left) and $f_s = 2$ Hz (right): excited target building (top); excited nearby building (bottom) .....	134
Figure 5-11 3-D soil model with semi-infinite lateral elements. ....	135
Figure 5-12 3D-3C modeled using lateral boundary condition as linear dashpots (a) as semi-infinite elements (b). ....	137
Figure 5-15 Comparison between lateral boundary conditions; dashpots and semi-infinite elements in a 3D-3C FF analysis: acceleration time history at the soil top. ....	138
Figure 5-16 Variation of the soil frequency with the side dimension of the, squared geometry, finite domain. ....	139

## List of Tables

Table 2-1 Stratigraphy and mechanical features of the analyzed multilayered soil profiles having different natural frequency.....	74
Table 2-2 Dimensions of the rectangular cross-section beams and columns .....	76
Table 2-3 Gof of the 1-D model in the case of linear soil behavior ( $f_b = f_s = f_q = 3.8$ Hz).79	
Table 2-4 Gof of 1-D model in the case of nonlinear soil behavior ( $f_b = f_s = f_q = 3.8$ Hz). .....	81
Table 2-5 Gof of 1-D model in the case of nonlinear soil and resonance ( $f_b = f_s = 3.8$ Hz). .....	85
Table 2-6 Gof of 1-D model in the case of SSI ( $f_b = 3.8 > f_s = 2.8$ Hz).....	86
Table 3-1 Gof of 1DT-3C model, with respect to a 3D-3C model for SSI analysis.....	96
Table 4-1 Stratigraphy and mechanical properties of the analyzed soil profiles.....	108
Table 4-2 Eurocode ground type and fundamental frequency of the analyzed soil profiles .	109
Table 4-3 Fundamental frequency of the analyzed frame structures .....	110
Table 4-4 Dimensions of rectangular cross-section beams for the analyzed buildings.....	111
Table 5-1 Stratigraphy and mechanical properties of the analyzed soil profiles.....	125
Table 5-2 Eurocode ground type and fundamental frequency of the analyzed soil profiles .	125
Table 5-3 Fundamental frequency of the analyzed frame structures .....	126
Table 5-4 Dimensions of rectangular cross-section beams for the analyzed buildings.....	126
Table 5-5 Gof of 1DT-3C wave propagation model in the case of a building having a nearby building compared with the case of isolated building.....	127



## Acknowledgements

First and most importantly, my sincerest gratitude goes to my supervisors, Paola Santisi and Anne Deshamps. I am grateful for their guidance throughout the three years of my thesis, for their patience, professionalism and wisdom. In particular, I am thankful to Paola for introducing me to this research field, for trusting me and for encouraging me.

I would like to thank the members of my thesis committee. Jean-François Semblat and Pierfrancesco Cacciola who kindly accepted to be referees for my thesis and provided their comments and suggestions on my manuscript. I am also thankful for Luca Lenti and Etienne Bertrand, who accepted to be members of my thesis jury.

I would also like to thank my thesis committee, Françoise Courboulex and Fernando Lopez Caballero, for their time and advices.

I thank all the members of the laboratories JAD and Géoazur, for the hangouts and time spent together at lunch and coffee breaks especially my colleagues Bjorn, Stefania, Eduard, Luis, Marcella, Lucrezia, Victor, Laurence, Giulia, Mehdi, Léo, Kevin, Alexandre, Alxis G., Alexis L., David M., Théa, Zoé, Alexianne, Nicolas, Emmanuelle, Mathilde, Laure, Sara, Jean-luc, Simon and David C. Also, I am thankful to my co-office David L. and Julie we've shared so much together.

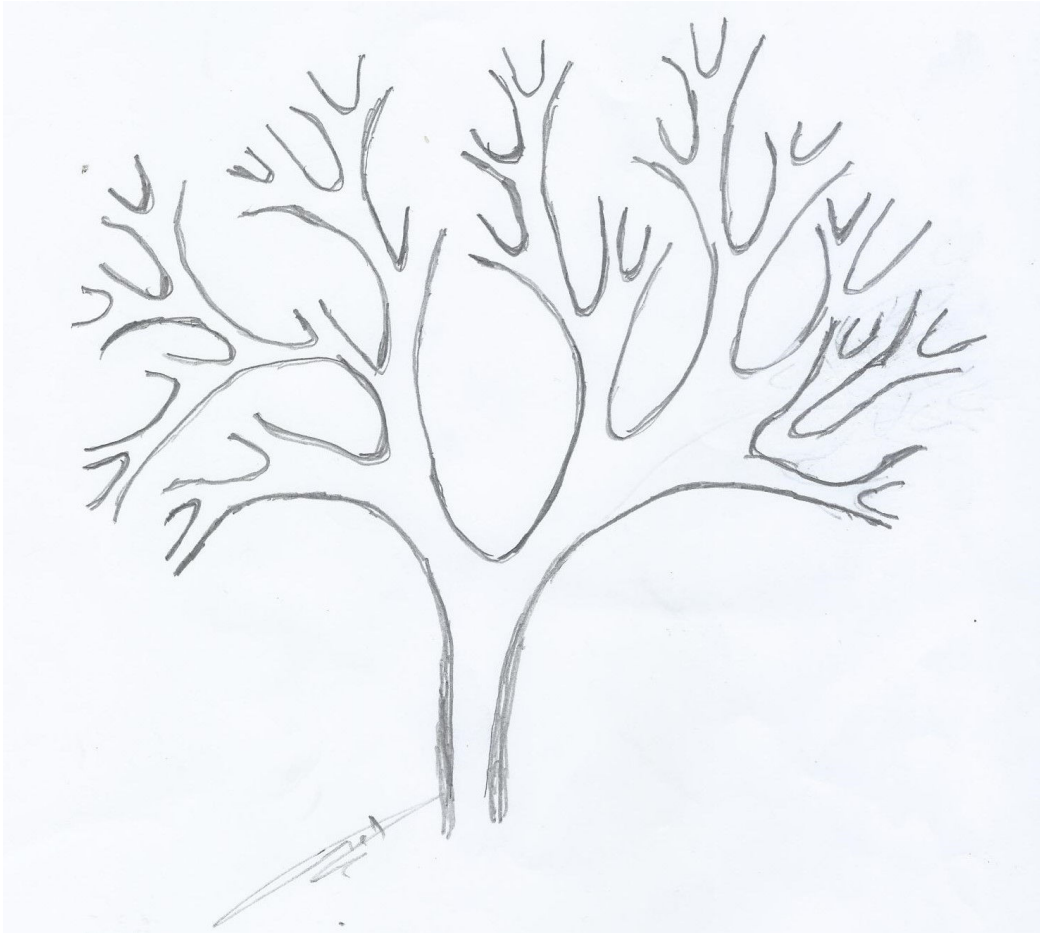
I want to thank Jean Marc Lacroix for his enormous help, I have learned a lot from him about clusters and codes.

I am also grateful to my friends Roula, Rita, Michelle, Rachelle, Christelle, Farah, Ralph, Tina and Joseph who have been there for me every time. Of course, special thanks to my F.R.I.E.N.D.S for their sense of humor.

My deepest appreciation goes to my father Milad, my mother Amal, my sisters Joelle and Nathalie and brothers in law François and Rami for their support, their prayers and their visits.

Finally, this research is performed using HPC resources from GENCI-[CINES] (Grant 2017-[A0010410071] and Grant 2018-[A0030410071]). This work has been funded by the region Provence-Alpes-Côte d'Azur (South-Eastern France), through a doctoral fellowship, and by the CNRS, through the project PEPS de site 2016 CNRS Université Nice Sophia Antipolis entitled "SSSI effects in the seismic response: identification of mechanical properties of buildings using MEMS and 3D modeling".





*Dedicated to my beloved family  
Milad, Amal, Joelle and Nathalie*



## Résumé étendu

Mon travail s'intéresse à la réponse sismique des structures dans leur environnement. Cette réponse sismique d'une structure dépend de la secousse incidente et de la propagation des ondes dans le sol et dans la structure elle-même. La structure étant couplée mécaniquement au sol, son excitation renvoie les ondes dans le sol. Ce phénomène est l'Interaction Sol Structure (ISS).

Selon les codes européens de conception parasismique en vigueur (CEN 2003), le mouvement en surface libre est actuellement utilisé comme chargement sismique au bas d'un bâtiment à base fixe (BF), pour la conception de bâtiments à fondation superficielle. Cette analyse en « deux étapes » (Saez et *al.*, 2011), ne permet donc pas de simuler numériquement l'ISS. Les effets d'ISS ne sont pris en compte que lorsque la réponse sismique de la structure est obtenue en résolvant le problème de l'équilibre dynamique appliquée à l'ensemble du domaine sol-structure : analyse en une étape. Nous avons montré que l'on pouvait, dans certaines conditions, considérer les effets de l'ISS comme une modification de la sollicitation sismique, influencée par les caractéristiques dynamiques structurelles, les paramètres mécaniques du sol et les caractéristiques de mouvement d'entrée.

Lors d'une sollicitation sismique, la topographie, la caractérisation géologique et géomécanique du sol affectent de manière significative le mouvement enregistré à surface libre. En particulier, de plus en plus les études s'attachent à comprendre les effets d'un comportement mécanique non linéaire dans les couches superficielles, comme dans les structures. Ces effets sont mis en évidence par exemple lors du benchmark PRENOLIN (Régnier et al. 2016) au cours duquel plusieurs relations constitutives non-linéaires ont été comparées par simulation numérique de la réponse sismique non-linéaire de site 1-D. Mais ces modèles testés exigent un nombre de paramètres important pour correctement reproduire la réponse du sol à un niveau de charge élevé. Comme pratiquement ces paramètres de sol peuvent être difficiles à déterminer, ces modélisations, importantes pour la compréhension des phénomènes, sont impossibles à introduire dans la réglementation. Je me suis attachée à concevoir un système équivalent plus simple : un modèle constitutif de sol efficace est celui qui est fiable et nécessite peu de paramètres à caractériser.

Plus largement, lorsque la construction est étendue à plus d'une structure, l'excitation sismique d'une structure est affectée par la présence des structures adjacentes. Cette interaction croisée entre structures voisines et le sol lors d'une sollicitation sismique est appelée interaction

structure-sol-structure (ISSS). Nous avons aussi abordé cette question fondamentale dans la construction des villes.

Afin d'étudier l'ISS et l'ISSS, une modélisation numérique du système sol-structure sous un chargement sismique est nécessaire. Plusieurs méthodes numériques ont été utilisées pour résoudre la propagation de l'onde dans un environnement complexe : les différences finies, les éléments finies (EF), les éléments spectraux, les éléments frontières et d'autres. Selon Chaljub *et al.* (2010), aucune méthode numérique unique ne peut être considérée comme la meilleure.

Dans mon travail, la solution directe de l'équation d'équilibre dynamique est résolue dans un schéma EF et le comportement non-linéaire des matériaux est pris en compte. Des conditions aux limites latérales périodiques sont adoptées, pour réduire le domaine du sol modélisé, lorsque l'hypothèse de périodicité est possible. Les résultats obtenus me permettent de proposer un modèle efficace pour la pratique de l'ingénierie qui tient compte de l'ISS.

### ***Modèle de propagation unidimensionnel d'onde à trois composantes pour l'interaction sol-structure***

Pour mettre en œuvre la simulation, un modèle de propagation unidirectionnelle (1D) est couplé à un modèle de bâtiment tridimensionnel (3-D) dans l'hypothèse de propagation d'onde verticale et de fondation superficielle rigide (modèle 1D-3C). Cette formulation est adaptée à la description de la colonne de sol par les données géotechniques généralement disponibles et permet de réduire le temps de calcul. Il est encore assez rare de connaître la géométrie et la stratigraphie d'un bassin sédimentaire qui serait nécessaire à une modélisation 3-D plus complète.

La loi de comportement d'Iwan (Iwan 1967), a été utilisée pour décrire le comportement non linéaire du sol sous chargement cyclique, en termes de contraintes totales. La solution du problème d'ISS est obtenue par solution directe de l'équation d'équilibre dynamique de l'ensemble. L'hypothèse de sol infiniment étendu dans les directions horizontales est traduite par une condition de périodicité latérale. Le mouvement sismique est imposé à la base de la colonne de sol en utilisant une condition absorbante qui prend en compte l'effet de l'élasticité du substratum rocheux.

Le modèle 1D-3C a été vérifié, dans le cas de comportement linéaire de sol et en utilisant un algorithme d'intégration implicite, par comparaison avec les résultats obtenus par le code maison SWAP\_3C (Santisi d'Avila and Lenti 2012) pour les études de réponse sismique du

sol à la surface libre et SFRINT\_3C (Santisi d'Avila and Lopez-Caballero 2018) pour les études de réponse sismique de sol et du bâtiment en considérant l'ISS. Ensuite, le modèle 1D-3C est validé, dans le cas de comportement non-linéaire de sol.

L'objectif est de prouver la pertinence du modèle de propagation 1D-3C dans un problème d'ISS, comparé à un modèle 3D-3C. Conceptuellement, ce dernier donne l'avantage de pouvoir modéliser la dalle de fondation par des éléments finis solides et donc de prendre en compte sa déformabilité. Par contre, dans le modèle de propagation 1D-3C, le même mouvement est imposé à la base de tous les poteaux du bâtiment simulant une base rigide. La comparaison quantitative des signaux obtenus par le modèle 1D-3C est effectuée en termes de pics en amplitude, d'intégrale d'Arias, d'intégrale en énergie, de spectre de Fourier et de réponse et de rapport de corrélation (coefficients du comparatif Goodness-of-fit proposés par Anderson, 2004). Les résultats obtenus dans le cas de propagation verticale montrent la fiabilité du modèle 1D-3C pour le sol quand les hypothèses de couches horizontales suffisamment étendues et de fondation superficielle rigide sont respectées. Le cas d'un champ d'onde incliné fera partie d'une étude ultérieure.

### ***Propagation unidirectionnelle d'onde à trois composantes dans un domaine de sol en forme de T pour l'ISS et l'ISSS***

L'approche de propagation unidirectionnelle d'une onde à trois composantes (1D-3C) est adoptée pour résoudre la réponse dynamique du sol. La technique de modélisation de propagation unidirectionnelle d'une onde trois composantes est étendue pour des analyses d'ISS et ISSS. Les résultats obtenus sur l'ISS montrent que cette interaction n'est observée dans le sol que dans les premières couches. Par conséquent, un modèle de sol 3-D est adopté jusqu'à une profondeur fixée, au-dessus de laquelle on considère que la déformation est influencée par l'ISS et l'ISSS, alors qu'un modèle de sol 1-D est adopté pour les couches de sol plus profondes, jusqu'à l'interface sol-substrat (modèle 1DT-3C). Le profil de sol en T est assemblé avec une ou plusieurs structures 3-D de type poteaux-poutres à l'aide d'un modèle par éléments finis, pour prendre en compte, respectivement, l'ISS et l'ISSS. Ce modèle permet de prendre en compte la déformabilité de la fondation et les effets de basculement et peut simuler l'interaction entre plusieurs bâtiments.

L'approche 1DT-3C est vérifiée par comparaison avec un modèle entièrement 3D-3C, dans le cas d'une propagation verticale dans un sol stratifié horizontalement. La technique de

modélisation 1DT-3C proposée est donc un outil pour la conception de bâtiments, permettant de prendre en compte l'ISS de manière efficace et simple. De fait, dans le cas d'une propagation verticale et de paramètres géotechniques homogènes dans chaque couche de sol, l'utilisation d'éléments solides unitaires pour les couches plus profondes, au lieu d'un domaine 3-D, représente une réduction du temps de calcul sans affecter les résultats.

L'effet d'ISS est défini comme la différence en termes d'accélération maximale  $a_{\max\_1\text{step}}/a_{\max\_2\text{step}}$  entre la solution en une étape (résolution directe du problème d'équilibre dynamique de l'ensemble sol-bâtiment) et la solution obtenue par la méthode en 2 étapes (mouvement à surface libre appliqué à un bâtiment à base fixe). Mon étude montre que cet effet est plus important dans le cas où le sol est plus mou et dans le cas d'un comportement de sol non linéaire. Des effets de résonance entre les fréquences du bâtiment, la fréquence associée au sol et le contenu fréquentiel du signal sismique produisent une réponse sismique amplifiée. L'effet d'ISS est observé pour les deux premiers modes de translation du bâtiment et est plus prononcé dans la direction du mode excité par la charge d'entrée.

### ***Spectre de réponse pour la conception parasismique tenant compte de l'interaction sol-structure***

Une analyse paramétrique de la réponse sismique des bâtiments en béton armé est développée et discutée pour identifier les paramètres clé du phénomène d'ISS, influençant la réponse structurelle, à introduire dans la conception parasismique de bâtiments.

La variation de l'accélération maximale en haut du bâtiment avec le rapport de fréquence bâtiment / sol est tracée pour plusieurs bâtiments, chargés par un mouvement à bande étroite qui excite leur fréquence fondamentale. Dans le cas de sols et de structures à comportement linéaire, une tendance similaire est obtenue pour différents bâtiments. En régime élastique linéaire, l'ISS peut être pris en compte à l'aide d'un facteur de correction appliqué au résultat d'une analyse en deux étapes (modèle de bâtiment à base fixe chargé par un signal sismique à surface libre). Ce facteur de correction dépend du rapport de fréquence fondamentale  $f_b/f_s$  du bâtiment au sol.

L'analyse paramétrique est répétée en introduisant l'effet de la non-linéarité du sol et du béton armé. L'effet de la non-linéarité du sol sur la réponse sismique des bâtiments est prépondérant par rapport à l'effet de la non-linéarité du béton armé. La non-linéarité du comportement du sol ou du sol et de la structure, tend à augmenter l'irrégularité de la réponse sismique des bâtiments.

De plus elle modifie la fréquence de vibration pendant le processus. Par conséquent, en tenant compte du comportement non-linéaire des matériaux, la réponse sismique des bâtiments considérant l'ISS ne peut plus être reproduite en appliquant un simple facteur de correction sur les résultats obtenus par l'analyse en deux étapes.

### ***Analyse de l'interaction structure-sol-structure***

La réponse sismique d'un bâtiment en béton armé est estimée en tenant compte de l'effet d'un bâtiment voisin, pour un sol et des structures à comportement linéaire. Cette approche permet une analyse efficace de l'interaction structure-sol-structure pour la pratique de l'ingénierie afin d'inspirer la conception d'outils pour la réduction du risque sismique et l'organisation urbaine. L'analyse effectuée à l'aide de la technique de modélisation 1DT-3C montre que l'ISSS est observée dans la direction du premier mode de vibration du bâtiment. L'ISSS donne, pour certains cas, une amplification jusqu'à 40 % du mouvement non prise en compte lorsque le bâtiment est considéré comme isolé. En outre, dans un sol meuble, la réponse sismique du bâtiment excité ne présente pas de variations importantes du fait de la présence de bâtiments voisins. L'effet de l'ISS l'emporte sur l'effet de l'ISSS.

### ***Conclusions et perspectives***

Dans les pratiques professionnelles, les normes de conception évoluent en fonction des nouvelles découvertes et des progrès croissants des capacités informatiques. Aujourd'hui, les codes de conception sismiques européens ne prennent toujours pas en compte l'ISS et l'ISSS dans la conception des structures. Cette recherche étudie les phénomènes d'interaction entre sol et structures, propose et valide des techniques de modélisation pour évaluer les réponses dynamiques des sols et des structures aux séismes, en prenant en compte l'ISS et l'ISSS.

L'approche de propagation des ondes sismiques 1DT-3C est proposée comme technique de modélisation pour la simulation de la réponse sismique des sols et des bâtiments, en tenant compte des effets de site, de la déformabilité des fondations, des effets de basculement et, éventuellement, de l'ISSS. Le modèle 1DT-3C consiste à adopter un modèle entièrement 3-D jusqu'à une profondeur fixe, au-dessus de laquelle les effets d'ISS et d'ISSS modifient le mouvement du sol et au-delà de laquelle un modèle 1-D est supposé être une approximation suffisante.

La technique de modélisation 1DT-3C proposée est un outil efficace pour la conception de bâtiments, permettant de prendre en compte facilement et efficacement les ISS et ISSS pour des comportements des matériaux linéaires et non-linéaires, offrant des avantages en terme de temps de modélisation et de calcul par rapport à un modèle entièrement 3-D. L'introduction des comportements non-linéaires est absolument nécessaire car les observations actuelles dans les zones soumises à de fortes sollicitations sismiques, montrent que ces effets sont importants. Par ailleurs cet outil s'adapte bien aux pratiques :

- les paramètres géotechniques peuvent assez simplement caractérisés pour un modèle de sol unidimensionnel en utilisant un forage, alors qu'une caractérisation 3D serait très lourde (plusieurs forage et mise en adéquation des observations).
- la définition des conditions aux limites est simple : le signal d'entrée et la condition aux limites d'absorption ne sont donnés que pour un seul élément.
- le maillage est considérablement réduit.

L'analyse paramétrique combinant 11 profils de sol et 5 structures différentes montre qu'en régime élastique linéaire l'ISS peut être pris en compte assez facilement à partir des résultats d'une étude traditionnelle en deux étapes. Elle permet donc de proposer une amélioration potentielle des spectres de réponse pour la conception parasismique proposés par l'Eurocode 8 en régime élastique.

Par contre le comportement non-linéaire du matériau provoque une modification de la réponse sismique du sol et des bâtiments, avec en particulier, une modification les fréquences caractéristiques. L'analyse paramétrique que je présente permet de tirer quelques résultats qualitatifs, mais montre qu'il n'y a pas de façon simple, pour la conception des bâtiments, de s'appuyer sur les modélisations traditionnelles qui se limitent à un comportement linéaire des matériaux.

La méthode proposée est efficace aussi pour une analyse de l'influence de l'ISSS sur un bâtiment cible. Je présente une analyse paramétrique le régime élastique linéaire. Les résultats montrent que si, dans le cas de sol mous, l'effet de l'ISS l'emporte sur l'effet de l'ISSS, dans les autres conditions de sol l'ISSS ne peut pas être négligé. L'analyse paramétrique donne des résultats préliminaires qui ne permettent pas encore de généraliser.

Cette recherche pourrait se prolonger par une analyse paramétrique et une étude statistique approfondies visant à généraliser la conception des structures dans les zones sismiques, en tenant compte des effets d'ISS. Pour permettre la vérification du modèle numérique, des

expériences sur des structures instrumentées à des échelles réelle ou proportionnelle pourraient être utilisées pour comparer observations et calculs numériques. L'approche de propagation des ondes 1D-3C pourrait évoluer pour modéliser les fondations profondes et les sols encaissants, en considérant un domaine 3-D atteignant une plus grande profondeur. Une analyse de contrainte efficace, prenant en compte la position de la nappe phréatique dans un modèle de propagation d'ondes 1DT-3C pour l'analyse de l'ISS, est actuellement développée dans le cadre de la thèse de doctorat de Stefania Gobbi. D'autres améliorations peuvent être introduites comme, la corrosion des barres d'acier dans le béton armé ou la considération des matériaux de construction différents tel que le bois et l'acier.



## Introduction

Earthquake engineering research is an interdisciplinary field involving structural and geotechnical engineers, seismologists, architects and urban planners. It is a discipline that studies the antiseismic conception of new structures and the ability of existing structures to survive an earthquake without severe damage. The building codes are based on actual knowledge concerning the seismic conception and design.

The need for such codes is initiated by several major earthquake disasters causing damage to structures hence, to population. The damage concerns reinforced concrete structures as well as wooden and steel structures and is observed in low-, mid- and high- rise buildings and that, either in lower, mid or upper story of structures. Earthquake damage also attains the soil leading to soil failure and eventual the collapse of the structures.

Due to variabilities in observations and seismic risk in regions the requisite for research in this field becomes higher in order to understand soil and structure responses to earthquakes and contribute in the progress of seismic codes. There are several seismic codes used in the world, most of them share similar fundamental design approaches and only differ in the techniques of application regarding local geological conditions and common new and old construction types. In France the first text aiming to prevent constructions to earthquake shakings was written in 1955 in the recommendation AS55. The text was updated through time with studies and new earthquake events. In 2005 the Eurocode 8, a new seismic code based on the European rules for construction, is employed in France to protect people and restrain structural damages to earthquakes. The metropolitan France presents moderated seismicity in which the eastern Provence presents the highest risk. For this reason, the region of Provence-Alpes-Côte d'Azur encourage research on seismic risk in the purpose of prevention of structural seismic damages.

Previous researches have shown that the interaction between the soil and the building induces modification in the dynamic response of the building (Veletsos and Meek 1974; Jennings 1970; Wolf 1985; Gazetas 1991). This modification of the structure response is not beneficial in all conditions and if it is the case, an overdesign is assumed.

The soil-structure interaction (SSI) has been the subject of many works, showing the importance of the SSI assessment in seismic structural design. In the Eurocode 8 the structure is considered as a simplified model using single degree of freedom (SDOF) and SSI is studied in a two-step analysis as named by Saez et al. (2011). This two-step analysis doesn't correctly model the interaction between the soil and the structure. An update to such procedure

considering the advances in theory and practice is mandatory. The lack of the previous version of the Eurocode 8 has encourage this research to consider SSI for structures with shallow foundation, model multilayered soil profiles and study the dynamic response of the assembly soil-structure.

The Eurocode 8 is limited to the elastic linear behavior of materials. However, evidence of nonlinearity in the soil has been observed for a long time now. In Japan, a seismological data is recorded in Kiban Kyoshin Network since 1995, following the Hyogo-Ken Nanbu earthquake of 1995 Kobe Japan, and provides evidence that soils tend to quickly reach nonlinearity properties for higher shaking amplitude. On the other hand, a non-cracked structure is an overstatement, cracks are created in concrete at early age and nonlinear behavior of the reinforced concrete should be considered to study the seismic response of a structure.

The aim of this research is to provide additional knowledge on structure and soil seismic responses, evaluate the accuracy of modeling techniques employed to replicate the SSI effect due to dynamic excitation and propose eventual advancement in the earthquake engineering field.

The progression of this research goes as following:

- Modeling technique for SSI (Chapter 2): The one-directional three-component (1D-3C) wave propagation approach is propagated in a one-dimensional (1-D) soil assembled with 3-D frame structure in a finite element (FE) scheme (1D-3C). The linear elasticity is employed, it is a simplification considered for structural design, assuming a behavior in elastic strain range, sufficiently far from yielding threshold. This hypothesis simplifies the numerical computations, avoiding modeling of nonlinear material behavior, accepting superposition principle and modeling concrete as a homogeneous material before cracking without the effect of reinforcing bars. Later the nonlinear behaving of materials is considered, in a dynamic analysis, introduces the hysteretic dissipation of energy in the assembly soil-structure and the system soil response is modified and depends on more parameters and on the time history, increasing the difficulty of prediction with simplified empirical tools.

The 1D-3C model is verified comparing with validated codes in a free field (FF) analysis using SWAP\_3C (proposed by Santisi d'Avila and Lenti 2012), and in a SSI analysis using SFRINT\_3C (proposed by Santisi d'Avila and Lopez-Caballero 2018), considering

linear and non-linear soil behaving. Analysis are undertaken using the 1D-3C model for SSI analysis.

- Advanced modeling technique for SSI and structure-soil-structure interaction (SSSI) (Chapter 3): Analysis using the 1D-3C model for SSI have shown evidence of the effect of SSI in the first layers of the soil and negligible or no effect in deeper soil. Based on this observation a T-shaped soil modeling is proposed (1DT-3C). It consists on modeling 3-D soil model until a certain thickness to be defined, depending on the SSI, connected to a 1-D soil modeled until the bedrock interface. The 3-D soil model permits the embedment of a 3-D foundation connected to the base node of the columns of the 3-D structure allowing rocking effect. The 1DT-3C present an efficient modeling technique for engineering practice, to consider SSI in any commercial FE code.

The proposed 1DT-3C model is verified, in linear and non-linear soil behaving, and SSI analysis are undertaken.

- Parametric investigation on SSI (Chapter 4): After verification of the proposed model for dynamic SSI and SSSI analyses, different computations are carried out to compare the structure and soil responses to earthquake, in the cases of linear and nonlinear behaving materials. A parametric analysis is performed to investigate the variation of the SSI effect with soil and structure dynamic features of the frequencies.
- Parametric investigation on SSSI (Chapter 5): Afterward a study on SSSI is held focusing on a target building and varying the nearby building and quake predominant frequency. The lateral boundary condition is investigated in order to assess a complex geometry of soil and structure plan for SSSI investigations.



## **Chapter 1 - Overview on soil and structural dynamics**

Continuous efforts have been made towards improving modeling techniques in earthquake engineering (characterization of geotechnical parameters, rheologic behavior, site effects, interaction between structure and soil, and with nearby structures), beside the continuous development of risk mitigation tools. Moreover, design codes need to evolve in the regulation of seismic loading definition using signals. Numerical methods that solve a dynamic soil-structure interaction problem is not currently adopted in the engineering practice for building design, but it remains a subject for researchers or taken into account in design of bridges, dams or towers. In the following, basic concepts of structural dynamics are introduced and previous research findings are presented.

## 1.1 Introduction to structural dynamic problem

In structural analysis, static and dynamic loading are considered. If the applied load has a long period, enough to be considered constant and neglect inertial forces it is static otherwise it is a dynamic load.

The structural dynamics aims to study the behavior of a structure under dynamic loadings. In particular, in earthquake engineering the structural response to earthquakes is analyzed.

### 1.1.1. Single degree of freedom (SDOF)

An adopted simplification to model structures under seismic loading is to represent the structure using a single degree of freedom oscillator (SDOF). It consists on a lumped mass  $m$  held by a massless column with stiffness  $k$ , damping coefficient  $c$  (Figure 1-1). The system is considered fixed at the bottom and subjected to earthquake loading,  $F(t) = -m\ddot{u}_g(t)$ , that is time dependent, according to Newton's second law, where  $\ddot{u}_g(t)$  is the ground acceleration at the building base. The differential equation of motion for the SDOF oscillator is

$$m\ddot{u}(t) + c\dot{u}(t) + ku(t) = F(t) \quad (1-1)$$

where  $m\ddot{u}(t)$ ,  $c\dot{u}(t)$ , and  $ku(t)$  are the inertial, viscous and elastic force, respectively. The dot represents time derivative and  $u(t)$ ,  $\dot{u}(t)$  and  $\ddot{u}(t)$  are the structural displacement, velocity and acceleration, respectively.

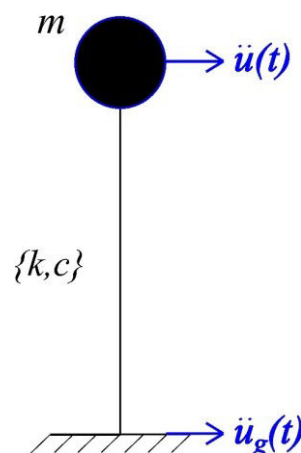


Figure 1-1 Single degree of freedom oscillator (SDOF) subjected to earthquake ground motion  $\ddot{u}_g(t)$ .

Dividing Eq. (1-1) by the mass  $m$  gives

$$\ddot{u}(t) + 2\zeta w_0 \dot{u}(t) + w_0^2 u(t) = -\ddot{u}_g(t) \quad (1-2)$$

where  $\ddot{u}_g(t)$  is the seismic loading,  $\zeta = c / c_r$  is the damping ratio,  $c_r = 2mw_0$  is the critical damping coefficient and  $w_0 = \sqrt{k/m}$  is the undamped angular frequency of the oscillator (Chopra 2001). The solution of the homogenous equation of motion ( $-\ddot{u}_g(t) = 0$ ) having initial static conditions  $u(0) = 0$ ,  $\dot{u}(0) = 0$  is written in

$$u(t) = e^{-\zeta w_0 t} [u(0) \cos(w_d t) + (\dot{u}(0) + \zeta w_0 u(0)) / w_d \sin(w_d t)] \quad (1-3)$$

where  $w_d = w_0 \sqrt{1 - \zeta^2}$ . The natural period of the oscillator is  $T_0 = 2\pi/w_0$  its frequency is  $f_0 = 1/T_0$  implying that more the structure is stiffer, higher is its natural frequency of vibration.

The increase of the damping ratio in Eq. (1-2) outcomes a slow to fast attenuation of the free vibration (Figure 1-2). Damping in structures originate from a low friction in materials but it is mostly due to damage in non-structural elements (Bachmann et al. 2012). The typical damping  $\zeta$  for buildings vary between 1 and 10%, this implies that the damped and undamped natural period and frequencies are almost identical.

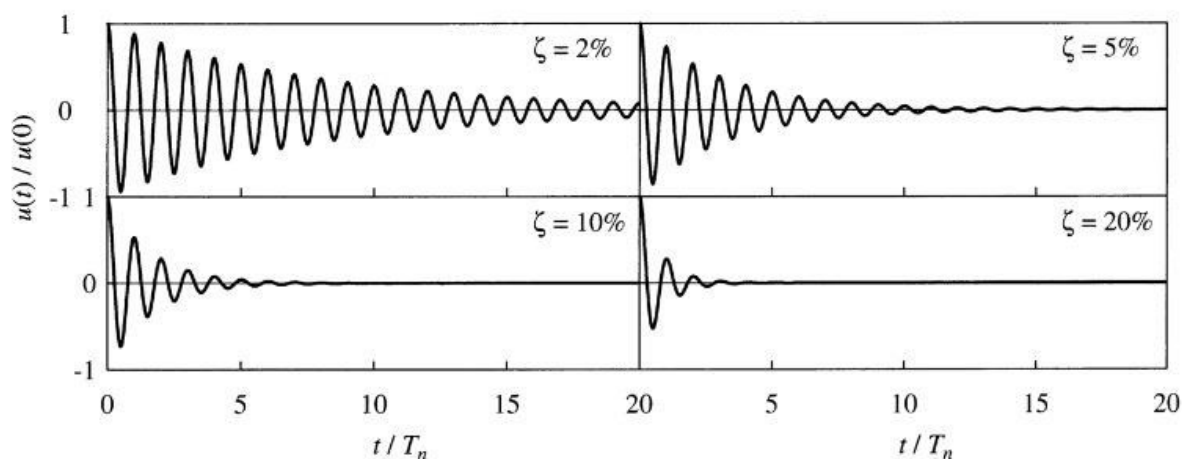


Figure 1-2 Free vibration of a SDOF system with different levels of damping:  $\zeta = 2, 5, 10,$  and  $20\%$ . (Chopra 2001)

### 1.1.2. Numerical solution of the dynamic equilibrium equation for SDOF oscillators

The dynamic equilibrium equation for a SDOF oscillator under seismic loading  $\ddot{u}_g(t)$  is written in Eq. (1-2), it can be rewritten as

$$\mathbf{y}_i = \boldsymbol{\theta}(\Delta t)\mathbf{y}_{i-1} + \boldsymbol{\gamma}_0(\Delta t)\mathbf{v} F_{i-1} + \boldsymbol{\gamma}_1(\Delta t)\mathbf{v} F_i \quad (1-4)$$

$$\dot{\mathbf{y}}_i = \mathbf{D}\mathbf{y}_i + \mathbf{v} F_i \quad (1-5)$$

where the subscript  $i$  is the iteration step,  $F_i = -\ddot{u}_g(t_i)$  and

$$\mathbf{y}_i = \begin{bmatrix} u(t_i) \\ \dot{u}(t_i) \end{bmatrix} \quad (1-6)$$

Eq. (1-4) and Eq. (1-5) can be solved by iteration, considering the static initial conditions  $u(0) = 0$ ,  $\dot{u}(0) = 0$ . The variables  $\boldsymbol{\theta}(\Delta t)$ ,  $\mathbf{v}$ ,  $\mathbf{D}$ ,  $\boldsymbol{\gamma}_0(\Delta t)$  and  $\boldsymbol{\gamma}_1(\Delta t)$  in Eq. (1-4) and Eq. (1-5) are defined as following

$$\boldsymbol{\theta}(\Delta t) = \begin{bmatrix} -w_0^2 g(\Delta t) & h(\Delta t) \\ -w_0^2 \dot{h}(\Delta t) & \dot{h}(\Delta t) \end{bmatrix}, \mathbf{v} = \begin{bmatrix} 0 \\ 1 \end{bmatrix}, \mathbf{D} = \begin{bmatrix} 0 & 1 \\ -w_0^2 & -2\zeta_0 w_0 \end{bmatrix} \quad (1-7)$$

$$\boldsymbol{\gamma}_0(\Delta t) = (\boldsymbol{\theta}(\Delta t) - \mathbf{L}(\Delta t)/\Delta t)\mathbf{D}^{-1}, \boldsymbol{\gamma}_1(\Delta t) = (\mathbf{L}(\Delta t)/\Delta t - \mathbf{I})\mathbf{D}^{-1} \quad (1-8)$$

where the functions presented in Eq. (1-7) and Eq. (1-8) are defined as

$$\mathbf{L}(\Delta t) = (\boldsymbol{\theta}(\Delta t) - \mathbf{I})\mathbf{D}^{-1} \quad (1-9)$$

$$g(\Delta t) = -1/w_0^2 e^{-\zeta w_0 \Delta t} (\cos(w_d \Delta t) + \zeta w_0/w_d \sin(w_d \Delta t)) \quad (1-10)$$

$$h(\Delta t) = -1/w_d e^{-\zeta w_0 \Delta t} \sin(w_d \Delta t) \quad (1-11)$$

$$\dot{h}(\Delta t) = e^{-\zeta w_0 \Delta t} (\cos(w_d \Delta t) - \zeta w_0/w_d \sin(w_d \Delta t)) \quad (1-12)$$

### 1.1.3. Dynamic study of a MDOF system in the frequency domain

The dynamic solution of a multiple degree of freedom (MDOF) structure under seismic loading  $\ddot{u}_g(t)$ , assuming linear constitutive behavior of materials, is written as

$$\mathbf{M}\ddot{\mathbf{u}}(t_i) + \mathbf{C}\dot{\mathbf{u}}(t_i) + \mathbf{K}\mathbf{u}(t_i) = -\mathbf{M}\boldsymbol{\tau}\ddot{u}_g(t_i) \quad (1-13)$$

where the  $\mathbf{M}$ ,  $\mathbf{K}$  and  $\mathbf{C}$  are the mass, stiffness and damping matrices respectively. The dot represents the time derivative, consequently,  $\mathbf{u}$ ,  $\dot{\mathbf{u}}$  and  $\ddot{\mathbf{u}}$  are the displacement, velocity and acceleration vectors, respectively, and  $\boldsymbol{\tau}$  is the influence vector.

Under the assumption of lumped mass, the structural model is simplified as in Figure 1-3 and the mass matrix is diagonal as  $\mathbf{M} = \text{diag}\{m_1, m_2 \dots m_n\}$ , where the subscript  $n$  represents the total number of stories in the building.

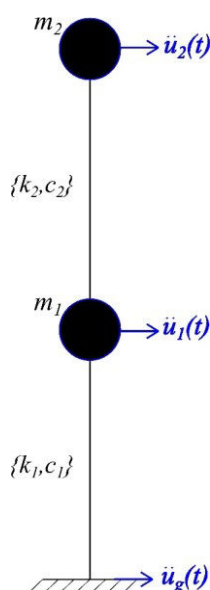


Figure 1-3 Multiple degree of freedom (MDOF) oscillator subjected to an earthquake ground motion  $\ddot{u}_g(t)$ .

The modal analysis can solve the dynamic equilibrium of a multiple degree of freedom MDOF system under the assumption of structural response resulting from the superposition of mode shapes. This, under the hypothesis of linear behaving materials. The dynamic equilibrium equation Eq. (1-13) can be written in modal coordinates by imposing the transformation  $\mathbf{u} = \boldsymbol{\phi}\mathbf{q}$ . Accordingly, it is

$$\mathbf{M}\boldsymbol{\phi}\ddot{\mathbf{q}}_i + \mathbf{C}\boldsymbol{\phi}\dot{\mathbf{q}}_i + \mathbf{K}\boldsymbol{\phi}\mathbf{q}_i = -\mathbf{M}\boldsymbol{\tau}\ddot{u}_{gi} \quad (1-14)$$

where  $\mathbf{q}_i$  is the modal displacement at the time step  $t_i$  and  $\boldsymbol{\phi}$  is the modal matrix compound by the eigenvectors obtained by solving

$$\mathbf{K}\boldsymbol{\phi} = \mathbf{M}\boldsymbol{\phi}\boldsymbol{\Omega}^2 \quad (1-15)$$

The natural angular frequencies are obtained as solution of

$$\det(\mathbf{K} - \lambda\mathbf{M}) = 0 \quad (1-16)$$

where  $\lambda$  is the vector of eigenvalues such that  $\lambda_j = w_{0j}^2$  and  $\boldsymbol{\Omega}_k^2 = \text{diag}\{w_{0j}^2\}$ . Each  $\lambda_j$  corresponds to the squared angular frequency of the structure such that  $w_{01} < w_{02} < \dots < w_{0j}$ . The subscript  $j$  represents the  $j^{\text{th}}$  mode shape.

The modal transformation corresponds to an operation of diagonalization of matrices  $\mathbf{M}$ ,  $\mathbf{K}$  and  $\mathbf{C}$ . Consequently, the dynamic equilibrium equation for the MDOF system in Eq. (1-14) is solved as a system of independent dynamic equilibrium equations of SDOF systems

$$\ddot{\mathbf{q}}_i + \boldsymbol{\Xi}\dot{\mathbf{q}}_i + \boldsymbol{\Omega}^2\mathbf{q}_i = -\boldsymbol{\phi}^T\mathbf{M}\boldsymbol{\tau}\Delta\ddot{\mathbf{u}}_{gi} \quad (1-17)$$

where  $\boldsymbol{\Xi} = \text{diag}\{2\zeta w_i\}$  and the modal matrix must be orthonormal with respect to the mass matrix and satisfy  $\boldsymbol{\phi}^T\mathbf{M}\boldsymbol{\phi} = \mathbf{I}$  and  $\boldsymbol{\phi}^T\mathbf{K}\boldsymbol{\phi} = \boldsymbol{\Omega}^2$ . Each one of Eq. (1-17) is solved as explained in section 1.1.2, since the analytical solution is known for the SDOF. The modal superposition is possible only for linear behavior of materials and proportionally damped structures.

#### 1.1.4. Dynamic equilibrium for MDOF structures

In the case of nonlinear behaving materials, i.e. when the stress-strain relationship is nonlinear, the dynamic equation is

$$\mathbf{M}\Delta\ddot{\mathbf{u}}(t_i) + \mathbf{C}_i\Delta\dot{\mathbf{u}}(t_i) + \mathbf{K}_i\Delta\mathbf{u}(t_i) = -\mathbf{M}\boldsymbol{\tau}\Delta\ddot{\mathbf{u}}_g(t_i) \quad (1-18)$$

where the stiffness and damping matrices vary during the process.

Time discretization is needed in order to solve this problem. According with the  $\alpha$ -method (Hughes 1987), at each time step  $t_i$  the following equation can be resolved

$$\begin{aligned} \mathbf{M}\Delta\ddot{\mathbf{u}}(t_i) + (1 + \alpha)\mathbf{C}(t_i)\Delta\dot{\mathbf{u}}(t_i) + (1 + \alpha)\mathbf{K}(t_i)\Delta\mathbf{u}(t_i) - \alpha\mathbf{C}(t_{i-1})\Delta\dot{\mathbf{u}}(t_{i-1}) \\ - \alpha\mathbf{K}(t_{i-1})\Delta\mathbf{u}(t_{i-1}) = (1 + \alpha)\Delta\mathbf{F}(t_i) - \alpha\Delta\mathbf{F}(t_{i-1}) \end{aligned} \quad (1-19)$$

In the following equation, for simplicity, the time instant  $t_i$  is indicated by the subscript  $i$ :

$$\begin{aligned} \mathbf{M}\Delta\ddot{\mathbf{u}}_i + (1 + \alpha)\mathbf{C}_i\Delta\dot{\mathbf{u}}_i + (1 + \alpha)\mathbf{K}_i\Delta\mathbf{u}_i - \alpha\mathbf{C}_{i-1}\Delta\dot{\mathbf{u}}_{i-1} - \alpha\mathbf{K}_{i-1}\Delta\mathbf{u}_{i-1} \\ = (1 + \alpha)\Delta\mathbf{F}_i - \alpha\Delta\mathbf{F}_{i-1} \end{aligned} \quad (1-20)$$

The increment of velocity  $\Delta\dot{\mathbf{u}}_i$  and acceleration  $\Delta\ddot{\mathbf{u}}_i$  at time step  $t_i$  are written in function of the increment of displacement  $\Delta\mathbf{u}_i$ , as following, and substituted in the Eq. (1-20)

$$\begin{aligned} \Delta\dot{\mathbf{u}}_i &= \gamma/\beta\Delta t \Delta\mathbf{u}_i - \gamma/\beta \dot{\mathbf{u}}_{i-1} + (1 - \gamma/2\beta) \Delta t\ddot{\mathbf{u}}_{i-1} \\ \Delta\ddot{\mathbf{u}}_i &= 1/\beta\Delta t^2 \Delta\mathbf{u}_i - 1/\beta\Delta t \dot{\mathbf{u}}_{i-1} + (1/2\beta) \Delta t\ddot{\mathbf{u}}_{i-1} \end{aligned} \quad (1-21)$$

at each time step, the displacement increment is obtained by modified equilibrium equation

$$\bar{\mathbf{K}}_i\Delta\mathbf{u}_i = \Delta\mathbf{F}_i + \mathbf{A}_{i-1} \quad (1-22)$$

where the modified stiffness matrix is

$$\bar{\mathbf{K}}_i = 1/\beta\Delta t^2 \mathbf{M} + (1 + \alpha)\gamma/\beta\Delta t \mathbf{C}_i + (1 + \alpha)\mathbf{K}_i \quad (1-23)$$

and the vector  $\mathbf{A}_{i-1}$  is dependent on the result of the previous time step and calculated as

$$\begin{aligned} \mathbf{A}_{i-1} &= [1/\beta\Delta t \mathbf{M} + (1 + \alpha)\gamma/\beta \mathbf{C}_i] \dot{\mathbf{u}}_{i-1} \\ &\quad + [1/2\beta \mathbf{M} + (1 + \alpha)(\gamma/2\beta - 1)\Delta t\mathbf{C}_i] \ddot{\mathbf{u}}_{i-1} \\ &\quad + \alpha\mathbf{C}_{i-1}\Delta\dot{\mathbf{u}}_{i-1} + \alpha\mathbf{K}_{i-1}\Delta\mathbf{u}_{i-1} - \alpha\Delta\mathbf{F}_{i-1} \end{aligned} \quad (1-24)$$

After evaluating the increment of displacement  $\Delta\mathbf{u}_i$  using Eq. (1-22), the increment of velocity  $\Delta\dot{\mathbf{u}}_i$  and the increment of acceleration  $\Delta\ddot{\mathbf{u}}_i$  are calculated using Eq. (1-21). The total displacement  $\mathbf{u}_i$ , velocity  $\dot{\mathbf{u}}_i$  and acceleration  $\ddot{\mathbf{u}}_i$  are then deduced as

$$\mathbf{u}_i = \mathbf{u}_{i-1} + \Delta\mathbf{u}_i \quad \dot{\mathbf{u}}_i = \dot{\mathbf{u}}_{i-1} + \Delta\dot{\mathbf{u}}_i \quad \ddot{\mathbf{u}}_i = \ddot{\mathbf{u}}_{i-1} + \Delta\ddot{\mathbf{u}}_i \quad (1-25)$$

The derivation introduces high frequency noise into the solution; numerical damping removes this high-frequency noise without having any significant effect on the meaningful, lower frequency response. The control over the amount of numerical damping is provided by the  $\alpha$ -method using the parameters  $\alpha, \beta = 0.25(1 - \alpha)^2$  and  $\gamma = 0.5 - \alpha$  such that  $-1/3 \leq \alpha \leq 0$  (Hughes 1987).

The Newmark algorithm is obtained for  $\alpha = 0$ , using  $2\beta \geq \gamma \geq 0.5$  in the case of unconditional stability.

## 1.2 Numerical methods

A numerical method is evaluated according to its efficiency, in terms of time, computer memory, and accuracy. According to Chaljub et al. (2010), no single numerical method can be considered as the best. Several methods have been used to solve wave propagation in media; finite difference method (FDM), boundary element method (BEM), spectral element method (SEM) and standard finite element method (FEM).

PRENOLIN benchmark (Régnier et al. 2016) has compared 20 codes with different numerical scheme and found a standard deviation in results of 0.065 in logarithmic unit for a low-frequency input motion at low PGA values, this deviation increases with the PGA but this may also be due to the differences in the nonlinear model implementation. In this paragraph four different numerical modeling methods are selected to be presented along with their advantages and disadvantages, that often depend on the application.

### 1.2.1 Finite difference method

The FDM has a long tradition in seismology and geophysics. It consists on replacing the partial derivatives by divided differences or combinations of point values of the function in a finite number of discrete nodes of the regular mesh (Moczo et al. 2004).

Considering  $u(x, y, z, t)$  a function in space and time. The approximation of the derivative, according to Taylor series of order one, is

$$\partial u(x, y, z, t) / \partial x \approx [u(x + \Delta x, y, z, t) - u(x, y, z, t)] / \Delta x + \theta(\Delta x) \quad (1-26)$$

Where  $\theta(\Delta x)$  is the error due to the approximation.

The FDM has been employed in SEISMOSOIL (<http://asimaki.caltech.edu/resources/index.html#software>) for analysis and signal processing of 1-D site-specific response problems, by Li and Assimaki (2010) using a modified hyperbolic soil model, in NOAH (Bonilla 2001), for wave propagation in saturated soil subjected to vertically incident ground motion and by Moczo et al. (2004) in an adjusted finite difference approximation.

The advantages that present this method are the simplicity of modeling and its low cost in computer memory. However, this method presents as inconvenient the limitation in representing a complex geometry as heterogeneity and topography. The regularity of the mesh,

forces a meshing relative to the minimum shear wave velocity and causes difficulty to consider complex topography and structures, requiring a small meshing and, consequently, an important computational time and memory.

### 1.2.2 Finite element method

The FEM is the most used for engineering applications. It consists of approaching, in a finite-dimensional subspace, a problem written in variational form (as minimization of energy in general) in an infinite dimensional space. In this case, the approximate solution is a function determined by a finite number of parameters (Hughes 1987).

Let us consider the following differential equation

$$\begin{cases} -u''(x) = f(x), & x \in ]0,1[ \\ u(0) = u(1) = 0 \end{cases} \quad (1-27)$$

to transform this differential system to variational form, the Galerkin method proposes a function  $v(x) \in V = \{C^1([0,1]) \text{ such that } v(0) = v(1) = 0\}$  and Eq. (1-27) is written

$$-\int_0^1 u''(x)v(x)dx = \int_0^1 f(x)v(x)dx \quad (1-28)$$

Integrating by part we obtain

$$-\int_0^1 u'(x)v'(x)dx = \int_0^1 f(x)v(x)dx \quad \forall v \in V \quad (1-29)$$

The problem is, hence, brought to solve the variational Eq. (1-29) approximating the problem in a sub-space  $\tilde{V}$  of finite dimension  $N$  posing  $\tilde{u}(x) = \sum_{j=1}^N u_j \phi_j(x) \in \tilde{V}$ , where  $\phi_j(x)$  are shape functions linearly independent in  $V$ .

The FEM has been widely employed, as example, Abaqus CAE (<https://www.3ds.com/products-services/simulia/products/abaqus/>), ASTER code (<http://www.code-aster.org>), CESAR ([www.cesar-lcpc.com](http://www.cesar-lcpc.com)) and OpenSees (<http://opensees.berkeley.edu/>), are softwares used for modeling, analyzing and visualization of results.

SWAP\_3C is a code for three-component seismic wave propagation, that uses line quadratic finite elements (Santisi d'Avila and Lenti 2012), verified and validated during the PRENOLIN

benchmark. The same 1D-3C wave propagation model is used for SSI analysis, by assembling the 1-D soil profile with a 3-D frame structure (Santisi d'Avila and Lopez-Caballero 2018).

The advantages of this method are the ability to model complex geometry as heterogeneity and topography, the feasibility to use adaptive mesh and the numerous available theories on the convergence of this method. The inconvenient is the expensive cost in computational time and memory.

### 1.2.3 Spectral element method

The SEM was initially used for fluid mechanics (Patera 1984). It derives from the FEM using polynomial functions ( $\phi_j(x)$ ) of high degree of type Chebyshev (Priolo et al. 1994) or Legendre (Komatitsch and Vilotte 1998).

The SEM is used in EFISPEC1D (<http://efispec.free.fr/>) software that solves 1-D wave propagation equations and by Mercerat et al. (2006).

The advantage of SEM is the accuracy in the convergence. The inconvenients are the loss of adaptive mesh (loss in geometry flexibility), comparing to FEM method, and the expensive cost in computational time and memory.

### 1.2.4 Boundary element method

When the domain of interest extends to infinity, the BEM represents a powerful alternative to FEM. It is founded on the boundary integral equation theory that describes the problem by equations with known and unknown boundary states. The discretization only concerns the surface rather than the volume, and reduces the dimension of the problem by one (Bonnet 1999; Hall 1994; Kythe 1995).

The BEM is mostly used for fracture or contact problems but it is also used in seismology to evaluate the topography effect and the wave propagation in alluvial basin (Bouchon and Sánchez-Sesma 2007; Mogi and Kawakami 2007; Semblat et al. 2002).

The BEM is especially advantageous in the case of problems with infinite or semi-infinite domains, it requires less computation time and memory when it provides more accurate solution at the interior nodes of the domain. Unfortunately, it presents some disadvantages as it is uncommon for engineering problems. Moreover, the boundary integral equations, requiring an explicit solution, available only for linear problems. Problems with nonlinearities are not accessible by BEM in its standard formulation. In addition, the BEM represents some

mathematical complications to choose the accurate boundary integral equations, a lot of mathematical analysis need to be performed. The inconvenient is also in terms of loss in geometry flexibility, BEM is not applicable for frame structures in 3-D analyses because of the large surface to volume ratio, this causes erroneous in the solution.

### **1.3 Site effect**

The geological characterization and topography nature of the soil affect significantly the registered signal at the free surface soil, caused by ground shaking with respect to the bedrock motion. The seismic site response has shown amplification of the seismic motion, comparing to that latter registered at bedrock surface, and this is due to seismic waves propagating in multilayered soft soil with different impedance contrast between layers (Bard et al. 1988; Bard and Bouchon 1985; Kawase and Aki 1989). These site effects are observed in many earthquakes: San Fernando, California February 9, 1971 (Hanks 1975), Mexico, Mexico City valley September 19, 1985 (Singh et al. 1988), Venezuela, Caracas valley July 29, 1967 (Papageorgiou and Kim 1991) etc.

#### *1.3.1. Impact of soil characterization*

In seismic site response, the shear wave velocity in the medium  $v_s$  is a key parameter for soil characterization. The average shear velocity of the top 30 m layers,  $v_{s30}$  is adopted as parameter to define the ground type in building codes. The soil stratigraphy influences the soil seismic response. In fact, when the seismic waves propagate across the layers, with different impedance contrast, some amplifications can be observed in the soil response.

As depicted in Figure 1-4, amplification in accelerographs of the May 13, 1995 earthquake (Ms 6.6, distance 130 km), is obtained at alluvial deposit surfaces in comparison with the reference borehole station (PRO).

The largest amplification is registered at the station TST, it represents the deepest deposit of sediments in the Mygdonian basin (197 m deep). The shown stations are part of EUROSEISTEST a European experimental site instrumented with a network of 21 high-resolution permanent accelerometers located in Mygdonia valley, epicenter area of the 1978 Stivos (Thessaloniki) earthquake Ms 6.5 (<http://euroseisdb.civil.auth.gr>).

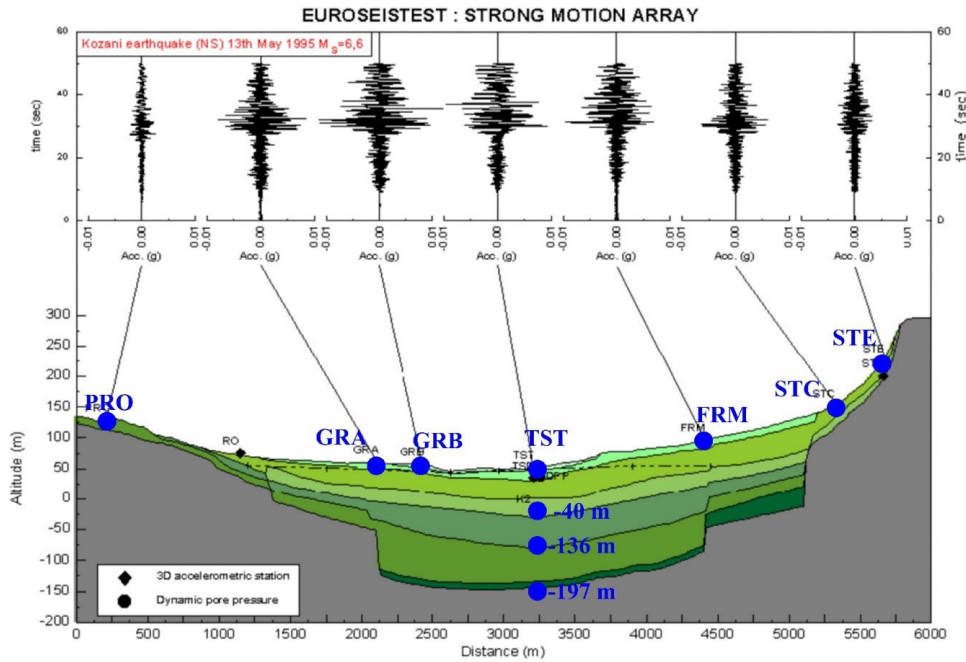


Figure 1-4 Time histories of the May 13, 1995 earthquake ( $M_s$  6.6, distance 130 km) recorded on north-south components of stations of the EUROSEISTEST network. (<http://euroseisdb.civil.auth.gr>)

Studies have shown that the geometry and material properties of the sedimentary basin govern the seismic amplification, for this reason it is very important to consider a correct characterization and modeling. Figure 1-5 shows the complete model gives amplification in the amplitude/frequency compared to the simplified model (Manakou et al. 2010; Pitilakis et al. 1999; Raptakis et al. 2000; Semblat et al. 2005). Moreover, in wave propagation modeling, the definition of the sediment-bedrock interface is mandatory.

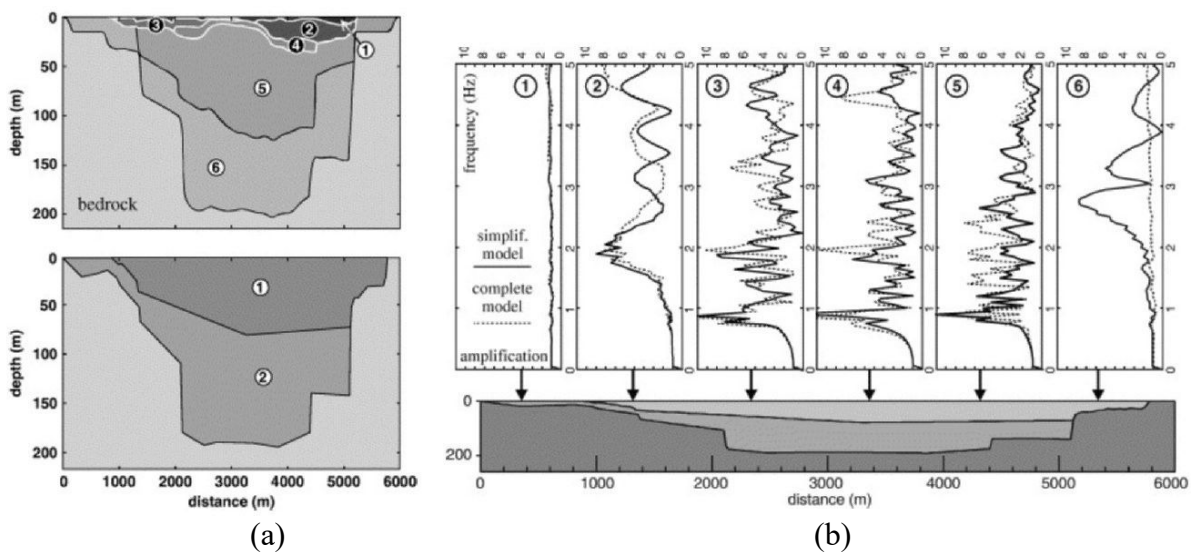


Figure 1-5 (a) Geotechnical model of the Mygdonia basin: complete model (top) and simplified model (bottom), (b) Amplification/frequency curves for various locations along the basin surface for simplified (continuous) and complete models (dashed). (Semblat et al. 2005)

### 1.3.2. Impact of the soil constitutive model

Besides the description of the geometry and the elastic parameters of sedimentary layers, the soil behavior is responsible for observed variabilities on site response (Chin and Aki 1991; Field et al. 1997). These variabilities have been mostly the result of a strong shaking. The spectral analysis of accelerograms show a shift in frequency peaks to lower frequency. Hence, to characterize the nonlinear soil behavior the simplest way is to compare the transfer function of the same site subjected to weak and strong ground motion. Figure 1-6 shows the evolution of the borehole site response with the PGA at the downhole sensor at site IWTH23 from earthquake recordings of the KiK-net database Japan (Régnier et al. 2013). It is noted a clear change in site response with respect to the PGA of the incoming motion, this is explained by the nonlinear constitution of the soil. The impact of nonlinear behavior of soils in site effects has been quantified (Castro-Cruz et al. 2017; Field et al. 1997; Kwok et al. 2008; Régnier et al. 2017).

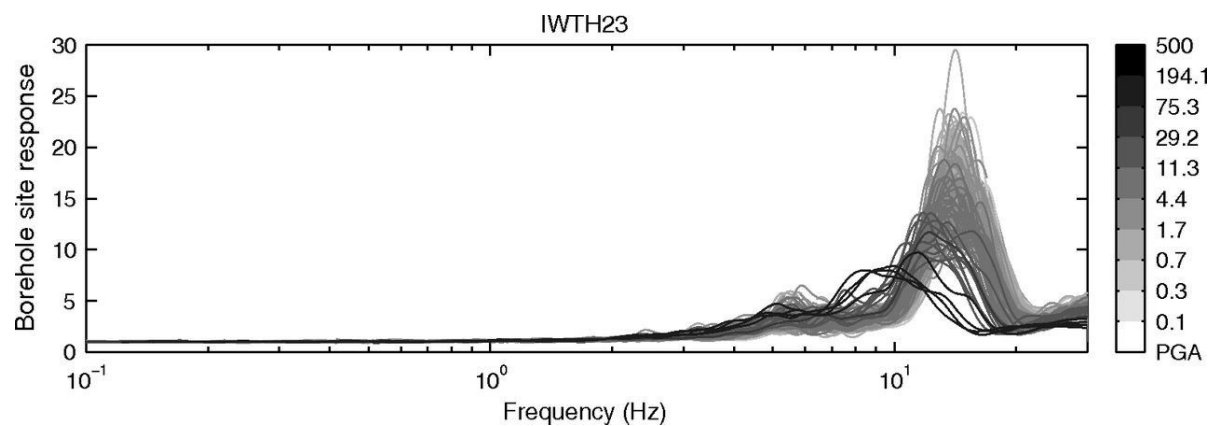


Figure 1-6 Reduction of the borehole site responses at IWTH23 with respect to the input-motion PGA ( $\text{cm/s}^2$ ). (Régnier et al. 2013)

Soil nonlinear behavior is manifested in the increase in damping and decrease in shear wave velocity, with the strengthening of the applied ground motion. Evidence of soil nonlinear behavior have been observed since a long time: we may cite data from Port Island in Kobe Japan, during the Hyogo-Ken Nanbu earthquake 1995 (Kawase et al. 1996), from California during the Loma Pietra earthquake 1985 (Chin and Aki 1991), from Mexico during Michoacan earthquake 1985 (Singh et al. 1988), from earthquake events in Japan (seismological data recorded in Kiban Kyoshin Network (Kik-net [www.kyoshin.bosai.go.jp](http://www.kyoshin.bosai.go.jp)) and other events around the world (Beresnev and Wen 1996).

Modeling the hysteretic behavior in soil, imply to characterize the nonlinear stress-strain relationship for different strain levels (Hardin and Drnevich 1972a; b). Numerous constitutive equations for the nonlinear behavior of soil have been developed. During the benchmark PRENOLIN (Régnier et al. 2016) on numerical simulation for 1-D nonlinear site response, the following nonlinear constitutive relationships are compared: extended hyperbolic model (Phillips and Hashash 2009), Iai's model (Iai and Ozutsumi 2011), isotropic hardening elasto-plastic soil model (Schanz et al. 1999), Iwan's model (Iwan 1967), Manzari-Dafalias model (Dafalias and Manzari 2004), modified Hujieux model (Aubry et al. 1982), multiyield model (Elgamal et al. 2003), Pisanò 3d elastic-plastic model (Pisanò and Jeremić 2014) and others. These models demand an increase of the number of parameters to reproduce better the soil response in higher level of loading. As the soil parameters can be difficult to determine, an efficient soil constitutive model is the one that is reliable and needs few parameters to be characterized.

#### ***1.4 Soil structure interaction***

The seismic response of a structure depends on the incident shake and the wave propagation in the soil to the ground level and in the structure itself. The excitation of the structure radiates waves back to the soil. This phenomenon is the soil-structure interaction (SSI).

According to the European seismic design codes (CEN 2003) the motion at free-field (FF, site prior handling) is currently used as seismic loading at the bottom of a fixed-base (FB) building, for structural design of buildings with shallow foundation. This two-step analysis (Figure 1-7), as named by Saez et al. (2011), does not permit to numerically simulate the soil-structure interaction (SSI) that modifies the seismic demand (seismic motion amplitude for structural design), influenced by structural dynamic features, soil mechanical parameters and input motion characteristics.

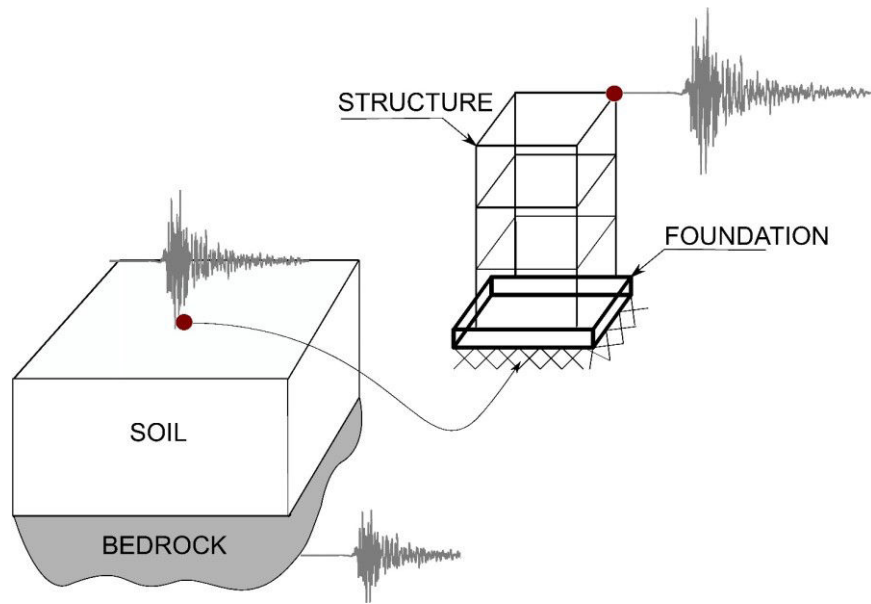


Figure 1-7 Two-step analyses; step one (left) Free Field analyses and step two (right) Fixed Base analyses.

#### 1.4.1. Observations on existing building and prototype experiments

The observations of a wave radiated back from a vibrating structure into the soil has been studied using earthquake records, ambient noise, shaking table and other alternative sources of dynamic excitation. An interesting early history on SSI is present in the work of Kausel (2010). Jennings (1970) observed, using vibration tests, large dynamic forces induced in the ground by the nine-story Millikan library building comparing surface ground records at about 4.8 km from the building with seismo-graph records on Mt. Wilson at 1463 m of altitude and about 9.7 km from the same building. Rocking motion up to 50% of the transverse motion registered at the top of a building is observed by Bard (1988), from California strong motion instrumentation program on strong motion data corresponding to buildings. In 1992, Celebi and Safak studied the recorded seismic response of the Pacific Park Plaza building in Emeryville, California during the Loma Prieta earthquake of October 17, 1989 ( $M_s = 7.1$ ). They noticed the largest SSI effect in the case where the soil is in resonance, the fundamental frequency of a building is in the same range of that of its relative soil (Celebi and Safak 1992; Safak and Celebi 1992). Chavez-Garcia and Cardenas (2002) investigate the SSI contribution on the ground motion in the Lake area of Mexico City using single and array measurements of ambient vibration. In this city, the structures are founded on soft soil and the frequency of the buildings coincide with that of the soil, both representing major factors in the SSI phenomenon, significantly altering the FF motion. Other studies also observed important impact of the soil-

structure resonance effects on SSI Ivanović et al. (2000) in Van Nuys California, Cornou et al. (2004) in Grenoble basin France and Ditommaso et al. (2010) in Potsdam Germany).

Mucciarelli et al. (2003) concluded that the SSI can significantly extend the motion duration and concentrate the amplification of response in a limited range of frequencies. Gueguen and Bard (2005) found out, during the Volvi test conducted on a scaled building, an asymmetric behavior of the reinforced concrete (RC) building regarding SSI and a reduction in the fundamental frequency of the building compared to the fundamental frequency of the system building-soil.

Exploring numerical simulation of series of shaking table tests, Paolucci et al. (2008) discussed evidence on the importance of nonlinear-inelastic foundation response to improve numerical SSI analysis results. Other experimental findings based on shaking table tests (Figure 1-8) have reported SSI evidence (Chau et al. 2009; Gallipoli et al. 2004; Hung et al. 2008; Lu et al. 2004; Maugeri et al. 2000; Shirato et al. 2008).



Figure 1-8 Photograph of a prototype model for the shaking table test. (Lu et al. 2004)

#### 1.4.2. Analytical study

A theory about vibration foundation is proposed in 1936 (Reissner 1936). According to Veletsos and Meek (1974), inertial interaction effects for buildings induce a lengthening of the natural period of the soil-structure system, because the structure is more flexible compared with the corresponding FB structure, and an increase of soil-structure system damping, due to dissipated energy and to radiated waves from the structure back into the soil. Wolf (1985) proposes the direct approach for SSI analyses that solves the dynamic equilibrium equation of

the soil-structure assembly, distinguishing the case of a FF motion applied to a FB model. Gazetas (1991) proposed the substructure approach SSI, analyzed as two separate interacting subdomains coupled through the concept of dynamic impedance functions, or two-step analysis as named by Saez et al. (2011) and shown Figure 1-7. Chopra and Gutierrez (1974), using an analytical simplified method, discuss SSI in the case of tall buildings, with reduced frequency of vibration, in very soft soil where the interaction has important effects on structural response. The dynamic response at the top of the building show a reduced frequency compared with the first FB mode shape. Using simplified numerical models, Jennings and Bielak (1973) show that the effect of SSI on the seismic response of buildings occurs predominantly in the direction of the fundamental mode shape. Moreover, the effects of interaction may be negligible for higher modes in the case of tall buildings having a translational first mode shape (of the FB structure). According to (Stewart et al. 1999a), two mechanisms of interaction take place between the structure, its foundation and soil: inertial and kinematic interaction. Inertia developed in the structure due to its own vibrations causes changes in seismic waves at the base of the structure, compared with the free FF that is the site prior handling. Furthermore, the presence of a deep foundation modifies seismic waves in the soil due to the stiffness contrast between soil and foundation. (Stewart et al. 1999b) studied the aptitude to SSI effects of 57 buildings in California, using an analytical approach, and observed that SSI is directly proportional to the structure to soil stiffness ratio.

#### *1.4.3. Numerical study*

Numerical methods are largely developed for SSI problems. The FEM is a common computing method in civil engineering, and extensively used for the SSI problems. To model the seismic propagation in 2-D and 3-D soil domain, a large domain of soil is requested to reproduce the condition of hindered horizontal strain. In FEM this represents an important computation time and internal memory consumption. Thus, various boundary conditions to limit the soil domain has been proposed. In 1969 Lysmer and Kuhlemeyer (1969) suggest viscous boundary considering only elastic systems. In 1974, nonreflecting plane boundary, allowing Dirichlet and Neumann conditions to alternate components at the boundary, is proposed by Smith (1974). In the following years other solutions have been proposed: in 1977, paraxial boundary by Clayton and Engquist (1977), in 1988, absorbing boundary condition by Barry et al. (1988) and in 1989 tied boundaries, reducing significantly the modeled soil domain, by Zienkiewicz et al.

(1989). Various extensions of these methods have been and still are being developed (Bielak et al. 2003; Nielsen 2006, 2014; Yoshimura et al. 2003).

#### *1.4.3.1. Simplified models for SSI analysis*

Using simplified numerical models (SDOF and MDOF models), Jennings and Bielak (1973) show that the effect of SSI on the seismic response of buildings occurs predominantly in the direction of the fundamental mode shape. Moreover, the effects of interaction may be negligible for higher modes in the case of tall buildings having a translational first mode shape (of the FB structure). According to Mylonakis and Gazetas (2000), the increase in fundamental period of a structure due to SSI does not necessarily lead to a smaller structural response and considering SSI as always beneficial is an oversimplification which may lead to unsafe structural design.

The application of a 1-D soil model is more suitable for engineering practice due to the accessible geotechnical characterization by using a single borehole investigation. The 1-D modeling of soil significantly reduces time and memory consumption and benefits simple boundary condition definition. Santisi d'Avila and Lopez-Caballero (2018) propose a one-directional three-component (1D-3C) wave propagation approach SFRINT\_3C for SSI problems, considering a 3-D frame structure rigidly connected to a 1-D soil profile. This latter solves the dynamic equilibrium equation using the direct method for the assembly of soil-building, using three-node line finite element (FE) for soil and Timoshenko beam elements for the frame structure.

#### *1.4.3.2. Two-dimensional and three-dimensional models for SSI analysis*

Two-dimensional model, have served in solving the SSI models in several studies (Gandomzadeh 2011; Saez et al. 2008). According to (Saez et al. 2011) SSI effects exist when the seismic response obtained by solving the dynamic equilibrium problem, applied to the assembly of soil domain and frame structure (one-step analysis Figure 1-9), is strongly different from that obtained by imposing the FF motion at the base of the FB structure (two-step analysis Figure 1-7). In a later study Saez et al. (2013) studied SSI in terms of total and effective stresses and conclude that SSI is generally beneficial or negligible for saturated soil condition. Furthermore, Lopez-Caballero and Modaressi-Farahmand-Razavi (2013) show that SSI effect increases with the building to soil fundamental frequency ratio.

Three-dimensional (3-D) wave propagation models have been proposed to obtain the six components of motion in soil and structure (such as the nuclear regulatory commission code for earthquake soil structure interaction, NRC ESSI simulator), by Coleman et al. (2013) and Jeremic et al. (2011), where the dynamic equilibrium problem is solved directly for the assembly of structure and a 3-D soil domain, incorporating the nonlinear behavior of soil in terms of effective stresses. This allows taking into account the propagation of body and surface waves and, at the same time, the spatial variability of the stratigraphy, rocking effect and the interaction with the foundation. Some other studies on SSI considering 3-D model are proposed (Iida 1998; Jeremic et al. 2009; Karapetrou et al. 2015; Mazzieri et al. 2013). Despite the evolution of 3-D numerical models, major uncertainties concerning the geotechnical model, difficulties related with the absorbing condition at the lateral boundaries, added to the high computational cost of an extended 3-D mesh make this kind of approach unusable for ordinary building design.

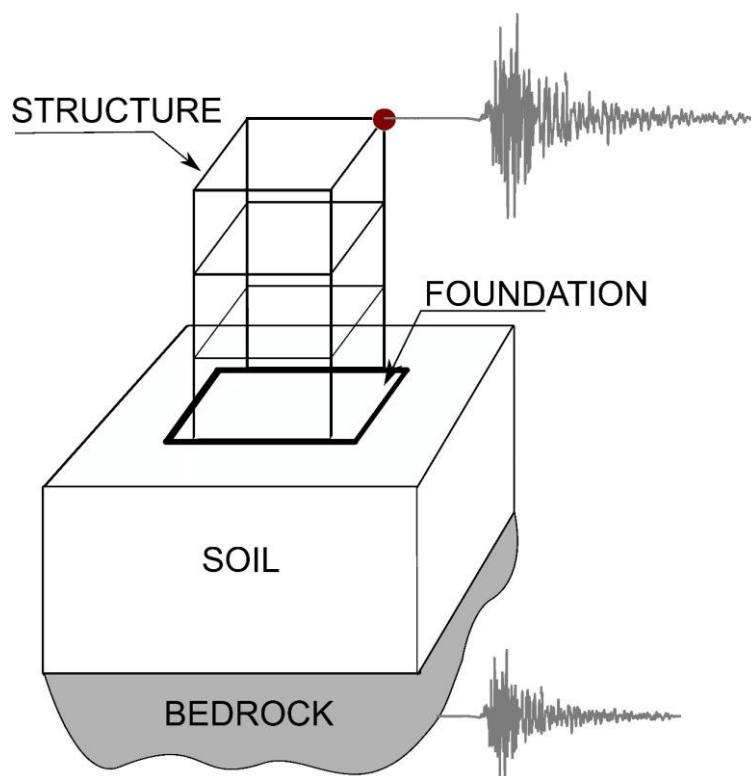


Figure 1-9 One-step analysis for SSI problems.

#### 1.4.3.3. *Large-scale model for SSI analysis*

The Large-Scale model is characterized by advantageous full-scale modelling, accurate calibration of soil properties and application of realistic time histories of horizontal force and overturning moment. On the other hand, large-scale model analysis ignores soil inertia forces,

and repetition of these analysis involve the treatment of a large amount of soil material. This model was employed by Shirato et al. (2008) for SSI problems and Gatti et al. for FF analysis.

### **1.5 Structure-soil-structure interaction**

Investigation on SSI has shown evident interference of the structure response to seismic motion with the response of the constructed soil. When the construction is extended to more than one structure, the adjacent structure is affected by the interference through the soil. This cross-interaction between neighbor structures and the soil, due to earthquake shaking, is called structure-soil-structure interaction (SSSI).

#### *1.5.1. Analytical study*

In 1971, Warburton et al. (1971) proposed a theory for the response of two geometrically identical masses of circular bases attached to a half-space and subjected to a harmonic excitation. In another paper, Warburton et al. (1972) have found, through an analytical study, that the unexcited mass affects only slightly the response of the excited mass. On the other hand, the unexcited mass is largely influenced by the excited mass even for significant inter-distance. When the adjacent mass has no more influence (increasing inter-distance), the SSI becomes more considerable with decreasing frequency of the soil.

SSSI investigations to understand the effect of a nearby building are undertaken by Luco and Contesse (1973), using a 2-D analytical model. The effects of the presence of a second structure are more important for a smaller structure located close to a larger structure, inducing a base motion for the smaller structure significantly different from that obtained by ignoring the presence of the nearby larger structure. According to Vicencio and Alexander (2018) SSSI effects increase when considering loose soil and closely spaced buildings. The most adverse effects, on building displacement, occur when there is a big difference of height between the buildings. Moreover, including the presence of nonlinearity in the soil can increase the size of adverse/beneficial SSSI effects, so it should not be neglected. The nonlinear SSSI response acceleration is amplified for the case of a smaller building flanked by a taller building; a beneficial effect can arrive for the taller building, but this reduction is not assured for the entire range of aspect ratios. Exploiting SSSI, a vibration barrier (ViBa) behaving as an oscillator is proposed by Cacciola et al. (2015) The ViBa is able to reduce the seismic energy on its neighborhood structures and their seismic response. An interesting complete review is present in the work of Lou et al. (2011)

### 1.5.2. Experimental study

In natural sciences, observations and experimental testing are principles of the scientific methods. Mizuno (1980) has experimentally observed the SSSI with the consequent variation and possible increase of the structural response caused by the radiation waves from a nearby structure. Moreover, the excitation of a nearby structure induces energy absorption from the ground. Under ambient vibration, the response of the building having low fundamental frequency becomes larger than that of a single building, while the response of the building having high natural frequency has an opposite tendency.

The experiments to study SSSI are challenging in the real scale. Prototype experiments are proposed with a scaling theory to justify the parameters of the experiment. Li et al. (2012) proposed a model scaled to the 1/15 (Figure 1-10) and show damages are more important in a SSSI comparing with that of SSI. Trombetta et al. (2014) investigate the SSSI by centrifuge tests. During high-intensity motions, the significance of SSSI is found to diminish; this could be due to a combination of superstructure yielding and saturation of footing forces. Consequently, from a design perspective, the results suggest that SSSI effects should be considered for low-to-moderate levels of earthquake shaking.



Figure 1-10 Prototype of a shaking table model scaled to the 1/15, SSI test model (left) and SSSI test model (right). (Li et al. 2012)

A related problem to SSSI is addressed considering more than two adjacent structures known as the site city interaction (SCI). Aldaikh et al. (2015 and 2016) experimented shaking table tests on a group of three building subjected to seismic excitation Figure 1-11 and showed that two adjacent buildings have a greater influence on a central building than this latter having only one adjacent building. Schwan et al. (2016) also studied site-city effect, experimenting shake table tests consisting on a site-city setup with up to 37 anisotropic resonant structures, and show that SSSI have significant effect of the seismic responses of the site and the buildings

adding that the denser the city the greater the effect. Tombari et al. (2018) performed shaking table tests using buildings in single story structures including ViBa buried in the soil, represented by viscoelastic silicone rubber, (Figure 1-12) and show reduction up to 46.2% of the maximum acceleration registered in both structure due to the existing of a third structure, ViBa, properly tuned to absorb dynamic energy.

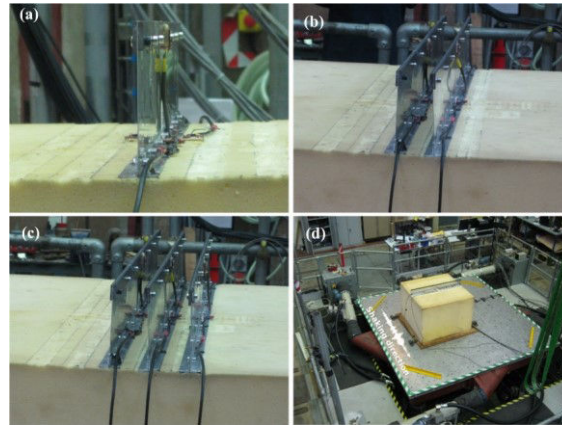


Figure 1-11 Overview of experiment: (a) single building; (b) two identical buildings; (c) three identical buildings; (d) experimental system mounted on the shaking table. (Aldaikh et al. 2016)

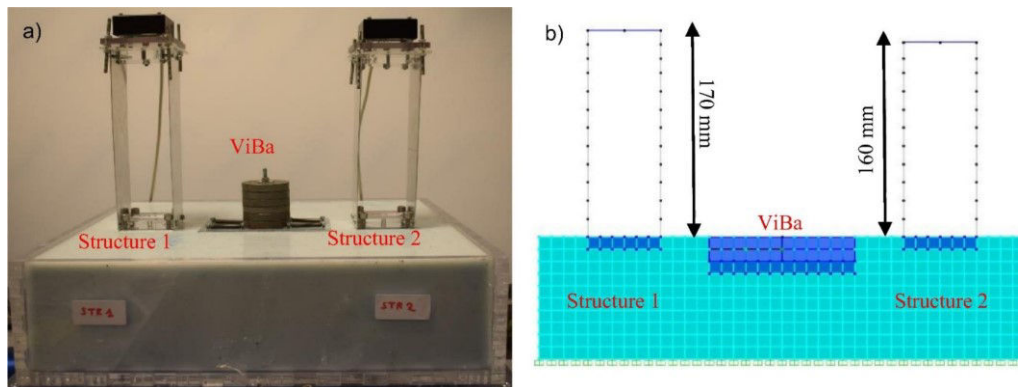


Figure 1-12 (a) Prototype and (b) Finite Element Model of two different structures protected by the ViBa. (Tombari et al. 2018)

### 1.5.3. Numerical study

Even if the FEM is efficient and very common in civil engineering, dealing with irregular geometry and material nonlinearity, the computation time and memory are serious for a large scale of soil. On the other hand, the BEM present advantages on the FEM because it demands a unique surface discretization without the need of a boundary condition definition as the FEM. The BEM present difficulties in complicated heterogenous medium and loses its advantage in

non-linear systems. In the 1990s a coupled BEM and FEM consisting on meshing only the structure while the soil is presented as elastic medium model using BEM (von Estorff and Firuziaan 2000; Mohammadi and Karabalis 1995; Yazdchi et al. 1999). The BE-FE method reduces the mesh size and allow to represent modal or hysteretic damping but remains limited to linear studies.

#### *1.5.3.1. Finite element method for SSSI analysis*

Various study has aborted the SSSI using FEM (Lin et al. 1987; Matthees and Magiera 1982). Bolisetti and Whittaker (2011) and Roy et al. (2015) investigating the SSSI effect for nuclear structures. Cacciola et al. (2017) employed FE approach assuming linear behavior for the soil and structures and studied the impact of a vibration barrier on an existing masonry structure. Nateghi-A and Rezaei-Tabrizi (2013) use a two-dimensional FE model to study the nonlinear dynamic response of two adjacent tall buildings having frame structure. In the cases wherein the soil and structure fundamental frequencies are near to each other, the interaction of the adjacent structures has an important effect on the increase of nonlinear responses, so it is not negligible. Varone et al. (2015) modeled the Vallerano valley located in Rome Italy in 2-D using the FE code CESAR-LCPC and highlighted the influence of the buildings in the local seismic response. Wang et al. (2013) draw attention to the interaction that touches ground and underground structure through the surrounding soil and model using the commercial software ANSYS an underground station with a nearby pile founded structure on a viscoelastic soil subjected to incident S wave. The obtained results show that the most important influence is due to the arrangement of the structures and the direction of the shaking.

#### *1.5.3.2. Boundary element method for SSSI analysis*

When it comes to site-city interaction the BEM is privileged. Semblat et al. (2000, 2004, 2008) proposed a 2-D model of Nice basin and studied the influence of various surface structures and densities of the city on seismic wave propagation. Schwan et al. (2016) studied a 2D numerical model considering up to 37 anisotropic resonant structures on elastic soil and concluded that site-city effect depends strongly on the city density and arrangement and detrimental effect is mostly observed on the city boundaries.

### *1.5.3.3. Coupled finite element and boundary element method for SSSI model*

Padrón et al. (2009) addressed the effect of SSSI on nearby buildings subjected to incident S or Rayleigh waves and has shown that nearby buildings can significantly increase the seismic response of structure. A parametric investigation is carried by Clouteau et al. (2012) investigating the effect of two adjacent buildings. They show that slight influence is due to the SSSI in the case of shallow foundation, however, this influence is more pronounced in the case of embedded foundation. On the other hand, Álamo et al. (2015) studied the SSSI effects on the dynamic response of three nearby buildings subjected to obliquely incident waves and observed impact caused by the angle of the incident wave on SSSI but not necessarily worse than the vertical incidence wave.

## **1.6 Conclusion**

The research presented in the following chapters aims to propose an efficient model for engineering practice, taking into account SSI. Consequently, the direct solution of the dynamic equilibrium equation is solved in a FE scheme. Moreover, a step by step solution is necessary to take into account the nonlinear behavior of materials. Periodic lateral boundary conditions are adopted to strongly reduce the soil domain when the periodicity assumption is possible.

## **Chapter 2 - One-dimensional three-component wave propagation model for soil-structure interaction**

European seismic design provisions consider, as seismic loading at the bottom of a FB building, a peak acceleration at the soil surface or a FF motion for structural design of buildings with shallow foundation. This two-step analysis, as named by Saez et al. (2011), does not permit to numerically simulate the SSI that modifies the seismic demand (seismic motion amplitude for structural design), influenced by structural dynamic features, soil mechanical parameters and input motion characteristics. Therefore, a numerical model accessible to engineers, that treats the SSI for buildings with shallow foundation, is proposed and discussed in this chapter.

The commands to create such a model in Abaqus software are presented in Appendix B.

## 2.1. 1D-3C wave propagation model

A 1-D soil profile is assembled with a 3-D frame structure in a FE scheme to treat the SSI problem (Figure 2-1a). A 1D-3C wave propagates in the soil domain from the bedrock until the building base. This model is based on the hypothesis of rigid shallow foundation, negligible rocking effects and negligible SSSI (it only permits the modeling of one structure). The discrete dynamic equilibrium equation for the assembly soil-structure is solved directly in a one-step analysis, as named by Saez et al. (2011).

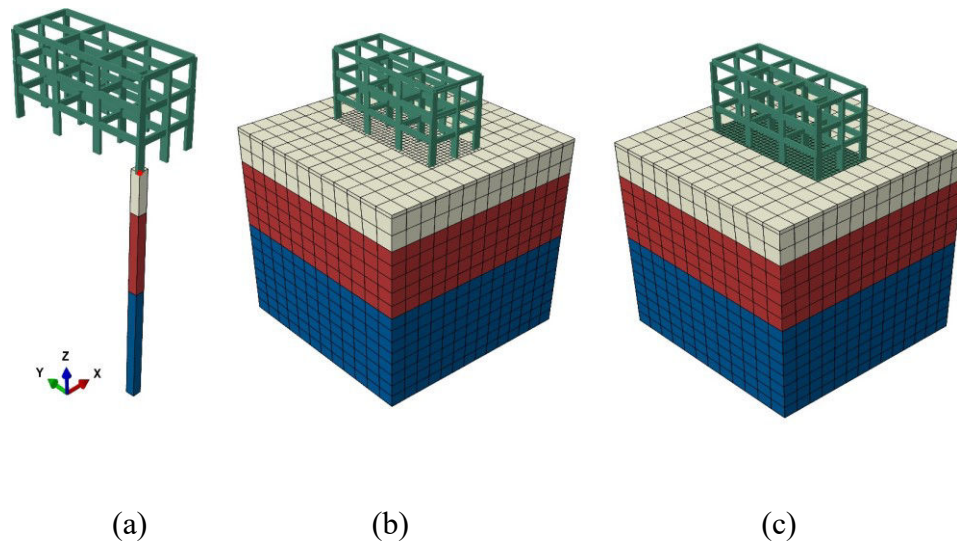


Figure 2-1 Assembly of a frame structure and a multilayer soil domain shaken by a three-component seismic motion, for SSI analysis: (a) 1D-3C wave propagation model, where the assembly is done in only one node; (b) 3D-3C wave propagation model, with connection node-to-node between building and soil; (c) 3D-3C model, where the foundation is modeled and embedded in the soil domain.

### 2.1.1. Spatial discretization of soil domain and boundary conditions

The soil basin is assumed as horizontally layered and infinitely extended along the horizontal directions  $x$  and  $y$ , in the  $xyz$ -coordinate system (Figure 2-1a). Consequently, no strain variation is considered in these directions. A periodic condition is applied at the lateral boundaries in the soil column, to impose zero strains  $\epsilon_x$  and  $\epsilon_y$ . According to Zienkiewicz et al. (1989) and Saez et al. (2011), this condition is verified because the lateral limits of the problem are considered to be far enough from the structure and it is obtained using tie constraints between lateral surfaces. Shear and pressure waves propagate vertically in  $z$ -direction from the top of the underlying elastic bedrock to the free surface. The soil is assumed to be a continuous and homogeneous medium, with nonlinear constitutive behavior. The hypothesis of vertical

propagation in a horizontally layered soil allows the 1-D spatial discretization of the soil domain. The soil column is modeled using 20-node solid FE, having three translational degrees of freedom per node Figure 2-2. The system of horizontal soil layers is bounded at the top by the free surface. Consequently, stresses normal to the free surface are assumed null.

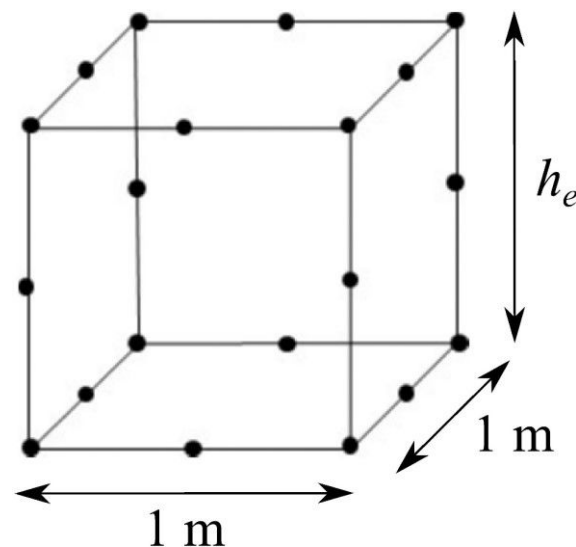


Figure 2-2 Unit area quadratic solid FE with 20 nodes, where  $h_e$  is the element height.

The minimum number of quadratic solid elements (Figure 2-2) per layer is defined as  $pfh_i/(2v_{si})$ , where  $h_i$  is the thickness of the  $i$ -th layer and  $v_{si}$  is the shear wave velocity in the medium, this latter related to the minimum wavelength of the seismic signal by the ratio  $v_{si}/f$ . The maximum frequency, above which the spectral content of the input signal can be considered negligible, is fixed as  $f = 15 \text{ Hz}$ . The minimum number of nodes per wavelength, to accurately represent the seismic signal, is assumed as the maximum between  $p = 2v_{si}/f$  (almost one element every meter) and  $p = 10$ . This criterium is adopted for the spatial discretization of soil domain in all the presented analyses of this research. Consequently, it will not be repeated in following chapters.

The soil column is bounded at the bottom by a semi-infinite bedrock having elastic behavior. A linear viscous dashpot is imposed at the bottom of the soil column, in each direction of motion, as absorbing boundary condition (as adopted by Bardet and Tobita 2001; Joyner and Chen 1975; Santisi d'Avila et al. 2013), to take into account the finite rigidity of the bedrock and allow energy to be radiated back into the underlying medium. The same absorbing condition can be properly adopted if borehole records are used and a high impedance contrast is imposed between soil and bedrock. This option guarantees a numerical damping, decreasing

with the assumed impedance contrast. A deconvolved rock outcropping motion is applied at the soil-bedrock interface and propagated along the soil profile.

In the adopted 1-D model of the soil domain, the solid elements have unit area in the horizontal plan Figure 2-2, to reduce modeling difficulties and computation time. In a 1D wave propagation model, the area of the soil column  $A$  appears as a constant in each term of the equilibrium equation Eq. (2-1), i.e. in the mass  $\mathbf{M}$ , stiffness  $\mathbf{K}$  and damping  $\mathbf{C}$  matrices and in the seismic loading vector ( $\mathbf{F}$ ). Consequently, the FF motion can be correctly obtained even if a unit area is adopted. This is not the case in SSI analyses where the area of the soil domain  $A$ , concerned by interaction effects, must be taken into account in the balance. In a commercial FE code, the area of the soil domain  $A$  can be considered by imposing a soil density of  $\rho A$  and an elasticity modulus in compression of  $E_0 A$ , where  $\rho$  and  $E_0$  are the soil density and elasticity modulus in compression, respectively, to correctly define the mass and stiffness of soil part (see Eq. (2-1) to Eq. (2-5), where  $\Delta \mathbf{a}$ ,  $\Delta \mathbf{v}$  and  $\Delta \mathbf{u}$  are the increments of acceleration, velocity and displacement, respectively, and the coefficients of matrix  $\mathbf{c}$  are  $\rho_b v_{sb}/n$ ,  $\rho_b v_{sb}/n$  and  $\rho_b v_{pb}/n$ . The parameters  $\rho_b$ ,  $v_{sb}$  and  $v_{pb}$  are the bedrock density and shear and compressional wave velocities in the bedrock, respectively. The parameter  $v_b$ ,  $\mathbf{N}$  and  $\mathbf{B}$  are the wave velocity in the bedrock, the shape functions matrix and displacement differentiation matrix, respectively. The superscript e denotes element).

$$\mathbf{M}\Delta \mathbf{a} + \mathbf{C}\Delta \mathbf{v} + \mathbf{K}\Delta \mathbf{u} = \Delta \mathbf{F} \quad (2-1)$$

$$\mathbf{M}^e = \rho_e A \int_0^h \mathbf{N}^T \mathbf{N} dz \quad (2-2)$$

$$\mathbf{K}^e = A \int_0^h \mathbf{B}^T \mathbf{E} \mathbf{B} dz \quad (2-3)$$

$$\mathbf{C}^{e=1} = A [\mathbf{N}^T \mathbf{c} \mathbf{N}] \quad (2-4)$$

$$\mathbf{F}^{e=1} = A [\mathbf{N}^T \mathbf{c} (2v_b)] \quad (2-5)$$

The damping coefficient of dashpots imposed at each node of the soil column base is proportional to  $\rho_b v_{sb} A_i$  for those in the horizontal directions and  $\rho_b v_{pb} A_i$  in the vertical direction.  $A_i = A/n$  is the influence area of each node and  $n$  is the number of nodes at the soil-bedrock interface. The seismic loading is applied at the soil-bedrock interface in terms of force. According to the applied boundary condition, the shear and normal stresses at the soil column base, at the bedrock interface, are  $\rho_b v_{sb} (v_x - 2v_{bx})$ ,  $\rho_b v_{sb} (v_y - 2v_{by})$  and  $\rho_b v_{sb} (v_z - 2v_{bz})$  respectively. The three components of the incident seismic motion at the bedrock level in terms of velocity  $v_{bx}$ ,  $v_{by}$  and  $v_{bz}$  in  $x$ -,  $y$ - and  $z$ -direction, respectively, can be obtained by halving the seismic motion at the outcropping bedrock. The three terms  $v_x$ ,  $v_y$

and  $v_z$  are the unknown velocities (incident and reflected motion), at the interface soil-bedrock interface, in  $x$ -,  $y$ - and  $z$ -direction, respectively that are evaluated during the process.

### 2.1.2. Soil constitutive relationship: Iwan's model

The nonlinearity of soil demands the linearization at each time step of the rate-type constitutive relationship. Consequently, the stress-strain relationship needs to be expressed in its incremental form. The adopted Iwan's 3-D elasto-plastic model for soils (Iwan 1967; Joyner and Chen 1975) satisfies Masing criterion (Kramer 1996) and does not depend on the number of loading cycles. According to Joyner (1975), the tangent constitutive matrix is deduced from the actual strain level and the strain and stress values at the previous time step. The stress increment is evaluated at each time step. The stress level depends on the strain increment and strain history but not on the strain rate. Therefore, this rheological model has no viscous damping. The energy dissipation process is purely hysteretic and does not depend on the frequency. The rheological formulation is in terms of total stresses and, consequently, it is appropriate in undrained conditions. The plasticity model uses von Mises yield surface that assumes pressure-independent behavior, that means yielding is independent of the average pressure stress. This assumption is acceptable for soils in undrained conditions.

The main feature of Iwan's model is that the mechanical parameters to calibrate the rheological model are easily obtained from laboratory dynamic tests on soil samples. The size of the yield surface is imposed by the first loading curve in the uniaxial stress case. The applied constitutive model does not depend on the selected backbone curve. In this research, the Poisson's ratio is assumed constant during the time history and, consequently, the normalized decay curve of the elastic modulus in compression is  $E/E_0 \approx G/G_0$ .

#### 2.1.2.1. Rheological model for soils in total stress analysis

The Iwan's constitutive model is a 3-D elasto-plastic model with kinematic hardening, suggested by Iwan (1967) and employed by Joyner (1975) and Joyner and Chen (1975) in a finite difference discretization of the soil domain. Iwan's model is applied by Bonilla (2001) in a finite difference formulation, by Santisi d'Avila and Lenti (2012) and Santisi d'Avila and Lopez-Caballero (2018) in a finite element scheme, with quadratic line elements having three nodes and three translational degrees of freedom each, and by Gandomzadeh (2011) in a 2-D finite element model. The same model is employed by Mercerat and Glinsky (2015) in

association with 1-D discontinuous Galerkin elements, by Oral (2016) using a 2-D spectral element mesh and in the proposed model using 3-D finite elements in Abaqus software.

As illustrated in Figure 2-3, the 1-D version of the stress-strain given by Iwan (1967) is composed of a series of  $n$  linear springs of spring constant  $G_i$ , calibrated to reproduce the stress-strain behavior measured in the laboratory and Coulomb friction units of stress threshold  $Y_i$ , arranged parallel to each other. Each friction unit remains locked until the stress on it exceeds its stress threshold  $Y_i$ , then it yields and the stress on it during yielding is equal to its yielding stress. The first spring reproduces the elastic behavior and the friction unit is set to  $Y_1 = 0$ . Each spring has stiffness expressed by spring constant  $G_i$ .

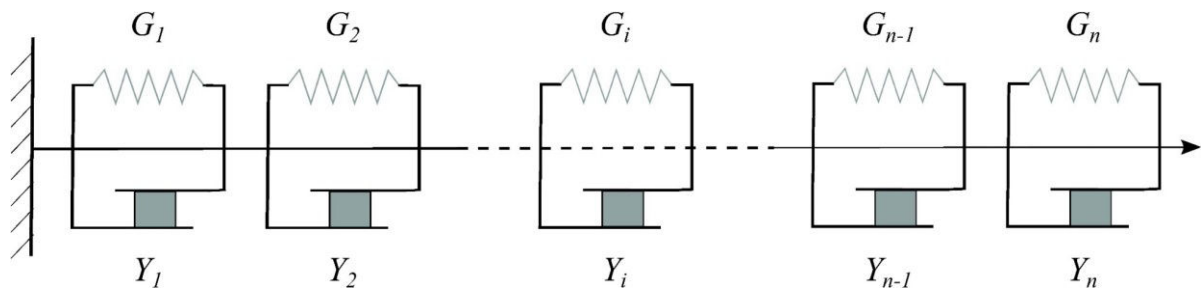


Figure 2-3 One-dimensional series-parallel rheological model proposed by Iwan in 1967.

In the present study, the soil behavior is assumed adequately described by a hyperbolic stress-strain curve (Hardin and Drnevich 1972a). This assumption yields a normalized shear modulus decay curve, expressed as  $G/G_0 = 1/(1 + |\gamma/\gamma_r|)$ , where  $\gamma_r$  is a reference shear strain corresponding to an actual tangent shear modulus equivalent to 50% of the elastic shear modulus, in a normalized shear modulus decay curve provided by laboratory test data (Figure 2-4a).

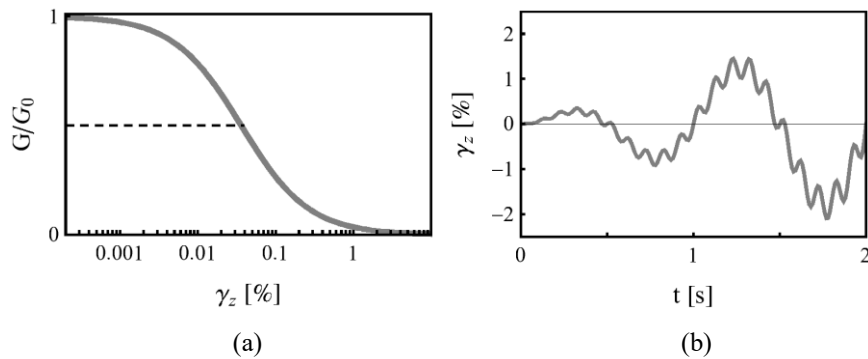


Figure 2-4 (a) Shear modulus decay curve and (b) shear strain time history.

The nonlinear isotropic-kinematic hardening model is used to simulate the inelastic material behavior subjected to cyclic loading. The kinematic hardening model, used to simulate the

inelastic material behavior subjected to cyclic loading, is linearly performed at a constant hardening rate to approximate the hardening behavior described by Prager hardening rule. The plasticity model assumes associated plastic flow, allowing isotropic yielding. Therefore, as the material yields, the inelastic deformation rate is in the direction of the normal to the yield surface (the plastic deformation is volume invariant).

From 1 to 3 dimensions, an extension of the standard incremental theory of plasticity (Fung 1965) is introduced, and the single yield surface stress space is replaced by a family of yields surfaces (Iwan 1967).

### 2.1.2.2. Yield surface

In Iwan's formulation the von Mises yielding criterion is assumed. The von Mises yield surface is expressed as

$$(\sigma_{xx} - \sigma_{yy})^2 + (\sigma_{xx} - \sigma_{zz})^2 + (\sigma_{zz} - \sigma_{yy})^2 + 6[\tau_{xy}^2 + \tau_{yz}^2 + \tau_{zx}^2] = 2Y_i^2 \quad (2-6)$$

It corresponds to a cylinder of circular base and infinite length with its axis inclined at equal angles to the three principal stresses. Figure 2-5 shows the distribution of the yield surfaces of the material behavior according to Iwan's model. Figure 2-5 top-left shows a virgin material. Then, a possible loading to a point A carrying along the yield surfaces as long as the material has not plastified, as a result of the kinematic hardening (Figure 2-5 top-right). Now the yield surfaces are altered by the loading to point A. Unloaded along the same path as the initial loading will not lead to the initial yield surfaces distribution (Figure 2-5 bottom-left). This loading and unloading leads to a linear hardening behavior exhibiting what is known as Bauschinger effect.

### 2.1.3. Elasto-plastic model in Abaqus

The plasticity model proposed in Abaqus has, similarly to Iwan's model, a combined kinematic and isotropic hardening. When the stress state reaches the yield surface, it translates, and this is kinematic hardening, or it grow, and this is isotropic hardening (Figure 2-6). The kinematic hardening causes the ratcheting effect. It is generated by accumulation of plastic strain over each loading cycle and is characterized by a shift of the stress-strain hysteresis loop along the strain axis (Figure 2-7).

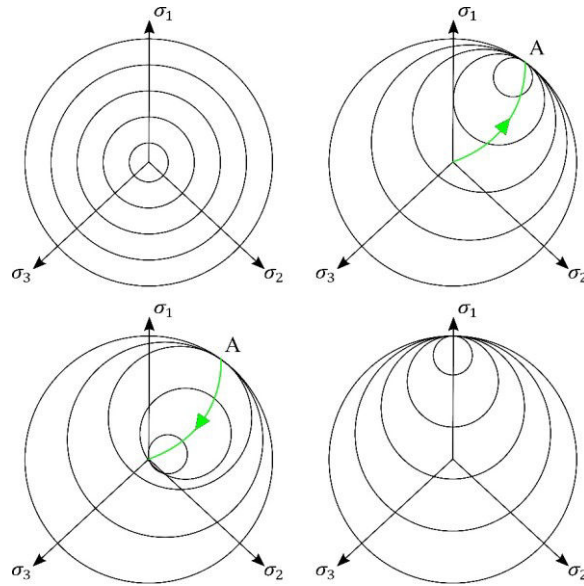


Figure 2-5 Schematic behavior of yield surfaces of Iwan model, in plane.

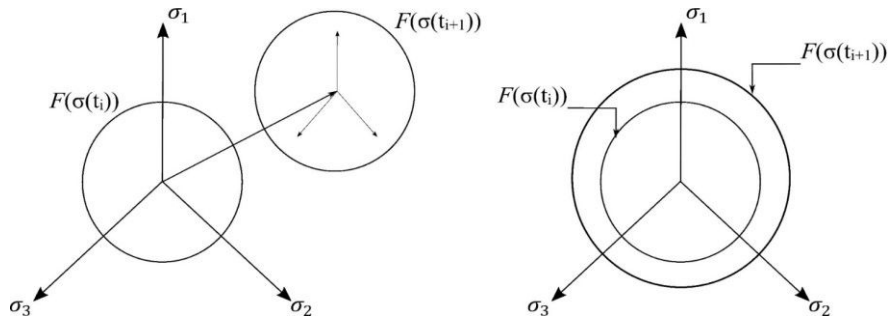


Figure 2-6 Yield surface transformation after kinematic hardening (left) or isotropic hardening (right).

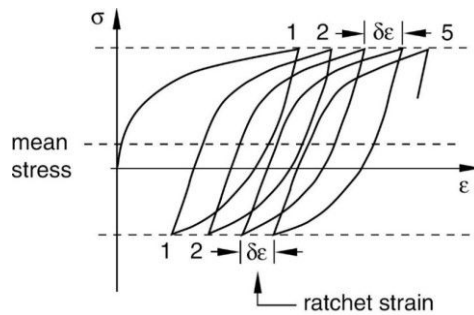


Figure 2-7 Ratchetting (Abaqus User Manual 2014, Figure 23.2.2–5)

The nonlinear behavior is characterized in Abaqus software providing the uniaxial first loading curve in terms of axial stresses and strains, deduced by the compressive modulus reduction curve. If resonance column tests provide shear modulus decay curves  $G/G_0(\gamma)$ , the demanded first loading curve is evaluated as  $\sigma(\epsilon) = E/E_0(\epsilon) E_0 \epsilon$ , where the axial stress  $\sigma(\epsilon)$  can be calculated from shear stress  $\tau(\gamma)$  as  $\sigma(\epsilon) = \sqrt{3} \tau(\gamma)$ ,  $E/E_0(\epsilon)$  is the normalized decay curve of

elastic modulus in compression versus axial strain  $\varepsilon$  that is assumed equal to  $G/G_0(\gamma)$  and  $\varepsilon = \sqrt{3}\gamma G_0/E_0$ .

An example of the hysteresis loops that this model produces for  $n = 80$  is shown in Figure 2-8. It illustrates the stress-strain response of a unit cube of soil, with a shear modulus decay curve represented in Figure 2-4a, subjected to cyclic one-component shear strain loading (Figure 2-4b) of increasing amplitude. Figure 2-8 has been obtained using an external Fortran routine (UMAT) integrated in Abaqus, corresponding to the constitutive model used in SWAP\_3C. Nevertheless, Iwan's model does not need to be an external Fortran routine in Abaqus, because the multi-surface plasticity model already implemented in Abaqus corresponds to the Iwan's model.

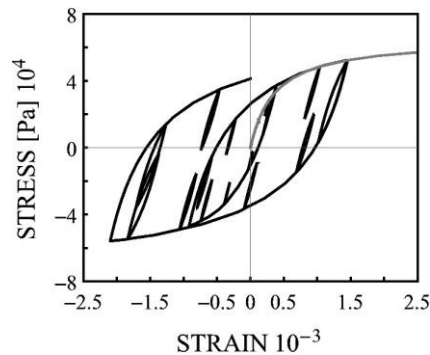


Figure 2-8 Hysteresis loop in a unit cube of soil obtained with the Fortran implementation of Iwan's model (UMAT/SWAP\_3C)

In Abaqus software, the first loading curve is discretized using the maximum number of intervals, equal to 98, and the nonlinear kinematic hardening with ratchetting is modeled using the maximum number of backstresses  $\alpha = 10$  (kinematic shift of the yield surface, Appendix C). The constitutive soil model in SWAP\_3C, the FE code used to verify the proposed modeling technique, is implemented using a number of backstresses  $\alpha$  corresponding to the number of intervals employed to discretize the uniaxial yield surface. Figure 2-8 shows hysteresis loops in the cases of 1-, 2- and 3-Component loading, obtained using the Iwan's model implemented in Abaqus with  $\alpha = 10$ . The same curves are obtained using SWAP\_3C with  $\alpha = 80$ . As discussed by Santisi d'Avila and Lenti (2012), the shear strength is reduced for 3C loading, compared with the uniaxial case. The first loading curve is corrected as  $\sigma(\varepsilon) = E/E_0(\varepsilon) E_0 A \varepsilon$  to consider the soil domain surface  $A$ , in the case of the 1-D model (unit-area solid elements for soil) for SSI analyses undertaken using a commercial FE code as Abaqus.

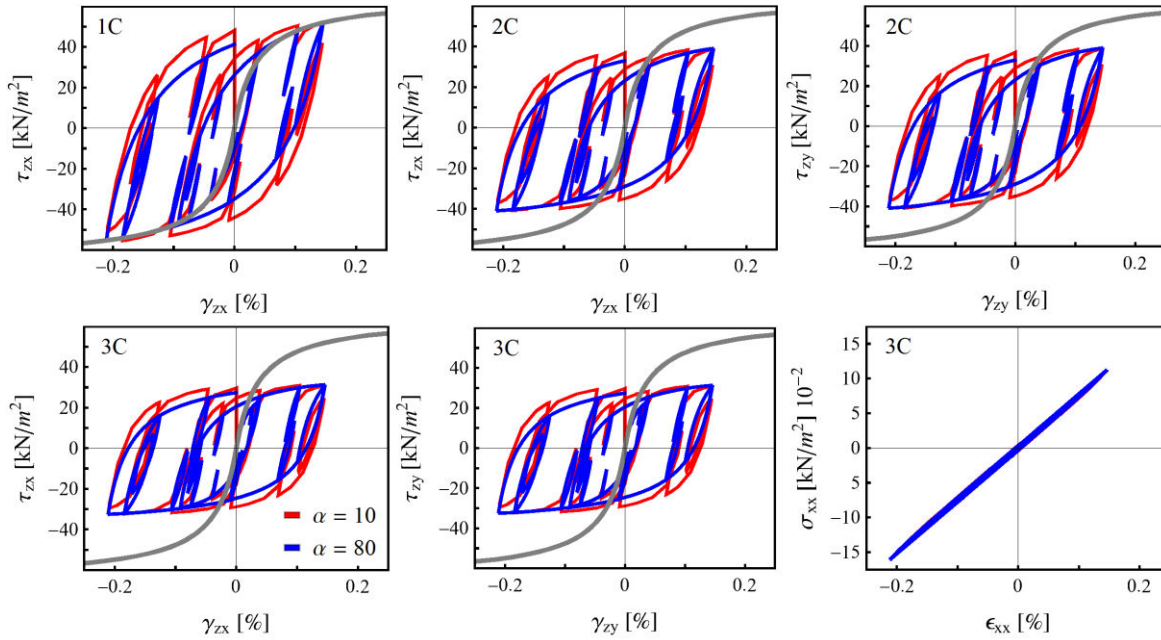


Figure 2-9 Hysteresis loops in a unit cube of soil loaded by a 1-, 2- and 3-Component strain, for a different number of backstresses in the kinematic hardening model.

#### 2.1.4. Building model

The 3-D frame structure is modeled using Timoshenko beam elements having six degrees of freedom per node. The transverse shear stiffness  $\chi GA$  of the beam cross-section is defined using a shear correction factor (Kaneko 1975) equal to  $\chi = (5(1 + \nu)) / (6 + 5\nu)$ . A linear constitutive behavior is assumed for the structure. The damping provided by non-structural components is taken into account according to Rayleigh approach (Chopra 2001). In fact, the damping submatrix related to the building is assumed as mass and stiffness proportional, using coefficients dependent on the first two FB natural frequencies. Live and dead loads are imposed on the beams in terms of mass per unit length.

The bases of building columns are all connected by a membrane rigid link under the assumption of rigid shallow foundation. According to the 1-D model approach, the building is rigidly connected at the bottom to the soil surface, under the assumption of rigid shallow foundation and negligible rocking effects. Rotational degrees of freedom of nodes at the base of columns are blocked.

In the 3D-3C model in Figure 2-1b, a rigid link imposed between the different column bases, directly assembled with the soil, implies that the same horizontal motion is transmitted at each building column base. Consequently, the 1D-3C wave propagation model (Figure 2-1a) and

the 3-D model with connection node-to-node between building and soil shown in Figure 2-1b are equivalent.

The advantages of the 1D-3C approach for SSI are that modelling difficulties and computation time are reduced compared with a 3D-3C approach. The dynamic equilibrium equation for the soil-structure assembly is solved in 11 minutes using the 1D-3C model and in 14 hours using the 3D-3C model, for an input motion of 120 s, on the CINES cluster using 1 core and 24 nodes. In fact, geotechnical parameters are easy to characterize for a 1-D soil model (using a single borehole investigation) and boundary condition definition is simple (the input signal and the absorbing boundary condition are given for only one element. Moreover, the mesh is considerably reduced Figure 2-1).

#### *2.1.5. Time discretization*

The discretization of seismic loading requires a time discretization to permit the problem solution. The implicit dynamic process is solved step-by-step by the Hilber-Hughes-Taylor algorithm (Hughes 1987), the so-called  $\alpha$ -method. The three parameters  $\alpha = -0.1$ ,  $\beta = 0.25(1 - \alpha)^2 = 0.3025$  and  $\gamma = 0.5 - \alpha = 0.6$  guarantee an unconditionally numerical stability of the time integration scheme and numerical damping to reduce high frequency content, without having any significant effect on the meaningful, lower frequency response. Material damping is purely hysteretic. The dynamic equilibrium equation is directly solved using a time step between  $dt = 10^{-4}$  s and the time step used for the input signal sampling. The building weight and gravity load are imposed as static initial condition in terms of strain and stress.

#### *2.1.6. Soil domain area concerned by the SSI*

The simulation of SSI effects requires the representation of an adequate soil volume. The soil depth is imposed by the position of the soil-bedrock interface, where the incident motion is imposed.

The soil domain area  $A$  is selected by evaluating the building base to bedrock transfer function (TF) that is the ratio of Fourier spectrum of acceleration signals at the building base and soil-bedrock interface. The frequency corresponding to the peak of this TF matches the soil column fundamental frequency in the FF case, when the soil domain area  $A$  is wide, and it is progressively lower with a decreasing soil area. The selected soil domain area is the smallest for which the peak of the building base to bedrock TF corresponds to a soil column fundamental

frequency equivalent to the FF case. In this research, a squared soil area is used, after evaluation of the building base to bedrock TF for both horizontal directions of motion and verification that the adopted dimension is convenient for both directions.

The building top to bottom TF, that provides the FB natural frequency of the building, is not influenced by the variation of the soil domain area. The building top to bedrock TF gives the frequency of the building-soil system. All the TF are evaluated in a linear elastic regime.

## 2.2. Input data

These input data are adopted in all the presented analyses of this research. Consequently, in following chapters, any used data will be referred to this section.

### 2.2.1. Soil data

The stratigraphy and mechanical parameters of soil profiles used in the verification phase are identified in Table 2-1. Soil properties are assumed constant in each soil layer. The soil density  $\rho$  and the shear and compressional wave velocities in the medium  $v_s$  and  $v_p$ , respectively, allow the computation of the elastic shear and P-wave moduli  $G_0 = \rho v_s^2$  and  $M_0 = \rho v_p^2$ . The shear wave velocity of each layer is fixed in such a way that the average shear wave velocity in the upper 30 m,  $v_{s30}$ , corresponds to the assumed fundamental frequency of the soil column  $f_s$ , according to  $f_s = v_{s30}/4H$ , where  $H$  is the soil profile depth. Densities and compressional wave velocities are deduced according to the relationships discussed by Boore (2015). The Poisson's ratio  $\nu = (0.5v_p^2/v_s^2 - 1)/(v_p^2/v_s^2 - 1)$  is evaluated as function of the compressional to shear velocity ratio. The at-rest lateral earth pressure can be obtained as  $K_0 = \nu/(1 - \nu)$ . The reference shear strain is assumed equal to  $\gamma_r = 0.35 \%$ .

Table 2-1 Stratigraphy and mechanical features of the analyzed multilayered soil profiles having different natural frequency.

Profile $f_s = 3.8$ Hz				Profile $f_s = 2.8$ Hz				Profile $f_s = 1.9$ Hz			
Depth (m)	$\rho$ (kg/m <sup>3</sup> )	$v_s$ (m/s)	$v_p$ (m/s)	Depth (m)	$\rho$ (kg/m <sup>3</sup> )	$v_s$ (m/s)	$v_p$ (m/s)	Depth (m)	$\rho$ (kg/m <sup>3</sup> )	$v_s$ (m/s)	$v_p$ (m/s)
0-5	1930	250	1417	0-5	1930	220	1365	0-5	1930	180	1293
5-15	1947	340	1568	5-15	1930	260	1435	5-15	1930	200	1329
15-30	2019	500	1815	15-30	1957	360	1601	15-30	1930	240	1400
> 30	2100	1000	2449	> 30	2100	1000	2449	> 30	2100	1000	2449

### 2.2.1. Building data

The two three-story buildings which floor plans are shown in Figure 2-10 are used for the following analyses. The choice of a limited number of spans is motivated by the fact that an increasing number of spans does not modify the natural frequencies associated to the first mode shapes, implying an increase of both mass and stiffness but a constant stiffness to mass ratio. Consequently, it is not useful, for the scope of the presented analysis, to increase the modeling and computation time. The number of stories is determined according to the desired fundamental frequency of the building, for the purpose of the analysis.

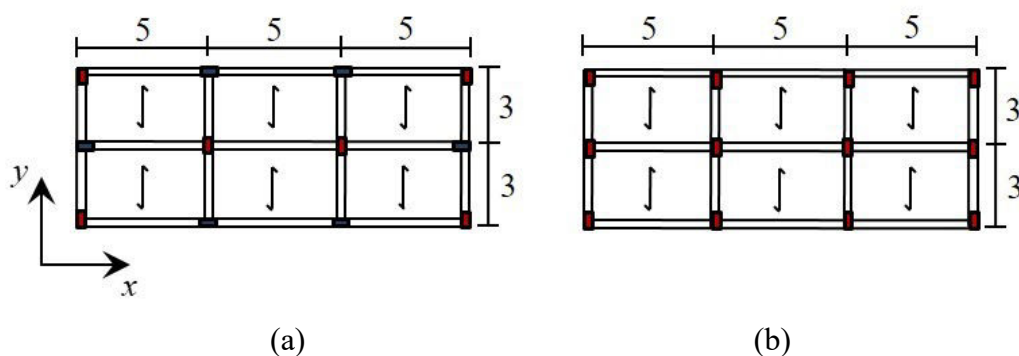


Figure 2-10 Floor plan of the two analyzed three-story buildings that have same (a) and different (b) inertia to horizontal motion in the two orthogonal directions  $x$  and  $y$ . The dimensions of the two buildings are the same; the difference is in the rectangular column orientation.

The building in Figure 2-10a has the same inertia to horizontal motion in the two orthogonal directions  $x$  and  $y$  due to column orientation, despite the rectangular floor plan. Its first and second natural frequencies are equal to  $f_b = 3.8$  Hz. The building in Figure 2-10b has very different inertia to horizontal displacement in the two orthogonal directions  $x$  and  $y$ , consequently, the first two natural frequencies are distinct. The first natural frequency is equal to  $f_{b1} = 2.8$  Hz and corresponds to a translational mode shape in  $x$ -direction, while the second one is  $f_{b2} = 4.7$  Hz and is related to a translational mode shape in  $y$ -direction. Building dimensions are indicated in Figure 2-10. The interstory height is 3.2 m. The rectangular cross-section of beams and columns are indicated in Table 2-2.

A live and dead load of  $140 \text{ kg/m}^2$  is distributed on beams in  $x$ -direction, according to their influence area, as mass per unit length. Mechanical properties of concrete are the elastic modulus in compression  $E = 31220 \cdot 10^6 \text{ N/m}^2$  and the Poisson's ratio  $\nu = 0.2$  (shear correction factor  $\chi = 0.857$ ). The reinforced concrete density is  $\rho = 2500 \text{ kg/m}^3$  and the damping ratio is  $\zeta = 5 \%$ .

Table 2-2 Dimensions of the rectangular cross-section beams and columns

Floor	Beam cm	Column cm
1	30×80	30×70
2	30×70	30×70
3	30×60	30×60

### 2.2.2.1. Soil area definition

Figure 2-11 shows the building bottom to bedrock TF for the soil profile and building having fundamental frequency  $f_s = f_b = 3.8$  Hz (Table 2-1 and Figure 2-10a), using different soil areas, in the case of seismic loading having predominant frequency  $f_q = 3.8$  Hz (Eq. (2-7) and Figure 2-12).

The selected soil area is the smallest that provides the soil column fundamental frequency equivalent to the FF case. The soil area  $A = 25 \text{ m} \times 25 \text{ m}$  is selected for the following analyses and a squared area is adopted, after evaluation of the building base to bedrock TF for both horizontal directions of motion and verification that the adopted dimension is convenient for both directions.

### 2.2.2. Input motion

A synthetic wavelet has been used as seismic loading in the following research, in order to use an input motion whose predominant frequency is close to the fundamental frequency of the building or the soil. A registered earthquake signal is also tested, to study the effect of a large-band seismic loading.

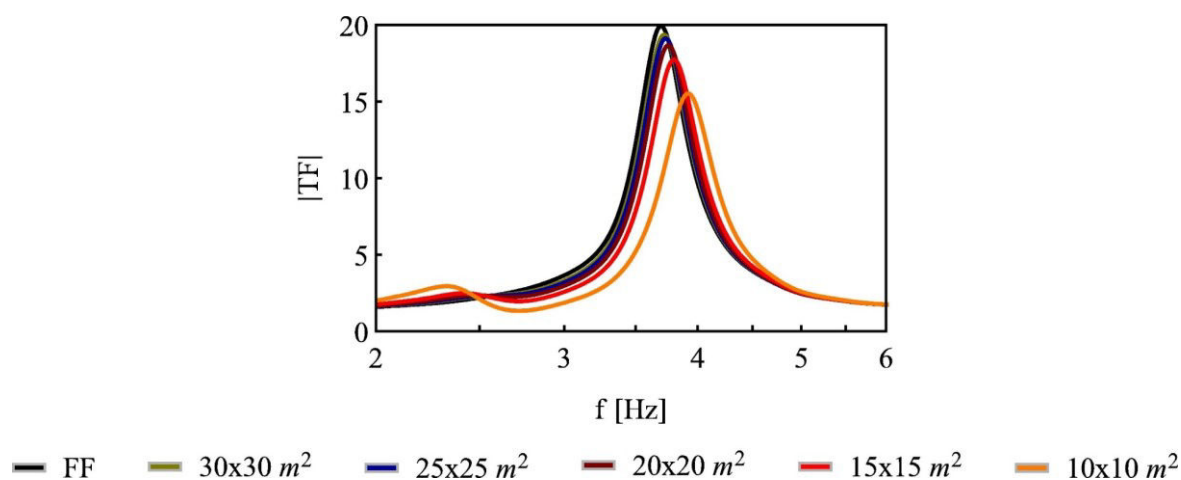


Figure 2-11 Building base to bedrock Transfer Function, evaluated for different soil areas, and free-field to bedrock Transfer Function.

### 2.2.2.1. Synthetic narrow-band

The seismic loading at the soil-bedrock interface (Mavroeidis and Papageorgiou 2002) has the following expression in terms of velocity:

$$v_0(t) = v_{0max}/2[1 + \cos(2\pi f_q/n(t - t_0))] \cos 2\pi f_q(t - t_0) \quad (2-7)$$

The motion duration is  $2t_0$ , where  $t_0 = n/2f_q$  is the time of envelope peak, the predominant frequency is  $f_q$  and  $n = 5$  is the number of cycles. The incident motion is obtained by deconvolution (halving) of rock outcrop motion. The peak acceleration on rock outcrop in North-South direction (NS) is imposed as  $a_{0max} = 0.2 \text{ m/s}^2$  and  $a_{0max} = 1.75 \text{ m/s}^2$  in the cases of linear and nonlinear soil behavior, respectively (Figure 2-12). East-West (EW) and Up-Down (UP) components of the incident motion have amplitude equal to the 90% and 50% of NS component.

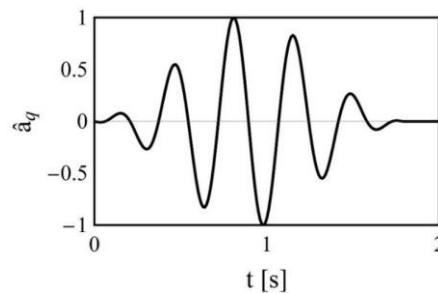


Figure 2-12 NS component of the synthetic seismic signal at the outcropping bedrock, in terms of normalized acceleration  $\hat{a}_q$ , for the predominant frequencies  $f_q = 2.8 \text{ Hz}$ .

### 2.2.2.2. Recorded large-band seismic loading

A recorded signal of the 6 April 2009 Mw 6.3 L'Aquila earthquake is used as input motion at the base of the horizontally multilayered soil, in terms of velocity, after deconvolution. The signal is recorded at the Antrodoco (ANT) station of the Italian strong motion network, localized in Lazio region (Italy), at an epicentral distance of 26.2 km. The ANT is a FF station in a flat surface (slope angle lower than  $15^\circ$ ) and on a stiff soil (type A in the Eurocode 8 soil classification). Consequently, the record is considered as rock outcropping motion. The PGA is  $0.2597 \text{ m/s}^2$  in North-South (NS) direction Figure 2-13a. The ground acceleration is  $0.1974 \text{ m/s}^2$  and  $0.1147 \text{ m/s}^2$  in East-West (EW) and Up-Down direction, respectively. The time step of recorded signals is  $dt = 5 \times 10^{-3} \text{ s}$ . The selected seismic signal is applied at the base of the horizontally multilayered soil profile in terms of velocity (Figure 2-13a).

The Fourier spectra, and the predominant frequency associated, of the NS, EW and UP components of 2009 Mw 6.3 L'Aquila earthquake recorded at ANT station are shown in Figure 2-13b.

### 2.2.3. Signal processing of the output motion

All numerical signals in the present analysis are filtered by a zero-phase-shift two pole Butterworth filter between 0.1 and 10 Hz, that is a band including the most relevant frequency content of the building.

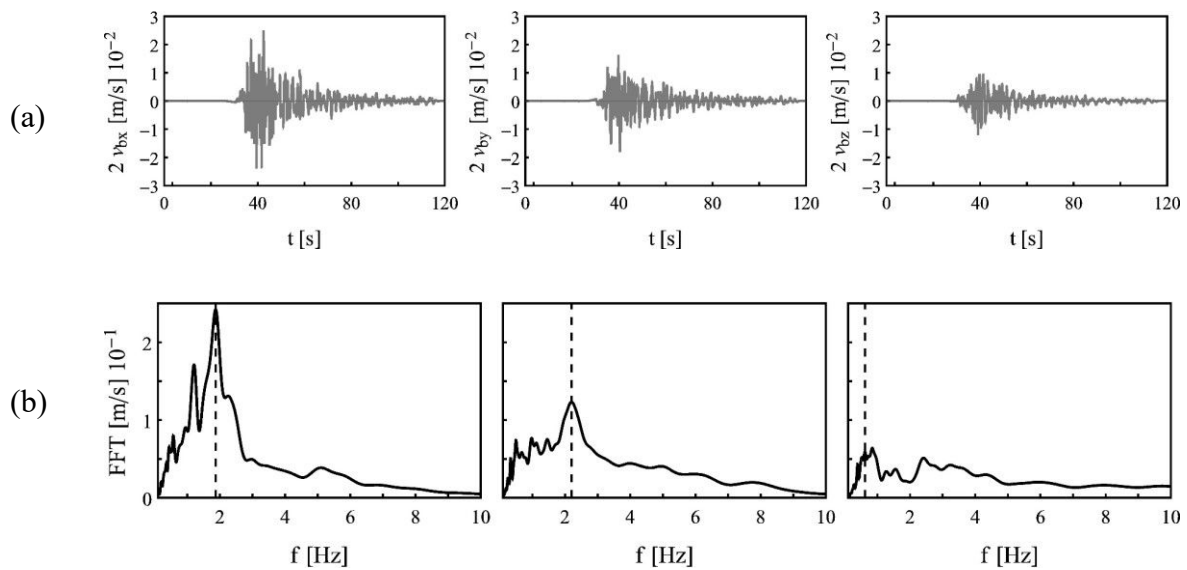


Figure 2-13 Velocity time history (a) and Fourier spectrum (b) for the NS, EW and UP components of the 2009 Mw 6.3 L'Aquila earthquake at recorded ANT station. Dashed lines show the predominant frequency in NS, EW and UP directions.

### 2.3. Verification of the proposed model

The adopted 1D-3C wave propagation model is verified, for linear and nonlinear behavior of soil, by comparison with the FF solution obtained by SWAP\_3C, the 1-D FE code proposed by Santisi d'Avila et al. (2013). The latter uses 3-node line elements for the spatial discretization of soil, where zero strains  $\epsilon_x$ ,  $\epsilon_y$  and  $\gamma_{xy}$  are directly imposed in the strain vector. The 1D-3C proposed model for SSI (assembly of 1-D soil and one 3-D building) is verified by comparison with SFRINT\_3C (Santisi d'Avila and Lopez-Caballero 2018).

Anderson's criteria (Anderson 2004) are employed to quantitatively estimate the reliability of results obtained using the proposed models, compared with reference numerical models. The Goodness-of-fit (Gof) is represented using grades between 0 and 10, assigned to ten parameters

characterizing a signal: Arias duration (C1), energy duration (C2), Arias intensity (C3), energy integral (C4), peak acceleration (C5), velocity (C6) and displacement (C7), response spectrum (C8), Fourier spectrum (C9) and cross correlation ratio (C10). Scores in the intervals 0-4, 4-6, 6-8 and 8-10 represent poor, fair, good and excellent fit, respectively.

### 2.3.1. Comparison with other codes

The three-story building in Figure 2-10a ( $f_b = 3.8$  Hz) is associated with the soil profile having  $f_s = 3.8$  Hz and subjected, at soil-bedrock interface, to the seismic loading with  $f_q = 3.8$  Hz (Figure 2-12). No numerical damping ( $\alpha = 0, \beta = 0.25$  and  $\gamma = 0.5$ ) is employed for the verification phase of SSI model because SFRINT\_3C (Santisi d'Avila and Lopez-Caballero 2018) considers only  $\beta$  and  $\gamma$ . The scores obtained in the case of linear soil behavior are listed in Table 2-3 and they guarantee an excellent fit. Figure 2-14 and Figure 2-15 show the obtained acceleration time histories in the FF case and for SSI, respectively, at different points.

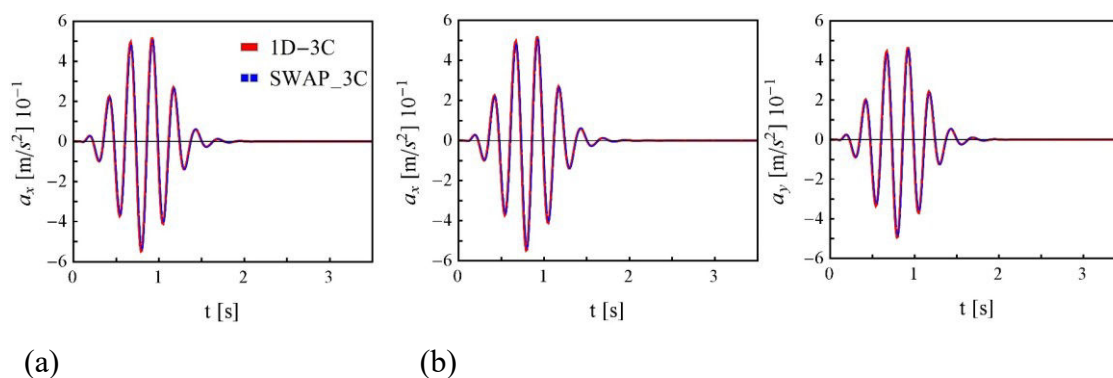


Figure 2-14 Acceleration time history at the soil surface, in the case of FF solution and linear soil behavior, for one- (a) and three-component (b) motion.

Table 2-3 Gof of the 1-D model in the case of linear soil behavior ( $f_b = f_s = f_q = 3.8$  Hz).

Compared models	Position	Direction	Anderson Criterion											
			C1	C2	C3	C4	C5	C6	C7	C8	C9	C10		
1D-1C FF	SWAP_3C	soil top	X	9.7	9.7	10	10	10	10	10	10	10	9.5	9.8
			X	9.7	9.7	10	10	10	10	10	10	10	9.5	9.8
1D-3C FF	SWAP_3C	soil top	Y	9.7	9.7	10	10	10	10	10	10	10	9.5	9.8
			Z	9.8	9.6	10	10	10	10	10	10	10	9.6	9.9
1D-1C SSI	SFRINT_3C	bldg. base	X	9.9	9.9	9.9	10	10	10	10	10	10	9.4	10
1D-1C SSI	SFRINT_3C	bldg. top	X	9.9	9.9	9.9	9.9	10	10	10	10	10	9.7	10
			X	9.9	9.9	9.9	10	10	10	10	10	10	9.4	10
1D-3C SSI	SFRINT_3C	bldg. base	Y	9.9	9.9	9.9	10	10	10	10	10	10	9.2	10
			Z	9.9	10	9.8	9.8	10	10	10	10	10	9.4	10

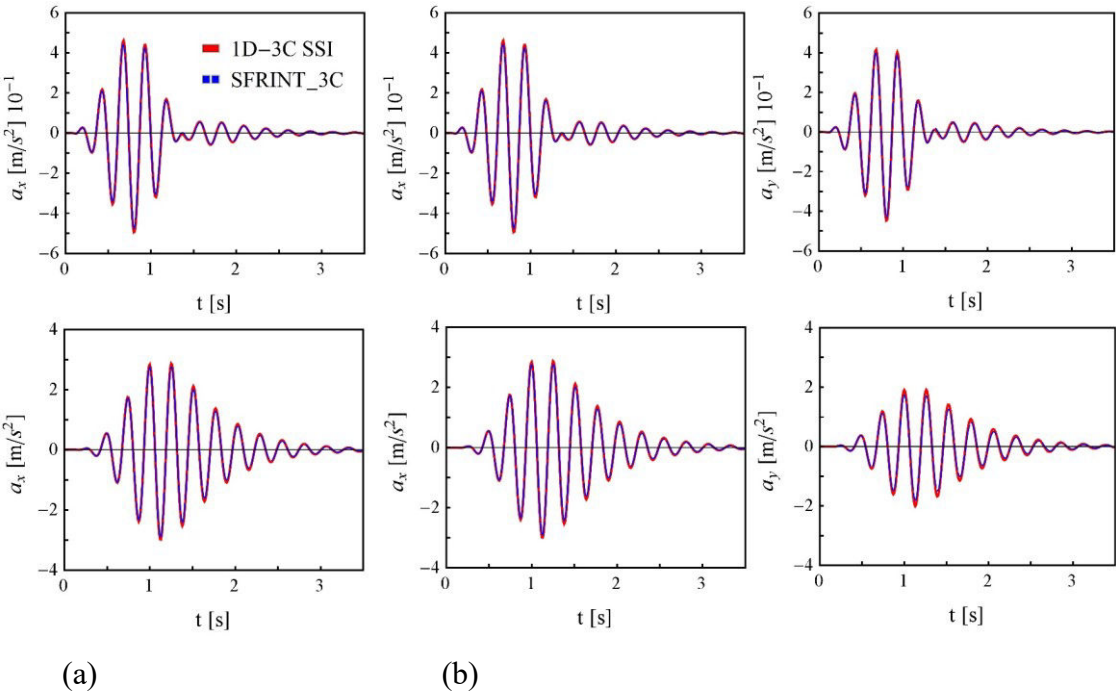


Figure 2-15 Acceleration time history at the soil surface (top) and at the building top (bottom), in the case of linear soil behavior, for one- (a) and three-component (b) motion.

The scores obtained in the case of nonlinear soil behavior are listed in Table 2-4 and they guarantee good and excellent fit. Some differences are due to the different implementation of the constitutive model for soil and convergence roots. Four scores are low, and the related curves are plotted in Figure 2-16. Some differences are observed between 1 s and 4 s, but they are assumed negligible and the verification of the proposed model is assured.

The acceleration time histories in the case of nonlinear soil are shown in Figure 2-17 and Figure 2-18, for the proposed model and the reference code (Santisi d’Avila and Lenti 2012; Santisi d’Avila and Lopez-Caballero 2018).

Table 2-4 Gof of 1-D model in the case of nonlinear soil behavior ( $f_b = f_s = f_q = 3.8$  Hz).

Compared models	Position	Direction	Anderson Criterion											
			C1	C2	C3	C4	C5	C6	C7	C8	C9	C10		
1D-1C FF	SWAP_3C	soil top	X	9.8	9.6	10	10	10	10	10	9.9	<b>4</b>	6.1	9.9
1D-3C FF	SWAP_3C	soil top	X	9.4	9.6	10	10	9.8	10	9.9	7.5	6.1	9.8	
			Y	9.4	9.6	10	10	9.8	10	9.9	7	6	9.8	
			Z	9.8	9.9	10	10	10	10	10	7	9.9		
1D-1C SSI	SFRINT_3C	bldg. base	X	9.6	9.4	9.9	10	10	10	9.9	<b>2.9</b>	6.6	9.5	
1D-1C SSI	SFRINT_3C	bldg. top	X	9.7	9.7	9.8	9.8	9.9	10	9.9	9.9	8.4	9.9	
			Y	9.7	9.7	9.8	9.8	10	10	10	10	8.6	10	
			Z	9.1	9.2	9.5	9.7	10	9.8	10	9.9	<b>5.6</b>	9.5	
1D-3C SSI	SFRINT_3C	bldg. base	X	9.2	9.4	9.7	10	9	10	9.9	8.2	7.2	9.2	
			Y	9.2	9.5	9.8	10	9.2	10	9.9	7.7	7	9.2	
			Z	8.9	9.2	9.7	9.9	10	9.9	10	9.8	<b>3.8</b>	8.7	

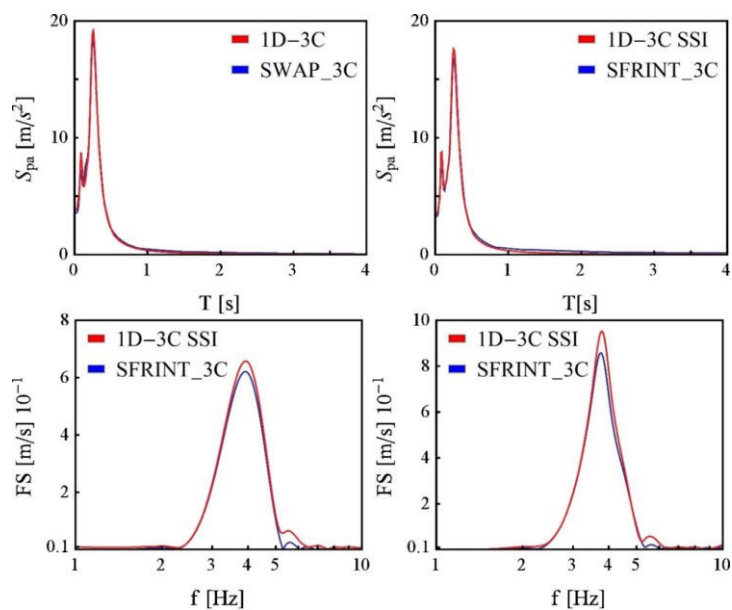


Figure 2-16 Parameters associated to lowest GoF scores: (top-left) Response spectrum for the 1C motion in  $x$ -direction at the FF, (top-right) Response spectrum for the 1C motion in  $x$ -direction at the building bottom, (bottom-left) Fourier spectrum for the 3C motion in  $z$ -direction at the building bottom (bottom-right) Fourier spectrum for the 3C motion in  $z$ -direction at the building top.

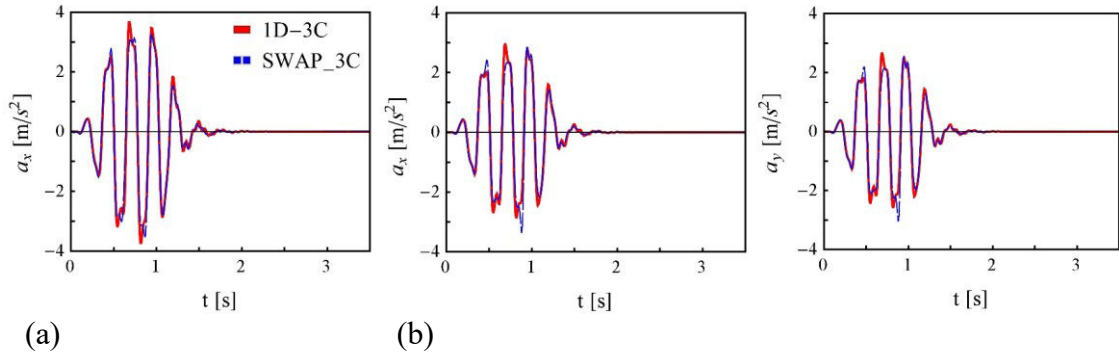


Figure 2-17 Acceleration time history at the soil surface, in the case of FF solution and nonlinear soil behavior, for one- (a) and three-component (b) motion.

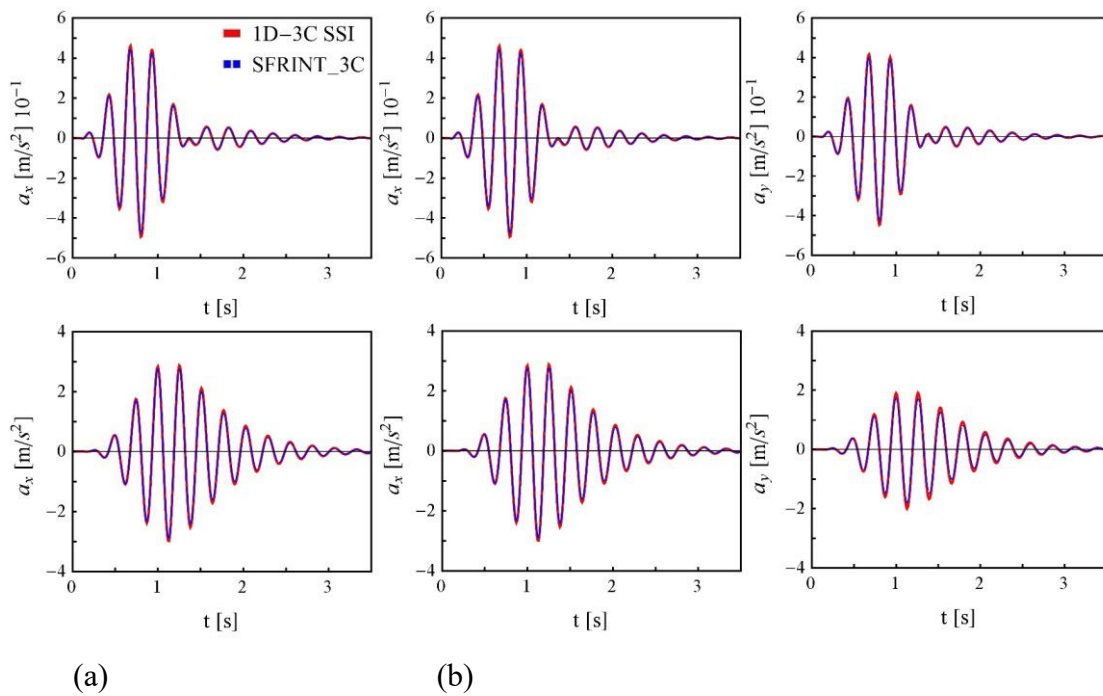


Figure 2-18 Acceleration time history at the building base (top) and top (bottom), in the case of nonlinear soil behavior, for one- (a) and three-component (b) motion.

**2.4. 1D-3C vs 3D-3C wave propagation model for vertical propagation**

Evaluation of the accuracy of the 1D-3C model, compared with the case of 3D-3C model where the periodicity condition is assumed, in the case of horizontally layered soil having nonlinear behavior is studied.

The employed models for this analysis are shown in Figure 2-1. The 1D-3C model, the 3D-3C model with connection node-to-node between building and soil and the 3D-3C model with

reinforced concrete foundation, named SFSI that stands for Soil-Foundation-Structure Interaction, are shown in Figure 2-1a, b and c, respectively.

A recorded signal of the 6 April 2009 Mw 6.3 L'Aquila earthquake (UTC 1:32) is employed as rock outcropping motion (Figure 2-13a). The selected seismic signal, recorded at an outcropping bedrock, is halved to consider the free surface effect and integrated to obtain the corresponding input data in terms of vertically incident velocities, before being forced at the base of the horizontally multilayered soil profile.

The three-story building in Figure 2-10a (same inertia in both orthogonal directions,  $f_b = 3.8$  Hz) is associated with the soil profile having  $f_s = 3.8$  Hz. The rigid foundation, embedded in the soil, has the same concrete properties as the structure. It is 16 m long by 7 m wide and 0.5 m deep.

The GoF criteria are listed in Table 2-5, giving excellent fit for all cases. A qualitative comparison of 1D-3C and 3D-3C models is shown in Figure 2-19 and

Figure 2-20, in terms of acceleration time history at the building bottom and top.

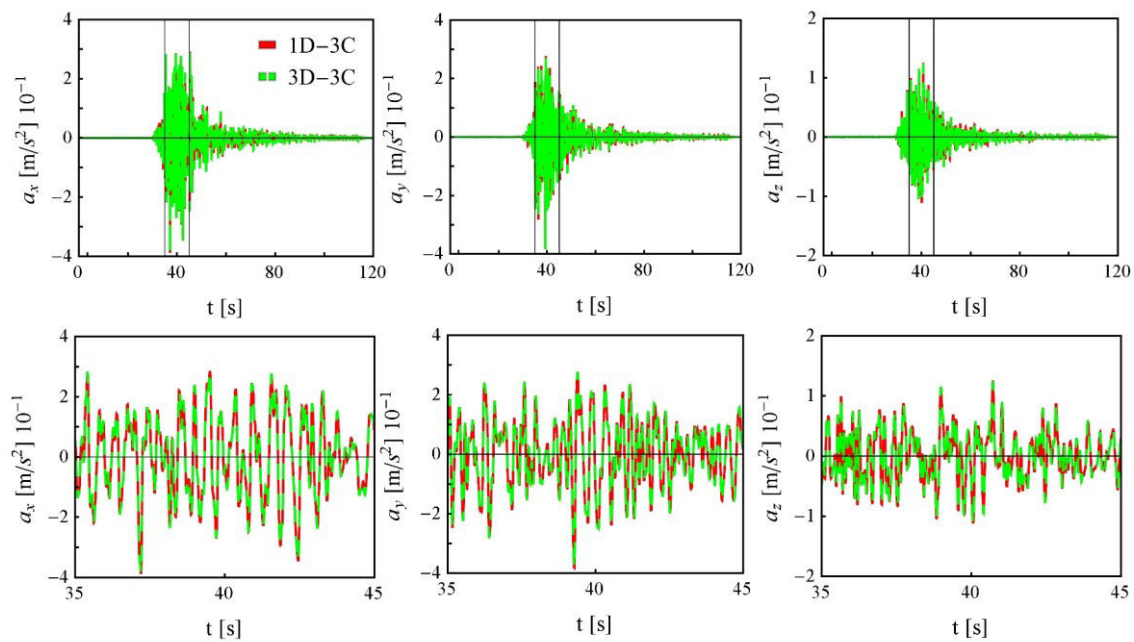


Figure 2-19 Simulated acceleration time history at the building bottom in the case of resonance ( $f_b = f_s = 3.8$  Hz) during the input signal duration (top) and in a 10 s time window over the largest amplitudes (bottom).

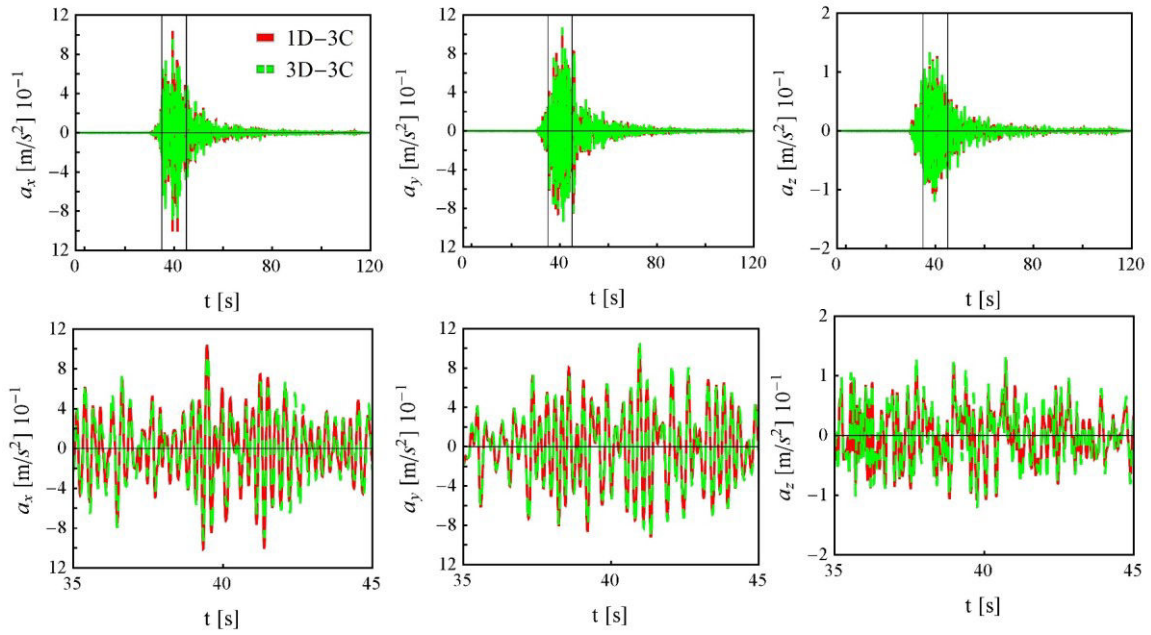


Figure 2-20 Simulated acceleration time history at the building top in the case of resonance ( $f_b = f_s = 3.8 \text{ Hz}$ ) during the input signal duration (top) and in a 10 s time window over the largest amplitudes (bottom).

The three-story building in Figure 2-10b (different inertia in both orthogonal directions, ( $f_b = 2.8 \text{ Hz}$ ) is associated with the soil profile having  $f_s = 3.8 \text{ Hz}$ . The rigid foundation, embedded in the soil, has the same concrete properties as the structure. It is 16 m long by 7 m wide and 0.5 m deep.

The GoF criteria are listed in Table 2-6, giving excellent fit for all cases. A qualitative comparison of 1D-3C and 3D-3C models is shown in Figure 2-21 and Figure 2-22, in terms of acceleration time history at the building bottom and top.

Table 2-5 Gof of 1D-3C model in the case of nonlinear soil and resonance  $f_b = f_s = 3.8$  Hz .

Compared Models		Position	Direction	Anderson Criterion										
				C1	C2	C3	C4	C5	C6	C7	C8	C9	C10	
1D-3C FF	3D-3C FF	soil top	X	10	10	10	10	10	10	10	10	10	10	10
			Y	10	10	10	10	10	10	10	10	10	10	10
			Z	10	10	10	10	10	10	10	10	10	9.9	10
1D-3C SSI	3D-3C SSI	bldg. base	X	10	10	10	10	10	10	10	10	10	10	10
			Y	10	10	10	10	10	10	10	10	10	9.8	10
			Z	9.9	10	10	10	10	10	10	10	10	9.2	9.9
1D-3C SSI	3D-3C SSI	bldg. top	X	9.9	9.9	10	10	10	10	10	10	10	10	10
			Y	9.8	9.9	10	10	10	10	10	10	10	9.8	10
			Z	9.9	10	10	10	10	10	10	10	10	9.1	9.9
3D-1C SSI	3D-1C SFSI	bldg. base	X	9.9	10	10	10	10	10	10	10	10	9.9	10
			Y	10	10	10	10	10	10	10	10	10	9.8	10
			Z	9.8	10	10	10	10	10	10	10	10	8.8	9.6
3D-1C SSI	3D-1C SFSI	bldg. top	X	9.5	9.7	10	10	10	10	10	10	10	9.7	9.6
			Y	9.9	9.9	10	10	10	10	10	10	10	9.8	10
			Z	9.7	9.9	9.8	10	10	10	10	10	10	8.9	9.6
1D-3C SSI	3D-3C SFSI	bldg. base	X	10	10	10	10	10	10	10	10	10	9.9	10
			Y	10	10	10	10	10	10	10	10	10	9.8	10
			Z	9.8	10	10	10	10	10	10	10	10	8.7	9.6
1D-3C SSI	3D-3C SFSI	bldg. top	X	9.4	9.6	10	10	9.9	10	10	10	10	9.7	9.4
			Y	9.7	9.8	10	10	10	10	10	10	10	9.7	9.9
			Z	9.6	9.9	9.7	10	10	10	10	10	10	8.8	9.7

Table 2-6 Gof of 1D-3C model in the case of nonlinear soil and SSI  $f_b = 3.8 > f_s = 2.8$  Hz

Compared Models		Position	Direction	Anderson Criterion											
				C1	C2	C3	C4	C5	C6	C7	C8	C9	C10		
1D-3C FF	3D-3C FF	soil top	X	10	10	10	10	10	10	10	10	10	9.9	10	
			Y	10	10	10	10	10	10	10	10	10	10	9.9	10
			Z	9.9	10	10	10	10	10	10	10	10	10	9.8	10
1D-3C SSI	3D-3C SSI	bldg. base	X	10	10	10	10	10	10	10	10	10	10	9.9	10
			Y	10	10	10	10	10	10	10	10	10	10	9.6	10
			Z	9.9	10	10	10	10	10	10	10	10	10	9.2	9.8
1D-3C SSI	3D-3C SSI	bldg. top	X	9.9	9.9	10	10	10	10	10	10	10	10	9.9	10
			Y	9.8	9.9	10	10	10	10	10	10	10	10	9.6	9.9
			Z	9.8	10	10	10	10	10	10	10	10	10	9.2	9.8
3D-3C SSI	3D-3C SFSI	bldg. base	X	10	10	10	10	10	10	10	10	10	10	9.8	10
			Y	10	10	10	10	10	10	10	10	10	10	9.9	10
			Z	9.8	9.9	10	10	10	10	10	10	10	10	8.7	9.6
3D-3C SSI	3D-3C SFSI	bldg. top	X	9.5	9.8	9.9	9.9	10	10	10	10	10	10	9.6	9.5
			Y	9.9	10	10	10	10	10	10	10	10	10	9.6	10
			Z	9.7	9.9	9.9	10	10	10	10	10	10	10	8.8	9.6
1D-3C SSI	3D-3C SFSI	bldg. base	X	10	10	10	10	10	10	10	10	10	10	9.7	10
			Y	10	10	10	10	10	10	10	10	10	10	9.6	10
			Z	9.7	9.9	10	10	10	10	10	10	10	10	8.6	9.6
1D-3C SSI	3D-3C SFSI	bldg. top	X	9.4	9.7	9.9	9.9	10	9.9	10	10	10	9.5	9.3	
			Y	9.7	9.9	10	10	10	10	10	10	10	10	9.3	9.8
			Z	9.6	9.9	9.9	10	10	10	10	10	10	10	8.6	9.5

## 2.5. SSI analysis

The proposed 1D-3C model is used to investigate SSI effects that exist, according to Saez et al. (2011), when the seismic response obtained by a one-step analysis (direct solution) is strongly different from that obtained by a two-step analysis and increases with the building to soil fundamental frequency ratio (Lopez Caballero and Farahmand Razavi 2008). The SSI is investigated in the case of resonance, when the fundamental frequency of building and soil column are close together hence, seismic response amplification is induced. In this analysis linear elastic materials are considered.

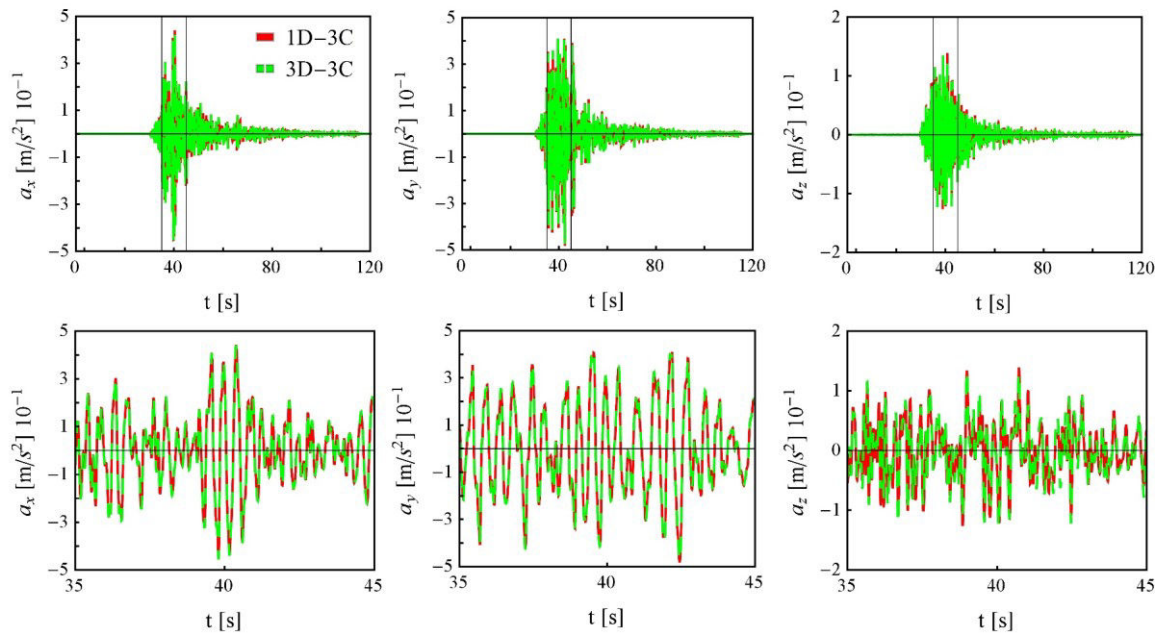


Figure 2-21 Simulated acceleration time history at the building bottom in the case of SSI ( $f_b = 3.8 > f_s = 2.8$  Hz) during the input signal duration (top) and in a 10 s time window over the largest amplitudes (bottom).

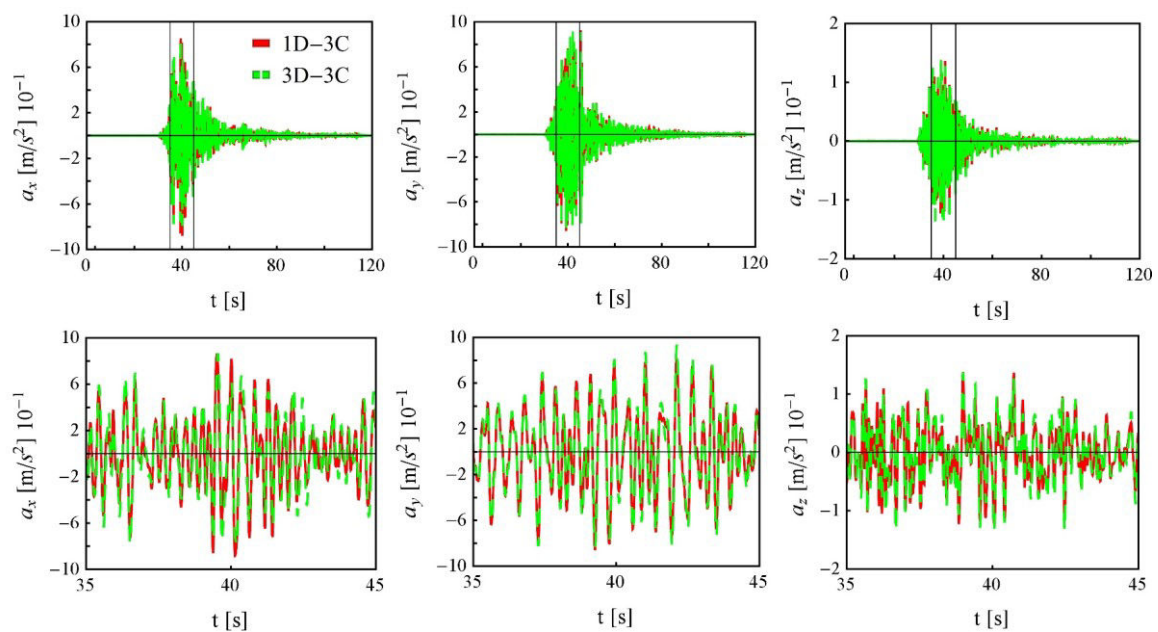


Figure 2-22 Simulated acceleration time history at the building top in the case of SSI ( $f_b = 3.8 > f_s = 2.8$  Hz) during the input signal duration (top) and in a 10 s time window over the largest amplitudes (bottom).

The three-story building having fundamental frequency  $f_b = 3.8$  Hz (Figure 2-10a) is placed on two different soil profiles having natural frequency  $f_s = 2.8$  Hz and 3.8 Hz (see Table 2-1) and linear behavior. The synthetic 3C motion having peak rock outcrop acceleration  $a_{0\max} = 0.2$  m/s<sup>2</sup> in  $x$ -and  $y$ -direction and halved in  $z$ -direction is applied at the soil-bedrock interface. The narrow band input with predominant frequency  $f_q = 3.8$  Hz is selected to excite the building.

Results in Figure 2-23 and Figure 2-24 show the building seismic response in the cases of resonance ( $f_b = 3.8$  Hz and  $f_s = 3.8$  Hz) and SSI ( $f_b = 3.8$  Hz and  $f_s = 2.8$  Hz) respectively. The ground motion and the acceleration at the building top are amplified in Figure 2-23, due to the resonance effect, compared with the case in Figure 2-24. The difference between one- and two-step analyses, due to SSI, is more pronounced in Figure 2-23, in the direction of the first mode shape, and in Figure 2-24, in the direction of the second mode shape in terms of acceleration at the building top. The differences in the building response in the two horizontal directions is because the building is rectangular shaped, even if the two first natural frequencies associated to the two translational modes are almost equal.

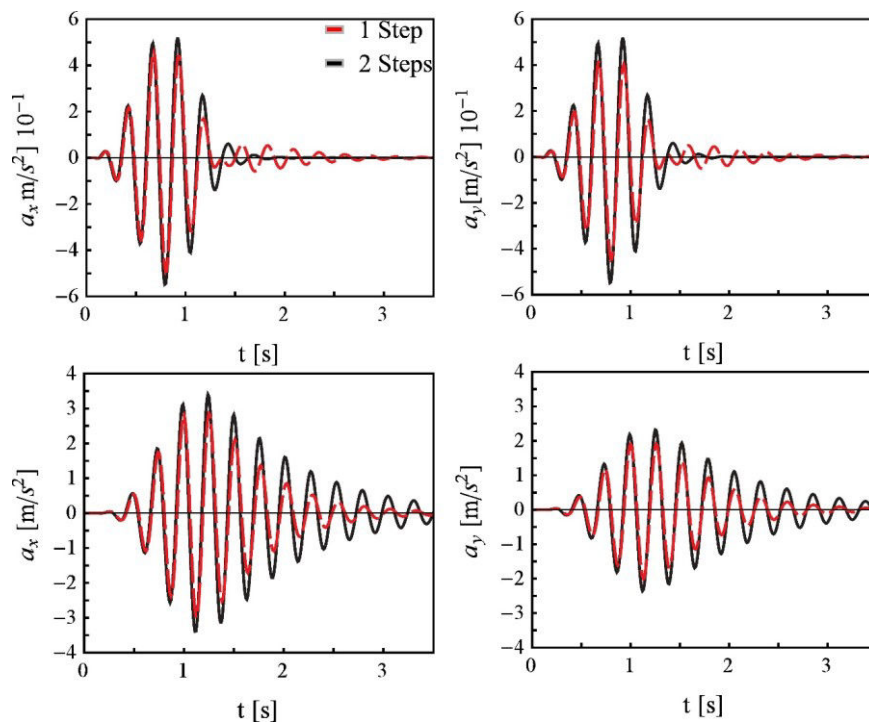


Figure 2-23 Horizontal acceleration time history in the cases of soil profile with fundamental frequency  $f_s = f_b = f_q = 3.8$  Hz, at building bottom (top) and at building top (bottom).

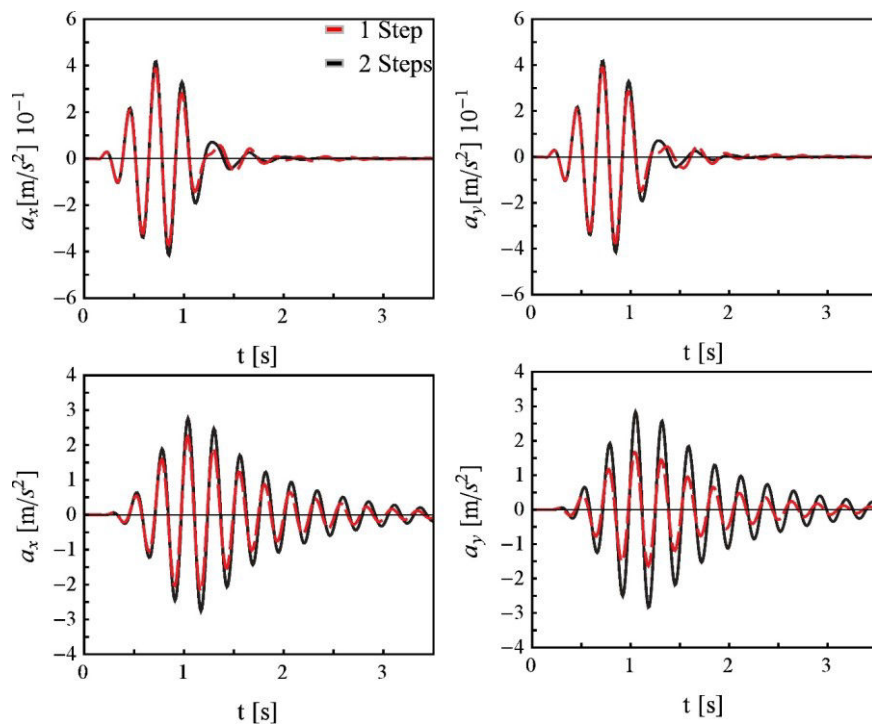


Figure 2-24 Horizontal acceleration time history in the cases of soil profile with fundamental frequency  $f_s = 2.8$  Hz, and  $f_b = f_q = 3.8$  Hz, at building bottom (top) and at building top (bottom).

## 2.6. Conclusion

The proposed 1D-3C seismic wave propagation model, used to simulate the response of soil and building to earthquakes taking into account site effects and SSI, is verified either comparing with SWAP\_3C code or with a 3D-3C model, for linear and nonlinear soil behavior. The proposed model avoids modeling problems related to the definition of boundary conditions and the lack of geotechnical data to produce a detailed 3-D soil model and strongly reduce the computational time. Consequently, it is suitable for professional practice.

The hypothesis of rigid shallow foundation with the same seismic motion at the base of all columns does not permit to consider the foundation deformability and rocking effects and this model cannot simulate the interaction between more buildings. Therefore, the 1D-3C model is limited to the study of SSI with rigid shallow foundation. Hence, in the next chapter an improved modeling technique is introduced to simulate the seismic response of soil and building also the foundation deformability, rocking effects and SSSI.



## **Chapter 3 - One-directional three-component wave propagation in a T-shaped soil domain for SSI and SSSI**

A modeling technique is proposed to take into account SSI in building design, considering rocking effects and the shallow foundation deformability. The one-directional three-component wave propagation is numerically simulated in a T-shaped horizontally layered soil domain assembled with a three-dimensional (3-D) frame structure. A 3-D soil model is used until a fixed depth and a 1-D model is supposed to be a sufficient approximation in deeper soil layers. The 1D-3C wave propagation approach in a T soil model (1DT-3C) is inspired by the consideration that SSI is detected in the near-surface soil layers. The proposed modeling approach is verified by comparison with a fully 3D-3C model for vertical propagation in horizontally layered soil and periodic lateral boundary condition. The 1DT-3C modeling technique is used to investigate the building response and SSI effects that vary with the frequency content of seismic loading and building-to-soil frequency ratio, respectively.

### 3.1. 1DT-3C wave propagation model for SSI and SSSI analyses

The proposed 1D-3C approach for SSI investigations, discussed in Chapter 2 - (Figure 3-1a), is limited to the case of rigid shallow foundation, negligible rocking effects, horizontally layered soil with periodic lateral boundary condition and homogeneous properties in each layer. Furthermore, the numerical simulation of seismic response of a group of buildings demands a fully 3-D soil domain Figure 3-1b.

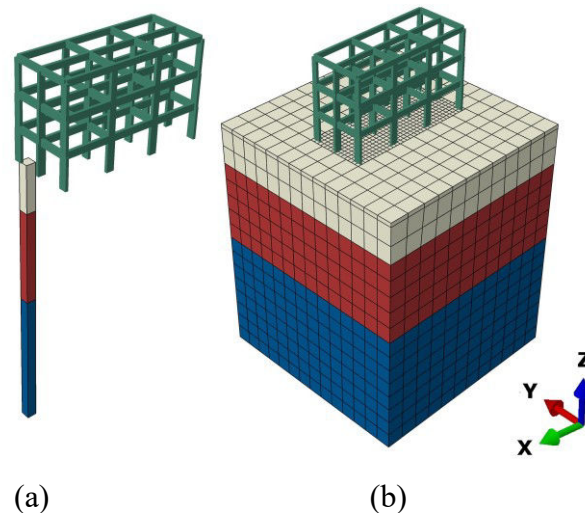


Figure 3-1 Assembly of a multilayer soil domain and a frame structure shaken by a three-component seismic motion: 1D-3C (a) and 3D-3C (b) model for SSI analysis.

In this research, a modeling technique is proposed to take into account the foundation deformability, rocking effects and the cross-interaction between neighbor structures and the soil. It is inspired by the consideration that SSI and SSSI are detected in the near-surface soil layers. The soil profile is assumed as horizontally layered and infinitely extended along the horizontal directions  $x$  and  $y$ , according to the  $xyz$  coordinate system represented in Figure 3-1. Consequently, no strain variation is considered in these directions. Shear and pressure waves propagate vertically in  $z$ -direction from the top of the underlying elastic bedrock to the soil surface. The soil is assumed to be a continuous and homogeneous medium, with nonlinear constitutive behavior. The discrete dynamic equilibrium equation for the assembly of soil domain and frame structure, including compatibility conditions, 3-D nonlinear constitutive relation and the imposed boundary conditions, is solved directly (one-step analysis). All the proposed modeling techniques, in this research, can be adopted independently of the constitutive relationship selected for soil and structure.

A fully 3-D soil model is adopted until a fixed depth  $h$  and a 1-D model is used for deeper soil layers Figure 3-2. Due to the T-shaped soil domain area, the proposed modeling technique is named as 1DT-3C approach for SSI and SSSI analyses Figure 3-3 (Appendix D).

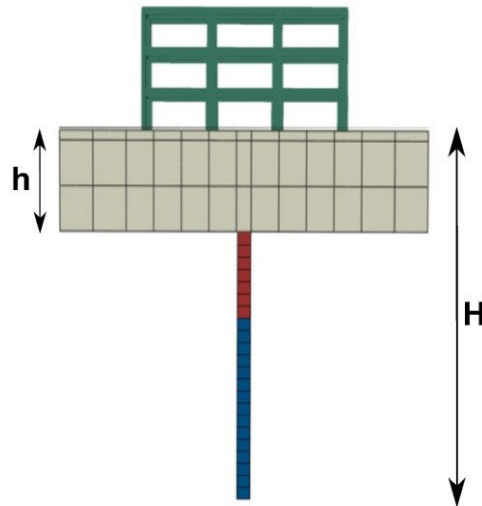


Figure 3-2 Section of the 1DT-3C model for SSI analysis where  $h$  is the thickness of the 3-D soil domain and  $H$  is the Thickness of the considered soil until bedrock interface.

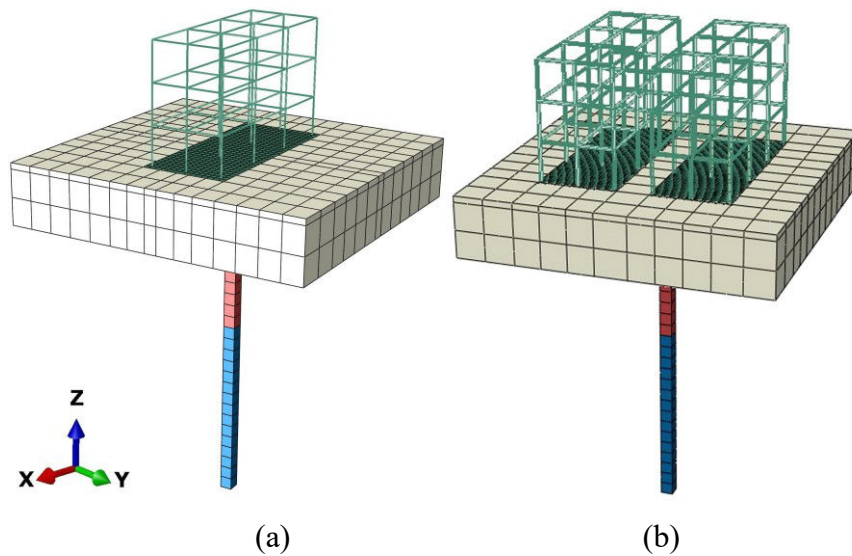


Figure 3-3 1DT-3C model for soil-structure interaction (a) and for structure-soil-structure (b) analysis.

A constraint equation is used to condense out the degrees of freedom at the base of the 3-D soil domain to those at the top of the unit area soil column. The foundation is modeled using 20-node solid FE and it is embedded in the soil domain. Consequently, the foundation

deformability and its rigid rotation, due to rocking effects, can be taken into account and the seismic motion at the base of each building column is independent.

The periodic lateral boundary condition is maintained at the lateral boundaries all along the depth. The lateral boundary condition could be defined using semi-infinite elements when the periodicity is not assured. The proposed 1DT-3C model, compared with a fully 3D-3C model, reduces the modeling time because the boundary condition definition is simple, especially in the case of periodic lateral boundary condition, because the input motion and the absorbing condition are defined in only one element at the base. Moreover, a one-dimensional soil profile can be characterized with a single borehole investigation, instead a 3-D soil domain needs more investigations to define in a reliable way the geotechnical model.

### ***3.2. Verification of the proposed model***

The 1DT-3C wave propagation approaches is verified by comparison with the case of 3-D soil domain, for vertical propagation, horizontally layered soil having nonlinear behavior and periodic lateral boundary condition. Anderson's criteria are employed to quantitatively estimate the reliability of results obtained using the proposed models, compared with the reference numerical model (Anderson 2004).

#### *3.2.1. Input data*

##### *3.2.1.1. Soil and building data*

The soil profiles with  $f_s = 3.8$  Hz and  $f_s = 1.9$  Hz are used in the verification phase. The stratigraphy and mechanical parameters of are introduced in Table 2-1. The two three-story buildings introduced in section 2.2 are used for the following analyses. The soil area  $A = 25 \text{ m} \times 25 \text{ m}$  is selected for the following analyses and a squared area is adopted, after evaluation of the building base to bedrock TF for both horizontal directions of motion and verification that the adopted dimension is convenient for both directions.

##### *3.2.1.2. 3-D soil thickness definition*

The depth of the fully 3-D soil domain is fixed using the results obtained using the 1D-3C wave propagation model in a SSI analysis and in linear elastic regime, compared with a simulation in FF conditions. Results of the Maximum shear strain and stress profiles with depth are shown in Figure 3-4. Only in the first meters the effect of SSI is not negligible. Hence, a 3-D soil

domain is assumed until a depth  $h = 5$  m, that corresponds to the interface between the first and second soil layers, and a 1-D model is used in deeper soil layers.

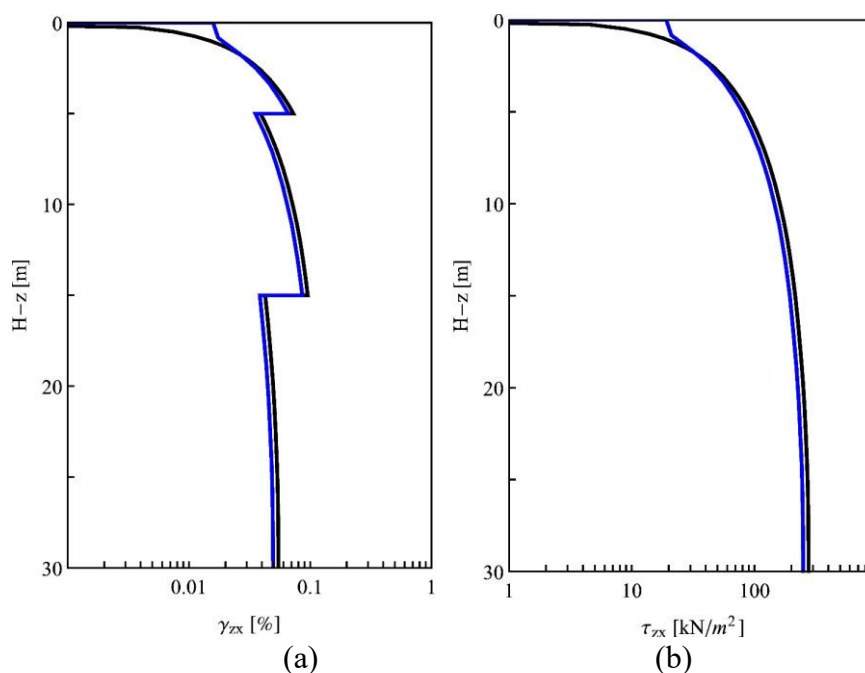


Figure 3-4 Maximum shear strain (a) and stress (b) profile with depth obtained using the 1D-3C wave propagation model for the SSI analysis in a linear elastic regime.

### 3.2.1.3. *Input motion*

The recorded signal of the 6 April 2009 Mw 6.3 L'Aquila earthquake (Chapter 2 - 2.2) is used as rock outcropping motion for the verification phase.

### 3.2.2. *Verification*

The 1DT-3C and the 3D-3C wave propagation approaches, in the case of vertical propagation in a horizontally layered soil for soil-foundation-structure interaction (SFSI) analysis shown in Figure 3-3a and Figure 3-1b respectively, are compared for the same case of building having  $f_b = 3.8$  Hz (Figure 2-10a), placed on the soil profile having  $f_s = 3.8$  Hz and nonlinear behavior. GoF show excellent fit of the 1DT-3C model compared with a 3D-3C model for SFSI analysis, as reported in Table 3-1. The acceleration time histories at the building bottom and the relative displacement time history at the building top are shown in Figure 3-5. The energy integral, the pseudo-acceleration response spectrum and Fourier spectrum in direction  $x$  are represented in Figure 3-6 to confirm the excellent fit given by the GoF scores (C4, C8 and C9, respectively, in Table 3-1). The correlation of the estimated acceleration in  $x$  direction is shown

in Figure 3-7. These comparisons with respect to the case of a 3D-3C model allow the verification of the 1DT-3C model, in the case of periodic lateral boundary condition and vertical propagation along a horizontally layered soil. Moreover, it is checked that the selected thickness  $h$  of the 3-D soil layer is suitable for this particular stratigraphy.

Table 3-1 Gof of 1DT-3C model, with respect to a 3D-3C model for SSI analysis.

Compared models	Position	Direction	Anderson criteria											
			C1	C2	C3	C4	C5	C6	C7	C8	C9	C10		
1DT-3C	3D-3C SFSI	bldg. base	X	10	10	10	10	10	10	10	10	10	9.5	10
			Y	10	10	10	10	10	10	10	10	10	9.3	10
			Z	9.7	10	9.9	10	10	10	10	10	10	8.4	9.9
1DT-3C	3D-3C SFSI	bldg. top	X	9.9	9.9	10	10	10	10	10	10	10	9.3	10
			Y	9.9	10	10	10	10	10	10	10	10	9.0	10
			Z	9.7	10	9.9	10	10	10	10	10	10	8.5	9.9

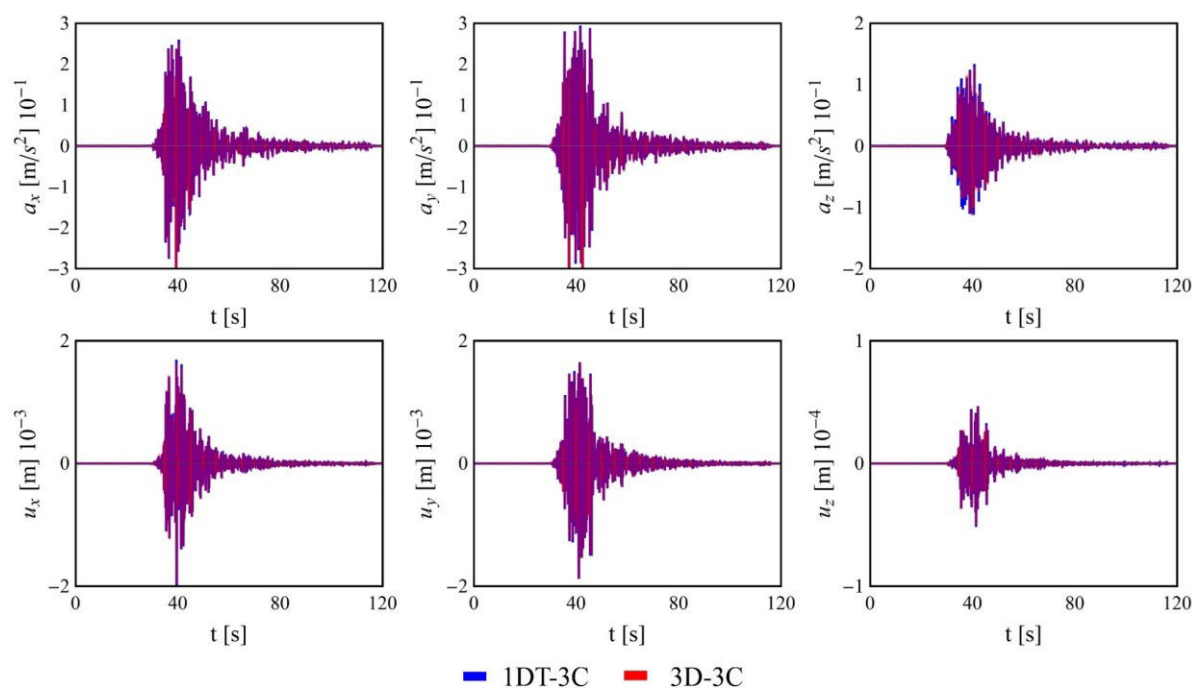


Figure 3-5 Comparison of 1DT-3C and 3D-3C models for SSI analysis: acceleration time history at the building bottom (top) and roof drift time history at the building top (bottom).

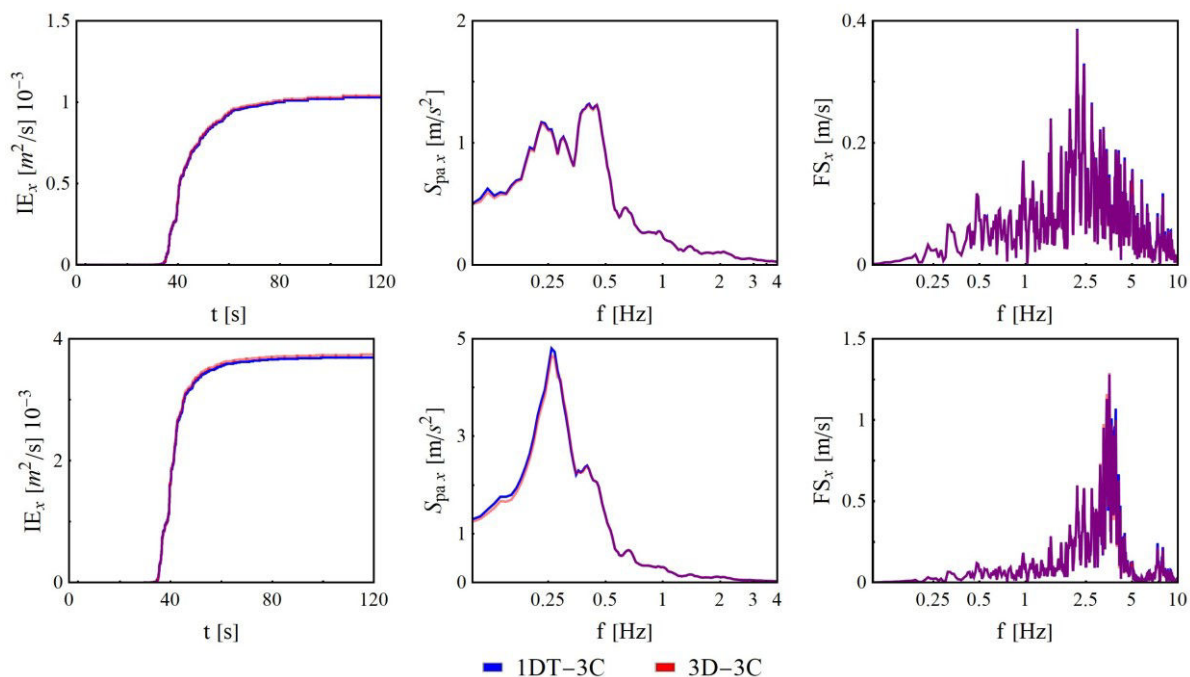


Figure 3-6 Comparison of 1DT-3C and 3D-3C models for SSI analysis: energy integral (IE), response spectrum acceleration ( $S_{pa}$ ) and Fourier spectrum (FS) for the horizontal x-component of motion at the building bottom (top) and top (bottom).

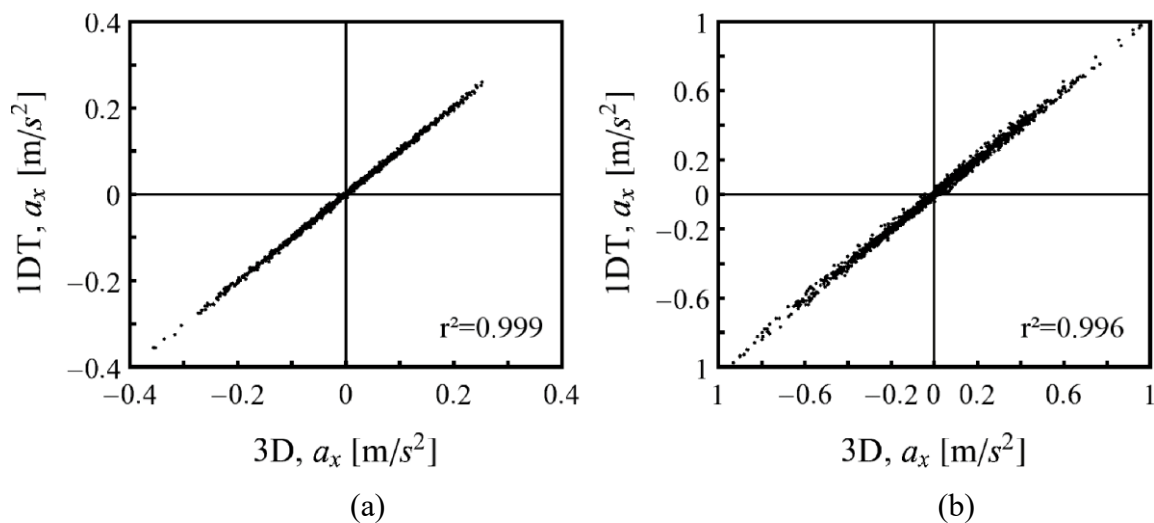


Figure 3-7 Comparison of 1DT-3C and 3D-3C models for SSI analysis: correlation coefficient of accelerations for the horizontal x-component of motion at the building bottom (a) and top (b).

### 3.3. SSI analysis

#### 3.3.1. Impact of the excitation frequency on the structural response

The 1DT-3C seismic wave propagation approach for SSI analysis is used in order to understand the impact of the seismic motion frequency content on the response of a building over a horizontally layered soil.

The building-soil system composed by a T-shaped soil profile having natural frequency  $f_s = 1.9$  Hz (Table 2-1) and a building having fundamental frequency  $f_b = 3.8$  Hz (Figure 2-10a) is first shaken by the synthetic narrow-band seismic loading (section 2.2) having predominant frequency  $f_q = f_b = 3.8$  Hz, close to the FB building frequency, and then by another having  $f_q = f_s = 1.9$  Hz, close to the soil column frequency.

Figure 3-8 shows an amplification of the acceleration at the building bottom in the case where the soil frequency is excited ( $f_q = f_s = 1.9$  Hz), that implies an amplification of the seismic loading for the building. However, the higher roof drift at the building top (Figure 3-8) is obtained for the case where the predominant frequency of the earthquake is close to the fixed-base frequency of the building ( $f_q = f_b = 3.8$  Hz).

This result signifies that the frequency content of the seismic load imposed at the bottom of the building is more important for the building deformation than the concept of expected maximum ground acceleration amplitude, derived from building design in static conditions and still used in design codes.

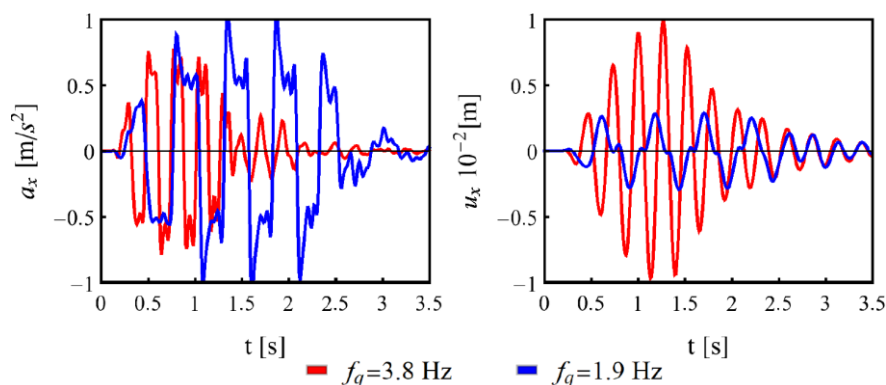


Figure 3-8 Acceleration time history at the building bottom (left) and roof drift at the building top (right), for the building-soil system composed by a T-shaped horizontally layered soil having frequency  $f_s = 1.9$  Hz and a building having fundamental frequency  $f_b = 3.8$  Hz, in the case of earthquake predominant frequency equal to  $f_q = f_s = 3.8$  Hz and  $f_q = f_s = 1.9$  Hz.

Furthermore, Figure 3-9 shows the building top to bottom TF in the cases of FB building and SSI analysis, using the 1DT-3C approach, for the two cases of soil profile having  $f_b = f_s = 3.8$  Hz and  $f_b = 3.8$  Hz  $>$   $f_s = 1.9$  Hz. It can be observed a reduction of the building fundamental frequency due to SSI, that is  $f_{SSI} = 3.6$  Hz. In this case of three-story building, the variation of frequency, also for softer soil ( $f_s = 1.9$  Hz), is not important because rocking effects are reduced. It is expected that more important rocking effects would reduce the building frequency when SSI is considered.

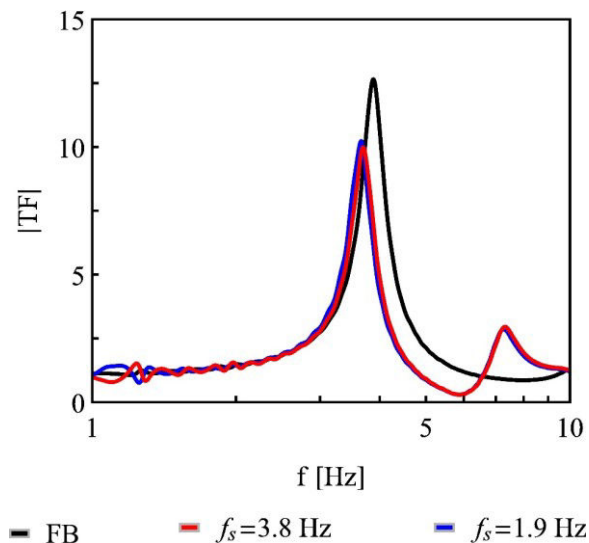


Figure 3-9 Building top to bottom transfer function estimated for a FB building and for SSI analysis in the cases of building-soil resonance ( $f_b = f_s = 3.8$  Hz) and softer soil ( $f_q = 3.8$  Hz  $>$   $f_s = 1.9$  Hz).

### 3.3.2. SSI estimation

The 1DT-3C seismic wave propagation model is used to compare the seismic response of a building-soil system shaken by a synthetic narrow-band seismic loading (section 2.2) having predominant frequency  $f_q$  equal to the fundamental frequency of the building,  $f_b$ . The analysis is done in both cases of horizontally layered soil having natural frequency  $f_s = f_b$  and  $f_s < f_b$ .

The building having  $f_b = 3.8$  Hz (Figure 2-10a) is placed at the surface of the soil profiles having  $f_s = 3.8$  Hz and  $f_s = 1.9$  Hz. The seismic input signal has predominant frequency  $f_q = f_b = 3.8$  Hz.

The acceleration time history at the building bottom and the roof drift at the building top are shown in Figure 3-10 for the cases of one-step analysis (building-soil system) and two-step analysis (FF motion at the base of a FB building).

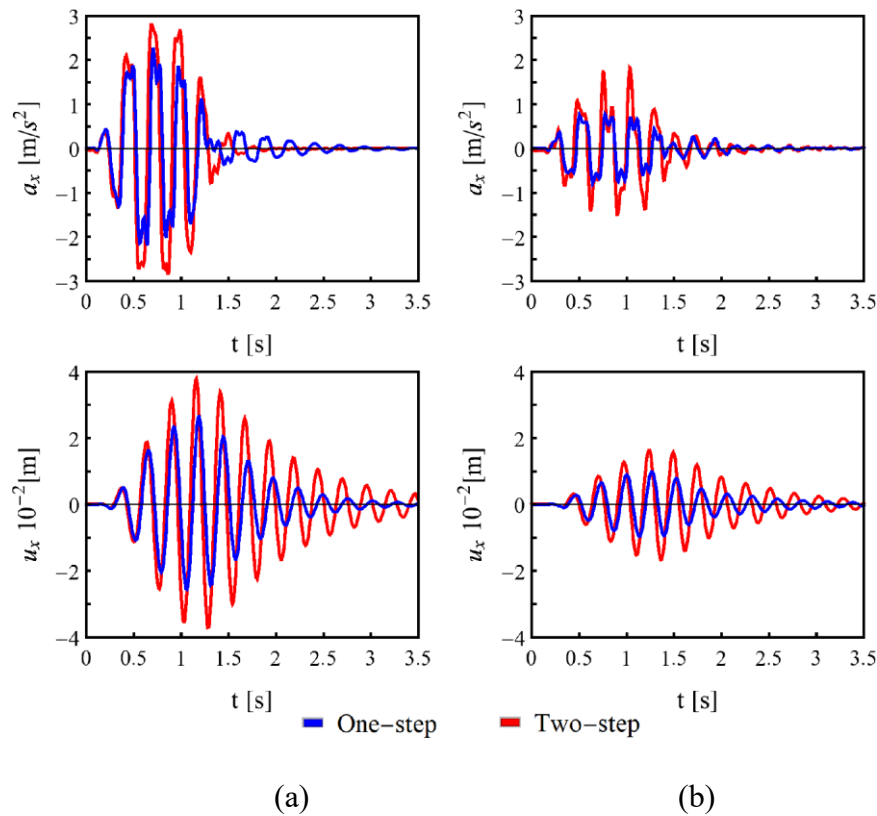


Figure 3-10 Acceleration time history at the building bottom and roof drift at the building top, for the building-soil system composed by a building having fundamental frequency  $f_b = 3.8$  Hz and a T-shaped horizontally layered soil having frequency  $f_s = f_b = 3.8$  Hz (a) and  $f_s = 1.9$  Hz  $< f_b = 3.8$  Hz (b), in the case of earthquake predominant frequency equal to  $f_q = f_b = 3.8$  Hz.

Taking into account the SSI using a one-step analysis gives a reduction of structural deformation. This SSI effect is quantitatively measured as the one-step to two-step ratio of the maximum acceleration at the building top,  $a_{\max\_1\text{step}}/a_{\max\_2\text{step}}$ . It is obtained  $a_{\max\_1\text{step}}/a_{\max\_2\text{step}} = 0.69$  and  $a_{\max\_1\text{step}}/a_{\max\_2\text{step}} = 0.57$ , for both  $x$ - and  $y$ -direction, in the cases  $f_s = f_b = f_q = 3.8$  Hz and  $f_s = 1.9$  Hz  $< f_b = f_q = 3.8$  Hz respectively. As expected, the SSI is more important in the case where the soil is softer (lower  $a_{\max\_1\text{step}}/a_{\max\_2\text{step}}$  ratio) in the case of nonlinear soil behavior. The resonance effect ( $f_s = f_b = f_q = 3.8$  Hz) produces an amplified seismic response, as can be observed by comparing Figure 3-10a and Figure 3-10b.

### 3.3.3. 1st vs 2nd natural frequency

The building represented in Figure 2-10b, having natural frequencies  $f_{b1} = 2.8$  Hz and  $f_{b2} = 4.7$  Hz, is placed at the surface of the soil profile having natural frequency  $f_s = 1.9$  Hz. Figure 3-11 and Figure 3-12 show the comparison between the results obtained by a one-step

analysis, using the 1DT-3C approach, and a two-step analysis, in terms of acceleration at the building bottom and the roof drift at the building top. In particular, the cases of input seismic loading (section 2.2) having predominant frequency equal to the first ( $f_q = f_{b1} = 2.8$  Hz) and second ( $f_q = f_{b2} = 4.7$  Hz) natural frequency of the building are shown in Figure 3-11 and Figure 3-12, respectively.

The one-step to two-step ratio of the maximum acceleration at the building top, quantitatively estimating the SSI effect, is  $a_{\max\_1\text{step}}/a_{\max\_2\text{step}} = 0.58$  for  $x$ -direction and  $a_{\max\_1\text{step}}/a_{\max\_2\text{step}} = 0.71$  for  $y$ -direction, in the case where  $f_q = f_{b1} = 2.8$  Hz and  $a_{\max\_1\text{step}}/a_{\max\_2\text{step}} = 0.65$  for  $x$ -direction and  $a_{\max\_1\text{step}}/a_{\max\_2\text{step}} = 0.56$  for  $y$ -direction, in the case where  $f_q = f_{b2} = 4.7$  Hz. SSI effect is observed for both translational mode shapes and, in the structure, it is more pronounced in the direction of the mode shape excited by the input load.

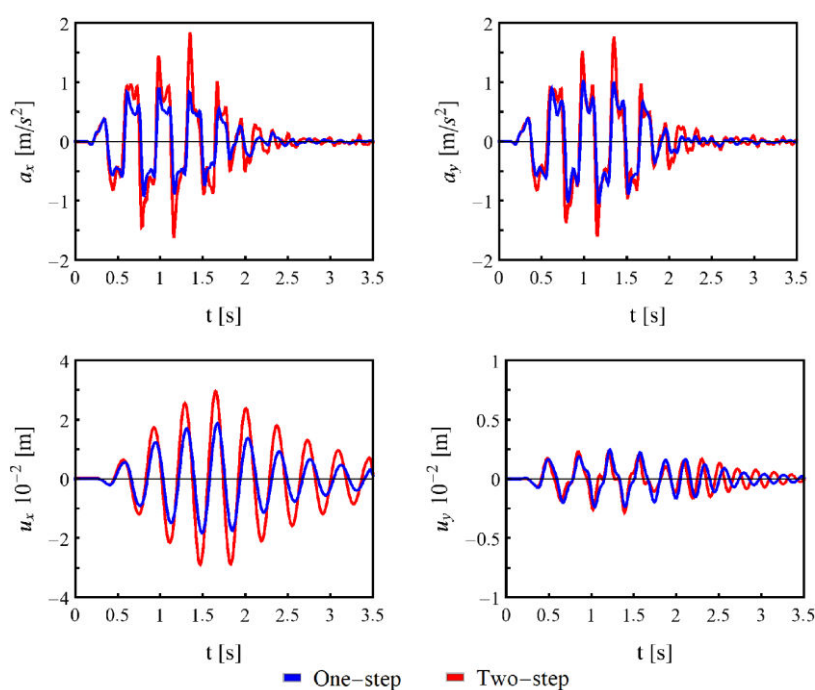


Figure 3-11 Acceleration time history at the building bottom and roof drift at the building top, for the building-soil system composed by a building having fundamental frequencies  $f_{b1} = 2.8$  Hz and  $f_{b2} = 4.7$  Hz and a T-shaped horizontally layered soil having frequency  $f_s = 1.9$  Hz, in the case of earthquake predominant frequency equal to  $f_q = f_{b1} = 2.8$  Hz.

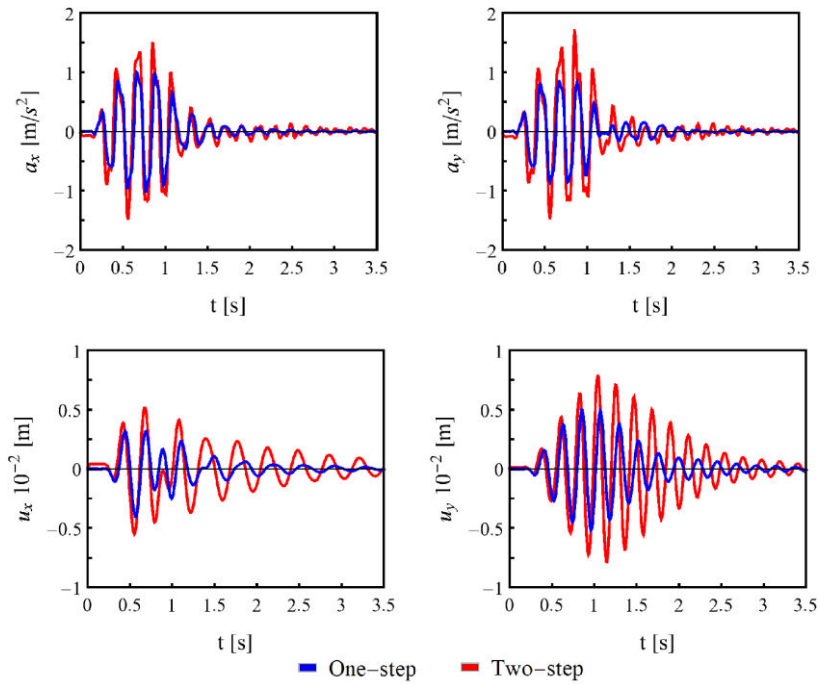


Figure 3-12 Acceleration time history at the building bottom and roof drift at the building top, for the building-soil system composed by a building having fundamental frequencies  $f_{b1} = 2.8$  Hz and  $f_{b2} = 4.7$  Hz and a T-shaped horizontally layered soil having frequency  $f_s = 1.9$  Hz, in the case of earthquake predominant frequency equal to  $f_q = f_{b2} = 4.7$  Hz.

### 3.4. Conclusion

The 1D-3C wave propagation is suitable for SSI analysis in the hypothesis of rigid shallow foundation, with the same seismic motion at the base of all columns. The latter model does not permit to consider the foundation deformability and rocking effects and furthermore cannot simulate the interaction between more buildings.

Therefore, the T-shaped model for 1D-3C seismic wave propagation is introduced (1DT-3C). It is proposed as modeling technique for the simulation of the response of soil and building to earthquakes, taking into account site effects, the foundation deformability, rocking effects and structure-soil-structure interaction. A fully 3-D model is adopted until a fixed depth, where SSI and SSSI effects are considered to modify the ground motion, and for deeper layers a 1-D model is used and supposed a sufficient approximation.

The 1DT-3C approach is verified by comparison with a fully 3-D model, in the case of vertical propagation in a horizontally layered soil. The proposed 1DT-3C modeling technique is an efficient tool for building design allowing SSI to be taken into account in an effective and easy way. In fact, in the case of vertical propagation and homogeneous geotechnical parameters in each soil layer, using unit area solid elements for deeper layers, instead of a 3-D domain,

represents a reduction of computational time without affecting the results. The dynamic equilibrium equation for the soil-structure assembly is solved in 1 hour 11 minutes using the 1DT-3C model and in 14 hours using the 3D-3C model, for an input motion of 120 s, on the CINES cluster using 1 core and 24 nodes.

The use of the 1DT-3C approach for SSI analyses shows that the frequency content of the seismic load imposed at the bottom of the building can be more significant for the building deformation than the concept of expected maximum ground acceleration amplitude, derived from building design in static conditions. The SSI effect is defined as difference between the direct solution of the dynamic equilibrium problem of the assembly of soil and building (one-step solution) and the FF motion applied to a FB building (two-step analysis), in terms of maximum acceleration ratio  $a_{\max\_1\text{step}}/a_{\max\_2\text{step}}$ . It appears more important in the case where the soil is softer, in the case of nonlinear soil behavior. The resonance between building, soil and earthquake frequency content produces an amplified seismic response. SSI effect is observed for both translational mode shapes and it is more pronounced, for the structural behavior, in the direction of the mode shape excited by the input load. In the next chapters, further studies are undertaken using the 1DT-3C wave propagation approach to understand the effect of SSI on the seismic building response and the effect of an adjacent building on structural seismic response.



## **Chapter 4 - Response spectrum for structural design considering soil-structure interaction**

In professional practice, the conception and design of civil engineering structures in seismic zones is done according to national seismic design codes to guarantee safety against earthquake. A good compromise between safety and cost is expected and parameters as the importance of the structure and the probability of seismic event occurrence during the life of a structure are considered. However, design norms evolve following research results and need to be actualized to introduce parameters not considered before.

Concerning environmental parameters in seismic zones, the motion amplification due to site effects is currently taken into account in the FF motion, without including the SSI neither the presence of nearby structures. It is investigated the importance of these parameters and if they should be introduced in the definition of seismic loading for structural design.

A parametric analysis is developed to investigate the interference of the structure response to seismic motion with the response of the constructed soil, considering soil profiles in the different ground types classified by the Eurocode 8 (CEN 2003) and multi-story multi-span RC buildings having frame structure, in a FE scheme suited for engineering practice. Even if previous studies (Jennings and Bielak, 1973; Bielak 1976; Chopra and Gutierrez 1974; Stewart et al., 1999b) considered the predominant effect of the first mode shape on SSI and SSSI, the seismic response of a building depends on several modes, especially considering the prescription of the Eurocode 8 (CEN 2003) where the sum of the effective modal masses for the modes taken into account has to amount to at least 90% of the total mass of the building. Consequently, the 3-D structure of each building has been modeled. The present parametric analyses are done in terms of total stress.

#### 4.1. 1DT-3C wave propagation model

The ground motion at the base of a frame structure and the building motion are estimated taking into account site effects and SSI. The 1D propagation of a three-component seismic wave in a T-shaped soil domain, with a building at the surface, is modeled in a FE scheme, as proposed by Fares et al. (2018). The modeling of a T-shaped soil domain is inspired by the consideration that the SSI is detected in the near-surface soil layers. A fully 3-D soil model is adopted until a fixed depth  $h$  and a 1-D model is used for deeper soil layers.

Shear and pressure waves propagate vertically in  $z$ -direction from the top of the underlying elastic bedrock to the soil surface. The soil basin is assumed as horizontally layered and infinitely extended along the horizontal directions  $x$  and  $y$ , according to the  $xyz$  coordinate system represented in Figure 4-1. Consequently, no strain variation is considered in these directions and, for this reason, a periodic lateral boundary condition is imposed using a tie constraint between lateral surfaces, under the assumption that the lateral limits of the problem are far enough from the structure. Continuity and homogeneity of materials is assumed for the structure and each soil layer.

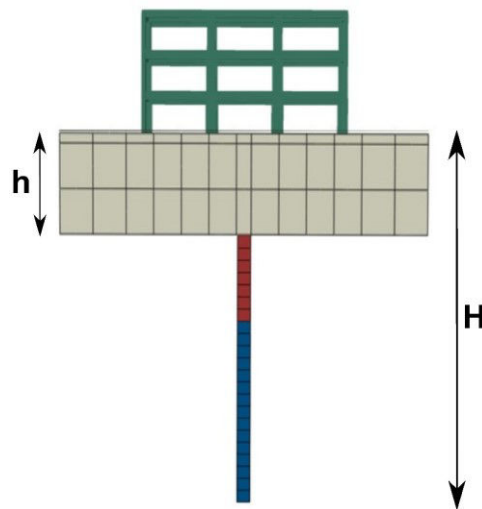


Figure 4-1 2-D section of the 1DT-3C model for SSI analysis where  $h$  is the thickness of the 3-D soil domain and  $H$  is the Thickness of the considered soil until bedrock interface.

The discrete dynamic equilibrium equation is solved directly for the assembly of soil domain and frame structure, including compatibility conditions, 3-D constitutive relation and the imposed boundary conditions. A constraint equation is used to condense out the degrees of freedom at the base of the 3-D soil domain to those at the top of the unit area soil column.

The dynamic process is solved step-by-step by the implicit Hilber-Hughes-Taylor algorithm (Hughes 1987). The three parameters  $\alpha = -0.1$ ,  $\beta = 0.25(1 - \alpha)^2 = 0.3025$  and  $\gamma = 0.5 - \alpha = 0.6$  guarantee an unconditionally numerical stability of the time integration scheme and numerical damping to reduce high frequency content, without having any significant effect on the meaningful, lower frequency response. The time step is automatically selected in the range between  $10^{-4}$  s and the time step used for the input signal sampling.

The Iwan's 3-D elasto-plastic model with isotropic and multilinear kinematic hardening (Iwan 1967; Joyner 1975; Joyner and Chen 1975) is adopted for soil. The main feature of Iwan's model is that the mechanical parameters to calibrate the rheological model are easily obtained from laboratory dynamic tests on soil samples. The rheological formulation is in terms of total stresses. The size of the yield surface is imposed by the backbone curve in the uniaxial stress case. In the present study, the soil behavior is assumed adequately described by a hyperbolic stress-strain curve (Hardin and Drnevich 1972a). This assumption yields a normalized shear modulus reduction curve expressed as  $G/G_0 = 1/(1 + |\gamma/\gamma_r|)$ , where  $G_0$  is the elastic shear modulus and  $\gamma_r$  is a reference shear strain corresponding to an actual tangent shear modulus equivalent to  $G/G_0 = 0.5$ .

The 3-D frame structure is modeled using Timoshenko beam elements. The building shallow foundation is rigidly connected to the soil, node-by-node. A linear constitutive behavior is assumed for the rigid foundation. The rotational degrees of freedom of nodes at the base of building columns are blocked. The damping due to non-structural elements is taken into account by the damping matrix that is assumed as mass and stiffness proportional, according to Rayleigh approach (Chopra 2000).

When the nonlinear behavior of reinforced concrete is taken into account, the constitutive relationships in terms of generalized strains and stresses are deduced by the analysis of a unit-length 3-D beam model, having solid FE for concrete and embedded steel bars. The cross-sectional behavior of RC beams under axial force, bending moment and shear is assumed independent, neglecting the coupling effect. The Lubliner's model (Lubliner et al. 1989) is selected for RC in compression and a linear behavior until the small tensile strength. A bilinear elasto-plastic behavior with hardening is adopted for the steel bars.

#### 4.2. Input data for the parametric analysis

A parametric analysis is developed to study the importance of SSI effects with the building to soil frequency ratio, for the different ground types in the Eurocode 8 classification (CEN 2003), in the cases of linear and nonlinear behavior of the building-soil system.

##### 4.2.1. Soil profiles

Stratigraphy and mechanical parameters of the eleven soil profiles used in the present parametric analysis are given in Table 4-1. Soil properties are assumed constant in each soil layer. The shear wave velocity profile is arbitrary fixed to obtain a selected fundamental frequency of the soil column (Table 4-2)

Table 4-1 Stratigraphy and mechanical properties of the analyzed soil profiles

Depth	Thickness	$\rho$	$v_s$	$v_p$	$\rho$	$v_s$	$v_p$	$\rho$	$v_s$	$v_p$
m	m	kg/m <sup>3</sup>	m/s	m/s	kg/m <sup>3</sup>	m/s	m/s	kg/m <sup>3</sup>	m/s	m/s
		Profile 1			Profile 2			Profile 3		
5	5	1999	450	1741	1957	360	1601	1937	320	1536
15	10	2108	750	2156	2020	500	1815	1976	400	1664
30	15	2166	950	2400	2092	700	2091	2058	600	1957
		Profile 4			Profile 5			Profile 6		
5	5	1930	280	1469	1930	250	1417	1930	240	1400
15	10	1957	360	1601	1947	340	1568	1932	310	1519
30	15	2039	550	1887	2020	500	1815	1994	440	1726
		Profile 7			Profile 8			Profile 9		
5	5	1930	230	1382	1930	220	1365	1930	200	1329
5	10	1930	280	1469	1930	260	1435	1930	240	1400
30	15	1976	400	1664	1957	360	1601	1930	300	1502
		Profile 10			Profile 11					
5	5	1930	180	1293	1930	160	1256			
15	10	1930	210	1347	1930	170	1275			
30	15	1930	250	1417	1930	180	1293			

Table 4-2 Eurocode ground type and fundamental frequency of the analyzed soil profiles

Soil profile	EC8 soil type	Frequency Hz
1	A	7.5
2	B	5.4
3	B	4.5
4	B	4.1
5	B	3.8
6	B	3.4
7	C	3.0
8	C	2.8
9	C	2.5
10	C	2.0
11	D	1.5

The soil density  $\rho$  and the compressional wave velocity  $v_p$  are deduced according to the relationships discussed by Boore (2015). Then, the elastic shear and P-wave moduli ( $G_0 = \rho v_s^2$  and  $M_0 = \rho v_p^2$ , respectively) are estimated. The Poisson's ratio is evaluated as function of the compressional to shear velocity ratio, according to the relation  $\nu = (0.5v_p^2/v_s^2 - 1)/(v_p^2/v_s^2 + 1)$  the reference shear strain is assumed equal to  $\gamma_r = 0.35 \text{ ‰}$  for all layers.

A squared soil area  $A = 25 \text{ m} \times 25 \text{ m}$  is selected for the following analyses, as explained above in Chapter 2 - 2.2, considering also that the maximum dimension of the building floor is 15 m. A 3-D soil domain is modeled until a depth  $h = 5 \text{ m}$ , that corresponds to the interface between the first and second soil layer, and a 1-D model is used in deeper soil layers (see Chapter 3 - 3.2.1).

#### 4.2.2. RC buildings

Concerning the five analyzed buildings, the number of stories is determined according to the desired fundamental frequency of the building (Table 4-3), for the purpose of the analysis. The building floor area is defined arbitrarily, because it is the building height that characterizes the building fundamental frequency.

The column orientation and the floor plan dimensions are indicated in the plans of Figure 2-10 and the mechanical properties of RC beams, altogether, previously introduced in Chapter 2 - 2.2, for the buildings listed in Table 4-3. The sum of considered dead and live load is  $700 \text{ kg/m}^2$ . This load is distributed on beams in x-direction, according to their influence

area, as mass per unit length. The interstory height is 3.2 m. All the analyzed buildings have a translational motion as first mode shape. The rectangular cross-section of beams is given in Table 4-4.

Table 4-3 Fundamental frequency of the analyzed frame structures

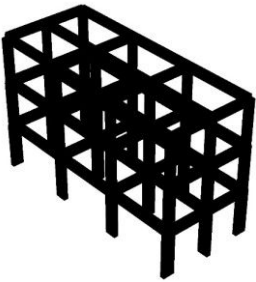
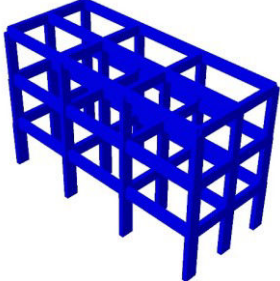
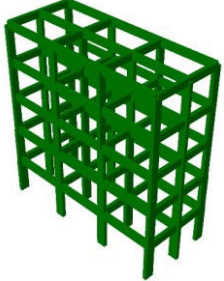
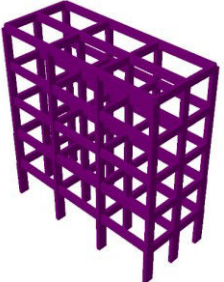
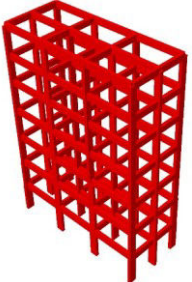
Building	Floors	Floor plan	Frequency Hz	Figure
1	3	a	3.8	
2	3	b	2.8	
3	5	a	2.2	
4	5	b	1.7	
5	7	a	1.5	

Table 4-4 Dimensions of rectangular cross-section beams for the analyzed buildings

Floor	Buildings 1-2		Buildings 3-4		Building 5	
	Beam cm	Column cm	Beam cm	Column cm	Beam cm	Column cm
1	30×80	30×70	30×70	30×80	30×80	30×70
2	30×70	30×70	30×70	30×70	30×70	30×70
3	30×60	30×60	30×60	30×60	30×60	30×60
4			30×60	30×60	30×60	30×60
5			30×60	30×60	30×60	30×60
6					30×60	30×60
7					30×60	30×60

When the nonlinear behavior of RC is taken into account, for the same concrete strength, the Hognestad's parabola is selected as first-loading curve (Appendix A). A cubic characteristic concrete strength  $R_{ck} = 30 \text{ N/mm}^2$  is assumed in compression. The rupture strain is fixed as  $\epsilon_{cu} = 3.5 \text{ ‰}$  and the concrete density is  $\rho_c = 2400 \text{ kg/m}^3$ . A linear behavior is assumed until the concrete tensile strength  $f_{ct} = 3.5 \text{ N/mm}^2$ .

Two 16 mm diameter and three 20 mm diameter longitudinal steel bars are used as top and bottom reinforcement, respectively, and 8 mm diameter stirrups with spacing of 150 mm.

The steel of bars has elastic modulus  $E_s = 210000 \text{ N/mm}^2$ , Poisson's ratio  $\nu_s = 0.3$  and density  $\rho_s = 7850 \text{ kg/m}^3$ . A bilinear elasto-plastic behavior with hardening is adopted, having yield stress  $f_{sy} = 450 \text{ N/mm}^2$ , yield strain  $\epsilon_{sy} = 2 \text{ ‰}$ , rupture stress  $f_{su} = 540 \text{ N/mm}^2$  and rupture strain  $\epsilon_{su} = 10 \text{ ‰}$ .

#### 4.2.3. Input motion

The recorded signal of the 6 April 2009 Mw 6.3 L'Aquila earthquake, and the synthetic narrow band loading (Chapter 2 - 2.2) are used as rock outcropping motion for this parametric analysis.

### 4.3. SSI analysis

The results obtained from the 55 combinations of building-soil system are presented in this section, trying to identify common aspects in the seismic response of buildings, with the purpose of understanding if a correction factor for the design response spectrum proposed by

the Eurocode 8 (CEN 2003) would be enough to take into account the SSI effect for RC buildings with shallow foundation.

#### 4.3.1. *Linear elastic analyses*

According to the purpose of correcting the actual approach imposed by the seismic design code and referring to results obtained by Trombetta et al. (2014) that show more important interaction effects in linear elastic conditions, a first part of this parametric analysis is undertaken considering linear behaving soil and structure.

The variation of the peak acceleration at the top of each analyzed building  $a_{max}$  with the soil natural frequency  $f_s$  is shown in Figure 4-2, in the two cases of synthetic narrow-band seismic loading having predominant frequency  $f_q$  close to the building fundamental frequency  $f_b$  and amplitude  $a_q = 0.1 \text{ m/s}^2$ , and the North-South component of the recorded large-band input loading (the 2009 Mw 6.3 L'Aquila earthquake:  $a_q = 0.26 \text{ m/s}^2$ ,  $f_q = 1.9 \text{ Hz}$ ) applied in the direction of the first mode shape of the building. The peak acceleration is normalized with respect to the maximum amplitude of the seismic load  $a_q$  to highlight the difference between a narrow- and large-band input, independently on the difference in terms of amplitude.

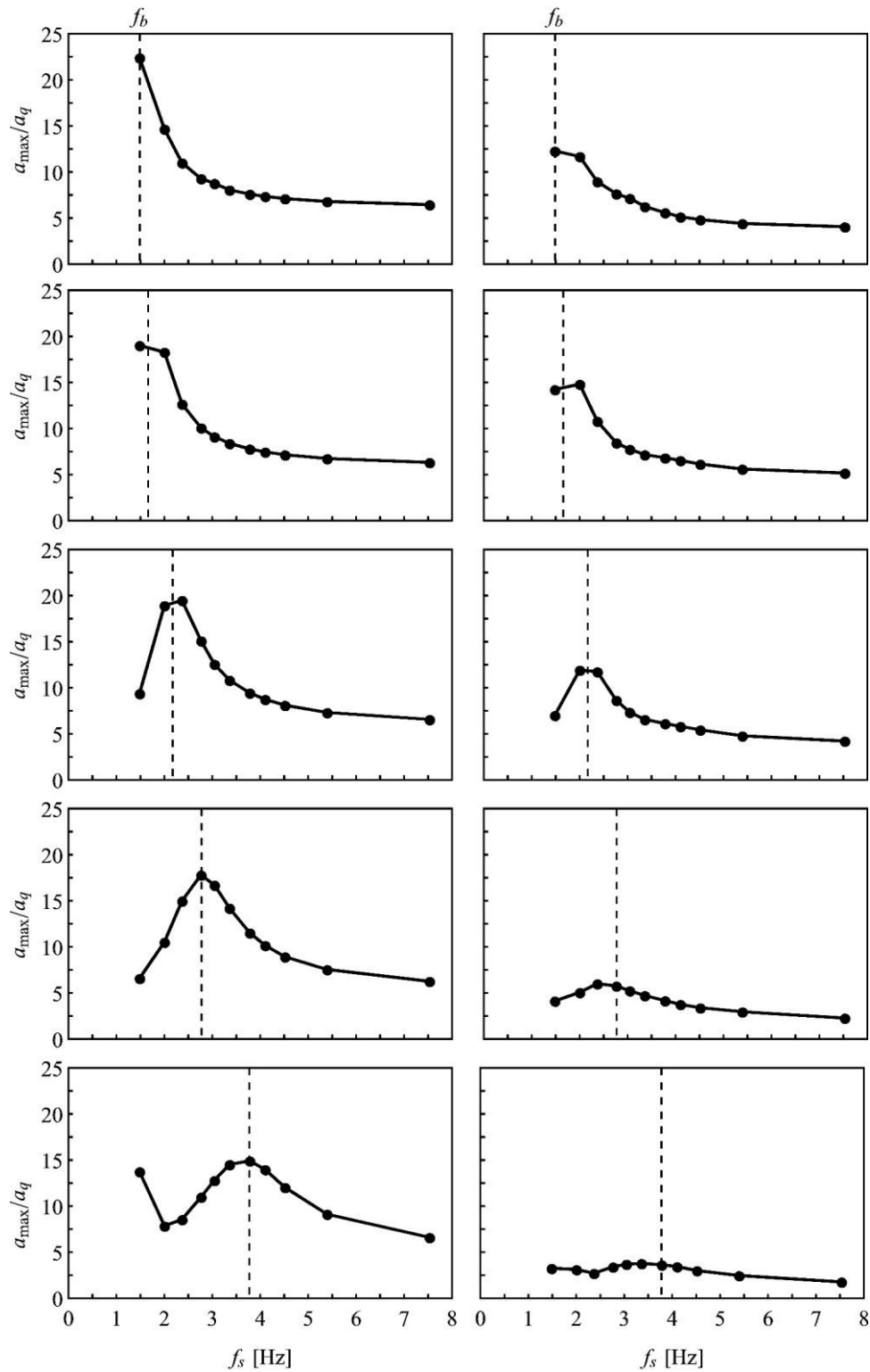


Figure 4-2 Variation of the peak acceleration at the top of five different buildings, normalized with respect to the maximum amplitude of the seismic load  $a_q$ , with the soil fundamental frequency: synthetic signal having predominant frequency close to the building fundamental frequency (left) and 2009 Mw 6.3 L'Aquila earthquake (right) as seismic loading. A vertical dashed line indicates the building fundamental frequency

The peak acceleration at the building top  $a_{\max}$  is maximum for the resonance of soil and building ( $f_s = f_b$ ). This, for both cases of excited building by a synthetic signal having  $f_q = f_b$ , but also for the recorded earthquake with distant predominant frequency. In the case of large-band input signal, the peak acceleration is higher for buildings having fundamental frequency close to  $f_q = 1.9$  Hz. The acceleration peak decreases, compared with resonance ( $f_s = f_b$ ), for  $f_s$  higher and lower than  $f_b$ . The same trend is obtained for all the structures.

Figure 4-3 shows the variation with the building to soil fundamental frequency ratio  $f_b/f_s$  of the peak acceleration at the top of each analyzed building, normalized with respect to its maximum  $\hat{a}_{\max}$ . It is confirmed that a similar result is achieved for all the structures, with a maximum seismic response for the resonance of soil and building.

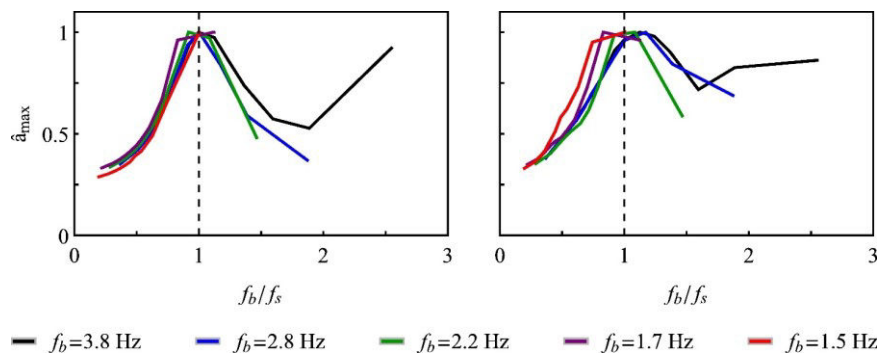


Figure 4-3 Variation with the building to soil fundamental frequency ratio of the peak acceleration at the top of five different buildings, normalized with respect to its maximum: synthetic signal having predominant frequency close to the building fundamental frequency (left) and 2009 Mw 6.3 L'Aquila earthquake (right) as seismic loading

The variation of the peak acceleration at the top of the building in a one-step analysis over that in a two-step analysis  $a_{\max}/a_{\max-2\text{step}}$  with the building to soil fundamental frequency ratio  $f_b/f_s$ , is shown in Figure 4-4, for the five analyzed buildings. According to Saez et al. (2011), the ratio  $a_{\max}/a_{\max-2\text{step}}$  is a measure of SSI effect. In the analyzed cases, the influence of SSI can reduce the acceleration peak at the top of the building of about 30% in the case of narrow-band seismic input having predominant frequency exciting the building fundamental frequency. In the case of large-band recorded earthquake, the influence of SSI can vary between 40% of reduction and 5% of increase of the acceleration peak at the top of the building. The similarity of all the cases is maintained, even if there is more variability in the case of recorded input loading. Consequently, an average curve for all analyzed cases could provide an acceleration ratio  $a_{\max}/a_{\max-2\text{step}}$  to quantify the SSI effect for any structure, known the

building to soil fundamental frequency ratio  $f_b/f_s$  in the studied case. This result suggests the definition of a correcting factor  $cf_{SSI} = a_{\max}/a_{\max-2step}$  of the design response spectrum that takes into consideration the SSI. In other words, the SSI effect could be predicted as  $a_{\max} = cf_{SSI} a_{\max-2step}$ , correcting the result obtained using a two-step analysis by the correcting factor  $cf_{SSI}$  read in a response spectrum considering SSI, similar to that in Figure 4-4, once the structure and soil dynamic features are known in terms of building to soil fundamental frequency ratio  $f_b/f_s$ .

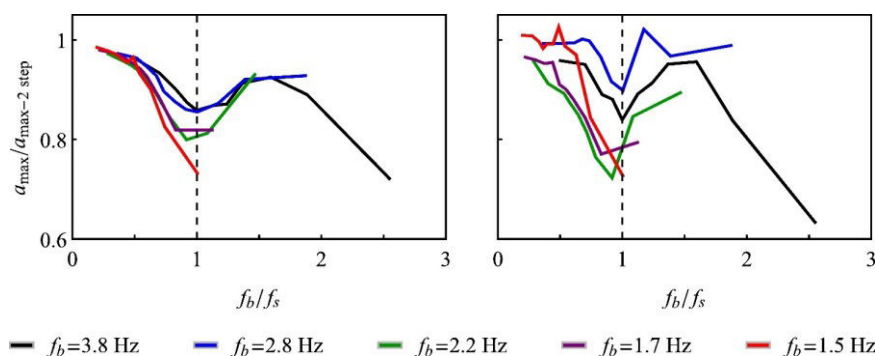


Figure 4-4 Variation of the peak acceleration at the top of the building in a one-step analysis over that in a two-step analysis with the building to soil fundamental frequency ratio, for five different buildings: synthetic signal having predominant frequency close to the building fundamental frequency (left) and 2009 Mw 6.3 L'Aquila earthquake (right) as seismic loading

The variation of the peak acceleration at the top of the building in a one-step analysis over that in a two-step analysis  $a_{\max}/a_{\max-2step}$  with the soil fundamental frequency  $f_s$ , is shown in Figure 4-5, for the five analyzed buildings. The variability of SSI effect is high, for ground types B, C and D, in particular for softer soils. Consequently, it is more convenient to generalize the problem by characterizing SSI with respect to the building to soil fundamental frequency ratio  $f_b/f_s$  (Figure 4-4).

#### 4.3.2. Effect on SSI of soil and structure nonlinear behavior

The variation with the soil natural frequency  $f_s$  of the peak acceleration  $a_{\max}$  at the top of the building is represented in Figure 4-6 in both cases of nonlinear behaving soil and nonlinear behaving structure and soil. The results are shown for a three- and seven-floor RC buildings, having fundamental frequency  $f_b = 1.5$  Hz and  $f_b = 3.8$  Hz, respectively, that are the most flexible and stiffest analyzed buildings (Table 4-3). A synthetic narrow-band seismic loading is used as incident motion at the soil-bedrock interface, having predominant frequency  $f_q$  close

to the building fundamental frequency  $f_b$  and an amplitude of  $a_q = 1.75 \text{ m/s}^2$  to trigger the nonlinear behavior in the soil.

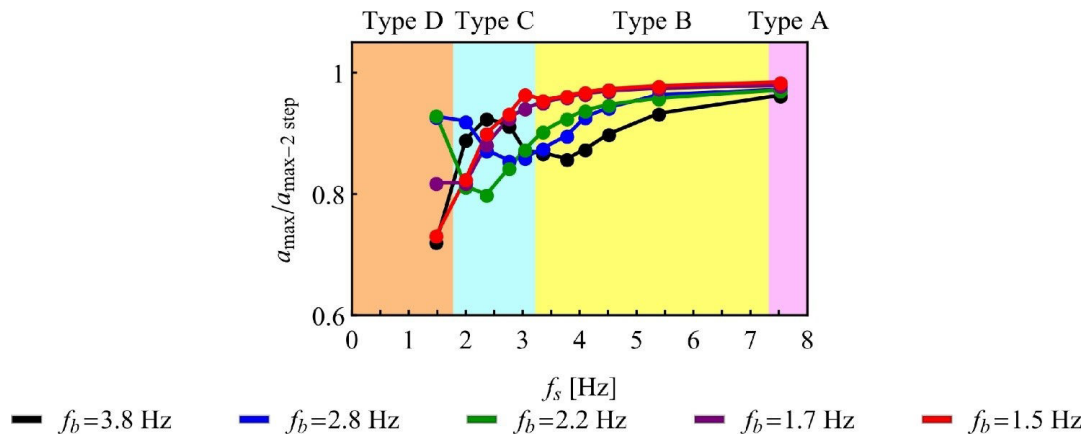


Figure 4-5 Variation of the peak acceleration at the top of the building in a one-step analysis over that in a two-step analysis with the soil fundamental frequency, for five different buildings and a synthetic signal having predominant frequency close to the building fundamental frequency as seismic loading. The ground type range is indicated by vertical boundaries

The peak acceleration at the building top  $a_{\max}$  decreases from stiff to soft soils (decreasing  $f_s$ ). This is due to the soil nonlinearity that, for the same amplitude of the input loading, is more pronounced in softer soils (decreasing  $f_s$ ) and is reduced progressively for stiff soils. A similar trend is obtained for both structures for nonlinear behaving soil, even if the seismic response in the stiffer building is reduced.

A difference is expected between the cases where the nonlinearity of RC is taken into account or not, because the constitutive curves in terms of generalized stresses, used for the nonlinear behaving RC beams, are deduced using a 3-D beam model with embedded steel bars, instead when the RC is assumed linear behaving the only elastic mechanical parameters of concrete are used, under the assumption of uncracked beam.

Comparing the case of nonlinear behaving building-soil system with the case of nonlinearity of soil only, the trend is maintained, but the attained acceleration level at the building top is reduced because the steel reinforcement is taken into account and for the energy dissipation due to the hysteretic behavior in the structure.

The nonlinearity of RC induces higher dissipation in more flexible buildings and a consequent lower acceleration.

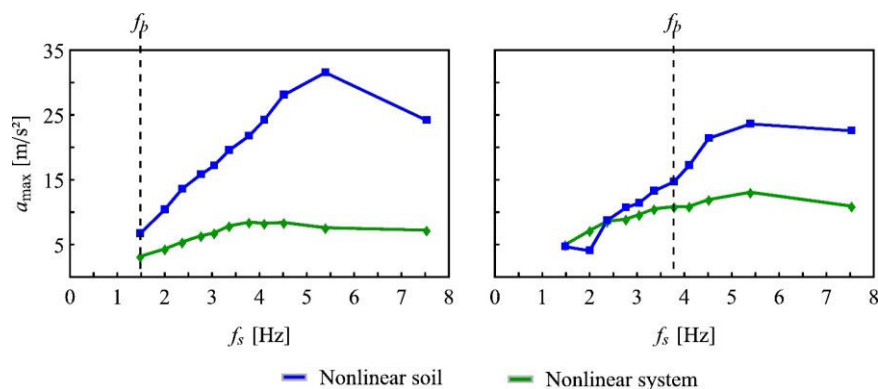


Figure 4-6 Variation with the soil fundamental frequency of the peak acceleration at the top of two buildings having fundamental frequency  $f_b = 1.5$  Hz (left) and  $f_b = 3.8$  Hz (right), in the case of nonlinear behaving soil and nonlinear behaving building-soil system. The synthetic input signal has predominant frequency close to the building fundamental frequency

Figure 4-7 shows the variation with the soil natural frequency  $f_s$  of the peak acceleration  $a_{\max}$  at the top of the same buildings, normalized with respect to the maximum amplitude of the seismic load  $a_q$ , for linear behaving building-soil system, nonlinear behaving soil and nonlinear behaving building-soil system. In softer soils (decreasing  $f_s$ ), the structural seismic response increases for linear behaving soil and decreases for nonlinear behaving soil. The nonlinearity increases with decreasing soil fundamental frequency  $f_s$ , for the same amplitude of the input loading. The peak acceleration at the building top decreases for increasing soil nonlinearity. Similar results are obtained for the seismic response of the building in a softer soil (decreasing  $f_s$  and higher soil nonlinearity), if the building nonlinearity is taken into account or not. The contribution of modeling the effect of steel bars and RC nonlinearity is more remarkable in the case of stiff soil and reduced soil nonlinearity.

The building seismic response is similar for both structures, when the nonlinearity of soil only or soil and structure is taken into account. In fact, the effect of maximum seismic response at the resonance of soil and building ( $f_s = f_b$ ) is lost.

The seismic response is reduced for nonlinear RC due to the energy dissipation and the steel reinforcement, taken into account in the model. Nevertheless, for softer soils, a negligible reduction of the building seismic response is obtained when the nonlinearity of the structure is also taken into account.

Figure 4-8 shows the variation of the peak acceleration  $a_{\max}$  at the top of the two analyzed buildings normalized with respect to the maximum amplitude of the seismic load

$a_q = 1.75 \text{ m/s}^2$ , with the building to soil fundamental frequency ratio  $f_b/f_s$ . The trend of these curves is similar for both structures when the nonlinearity of materials is taken into account.

The comparison of the structural response in the cases where the nonlinearity is taken into account, for the soil only or soil and structure, with the case of linear behaving system (Figure 4-7 and Figure 4-8), suggests the preponderance on the structural seismic response of soil nonlinearity effect, compared with the structure nonlinearity.

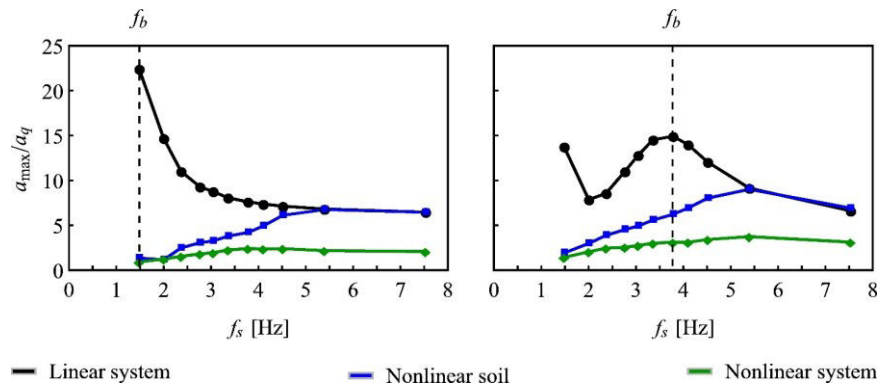


Figure 4-7 Variation with the soil fundamental frequency of the peak acceleration, normalized with respect to the maximum amplitude of the seismic load  $a_q$ , at the top of two buildings having fundamental frequency  $f_b = 1.5$  Hz (left) and  $f_b = 3.8$  Hz (right), for the cases of linear behaving building-soil system, nonlinear behaving soil and nonlinear behaving building-soil system. The synthetic input signal has predominant frequency close to the building fundamental frequency

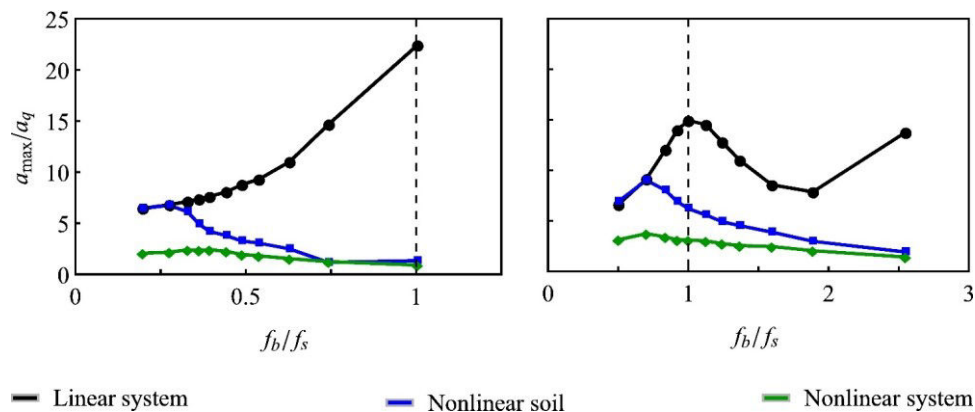


Figure 4-8 Variation with the building to soil fundamental frequency ratio of the peak acceleration, normalized with respect to the maximum amplitude of the seismic load  $a_q$ , at the top of two buildings having fundamental frequency  $f_b = 1.5$  Hz (left) and  $f_b = 3.8$  Hz (right), for the cases of linear behaving building-soil system, nonlinear behaving soil and nonlinear behaving building-soil system. The synthetic input signal has predominant frequency close to the building fundamental frequency

The curves representing the variation with the building to soil fundamental frequency ratio  $f_b/f_s$  of the peak acceleration at the building top, normalized with respect to its maximum ( $\hat{a}_{\max}$ ), have been obtained for different buildings, in the case of linear behaving building-soil systems, and superposed (Figure 4-3), obtaining an average curve with small variance. Nevertheless, according to Figure 4-9, when the nonlinearity of materials is attained, the seismic response of the two analyzed buildings (the stiffest and the supplest), in terms of peak acceleration at the building top, have the same trend with the building to soil fundamental frequency ratio  $f_b/f_s$ , but it attains a maximum for a different value of  $f_b/f_s$  and not for the elastic resonance case ( $f_b/f_s = 1$ ). Moreover, the influence on the structural seismic response of the nonlinearity of RC structure is less pronounced, compared with the effect of soil nonlinearity.

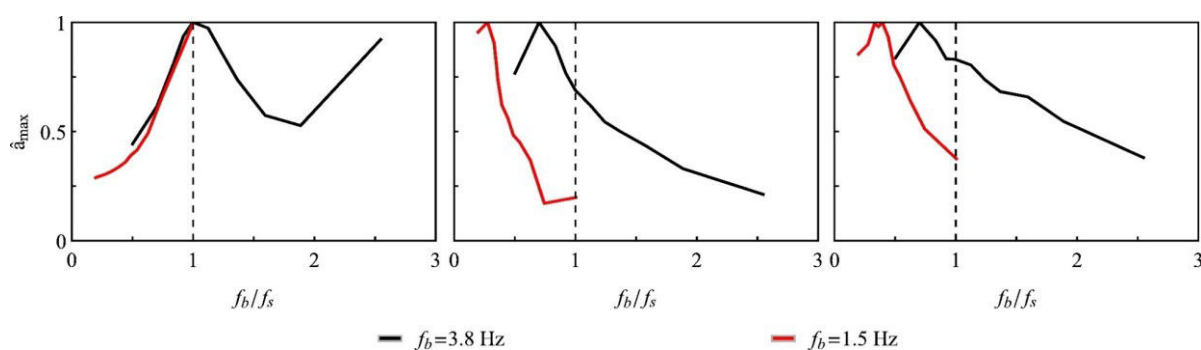


Figure 4-9 Variation with the building to soil fundamental frequency ratio of the peak acceleration at the top of two analyzed buildings, normalized with respect to its maximum, for the cases of linear behaving building-soil system (left), nonlinear behaving soil (middle) and nonlinear behaving building-soil system (right). The synthetic input signal has predominant frequency close to the building fundamental frequency

The attainment of strains in the nonlinear plastic range, for soil or soil and structure, tends to increase the irregularity of the structural seismic response and modifies the vibration frequency during the process. Consequently, the building to soil fundamental frequency ratio  $f_b/f_s$  is modified compared with the elastic regime and the curves in Figure 4-9 do not give similar structural response for all the analyzed buildings, depending only on the parameter  $f_b/f_s$ , as in the case of linear behaving building-soil system (Figure 4-3).

The variation with the building to soil fundamental frequency ratio  $f_b/f_s$  of the peak acceleration at the top of the three- and seven-floor RC buildings, having fundamental frequency  $f_b = 1.5$  Hz and  $f_b = 3.8$  Hz (Table 4-3), respectively, is shown normalized with respect to the peak acceleration at the top of the building in a two-step analysis

( $a_{\max}/a_{\max-2\text{step}}$ ) in Figure 4-10. This, for the cases of linear behaving building-soil system, nonlinear behaving soil and nonlinear behaving building-soil system. Taking into account the nonlinear behavior of materials, the structural seismic response considering SSI becomes unpredictable using a correction factor depending only on the elastic building to soil fundamental frequency ratio  $f_b/f_s$ , applied to a two-step analysis. According to Figure 4-10, the variability of SSI effect is higher when the nonlinearity of materials is taken into account and the nonlinearity of the structure strongly modifies the influence of SSI, compared with the case of nonlinear behaving soil only.

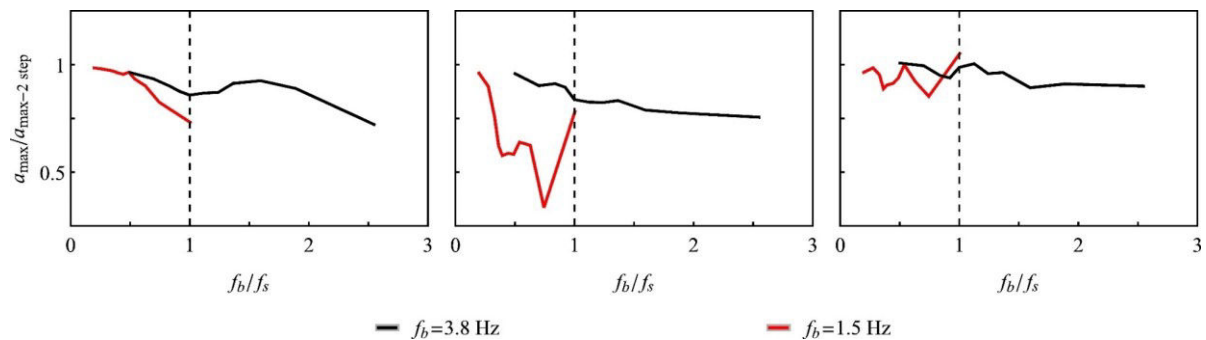


Figure 4-10 Variation with the building to soil fundamental frequency ratio of the peak acceleration at the top of the building in a one-step analysis over that in a two-step analysis, for the two analyzed buildings, in the cases of linear behaving building-soil system (left), nonlinear behaving soil (middle) and nonlinear behaving building-soil system (right). The synthetic input signal has predominant frequency close to the building fundamental frequency

#### 4.4. Conclusion

The extensive application of 3-D SSI models in the usual engineering practice is hindered by the lack of geotechnical data that makes more difficult realizing a reliable soil model and, on the other hand, the dimension of soil domain results in a significant modeling and computation time. The proposed 1DT-3C model, compared with a fully 3-D model, reduces the modeling and computation time. In fact, geotechnical parameters are easy to characterize for a one-dimensional soil model (using a single borehole investigation) and boundary condition definition is simple (the input signal and the absorbing boundary condition are given for only one element. Moreover, the mesh is considerably reduced.

- The SSI, estimated as the peak acceleration at the building top in a one-step analysis over that in a two-step analysis, is maximum for the resonance of soil and building, for both cases of synthetic narrow-band signal exciting the building and for recorded large-band seismic signal, and for the five selected RC frame structures.

- In the analyzed cases, the SSI effect reduces the seismic response of about 30-40% for the resonance of soil and building and can induce some negligible amplification for other values of the building to soil frequency ratio. The results are similar for all the analyzed structures, with an increase of variability in the case of large-band input exciting the building fundamental frequency, compared with the narrow-band input signal.
- In the linear elastic regime, the SSI can be taken into account using a correction factor applied to the result of a two-step analysis (FB building model loaded by a FF seismic signal). This correction factor depends on the building to soil fundamental frequency ratio  $f_b/f_s$ .
- With an increasing soil softness and attained nonlinearity, the structural seismic response increases for linear behaving soil and decreases for nonlinear behaving soil (the attained nonlinearity level increases).
- The effect of soil nonlinearity on the structural seismic response is preponderant compared with the effect of the RC nonlinearity.
- The attainment of strains in the nonlinear plastic range, for soil or soil and structure, tends to increase the irregularity of the structural seismic response. Moreover, the nonlinearity of soil and structure modifies the vibration frequency during the process. Consequently, taking into account the nonlinear behavior of materials, the structural seismic response considering SSI becomes unpredictable using a simple correction factor depending only on the elastic building to soil fundamental frequency ratio  $f_b/f_s$ , applied to a two-step analysis.

The present parametric analysis confirms some results of the literature concerning SSI analyses and shows that general results can be obtained in a linear elastic regime for structural design taking into account SSI. Coupling seismic site effects and SSI for nonlinear behaving materials demands a specific one-step SSI analysis.



## **Chapter 5 - Structure-soil-structure interaction analysis**

The effect of an adjacent structure whose interference passes through the soil (named SSSI) is studied, questioning about the validity of actual seismic design which considers structures isolated from surroundings. The proposed advanced model, suited for engineering practice, can be adopted to explore the coupling of seismic site effects, due to soil stratigraphy and nonlinearity, with dynamic features of superstructures, foundation deformability and earthquake motion.

In this research, a linear behaving soil-building system is used to identify the key parameters that influence the SSSI phenomenon and understand if a simple procedure can be proposed for structural design. This, in the case of two nearby buildings. This work is inspired by the possibility of using vibration barriers for risk mitigation. The idea of an oscillator absorbing the energy of earthquakes and protecting buildings is a smart solution if well designed. It is important to study the phenomenon of SSSI before proposing a procedure for vibration barrier design.

### 5.1. 1DT-3C wave propagation model for SSSI analysis

The proposed 1D-3C wave propagation model for SSI investigations is limited to the case of rigid shallow foundation. Rocking effects cannot be reproduced. Furthermore, the numerical simulation of seismic response of a group of buildings demands a fully 3-D model.

The proposed T soil model for 1DT-3C wave propagation permits the consideration of a city, deep foundation, rocking effect and soil spatial stratigraphy. The modeling of a T-shaped soil domain is inspired by the consideration that the SSI is detected in the near-surface soil layers. A fully 3-D soil model is adopted until a fixed depth  $h$  and a 1-D model is used for deeper soil layers (Figure 5-1).

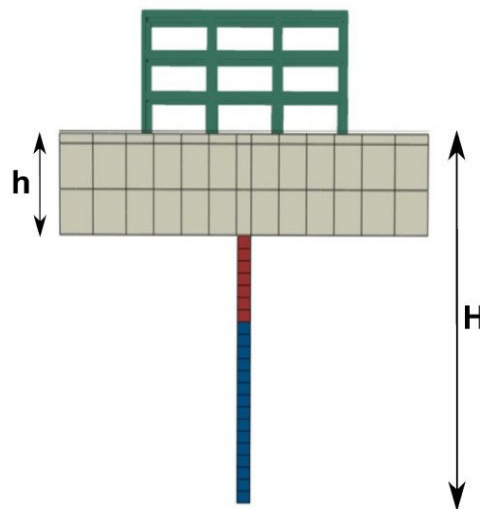


Figure 5-1 2-D section of the 1DT-3C model for SSI analysis where  $h$  is the thickness of the 3-D soil domain and  $H$  is the Thickness of the considered soil until bedrock interface.

### 5.2. Input data for the parametric analysis

A parametric analysis is developed to study the importance of SSSI effects for different ground types in the Eurocode 8 classification (CEN 2003), in the case of linear of the building-soil system.

#### 5.2.1. Soil profiles

Stratigraphy and mechanical parameters of the eleven soil profiles used in the present parametric analysis are given in Table 5-1. Soil properties are assumed constant in each soil layer. The shear wave velocity profile is arbitrary fixed to obtain a selected fundamental frequency of the soil column (Table 5-2).

The soil density  $\rho$  and the compressional wave velocity  $v_p$  are deduced according to the relationships discussed by Boore (2015). Then, the elastic shear and P-wave moduli ( $G_0 = \rho v_s^2$  and  $M_0 = \rho v_p^2$ , respectively) are estimated. The Poisson's ratio is evaluated as function of the compressional to shear velocity ratio, according to the relation  $\nu = (0.5v_p^2/v_s^2 - 1)/(v_p^2/v_s^2 - 1)$ . The reference shear strain is assumed equal to  $\gamma_r = 0.35 \text{ ‰}$  for all layers.

Table 5-1 Stratigraphy and mechanical properties of the analyzed soil profiles

Profile 1				Profile 2				Profile 3			
Depth (m)	$\rho$ (kg/m <sup>3</sup> )	$v_s$ (m/s)	$v_p$ (m/s)	Depth (m)	$\rho$ (kg/m <sup>3</sup> )	$v_s$ (m/s)	$v_p$ (m/s)	Depth (m)	$\rho$ (kg/m <sup>3</sup> )	$v_s$ (m/s)	$v_p$ (m/s)
0-5	1930	220	1365	0-5	1930	180	1293	0-5	1930	160	1256
5-15	1930	260	1435	5-15	1930	210	1347	5-15	1930	170	1275
15-30	1957	360	1601	15-30	1930	250	1417	15-30	1930	180	1293
> 30	2100	1000	2449	> 30	2100	1000	2449	> 30	2100	1000	2449

Table 5-2 Eurocode ground type and fundamental frequency of the analyzed soil profiles

Soil profile	EC8 soil type	Frequency Hz
1	C	2.8
2	C	2.0
3	D	1.5

A squared soil area  $A = 25 \text{ m} \times 25 \text{ m}$  is selected for the following analyses, as explained above in Chapter 2 - 2.2, considering also that the maximum dimension of the building floor is 15 m. A 3-D soil domain is modeled until a depth  $h = 5 \text{ m}$ , that corresponds to the interface between the first and second soil layer, and a 1-D model is used in deeper soil layers (see Chapter 3 - 3.2.1).

### 5.2.2. Buildings characteristics

Concerning the analyzed buildings, the number of stories is determined according to the desired fundamental frequency of the building (Table 5-3), for the purpose of the analysis. The building floor area is defined arbitrarily, because it is the building height that characterizes the building fundamental frequency.

The column orientation and the floor plan dimensions are indicated in the plans of Figure 2-10 and the mechanical properties of RC beams, altogether, previously introduced in Chapter 2 - 2.2, for the buildings listed in Table 5-3.

Table 5-3 Fundamental frequency of the analyzed frame structures

Building	Floors	Floor plan	Frequency Hz
1	3	a	3.8
2	3	b	2.8
3	5	a	2.2
4	7	a	1.5

Table 5-4 Dimensions of rectangular cross-section beams for the analyzed buildings

Floor	Buildings 1-2		Building 3		Building 4	
	Beam cm	Column cm	Beam cm	Column cm	Beam cm	Column cm
1	30×80	30×70	30×70	30×80	30×80	30×70
2	30×70	30×70	30×70	30×70	30×70	30×70
3	30×60	30×60	30×60	30×60	30×60	30×60
4			30×60	30×60	30×60	30×60
5			30×60	30×60	30×60	30×60
6					30×60	30×60
7					30×60	30×60

### 5.2.3. Input motion

The recorded signal of the 6 April 2009 Mw 6.3 L'Aquila earthquake, and the synthetic narrow band loading are used as rock outcropping motion for this parametric analysis (Chapter 2 - 2.2).

## 5.3. SSSI analysis

### 5.3.1. SSSI versus SSI

The 1DT-3C seismic wave propagation model is used to compare the seismic response of a building when it is isolated and in the case of presence of a nearby building, in order to investigate the influence of SSSI.

The analysis is undertaken using the soil profile with  $f_s = 2.8$  Hz (Table 5-1), the 2009 Mw 6.3 L'Aquila earthquake as seismic loading, the buildings in Figure 2-10a, with the same inertia in both orthogonal directions ( $f_x = f_y = 3.8$  Hz), and the building in Figure 2-10b, with different inertia in two orthogonal directions ( $f_x = 2.8$  Hz,  $f_y = 4.7$  Hz).

Table 5-5 Gof of 1DT-3C wave propagation model in the case of a building having a nearby building compared with the case of isolated building.

Compared Models		Position	$\vec{x}$	Anderson Criterion									
				C1	C2	C3	C4	C5	C6	C7	C8	C9	C10
1DT-3C SSSI $f_{b1} = f_{b2}$ $= 3.8$ Hz	1DT-3C SSI $f_b = 3.8$ Hz	$f_b = 3.8$ Hz bldg. base	x	9.7	9.8	9.8	9.9	10	9.9	10	10	9.6	9.8
			y	9.8	9.8	10	10	10	10	10	10	9.3	9.9
			z	9.8	9.9	9.9	10	9.9	10	10	10	9.5	9.8
1DT-3C SSSI $f_{b1} = 3.8$ Hz $f_{b2} = 2.8$ Hz	1DT-3C SSI $f_b = 3.8$ Hz	$f_b = 3.8$ Hz bldg. base	x	9.9	9.9	10	10	10	10	10	10	9.8	10
			y	9.8	9.9	10	10	10	10	10	10	9.5	9.9
			z	9.9	9.9	9.9	10	9.8	10	10	10	9.6	9.9
1DT-3C SSSI $f_{b1} = f_{b2}$ $= 3.8$ Hz	1DT-3C SSI $f_b = 3.8$ Hz	$f_b = 3.8$ Hz bldg. top	x	9.8	9.9	9.9	10	10	10	10	10	9.8	9.9
			y	9.9	9.9	10	10	10	10	10	10	9.8	10
			z	9.8	10	10	10	9.9	10	10	10	9.8	10
1DT-3C SSSI $f_{b1} = 3.8$ Hz $f_{b2} = 2.8$ Hz	1DT-3C SSI $f_b = 3.8$ Hz	$f_b = 3.8$ Hz bldg. top	x	9.8	9.8	10	10	9.9	10	10	10	9.6	9.8
			y	9.8	9.8	10	10	10	10	10	10	9.5	9.9
			z	9.9	9.9	9.9	10	9.8	10	10	10	9.7	9.9
1DT-3C SSSI $f_{b1} = f_{b2}$ $= 2.8$ Hz	1DT-3C SSI $f_b = 2.8$ Hz	$f_b = 2.8$ Hz bldg. base	x	8.2	8.3	9.2	9.9	8.5	9.4	10	9.4	6.3	<b>3.2</b>
			y	8.7	8.9	9.7	8	9.8	9.6	8.8	9.4	<b>5.3</b>	<b>2.8</b>
			z	9.4	9.9	9.8	10	9.9	9.9	10	9.9	8	8.1
1DT-3C SSSI $f_{b1} = 3.8$ Hz	1DT-3C SSI $f_b = 2.8$ Hz	$f_b = 2.8$ Hz bldg. base	x	8.2	8.3	9.3	9.9	8.4	9.4	10	9.4	6.4	<b>3.2</b>
			y	8.6	8.9	9.7	8.1	9.9	9.7	8.8	9.5	<b>5.3</b>	<b>2.6</b>
			z	9.4	9.8	9.7	10	10	9.9	10	9.9	7.9	8
1DT-3C SSSI $f_{b1} = f_{b2}$ $= 2.8$ Hz	1DT-3C SSI $f_b = 2.8$ Hz	$f_b = 2.8$ Hz bldg. top	x	8.9	8.5	10	10	9.9	9.9	10	9.6	6.4	<b>3.4</b>
			y	8.6	8.5	7.3	9.7	9.3	9.6	10	9.5	<b>5.5</b>	<b>3.1</b>
			z	9.2	9.8	9.8	10	10	10	10	9.9	7.7	7.6
1DT-3C SSSI $f_{b1} = 3.8$ Hz $f_{b2} = 2.8$ Hz	1DT-3C SSI $f_b = 2.8$ Hz	$f_b = 2.8$ Hz bldg. top	x	8.9	8.6	9.9	10	10	10	10	9.6	6.5	<b>4</b>
			y	8.5	8.4	<b>5.4</b>	9.2	9.1	9.4	10	9.5	<b>5.5</b>	<b>3</b>
			z	9.3	9.8	9.8	10	10	9.9	10	9.9	7.7	7.5

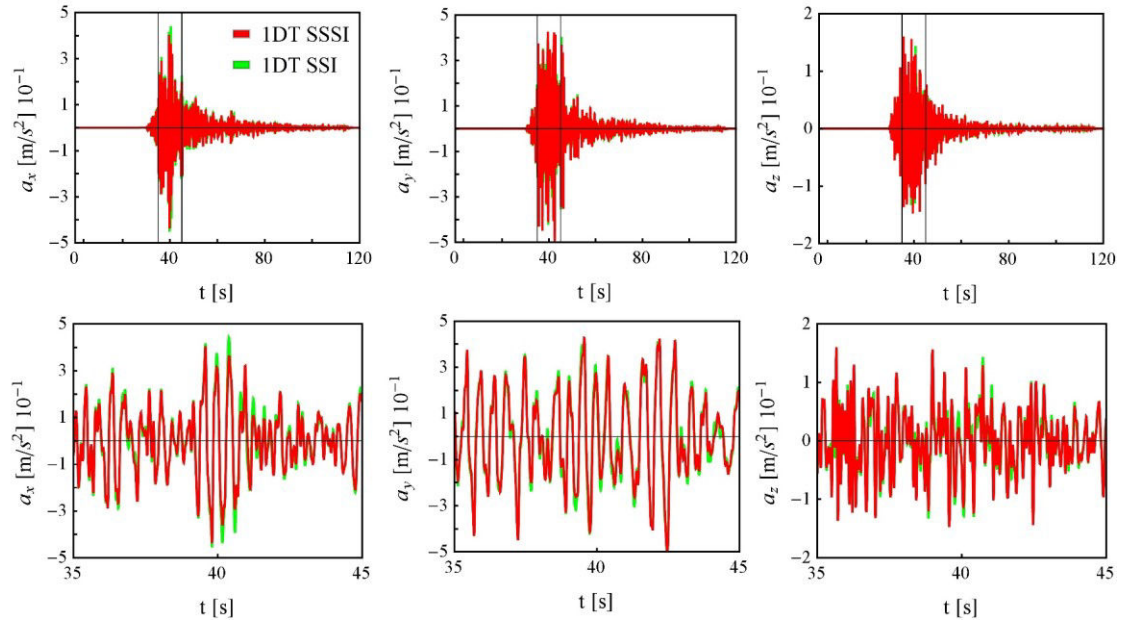


Figure 5-2 Simulated acceleration time history of the building with  $f_{b1} = f_{b2} = 3.8$  Hz at the building bottom, in the case of a nearby building with  $f_{b1} = f_{b2} = 3.8$  Hz, during the input signal duration (top) and in a 10 s time window over the largest amplitudes (bottom).

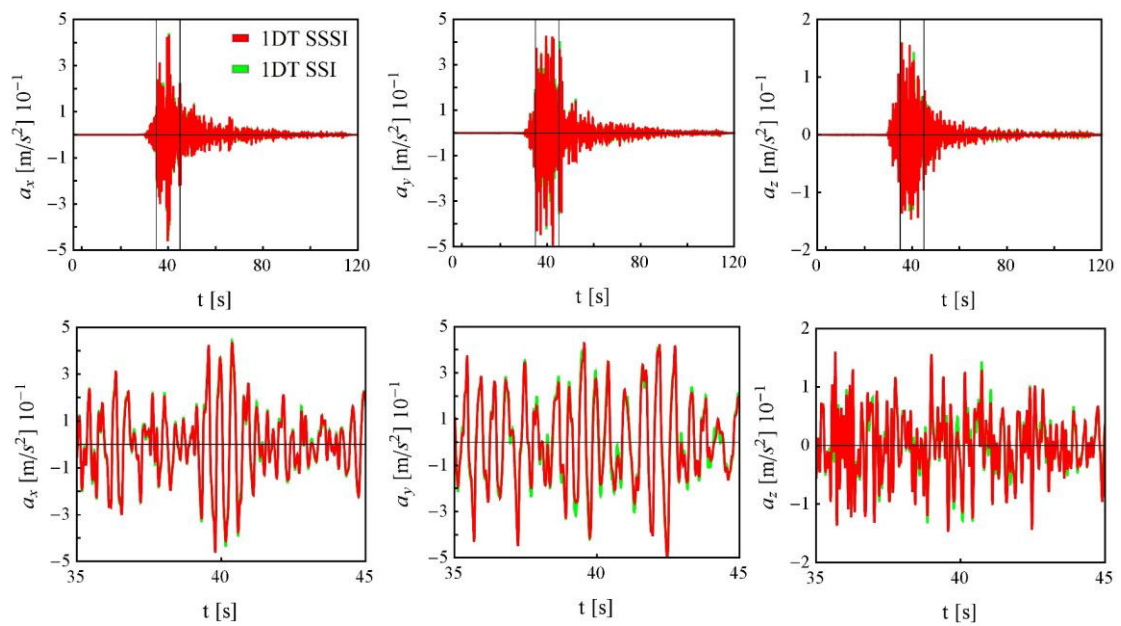


Figure 5-3 Simulated acceleration time history of the building with  $f_{b1} = f_{b2} = 3.8$  Hz at the building bottom, in the case of a nearby building with  $f_{b1} = 2.8$  Hz different than  $f_{b2} = 4.7$  Hz, during the input signal duration (top) and in a 10 s time window over the largest amplitudes (bottom).

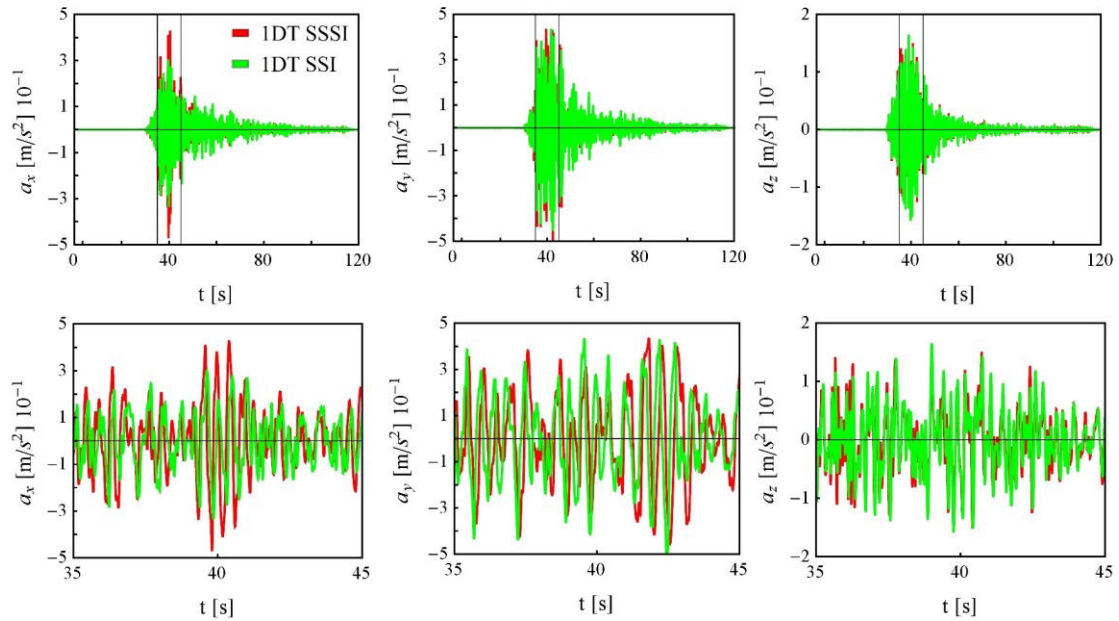


Figure 5-4 Simulated acceleration time history of the building with  $f_{b1} = 2.8$  Hz different than  $f_{b2} = 4.7$  Hz at the building bottom, in the case of a nearby building with  $f_{b1} = 2.8$  Hz different than  $f_{b2} = 4.7$  Hz, during the input signal duration (top) and in a 10 s time window over the largest amplitudes (bottom).

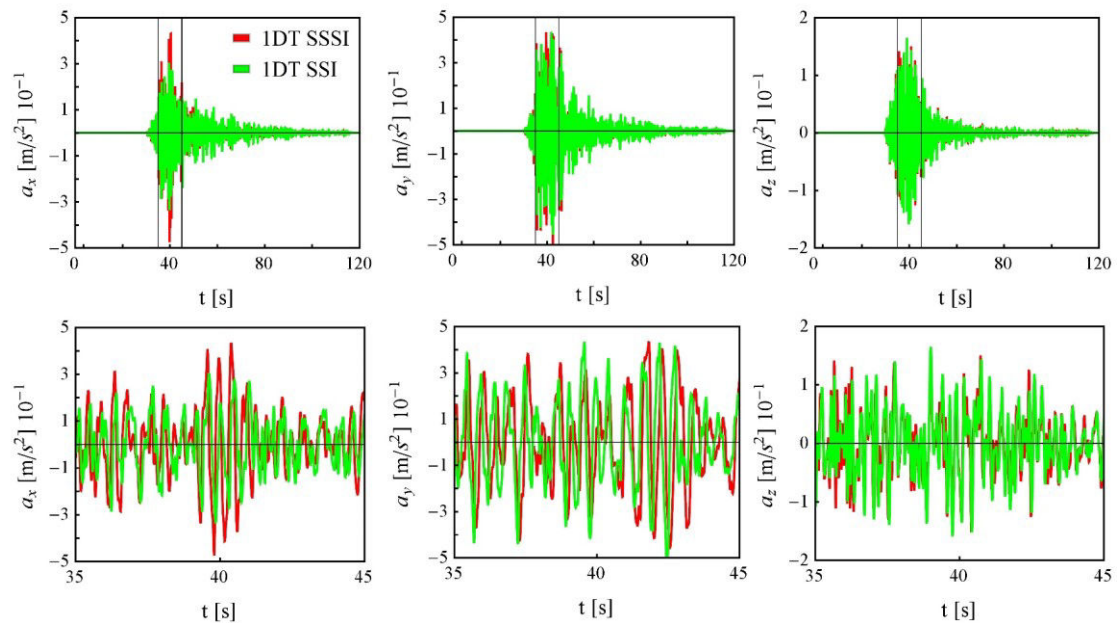


Figure 5-5 Simulated acceleration time history of the building with  $f_{b1} = 2.8$  Hz different than  $f_{b2} = 4.7$  Hz at the building bottom, in the case of a nearby building with  $f_{b1} = f_{b2} = 3.8$  Hz, during the input signal duration (top) and in a 10 s time window over the largest amplitudes (bottom).

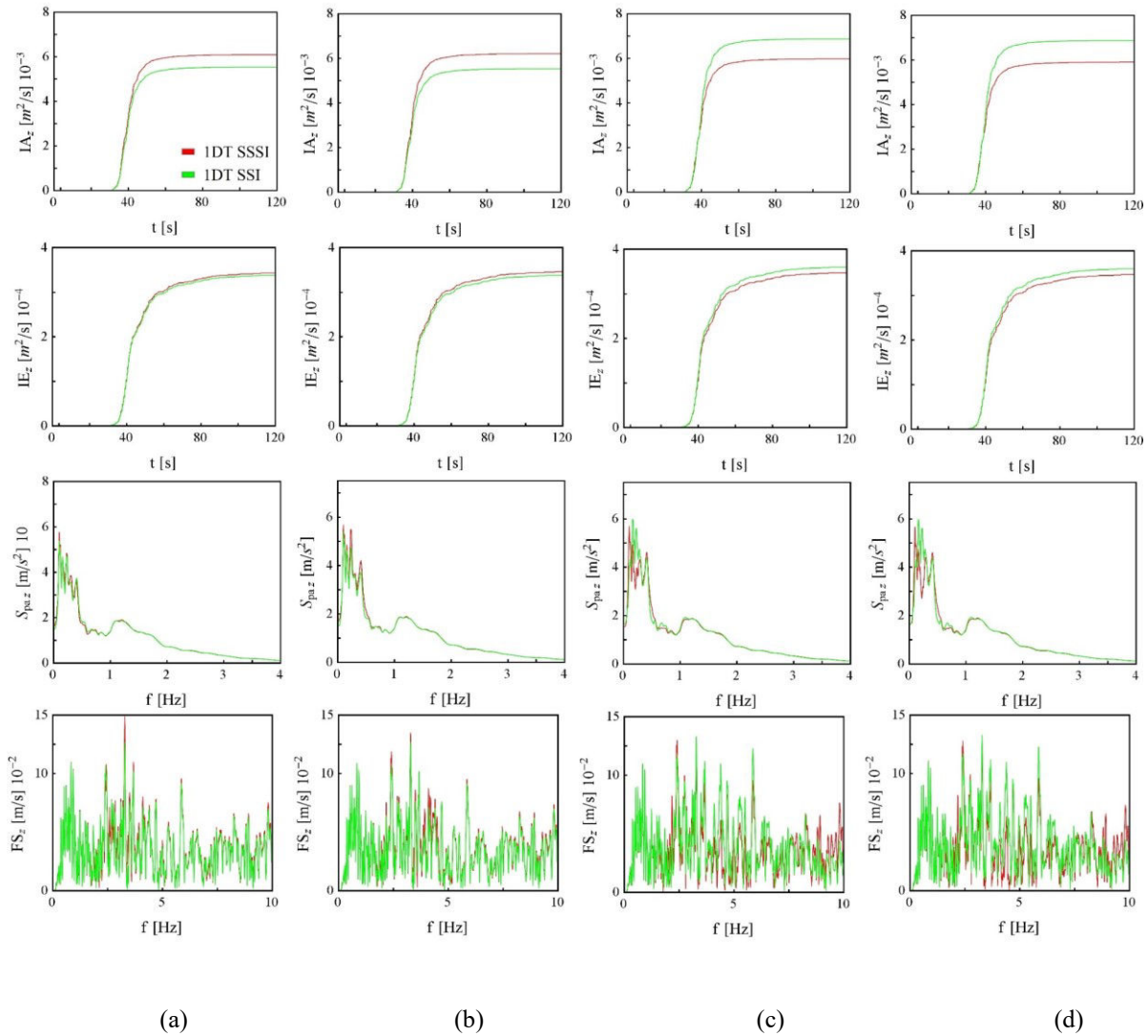


Figure 5-6 Comparison of results obtained using the 1DT-3C wave propagation model for isolated building and SSSI, in terms of Arias integral (AI), energy integral (IE), pseudo-acceleration response spectrum ( $S_{pa}$ ) and Fourier spectrum (FS) for the vertical component (z) of motion and  $f_s = 2.8$  Hz : (a) building with  $f_{b1} = f_{b2} = 3.8$  Hz at the building bottom, in the case of a nearby building with  $f_{b1} = f_{b2} = 3.8$  Hz; (b) building with  $f_{b1} = f_{b2} = 3.8$  Hz at the building bottom, in the case of a nearby building with  $f_{b1} = 2.8$  Hz different than  $f_{b2} = 4.7$  Hz; (c) building with  $f_{b1} = 2.8$  Hz different than  $f_{b2} = 4.7$  Hz at the building bottom, in the case of a nearby building with  $f_{b1} = 2.8$  Hz different than  $f_{b2} = 4.7$  Hz; (d) building with  $f_{b1} = 2.8$  Hz different than  $f_{b2} = 4.7$  Hz at the building bottom, in the case of a nearby building with  $f_{b1} = f_{b2} = 3.8$  Hz.

The seismic response of each building, influenced by a nearby more flexible or stiffer building, is investigated. Anderson's criteria are employed to quantitatively estimate the differences in results obtained, comparing the response of an isolated building and a building having a nearby building (Anderson 2004). According to Gof scores in Table 5-5, Figure 5-2 and Figure 5-3, where the case with one building is assumed as reference and the influence of the nearby building is observed, it can be deduced that the building with  $f_x = f_y = 3.8$  Hz is not influenced

by a nearby building. On the contrary, the building with  $f_x = 2.8\text{Hz}$  different than  $f_y = 4.7\text{ Hz}$  is influenced by SSSI effects, both considered cases.

In terms of peak acceleration of the building with  $f_x = 2.8\text{Hz}$  different than  $f_y = 4.7\text{ Hz}$  at the building bottom (Table 5-5, Figure 5-4, Figure 5-5 and Figure 5-6), the SSSI is observed in the direction of the first translational mode shape (x) of the building.

Considering SSSI gives an amplification of motion, not taken into account when the building is considered isolated.

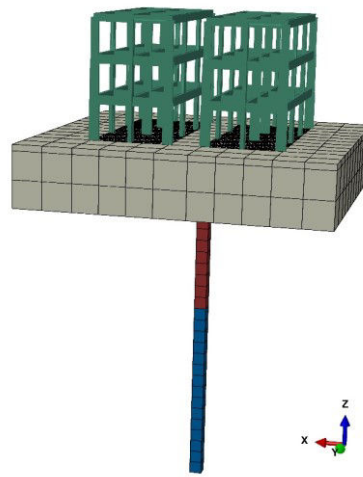


Figure 5-7 1DT-3C for SSSI analysis

### 5.3.2. SSSI parametric analysis

The effect of a nearby building, in the linear elastic regime, is investigated for three buildings (Table 5-3), with fundamental frequency  $f_{b1} = 1.5\text{ Hz}$  (the supplest),  $f_{b1} = 2.2\text{ Hz}$  (intermediate) and  $f_{b1} = 3.8\text{ Hz}$  (the stiffest). Two soft soil profiles have been selected for the analysis, to highlight the SSSI effect, whose natural frequencies are  $f_s = 1.5\text{ Hz}$  (ground type D, see Table 5-2) and  $f_s = 2\text{ Hz}$  (the softest analyzed soil of ground type C).

In a first part of the analysis, the seismic response of a target building having fundamental frequency  $f_{b1}$  is investigated using a synthetic seismic signal having predominant frequency  $f_q = f_{b1}$ , in the five cases where one of the buildings in Table 5-3 is placed at a distance of 1m (distance between the shallow foundations), as shown in Figure 5-7.

The variation of the peak acceleration at the top of the excited building with the fundamental frequency of the nearby building  $f_{b2}$  is shown in Figure 5-8, for the two selected soil profiles.

The seismic response of the excited building does not have important variations caused by the different buildings placed nearby. This effect suggests that when the first mode shape of the building is excited ( $f_q = f_{b1}$ ), the SSSI is less evident. The maximum accelerations at the top of the excited building are obtained in the case of resonance of the building-soil system ( $f_q = f_{b1} = f_s$ ). Whereas, a slight increase of the seismic response of the building having fundamental frequency far from the soil profiles ( $f_{b1} = 3.8$  Hz), is noticed for the softest soil with  $f_s = 1.5$  Hz (Figure 5-8).

In a second part of the analysis, the seismic response of a target building having fundamental frequency  $f_{b1}$  is investigated in the five cases where one of the buildings in Table 5-3, having fundamental frequency  $f_{b2}$ , is placed at a distance of 1 m (Figure 5-7) and the system is excited using a synthetic seismic signal having predominant frequency equal to that of the nearby building ( $f_q = f_{b2}$ ).

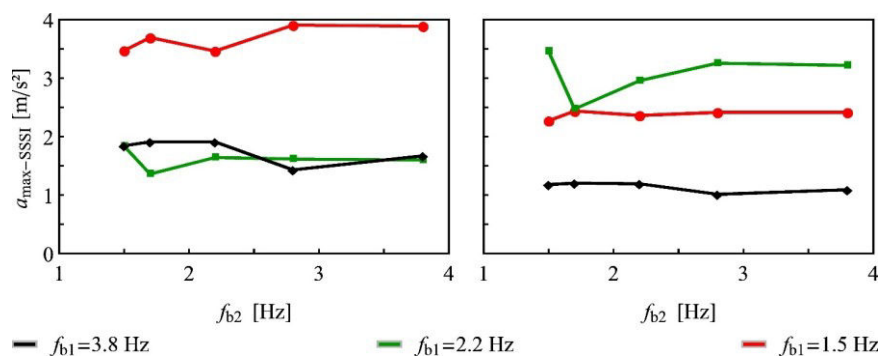


Figure 5-8 Variation of the peak acceleration at the top of the excited building with the natural frequency of the nearby building, for the cases of soil profile having natural frequency  $f_s = 1.5$  Hz (left) and  $f_s = 2$  Hz (right)

Figure 5-9 shows the variation of the peak acceleration at the top of the target building in a SSSI analysis over that in a SSI analysis (single building)  $a_{\max}/a_{\max-SSI}$  with the fundamental frequency of the nearby building  $f_{b2}$ , in a soft soil, in both cases of seismic loading exciting the target ( $f_q = f_{b1}$ ) and nearby building ( $f_q = f_{b2}$ ). A similar result is obtained for the two selected soil profiles. When the target building is excited, its structural seismic response can attain a reduction of 30 % or an increment of 5 %, in the analyzed cases. Instead, when the nearby building is excited the seismic response of the target building has a variability of  $\pm 40$  %.

In a soft soil, when the nearby building is quite stiff ( $f_{b2} > 2.8$  Hz) the SSSI induces a slight 10 % reduction of the seismic response, compared with the case of single building, with small

variability for the different analyzed buildings. This suggests that a stiff nearby building does not have a remarkable effect on the seismic response of the target building.

Figure 5-10 shows the variation of the peak acceleration at the top of the target building in a SSSI analysis over that in a SSI analysis (single building)  $a_{\max}/a_{\max-SSI}$  with the target to nearby building fundamental frequency ratio  $f_{b1}/f_{b2}$ , in a soft soil, in both cases of seismic loading exciting the target ( $f_q = f_{b1}$ ) and nearby building ( $f_q = f_{b2}$ ). A similar result is obtained for the two selected soil profiles. When the target building is excited, its structural seismic response can attain a reduction until 30 % for a target to nearby building fundamental frequency ratio  $f_{b1}/f_{b2} \approx 1.3$ . Instead, when the nearby building is excited, the seismic response of the target building has a variability of  $\pm 40\%$  for a target to nearby building fundamental frequency ratio  $f_{b1}/f_{b2} \approx 1$  that is when the nearby building is more flexible.

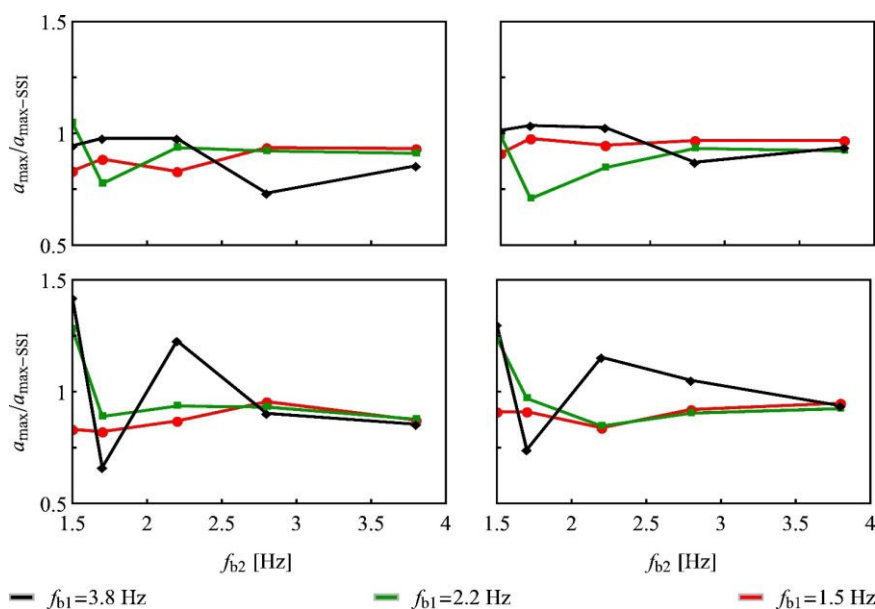


Figure 5-9 Variation of the peak acceleration at the top of the target building in a SSSI analysis over that in a SSI analysis (single excited building) with the natural frequency of the nearby building, for the cases of soil profile having natural frequency  $f_s = 1.5$  Hz (left) and  $f_s = 2$  Hz (right): excited target building (top); excited nearby building (bottom)

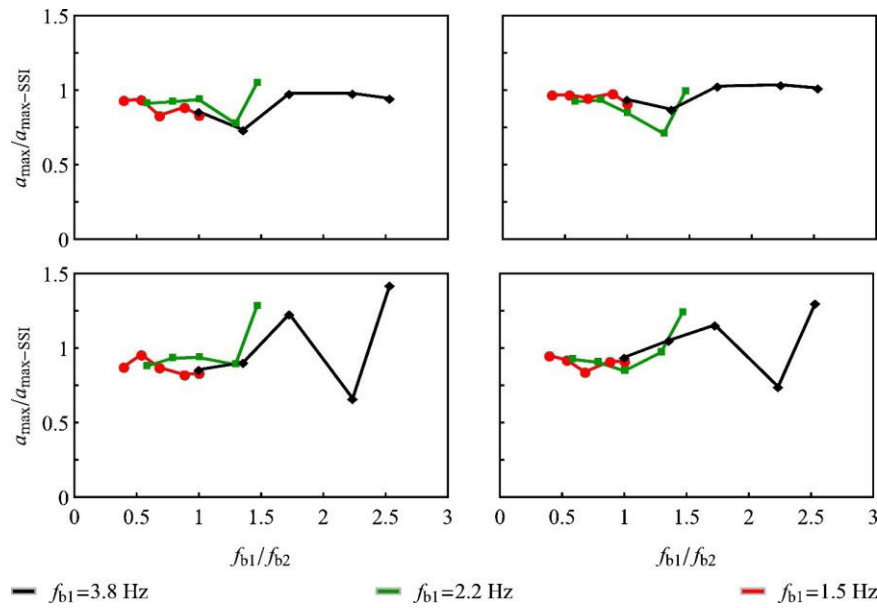


Figure 5-10 Variation of the peak acceleration at the top of the target building in a SSSI analysis over that in a SSI analysis (single excited building) with the target to nearby building fundamental frequency ratio, for the cases of soil profile having natural frequency  $f_s = 1.5$  Hz (left) and  $f_s = 2$  Hz (right): excited target building (top); excited nearby building (bottom)

#### 5.4. Semi-infinite elements and dashpot boundary conditions

When the periodicity assumption is not verified, for example when it is studied the dynamic response of soil representing any irregularity in the geometry, as nonsymmetrical city plan, complicated topography or spatial stratigraphy, it is mandatory to model the far field, where the reflected waves are far enough to be neglected in the analyzed zone an absorbing lateral boundary condition is necessary to dissipate energy out of the truncated domain and reduce soil domain. Nevertheless, due to the impossibility to impose zero horizontal strains, the soil domain to be modeled is much larger compared with the case of periodic lateral condition.

Abaqus software provides semi-infinite elements, to model the far field region, based on the work of Lysmer and Kuhlemeyer (1969) to assembly with the standard finite elements used to model the region of interest (Figure 5-11 ).

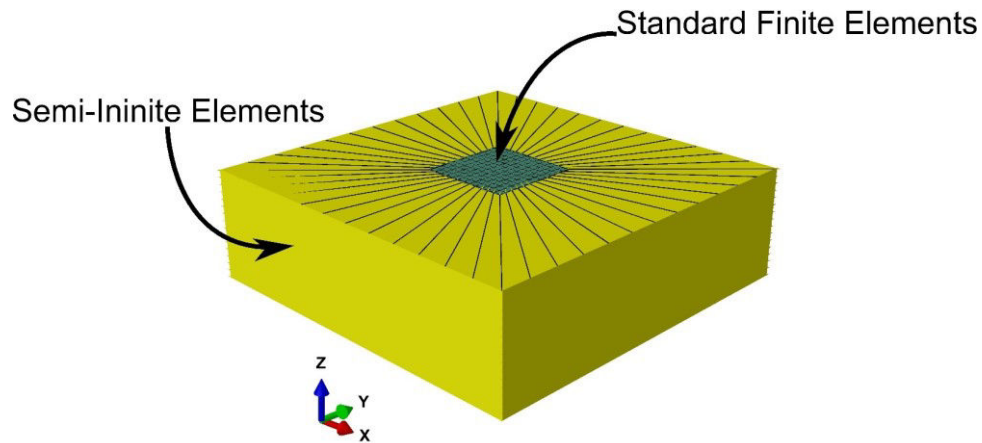


Figure 5-11 3-D soil model with semi-infinite lateral elements.

The solution of the infinite element representing the far field is considered linear and have no influence on the truncated domain of interest and the damping on this boundary is introduced such that

$$\sigma_{xx} = -d_p \dot{u}_x \quad (5-1)$$

and

$$\sigma_{xy} = -d_s \dot{u}_y \quad (5-2)$$

$$\sigma_{xz} = -d_s \dot{u}_z \quad (5-3)$$

where  $d_p$  and  $d_s$  are damping constants,  $\dot{u}_x$ ,  $\dot{u}_y$  and  $\dot{u}_z$  are the velocities in x, y and z direction respectively,  $\sigma_{xx}$  is the normal stress and  $\sigma_{xy}$  and  $\sigma_{xz}$  are shear stresses.

We consider plane wave traveling along the x-direction, to calculate the damping constants,. The solution exists in two forms, the plane longitudinal wave solution, written in this form

$$u_x = f(x \pm v_p t), \quad u_y = u_z = 0 \quad (5-4)$$

and the shear wave solution, written in this form

$$u_y = f(x \pm v_s t), \quad u_x = u_z = 0 \quad (5-5)$$

or

$$u_z = f(x \pm v_s t), \quad u_x = u_y = 0 \quad (5-6)$$

where  $v_p$  and  $v_s$  are the body and shear wave velocity respectively,  $f(x - vt)$  represents the wave propagating in the positive x-direction and  $f(x + vt)$  represents the wave propagating in the negative x-direction.

Now, considering the plane solution  $u_x$  will be equal to the sum of the propagating wave approaching to the boundary  $f(x - v_p t)$  and the reflected wave away from the boundary  $f(x + v_p t)$ , the total displacement is then written  $u_x = f(x - v_p t) + f(x + v_p t)$ . In order to obtain a silent boundary, the reflection is set equal to zero  $f(x + v_p t) = 0$ , which implies that the damping coefficient is written as following

$$d_p = \rho v_p \quad (5-7)$$

where  $\rho$  is the soil density.

Similarly,

$$d_s = \rho v_s \quad (5-8)$$

Proof:

$$u_x = f(x - v_p t) + f(x + v_p t) \quad (5-9)$$

$$\dot{u}_x = -v_p [f'(x - v_p t) - f'(x + v_p t)] \quad (5-10)$$

$$\varepsilon = 1/2 [\partial u / \partial x + (\partial u / \partial x)^T] \quad (5-11)$$

$$\varepsilon_{xx} = f'(x - v_p t) + f'(x + v_p t)$$

$$\boldsymbol{\sigma} = \lambda \mathbf{II} : \boldsymbol{\varepsilon} + 2G \boldsymbol{\varepsilon}$$

$$\begin{aligned} \sigma_{xx} &= (\lambda + 2G)[f'(x - v_p t) + f'(x + v_p t)] \\ &= d_p v_p [f'(x - v_p t) - f'(x + v_p t)] \end{aligned} \quad (5-12)$$

Since  $f(x + v_p t) = 0$ ,  $f'(x + v_p t)$  is then equal to 0 and  $f'(x - v_p t) \neq 0$ ,

$$\lambda + 2G = d_p v_p \quad (5-13)$$

$$d_p = (\lambda + 2G) / c_p \quad (5-14)$$

where  $\lambda$  is Lamé's constant,  $\lambda = E\nu/(1 + \nu)(1 - 2\nu)$ ,  $G$  is the shear modulus  $G = E/2(1 + \nu) = 1/2 (\rho v_p^2 - \lambda) = \rho v_s^2$ ,  $\nu$  and  $E$  are the Poisson's ratio and the Young's modulus, respectively.

Hence,

$$d_p = \rho v_p \quad (5-15)$$

#### 5.4.1. Semi-infinite elements vs dashpots

A verification is undertaken using dashpot (Figure 5-12a) and semi-infinite elements (Figure 5-12b) as lateral boundary condition. The 3D-3C model is used for a FF analysis of a homogeneous one-layer soil of 30 m depth. The soil parameters are density equal to 1930 Kg/m<sup>3</sup>, Young modulus equal to 253219 10<sup>3</sup> N/m<sup>2</sup> and a Poisson ratio equal to 0.4875, is considered. The frequency of this soil profile is  $f_s = 1.75$  Hz.

The narrow band synthetic signal with  $f_q = 3.8$  Hz is imposed at the soil-bedrock interface (Chapter 2 - 2.2).

Figure 5-13 shows the comparison between the FF response of the 3D-3C model using dashpot or semi-infinite elements as lateral boundary condition. The time histories for the acceleration registered at the top of the FF soil are similar in both lateral boundary conditions.

Consequently, this test confirms that both modeling techniques are equivalent.

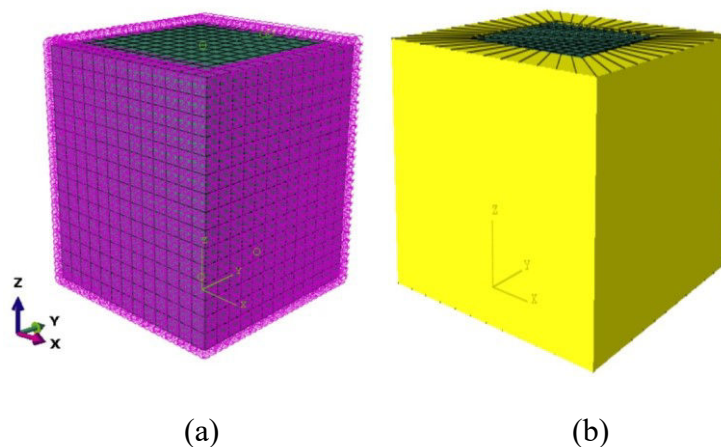


Figure 5-12 3D-3C modeled using lateral boundary condition as linear dashpots (a) as semi-infinite elements (b).

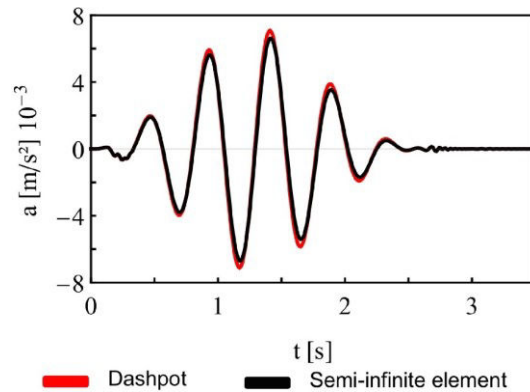


Figure 5-13 Comparison between lateral boundary conditions; dashpots and semi-infinite elements in a 3D-3C FF analysis: acceleration time history at the soil top.

#### 5.4.2. Domain truncation definition

In this analysis the 3D-3C model having semi-infinite lateral boundary condition is used for a FF analysis of the homogeneous one-layer soil presented in section 5.4.1, subjected to a narrow band synthetic signal with  $f_q = 1.75$  Hz at the soil-bedrock interface (Chapter 2 - 2.2).

In order to define the dimension of the truncated domain, a parametric analysis is run using several dimensions for the finite domain:  $25 \times 25$  m<sup>2</sup>,  $80 \times 80$  m<sup>2</sup>,  $150 \times 150$  m<sup>2</sup>,  $300 \times 300$  m<sup>2</sup>, the frequency is calculated for each case using modal analysis.

Figure 5-14 shows the variation of the soil frequency with the dimension of the soil. It is noticed that in order to get the frequency of the soil obtained using a periodic condition, a large domain needs to be modeled using the semi-infinite elements as lateral boundary condition. Hence, the use of the semi-infinite or dashpots as absorbing lateral boundary conditions is only interesting when modeling a large-scale geometry, as a city, or in the case of important site or site-city effects where the periodicity is not verified and it is required a “far” field for the waves to dissipate. Therefore, for engineering practice the tie boundary condition remains the preferred lateral boundary condition for SSI and SSSI analysis.

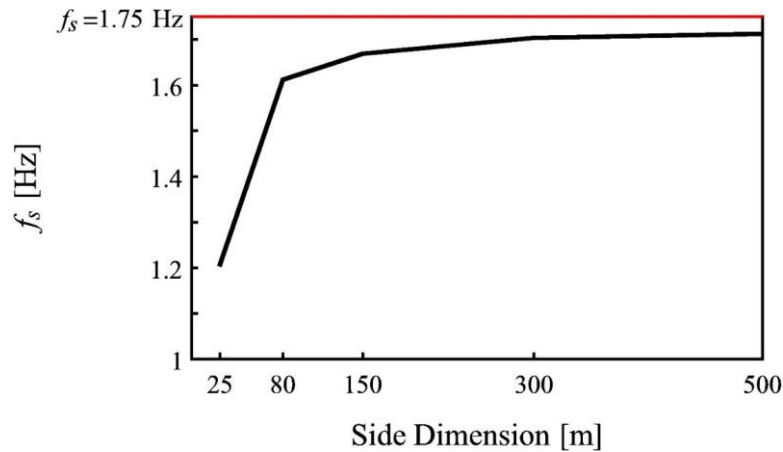


Figure 5-14 Variation of the soil frequency with the side dimension of the, squared geometry, finite domain.

### 5.5. Conclusion

The analysis done using the 1DT-3C modeling technique show that SSSI is observed in the direction of the first translational mode shape of the building. Considering SSSI gives an amplification of motion, not taken into account when only an isolated building is considered. In addition;

- In a soft soil, the seismic response of the excited building does not have important variations caused by the different buildings placed nearby. This effect suggests that when the first mode shape of the building is excited ( $f_q = f_{b1}$ ), the SSSI is less evident.
- The structural seismic response in a SSSI analysis, compared with the case of single building, attains 30 % of reduction and the variability is less pronounced, when the target building is excited. Instead, when the nearby building is excited the seismic response of the target building has a variability of  $\pm 40$  %.
- In a soft soil, a stiff nearby building does not have a remarkable effect on the seismic response of the target building, inducing a slight 10 % reduction of the seismic response, compared with the case of single building, with small variability for the different buildings.
- In a soft soil, when the target building is excited, its structural seismic response can attain a reduction until 30 % for a target to nearby building fundamental frequency ratio  $f_{b1}/f_{b2} \approx 1.3$ .

- In a soft soil, when the nearby building is excited, the seismic response of the target building has a variability of  $\pm 40\%$  when the nearby building is more flexible, for a target to nearby building fundamental frequency ratio  $f_{b1}/f_{b2} \approx 1.3$ .

- The 3D-3C model is considered to study lateral boundary condition influence on soil response. The periodicity lateral boundary condition that induces zero horizontal stresses in the soil, remains the preferred assumption for engineering practice, due to the important reduction of the soil domain to analyze. When the periodicity assumption is not verified, the dashpots represent a satisfactory absorbing boundary condition. They can be applied as lateral boundary condition. However, the modeled soil domain becomes important, because the condition of zero horizontal stresses is not imposed but is attained using huge soil domain.

The increased number of influencing parameters in a SSSI analysis (stiffness of soil, relative stiffness of buildings and which building is excited) demands further work for a generalization of results.

## Chapter 6 - Conclusions and perspectives

In professional practice, the concept of design of a civil engineering structure that resists to horizontal forces was introduced in the 1970s in European seismic design codes to guarantee safety against earthquakes and other phenomena that acts horizontally on a structure as wind. However, design norms advance according to new findings and with the increasing progress of computer capacities. Today, the European seismic design codes still do not consider SSI and SSSI in the conception of structures. This research proposes modeling techniques to evaluate soil and structure dynamic responses to earthquakes, taking into account SSI and SSSI for conception purposes. This research aims to introduce in building design parameters taking into account SSI and in the urban planning the concept of SSSI.

The 3-D soil model permits taking into account the spatial variability of soil properties, topography effects, foundation deformability, rocking effects and the presence of a group of buildings at the soil surface. On the other hand, the 1-D model avoids modeling problems related to the definition of lateral boundary conditions and the lack of geotechnical data to produce a detailed 3-D soil model and strongly reduces the computational time. A one-direction three-component (1D-3C) seismic wave propagation approach is proposed to take into account SSI in professional practice using any commercial FE code. The seismic response of soil and building can be simulated considering site effects and soil-structure interaction for linear and nonlinear soil behavior.

The 1D-3C wave propagation model for SSI is limited to the assumption of rigid shallow foundation, and negligible rocking effects. The 1DT-3C seismic wave propagation approach is proposed as modeling technique for the simulation of the seismic response of soil and building, taking into account site effects, the foundation deformability, rocking effects and, eventually, SSSI. The 1DT model consists on adopting a fully 3-D model until a fixed depth, where SSI and SSSI effects are considered to modify the ground motion and a 1-D model is supposed a sufficient approximation.

The 1DT-3C wave propagation approach is verified by comparison with a fully 3-D model, in the case of vertical propagation in a horizontally layered soil, considering linear and nonlinear soil behavior. The proposed 1DT-3C modeling technique is an efficient tool for building design allowing SSI to be taken into account in an effective and easy way, providing benefits in modeling and computation time comparing to a fully 3-D model. In fact, geotechnical parameters are easy to characterize for a one-dimensional soil model (using a single borehole

investigation) and boundary condition definition is simple (the input signal and the absorbing boundary condition are given for only one element moreover, the mesh is considerably reduced. The dynamic equilibrium equation for the soil-structure assembly is solved in 1 hour 11 minutes using the 1DT-3C model and in 14 hours using the 3D-3C model, for an input motion of 120 s, on the CINES cluster using 1 core and 24 nodes.

The proposed 1DT-3C approach is used modeling different soil profiles and structure frames in the objective to understand the SSI phenomenon. The results for SSI analyses show that:

- The frequency content of the seismic load imposed at the bottom of the building can be more significant for the building deformation than the concept of expected maximum ground acceleration amplitude, derived from building design in static conditions.
- The SSI effect appears more important in the case where the soil is softer.
- The resonance between building, soil and earthquake frequency content produces an amplified seismic response.
- The SSI effect is observed at the soil surface for both translational mode shapes and it is more pronounced, for the structural behavior, in the direction of the building mode shape excited by the input load.

The results confirm the impact of SSI effect on responses of both soil and buildings. Further studies are undertaken, using the 1DT-3C wave propagation approach, to understand the effect of SSI on the structural seismic response for building seismic design. The SSI effect, defined as the difference between the direct solution of the dynamic equilibrium problem of the assembly of soil and building (one-step solution) and the FF motion applied to a fixed-base building (two-step analysis), in terms of maximum acceleration ratio  $a_{\max\_1\text{step}}/a_{\max\_2\text{step}}$ , is estimated for different cases. A parametric analysis combining 11 soil profiles and 5 different frame structures is undertaken, in linear elastic regime, using a synthetic narrow-band signal with predominant frequency equal to that of the structure and a recorded large-band seismic signal of L'Aquila earthquake (Mw 6.3). The results show that:

- The SSI ratio  $a_{\max\_1\text{step}}/a_{\max\_2\text{step}}$  is maximum for the resonance of soil and building, for both cases of synthetic narrow-band signal exciting the building and for recorded large-band seismic signal, and for the five selected RC frame structures.
- In the analyzed cases, the SSI effect reduces the seismic response of about 30-40% for the resonance of soil and building and can induce some negligible amplification for

other values of the building to soil frequency ratio. The results are similar for all the analyzed structures, with an increase of variability in the case of large-band input exciting the building fundamental frequency, compared with the narrow-band input signal.

- The SSI can be taken into account using a correction factor applied to the result of a two-step analysis (FB building model loaded by a FF seismic signal). This correction factor depends on the building to soil fundamental frequency ratio  $f_b/f_s$ .
- The variability of SSI effect is high, for ground types B, C and D, in particular for softer soils. Consequently, it is more convenient to generalize the problem by characterizing SSI with respect to the building to soil fundamental frequency ratio  $f_b/f_s$ .

This parametric analysis is repeated to investigate the influence of nonlinear soil behavior and nonlinear RC behavior on structural seismic response and SSI, compared with the linear behaving assumption. The results give:

- With an increasing soil softness and attained nonlinearity, the structural seismic response increases for linear behaving soil and decreases for nonlinear behaving soil (the attained nonlinearity level increases).
- The effect of soil nonlinearity on the structural seismic response is preponderant compared with the effect of the RC nonlinearity.
- The attainment of strains in the nonlinear plastic range, for soil or soil and structure, tends to increase the irregularity of the structural seismic response. Moreover, the nonlinearity of soil and structure modifies the vibration frequency during the process. Consequently, taking into account the nonlinear behavior of materials, the structural seismic response considering SSI becomes unpredictable using a simple correction factor depending only on the elastic building to soil fundamental frequency ratio  $f_b/f_s$ , applied to a two-step analysis.

This parametric analysis confirms some results of the literature concerning SSI analyses and shows that general results can be obtained in a linear elastic regime for structural design taking into account SSI. Coupling seismic site effects and SSI for nonlinear behaving materials demands a specific one-step SSI analysis.

A parametric analysis, using the 1DT-3C modeling technique in the linear elastic regime, is developed to study the influence of SSSI on a target building having different nearby structure. Results show that:

- SSSI is observed in the direction of the first translational mode shape of the building. Considering SSSI gives an amplification of motion, not taken into account when only an isolated building is considered.
- In a soft soil, the seismic response of the excited building does not have important variations caused by the different buildings placed nearby. This effect suggests that when the first mode shape of the building is excited ( $f_q = f_{b1}$ ), the SSSI is less evident.
- The structural seismic response in a SSSI analysis, compared with the case of single building, attains 30 % of reduction and the variability is less pronounced, when the target building is excited. Instead, when the nearby building is excited the seismic response of the target building has a variability of  $\pm 40$  %.
- In a soft soil, a stiff nearby building does not have a remarkable effect on the seismic response of the target building, inducing a slight 10 % reduction of the seismic response, compared with the case of single building, with small variability for the different buildings.
- In a soft soil, when the target building is excited, its structural seismic response can attain a reduction until 30 % for a target to nearby building fundamental frequency ratio  $f_{b1}/f_{b2} \approx 1.3$ .
- In a soft soil, when the nearby building is excited, the seismic response of the target building has a variability of  $\pm 40$  % when the nearby building is more flexible, for a target to nearby building fundamental frequency ratio  $f_{b1}/f_{b2} \approx 1.3$ .
- The periodicity lateral boundary condition that induces zero horizontal stresses in the soil, remains the preferred assumption for engineering practice, due to the important reduction of the soil domain to analyze. When the periodicity assumption is not verified, the dashpots represent a satisfactory absorbing boundary condition. They can be applied as lateral boundary condition. However, the modeled soil domain becomes important, because the condition of zero horizontal stresses is not imposed but is attained using huge soil domain. The increased number of influencing parameters in a SSSI analysis

(stiffness of soil, relative stiffness of buildings and which building is excited) demands further work for a generalization of results.

In conclusion, this research provides a 1DT-3C modeling technique to study SSI and SSSI effects, for linear and nonlinear material behavior. Furthermore, it shows a potential improvement of the design spectra proposed by the Eurocode 8 in the elastic regime. The nonlinear behavior of material causes a change in the seismic response of soil and buildings hence, results are unpredictable using only the parameters adopted for linear material behavior. The 1DT-3C wave propagation approach used for SSSI analysis is a tool to inspire the design of seismic risk mitigation tools and urban organization. The parametric analysis gives preliminary results that do not permit a generalization yet.

The evolution of this research can evolve in an extensive parametric analysis and statistical study to generalize the conception of structures in seismic zones considering SSI effects in the Eurocode 8. On the other hand, the 1DT-3C modeling technique can help the design of risk mitigation tools. To allow the verification of the numerical model, experiments on instrumented structures in real and proportional scales could be used to compare the numerical and experimental structural response to dynamic loading.

The 1DT-3C wave propagation approach could evolve to model underground floors and deep foundations, with 3-D soil domain arriving at a greater depth. An effective stress analysis, taking into account the water table position in a 1DT-3C wave propagation model for SSI, is currently developed in the framework of the PhD thesis of Stefania Gobbi.

Other improvements can be the introduction of, corrosion of the steel bars in the reinforced concrete or different construction material for the structure can be adopted as wood and steel.



## References

- Abaqus User Manual. (2014). “Abaqus Theory Guide. Version 6.14.” *Dassault Systemes Simulia Corporation*.
- Álamo, G. M., Padrón, L. A., Aznárez, J. J., and Maeso, O. (2015). “Structure-soil-structure interaction effects on the dynamic response of piled structures under obliquely incident seismic shear waves.” *Soil Dynamics and Earthquake Engineering*, 78, 142–153.
- Aldaikh, H., Alexander, N. A., Ibraim, E., and Knappett, J. (2016). “Shake table testing of the dynamic interaction between two and three adjacent buildings (SSSI).” *Soil Dynamics and Earthquake Engineering*, 89, 219–232.
- Aldaikh, H., Alexander, N. A., Ibraim, E., and Oddbjornsson, O. (2015). “Two dimensional numerical and experimental models for the study of structure–soil–structure interaction involving three buildings.” *Computers & Structures*, 150, 79–91.
- Anderson, J. G. (2004). “Quantitative measure of the goodness-of-fit of synthetic seismograms.” *13th World Conference on Earthquake Engineering Conference Proceedings, Vancouver, Canada, Paper*.
- Aubry, D., Hujeux, J. C., Lassoudiere, F., and Meimon, Y. (1982). “A double memory model with multiple mechanisms for cyclic soil behaviour.” *Proceedings of the Int. Symp. Num. Mod. Geomech*, 3–13.
- Bachmann, H., Ammann, W. J., Deischl, F., Eisenmann, J., Floegl, I., Hirsch, G. H., Klein, G. K., Lande, G. J., Mahrenholtz, O., and Natke, H. G. (2012). *Vibration problems in structures: practical guidelines*. Birkhäuser.
- Bard, P.-Y. (1988). “The importance of rocking in building motion: an experimental evidence.” *Proc. of the Ninth World Conference on Earthquake Engineering*, 333–338.
- Bard, P.-Y., and Bouchon, M. (1985). “The two-dimensional resonance of sediment-filled valleys.” *Bulletin of the Seismological Society of America*, 75(2), 519–541.
- Bard, P.-Y., Campillo, M., Chavez-Garcia, F. J., and Sanchez-Sesma, F. (1988). “The Mexico Earthquake of September 19, 1985—A Theoretical Investigation of Large- and Small-scale Amplification Effects in the Mexico City Valley.” *Earthquake Spectra*, 4(3), 609–633.
- Bardet, J. P., and Tobita, T. (2001). “A Computer Program for Non-linear Earthquake Response Analyses of Layered Soil Deposits.” *Department of Civil Engineering, University of Southern California*.
- Barry, A., Bielak, J., and MacCamy, R. C. (1988). “On absorbing boundary conditions for wave propagation.” *Journal of Computational Physics*, 79(2), 449–468.
- Beresnev, I. A., and Wen, K.-L. (1996). “Nonlinear soil response—A reality?” *Bulletin of the Seismological Society of America*, 86(6), 1964–1978.
- Bielak, J. (1976). “Modal Analysis for Building-Soil Interaction.” *Journal of the Engineering Mechanics Division*, 102(5), 771–786.

- Bielak, J., Loukakis, K., Hisada, Y., and Yoshimura, C. (2003). "Domain reduction method for three-dimensional earthquake modeling in localized regions, Part I: Theory." *Bulletin of the Seismological Society of America*, 93(2), 817–824.
- Bolisetti, C., and Whittaker, A. S. (2011). "Seismic structure–soil–structure interaction in nuclear power plant structures." *Transactions, SMiRT*, 21, 6–11.
- Bonilla, L. F. (2001). "NOAH: users manual." *Institute for Crustal Studies, University of California, Santa Barbara*, 38.
- Bonnet, M. (1999). "Boundary Integral Equation Methods for Solids and Fluids." *Meccanica*, 34(4), 301–302.
- Boore, D. M. (2015). "Notes on relating density to velocity for use in site amplification calculations." [http://www.daveboore.com/daves\\_notes.html](http://www.daveboore.com/daves_notes.html).
- Bouchon, M., and Sánchez-Sesma, F. J. (2007). "Boundary Integral Equations and Boundary Elements Methods in Elastodynamics." *Advances in Geophysics*, Advances in Wave Propagation in Heterogenous Earth, R.-S. Wu, V. Maupin, and R. Dmowska, eds., Elsevier, 157–189.
- Cacciola, P., Banjanac, N., and Tombari, A. (2017). "Vibration Control of an existing building through the Vibrating Barrier." *Procedia Engineering*, X International Conference on Structural Dynamics, EUROODYN 2017, 199, 1598–1603.
- Cacciola, P., Espinosa, M. G., and Tombari, A. (2015). "Vibration control of piled-structures through structure-soil-structure-interaction." *Soil Dynamics and Earthquake Engineering*, 77, 47–57.
- Castro-Cruz, D., Régnier, J., Bertrand, E., and Courboux, F. (2017). "Seismic non-linear behavior of soil inferred by analysis of borehole data." *16th European Conference On Earthquake Engineering*.
- Celebi, M., and Safak, E. (1992). "Seismic response of Pacific Park Plaza. I: Data and preliminary analysis." *Journal of Structural Engineering*, 118(6).
- CEN. (2003). "EN 1998-5: Eurocode 8: Design of structures for earthquake resistance - Part 5: Foundations, retaining structures and geotechnical aspects."
- Chaljub, E., Moczo, P., Tsuno, S., Bard, P.-Y., Kristek, J., Käser, M., Stupazzini, M., and Kristekova, M. (2010). "Quantitative Comparison of Four Numerical Predictions of 3D Ground Motion in the Grenoble Valley, FranceQuantitative Comparison of Four Numerical Predictions of 3D Ground Motion in the Grenoble Valley." *Bulletin of the Seismological Society of America*, 100(4), 1427–1455.
- Chau, K. T., Shen, C. Y., and Guo, X. (2009). "Nonlinear seismic soil–pile–structure interactions: Shaking table tests and FEM analyses." *Soil Dynamics and Earthquake Engineering*, 29(2), 300–310.
- Chavez-Garcia, F. J., and Cardenas, M. (2002). "The contribution of the built environment to the 'free-field' ground motion in Mexico City." *Soil Dynamics and Earthquake Engineering*, 22(9), 773–780.
- Chin, B.-H., and Aki, K. (1991). "Simultaneous study of the source, path, and site effects on strong ground motion during the 1989 Loma Prieta earthquake: A preliminary result on pervasive nonlinear site effects." *Bulletin of the Seismological Society of America*, 81(5), 1859–1884.
- Chopra, A. K. (2001). "Dynamics of structures: Theory and applications."

- Chopra, A. K., and Gutierrez, J. A. (1974). "Earthquake response analysis of multistorey buildings including foundation interaction." *Earthquake Engineering & Structural Dynamics*, 3(1), 65–77.
- Clayton, R., and Engquist, B. (1977). "Absorbing boundary conditions for acoustic and elastic wave equations." *Bulletin of the Seismological Society of America*, 67(6), 1529–1540.
- Clouteau, D., Broc, D., Devésá, G., Guyonvarh, V., and Massin, P. (2012). "Calculation methods of Structure–Soil–Structure Interaction (3SI) for embedded buildings: Application to NUPEC tests." *Soil Dynamics and Earthquake Engineering*, 32(1), 129–142.
- Coleman, J., Jeremic, B., and Whittaker, A. (2013). "Nonlinear time domain seismic soil structure interaction (SSI) analysis for nuclear facilities and draft Appendix B of ASCE 4." *SMiRT-22*, 18–23.
- Cornou, C., Gueguen, P., Bard, P.-Y., and Haghshenas, E. (2004). "Ambient noise energy bursts observation and modeling: Trapping of harmonic structure-soil induced-waves in a topmost sedimentary layer." *Journal of seismology*, 8(4), 507–524.
- Dafalias, Y. F., and Manzari, M. T. (2004). "Simple plasticity sand model accounting for fabric change effects." *Journal of Engineering mechanics*, 130(6), 622–634.
- Ditommaso, R., Parolai, S., Mucciarelli, M., Eggert, S., Sobiesiak, M., and Zschau, J. (2010). "Monitoring the response and the back-radiated energy of a building subjected to ambient vibration and impulsive action: the Falkenhof Tower (Potsdam, Germany)." *Bulletin of Earthquake Engineering*, 8(3), 705–722.
- Elgamal, A., Yang, Z., Parra, E., and Ragheb, A. (2003). "Modeling of cyclic mobility in saturated cohesionless soils." *International Journal of Plasticity*, 19(6), 883–905.
- von Estorff, O., and Firuziaan, M. (2000). "Coupled BEM/FEM approach for nonlinear soil/structure interaction." *Engineering Analysis with Boundary Elements*, 24(10), 715–725.
- Fares, R., Santisi d'Avila, M. P., and Deschamps, A. (2018). "Soil-Structure Interaction analysis using a 1DT-3C wave propagation model." *Soil Dynamics and Earthquake Engineering*.
- Field, E. H., Johnson, P. A., Beresnev, I. A., and Zeng, Y. (1997). "Nonlinear ground-motion amplification by sediments during the 1994 Northridge earthquake." *Nature*, 390(6660), 599–602.
- Fung, Y. C. (1965). *Foundations of solid mechanics*. Prentice-Hall, Englewood Cliffs, N.J.
- Gallipoli, M. R., Mucciarelli, M., Castro, R. R., Monachesi, G., and Contri, P. (2004). "Structure, soil–structure response and effects of damage based on observations of horizontal-to-vertical spectral ratios of microtremors." *Soil Dynamics and Earthquake Engineering*, 24(6), 487–495.
- Gandomzadeh, A. (2011). "Dynamic soil-structure interaction: effect of nonlinear soil behavior." Université Paris-Est.
- Gatti, F., Lopez Caballero, F., Paolucci, R., and Clouteau, D. (n.d.). "Preliminary calibration of the numerical large-scale scenario of the Niigata-Ken Chuetsu-Oki earthquake."
- Gazetas, G. (1991). "Formulas and Charts for Impedances of Surface and Embedded Foundations." *Journal of Geotechnical Engineering*, 117(9), 1363–1381.

- Gueguen, P., and Bard, P.-Y. (2005). "Soil-structure and soil-structure-soil interaction: experimental evidence at the Volvi test site." *Journal of Earthquake Engineering*, 9(05), 657–693.
- Hall, W. S. (1994). "Boundary Element Method." *The Boundary Element Method, Solid Mechanics and Its Applications*, Springer, Dordrecht, 61–83.
- Hanks, T. C. (1975). "Strong ground motion of the San Fernando, California, earthquake: Ground displacements." *Bulletin of the Seismological Society of America*, 65(1), 193–225.
- Hardin, B. O., and Drnevich, V. P. (1972a). "Shear modulus and damping in soils: design equations and curves." *Journal of the Soil mechanics and Foundations Division, ASCE*, 98(7), 667–692.
- Hardin, B. O., and Drnevich, V. P. (1972b). "Shear modulus and damping in soils: measurement and parameter effects." *Journal of the Soil mechanics and Foundations Division, ASCE*, 98(6).
- Hughes, T. J. R. (1987). "The finite element method - linear static and dynamic finite element analysis." *Prentice Hall Englewood Cliff*, 490–567.
- Hung, H. H., Chang, K. C., Liu, K. Y., and Ho, T. H. (2008). "An experimental study on rocking response of bridge spread foundations." *Proceedings of the 14th World Conference on Earthquake Engineering*.
- Iai, S., and Ozutsumi, O. (2011). "Yield and cyclic behaviour of a strain space multiple mechanism model for granular materials." *International Journal for Numerical and Analytical Methods in Geomechanics*, 29(4), 417–442.
- Iida, M. (1998). "Three-dimensional non-linear soil–building interaction analysis in the lakebed zone of Mexico city during the hypothetical Guerrero earthquake." *Earthquake Engineering & Structural Dynamics*, 27(12), 1483–1502.
- Ivanović, S. S., Trifunac, M. D., Novikova, E. I., Gladkov, A. A., and Todorovska, M. I. (2000). "Ambient vibration tests of a seven-story reinforced concrete building in Van Nuys, California, damaged by the 1994 Northridge earthquake." *Soil Dynamics and Earthquake Engineering*, 19(6), 391–411.
- Iwan, W. D. (1967). "On a Class of Models for the Yielding Behavior of Continuous and Composite Systems." *Journal of Applied Mechanics*, 34(3), 612–617.
- Jennings, P. C. (1970). "Distant motions from a building vibration test." *Bulletin of the Seismological Society of America*, 60(6), 2037–2043.
- Jennings, P. C., and Bielak, J. (1973). "Dynamics of building-soil interaction." *Bulletin of the Seismological Society of America*, 63(1), 9–48.
- Jeremic, B., Jie, G., Preisig, M., and Tafazzoli, N. (2009). "Time domain simulation of soil–foundation–structure interaction in non-uniform soils." *Earthquake Engineering & Structural Dynamics*, 38(5), 699–718.
- Jeremic, B., Tafazzoli, N., Kamrani, B., Tasiopoulou, P., and Jeong, C.-G. (2011). "Report to NRC on: Investigation of Analysis Methods to Incorporate Multi-Dimensional Loading and Incoherent Ground Motions in Soil-Structure Interaction Analysis."
- Joyner, W. B. (1975). "A method for calculating nonlinear seismic response in two dimensions." *Bulletin of the Seismological Society of America*, 65(5), 1337–1357.

- Joyner, W. B., and Chen, A. T. F. (1975). "Calculation of nonlinear ground response in earthquakes." *Bulletin of the Seismological Society of America*, 65(5), 1315–1336.
- Kaneko, T. (1975). "On Timoshenko's correction for shear in vibrating beams." *Journal of Physics D: Applied Physics*, 8(16), 1927.
- Karapetrou, S. T., Fotopoulou, S. D., and Pitilakis, K. D. (2015). "Seismic vulnerability assessment of high-rise non-ductile RC buildings considering soil–structure interaction effects." *Soil Dynamics and Earthquake Engineering*, 73, 42–57.
- Kausel, E. (2010). "Early history of soil–structure interaction." *Soil Dynamics and Earthquake Engineering*, 30(9), 822–832.
- Kawase, H., and Aki, K. (1989). "A study on the response of a soft basin for incident S, P, and Rayleigh waves with special reference to the long duration observed in Mexico City." *Bulletin of the Seismological Society of America*, 79(5), 1361–1382.
- Kawase, H., Satoh, T., and Fukutake, K. (1996). "Simulation of the borehole records observed at the Port Island in Kobe, Japan, during the Hyogo-ken Nanbu earthquake of 1995." *Proc. of the 11th World Conf. on Earthquake Engineering*.
- Komatitsch, D., and Vilotte, J.-P. (1998). "The spectral element method: An efficient tool to simulate the seismic response of 2D and 3D geological structures." *Bulletin of the Seismological Society of America*, 88(2), 368–392.
- Kramer, S. L. (1996). "Geotechnical earthquake engineering. In prentice–Hall international series in civil engineering and engineering mechanics." *Prentice-Hall, New Jersey*.
- Kwok, A. O. L., Stewart, J. P., and Hashash, Y. M. A. (2008). "Nonlinear Ground-Response Analysis of Turkey Flat Shallow Stiff-Soil Site to Strong Ground Motion." *Bulletin of the Seismological Society of America*, 98(1), 331–343.
- Kythe, P. K. (1995). *An Introduction to Boundary Element Methods*. CRC Press.
- Li, P. Z., Hou, X. Y., Liu, Y. M., and Lu, X. L. (2012). "Shaking table model tests on dynamic structure-soil-structure interaction during various excitations." *Proceedings of the 15th World Conference on Earthquake Engineering, Lisbon, Portugal*, 23–28.
- Li, W., and Assimaki, D. (2010). "Site- and Motion-Dependent Parametric Uncertainty of Site-Response Analyses in Earthquake Simulations." *Bulletin of the Seismological Society of America*, 100(3), 954–968.
- Lin, H.-T., Roesset, J. M., and Tassoulas, J. L. (1987). "Dynamic interaction between adjacent foundations." *Earthquake Engineering & Structural Dynamics*, 15(3), 323–343.
- Lopez Caballero, F., and Farahmand Razavi, A. M. (2008). "Numerical simulation of liquefaction effects on seismic SSI." *Soil Dynamics and Earthquake Engineering*, 28(2), 85–98.
- Lopez-Caballero, F., and Modaressi-Farahmand-Razavi, A. (2013). "Numerical simulation of mitigation of liquefaction seismic risk by preloading and its effects on the performance of structures." *Soil Dynamics and Earthquake Engineering*, 49, 27–38.
- Lou, M., Wang, H., Chen, X., and Zhai, Y. (2011). "Structure–soil–structure interaction: Literature review." *Soil Dynamics and Earthquake Engineering*, 31(12), 1724–1731.

- Lu, X., Li, P., Chen, Y., and Chen, B. (2004). "Shaking table model testing on dynamic soil-structure interaction system." *Proc., 13th World Conf. on Earthquake Eng.*
- Lublinter, J., Oliver, J., Oller, S., and Onate, E. (1989). "A plastic-damage model for concrete." *International Journal of Solids and Structures*, 25(3), 299–326.
- Luco, J. E., and Contesse, L. (1973). "Dynamic structure-soil-structure interaction." *Bulletin of the Seismological Society of America*, 63(4), 1289–1303.
- Lysmer, J., and Kuhlemeyer, R. L. (1969). "Finite dynamic model for infinite media." *Journal of the Engineering Mechanics Division*, 95(4), 859–878.
- Manakou, M. V., Raptakis, D. G., Chávez-García, F. J., Apostolidis, P. I., and Pitilakis, K. D. (2010). "3D soil structure of the Mygdonian basin for site response analysis." *Soil Dynamics and Earthquake Engineering*, 30(11), 1198–1211.
- Matthees, W., and Magiera, G. (1982). "A sensitivity study of seismic structure-soil-structure interaction problems for nuclear power plants." *Nuclear Engineering and Design*, 73(3), 343–363.
- Maugeri, M., Musumeci, G., Novità, D., and Taylor, C. A. (2000). "Shaking table test of failure of a shallow foundation subjected to an eccentric load." *Soil Dynamics and Earthquake Engineering*, 20(5), 435–444.
- Mavroeidis, G. P., and Papageorgiou, A. S. (2002). "Near-source strong ground motion: characteristics and design issues." *The 17th US National Conference on Earthquake Engineering (7NCEE)*, Boston, Massachusetts, 25.
- Mazzieri, I., Stupazzini, M., Guidotti, R., and Smerzini, C. (2013). "SPEED: SPectral Elements in Elastodynamics with Discontinuous Galerkin: A non-conforming approach for 3D multi-scale problems." *International Journal for Numerical Methods in Engineering*, 95(12), 991–1010.
- Mercerat, E. D., and Glinsky, N. (2015). "A nodal discontinuous Galerkin method for non-linear soil dynamics." *6th International Conference Earthquake Geotechnical Engineering*.
- Mercerat, E. D., Vilotte, J. P., and Sánchez-Sesma, F. J. (2006). "Triangular Spectral Element simulation of two-dimensional elastic wave propagation using unstructured triangular grids." *Geophysical Journal International*, 166(2), 679–698.
- Mizuno, H. (1980). "Effects of structure–soil–structure interaction during various excitations." *7th World Conference on Earthquake Engineering*, 149–156.
- Moczo, P., Kristek, J., and Halada, L. (2004). "The finite-difference method for seismologists." *An Introduction*. Comenius University, Bratislava.
- Mogi, H., and Kawakami, H. (2007). "Analysis of Scattered Waves on Ground with Irregular Topography Using the Direct Boundary Element Method and Neumann Series Expansion." *Bulletin of the Seismological Society of America*, 97(4), 1144–1157.
- Mohammadi, M., and Karabalis, D. L. (1995). "Dynamic 3-D soil–railway track interaction by BEM–FEM." *Earthquake Engineering & Structural Dynamics*, 24(9), 1177–1193.
- Mucciarelli, M., Gallipoli, M. R., Ponzo, F., and Dolce, M. (2003). "Seismic waves generated by oscillating buildings: analysis of a release test." *Soil Dynamics and Earthquake Engineering*, 23(4), 255–262.

- Mylonakis, G., and Gazetas, G. (2000). “Seismic soil-structure interaction: beneficial or detrimental?” *Journal of Earthquake Engineering*, 04(03), 277–301.
- Nateghi-A, F., and Rezaei-Tabrizi, A. (2013). “Nonlinear dynamic response of tall buildings considering structure–soil–structure effects.” *The Structural Design of Tall and Special Buildings*, 22(14), 1075–1082.
- Nielsen, A. H. (2006). “Absorbing boundary conditions for seismic analysis in ABAQUS.” *ABAQUS Users’ Conference*, 359–376.
- Nielsen, A. H. (2014). “Towards a complete framework for seismic analysis in Abaqus.” *Proceedings of the ICE-Engineering and Computational Mechanics*, 167(1), 3–12.
- Oral, E. (2016). “Modélisation multi-dimensionnelle de la propagation des ondes sismiques dans des milieux linéaires et non-linéaires.”
- Padrón, L. A., Aznárez, J. J., and Maeso, O. (2009). “Dynamic structure–soil–structure interaction between nearby piled buildings under seismic excitation by BEM–FEM model.” *Soil Dynamics and Earthquake Engineering*, 29(6), 1084–1096.
- Paolucci, R., Shirato, M., and Yilmaz, M. T. (2008). “Seismic behaviour of shallow foundations: Shaking table experiments vs numerical modelling.” *Earthquake Engineering & Structural Dynamics*, 37(4), 577–595.
- Papageorgiou, A. S., and Kim, J. (1991). “Study of the propagation and amplification of seismic waves in Caracas Valley with reference to the 29 July 1967 earthquake: SH waves.” *Bulletin of the Seismological Society of America*, 81(6), 2214–2233.
- Patera, A. T. (1984). “A spectral element method for fluid dynamics: Laminar flow in a channel expansion.” *Journal of Computational Physics*, 54(3), 468–488.
- Phillips, C., and Hashash, Y. M. (2009). “Damping formulation for nonlinear 1D site response analyses.” *Soil Dynamics and Earthquake Engineering*, 29(7), 1143–1158.
- Pisanò, F., and Jeremić, B. (2014). “Simulating stiffness degradation and damping in soils via a simple visco-elastic–plastic model.” *Soil Dynamics and Earthquake Engineering*, 63, 98–109.
- Pitilakis, K., Raptakis, D., Lontzetidis, K., Tika-Vassilikou, T., and Jongmans, D. (1999). “Geotechnical and geophysical description of euro-seistest, using field, laboratory tests and moderate strong motion recordings.” *Journal of Earthquake Engineering*, 03(03), 381–409.
- Priolo, E., Carcione, J. M., and Seriani, G. (1994). “Numerical simulation of interface waves by high-order spectral modeling techniques.” *The Journal of the Acoustical Society of America*, 95(2), 681–693.
- Raptakis, D., Chávez-García, F. J., Makra, K., and Pitilakis, K. (2000). “Site effects at Euroseistest—I. Determination of the valley structure and confrontation of observations with 1D analysis.” *Soil Dynamics and Earthquake Engineering*, 19(1), 1–22.
- Régnier, J., Bonilla, L.-F., Bard, P.-Y., Bertrand, E., Hollender, F., Kawase, H., Sicilia, D., Arduino, P., Amorosi, A., Asimaki, D., Boldini, D., Chen, L., Chiaradonna, A., DeMartin, F., Ebrille, M., Elgamal, A., Falcone, G., Foerster, E., Foti, S., Garini, E., Gazetas, G., Gélis, C., Ghofrani, A., Giannakou, A., Gingery, J. R., Glinsky, N., Harmon, J., Hashash, Y., Iai, S., Jeremić, B., Kramer, S., Kontoe, S., Kristek, J., Lanzo, G., Lernia, A. di, Lopez-Caballero, F., Marot, M., McAllister, G., Mercerat, E. D., Moczo, P., Montoya-Noguera, S., Musgrove, M., Nieto-Ferro, A., Pagliaroli, A.,

- Pisanò, F., Richterova, A., Sajana, S., d'Avila, M. P. S., Shi, J., Silvestri, F., Taiebat, M., Tropeano, G., Verrucci, L., and Watanabe, K. (2016). "International benchmark on numerical simulations for 1D, nonlinear site response (PRENOLIN): Verification phase based on canonical cases." *Bulletin of the Seismological Society of America*, 106(5), 2112–2135.
- Régnier, J., Cadet, H., and Bard, P.-Y. (2017). "Impact of non-linear soil behavior on site response amplitude." *16th World Conference on Earthquake Engineering*, Santiago, Chile.
- Régnier, J., Cadet, H., Bonilla, L. F., Bertrand, E., and Semblat, J.-F. (2013). "Assessing Nonlinear Behavior of Soils in Seismic Site Response: Statistical Analysis on KiK-net Strong-Motion Data Assessing Nonlinear Behavior of Soils in Seismic Site Response." *Bulletin of the Seismological Society of America*, 103(3), 1750–1770.
- Reissner, E. (1936). "Stationäre, axialsymmetrische, durch eine schüttelnde Masse erregte Schwingungen eines homogenen elastischen Halbraumes." *Ingenieur-Archiv*, 7(6), 381–396.
- Roy, C., Bolourchi, S., and Eggers, D. (2015). "Significance of structure–soil–structure interaction for closely spaced structures." *Nuclear Engineering and Design*, 295, 680–687.
- Saez, E., Lopez Caballero, F., and Modaressi-Farahmand-Razavi, A. (2011). "Effect of the inelastic dynamic soil–structure interaction on the seismic vulnerability assessment." *Structural Safety*, 33(1), 51–63.
- Saez, E., Lopez Caballero, F., and Modaressi-Farahmand-Razavi, A. (2013). "Inelastic dynamic soil–structure interaction effects on moment-resisting frame buildings." *Engineering Structures*, 51, 166–177.
- Saez, E., Lopez-Caballero, F., and Modaressi-Farahmand-Razavi, A. (2008). "Effects of non-linear soil behaviour on the seismic performance evaluation of structures." *Ital Geotech J*, 2, 63–76.
- Safak, E., and Celebi, M. (1992). "Seismic Response of Pacific Park Plaza. II: System Identification." *Journal of Structural Engineering*, 118(6).
- Santisi d'Avila, M. P., and Lenti, L. (2012). "Modeling strong seismic ground motion: 3D loading path vs wavefield polarization." *Geophysical Journal International*.
- Santisi d'Avila, M. P., and Lopez-Caballero, F. (2018). "Analysis of nonlinear soil-structure interaction effects: 3D frame structure and 1-Directional propagation of a 3-Component seismic wave." *Computers & Structures*.
- Santisi d'Avila, M. P., Semblat, J.-F., and Lenti, L. (2013). "Strong ground motion in the 2011 Tohoku earthquake: A one-directional three-component modeling." *Bulletin of the Seismological Society of America*, 103(2B), 1394–1410.
- Schanz, T., Vermeer, P. A., and Bonnier, P. G. (1999). "The hardening soil model: formulation and verification." *Beyond 2000 in computational geotechnics*, 281–296.
- Schwan, L., Boutin, C., Padrón, L., Dietz, M., Bard, P.-Y., and Taylor, C. (2016). "Site-city interaction: theoretical, numerical and experimental crossed-analysis." *Geophysical Journal International*, 205(2), 1006–1031.

- Semblat, J. F., Duval, A. M., and Dangla, P. (2002). "Seismic site effects in a deep alluvial basin: numerical analysis by the boundary element method." *Computers and Geotechnics*, 29(7), 573–585.
- Semblat, J. F., Kham, M., Parara, E., Bard, P. Y., Pitilakis, K., Makra, K., and Raptakis, D. (2005). "Seismic wave amplification: Basin geometry vs soil layering." *Soil Dynamics and Earthquake Engineering*, 11th International Conference on Soil Dynamics and Earthquake Engineering (ICSDEE): Part 1, 25(7), 529–538.
- Semblat, J.-F., Duval, A.-M., and Dangla, P. (2000). "Numerical analysis of seismic wave amplification in Nice (France) and comparisons with experiments." *Soil Dynamics and Earthquake Engineering*, 19(5), 347–362.
- Semblat, J.-F., Kham, M., and Bard, P.-Y. (2008). "Seismic-Wave Propagation in Alluvial Basins and Influence of Site-City Interaction." *Bulletin of the Seismological Society of America*, 98(6), 2665–2678.
- Semblat, J.-F., Kham, M., Bard, P.-Y., and Guéguen, P. (2004). "Could 'site-city interaction' modify site effects in urban areas?" *13th world conference on earthquake engineering, Vancouver, paper*.
- Shirato, M., Kouno, T., Asai, R., Nakatani, S., Fukui, J., and Paolucci, R. (2008). "large-scale experiments on nonlinear behavior of shallow foundations subjected to strong earthquakes." *SOILS AND FOUNDATIONS*, 48(5), 673–692.
- Singh, S. K., Lermo, J., Domínguez, T., Ordaz, M., Espinosa, J. M., Mena, E., and Quaas, R. (1988). "The Mexico Earthquake of September 19, 1985—A Study of Amplification of Seismic Waves in the Valley of Mexico with Respect to a Hill Zone Site." *Earthquake Spectra*, 4(4), 653–673.
- Smith, W. D. (1974). "A nonreflecting plane boundary for wave propagation problems." *Journal of Computational Physics*, 15(4), 492–503.
- Stewart, J. P., Fenves, G. L., and Seed, R. B. (1999a). "Seismic Soil-Structure Interaction in Buildings. I: Analytical Methods." *Journal of Geotechnical and Geoenvironmental Engineering*, 125(1), 26–37.
- Stewart, J. P., Seed, R. B., and Fenves, G. L. (1999b). "Seismic Soil-Structure Interaction in Buildings. II: Empirical Findings." *Journal of Geotechnical and Geoenvironmental Engineering*, 125(1), 38–48.
- Tombari, A., Espinosa, M. G., Alexander, N. A., and Cacciola, P. (2018). "Vibration control of a cluster of buildings through the Vibrating Barrier." *Mechanical Systems and Signal Processing*, 101, 219–236.
- Trombetta, N. W., Benjamin Mason, H., Hutchinson, T. C., Zupan, J. D., Bray, J. D., and Kutter, B. L. (2014). "Nonlinear soil–foundation–structure and structure–soil–structure interaction: engineering demands." *Journal of Structural Engineering*, 141(7), 04014177.
- Varone, C., Lenti, L., Martino, S., and Semblat, J.-F. (2015). "Interaction site-ville à Rome: modélisation géologique et numérique des effets de l'urbanisation récente." *9e Colloque National AFPS*, Marne-la-Vallée.
- Veletsos, A. S., and Meek, J. W. (1974). "Dynamic behaviour of building-foundation systems." *Earthquake Engineering & Structural Dynamics*, 3(2), 121–138.

- Vicencio, F., and Alexander, N. A. (2018). “Dynamic interaction between adjacent buildings through nonlinear soil during earthquakes.” *Soil Dynamics and Earthquake Engineering*, 108, 130–141.
- Wang, H., Lou, M., Chen, X., and Zhai, Y. (2013). “Structure–soil–structure interaction between underground structure and ground structure.” *Soil Dynamics and Earthquake Engineering*, 54, 31–38.
- Warburton, G. B., Richardson, J. D., and Webster, J. J. (1971). “Forced Vibrations of Two Masses on an Elastic Half Space.” *Journal of Applied Mechanics*, 38(1), 148–156.
- Warburton, G. B., Richardson, J. D., and Webster, J. J. (1972). “Harmonic Response of Masses on an Elastic Half Space.” *Journal of Engineering for Industry*, 94(1), 193–200.
- Wolf, J. P. (1985). *Dynamic soil-structure interaction*. Prentice Hall int.
- Yazdchi, M., Khalili, N., and Valliappan, S. (1999). “Dynamic soil–structure interaction analysis via coupled finite-element–boundary-element method.” *Soil Dynamics and Earthquake Engineering*, 18(7), 499–517.
- Yoshimura, C., Bielak, J., Hisada, Y., and Fernández, A. (2003). “Domain reduction method for three-dimensional earthquake modeling in localized regions, part II: Verification and applications.” *Bulletin of the Seismological Society of America*, 93(2), 825–841.
- Zienkiewicz, O. C., Bicanic, N., and Shen, F. Q. (1989). “Earthquake input definition and the transmitting boundary conditions.” *Advances in Computational Nonlinear Mechanics*, International Centre for Mechanical Sciences, I. S. Dolićsinis, ed., Springer Vienna, 109–138.

## Appendix A - Nonlinear behavior of RC

The behavior of reinforced concrete is no longer linear when cracks initiate in beams and columns, and the steel start working. The distribution of steel in a beam section or column section is not necessary uniform and symmetrical, consequently, an homogenization is difficult. The constitutive laws for RC sections are deduced in terms of generalized stresses and strains and used in the nodes of a 1-D beam element.

### Constitutive relationship in terms of generalized stresses

A 3-D beam having a rectangular section with cross-sectional area  $A = 30 \times 60 \text{ cm}^2$  and a length of 1 m (Figure E-1), is used as example to explain the adopted procedure.

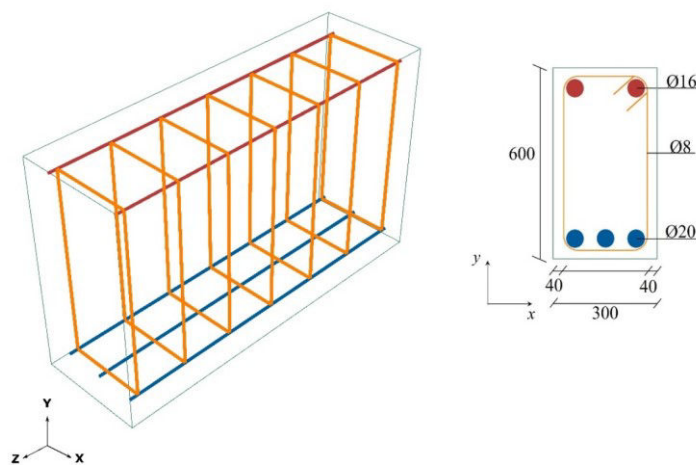


Figure E-1 Reinforced unit length 3-D beam (left) and beam cross-section (right)

When the nonlinear behavior of RC is taken into account, the Hognestad's parabola is selected as first-loading curve plotted in Figure E-2 for a cubic characteristic concrete strength  $R_{ck} = 30 \text{ N/mm}^2$  in compression.

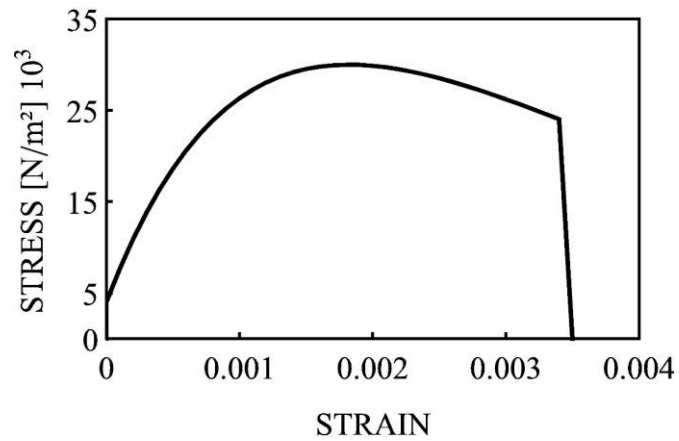


Figure E-2 Hognestad's parabola.

### Axial behavior

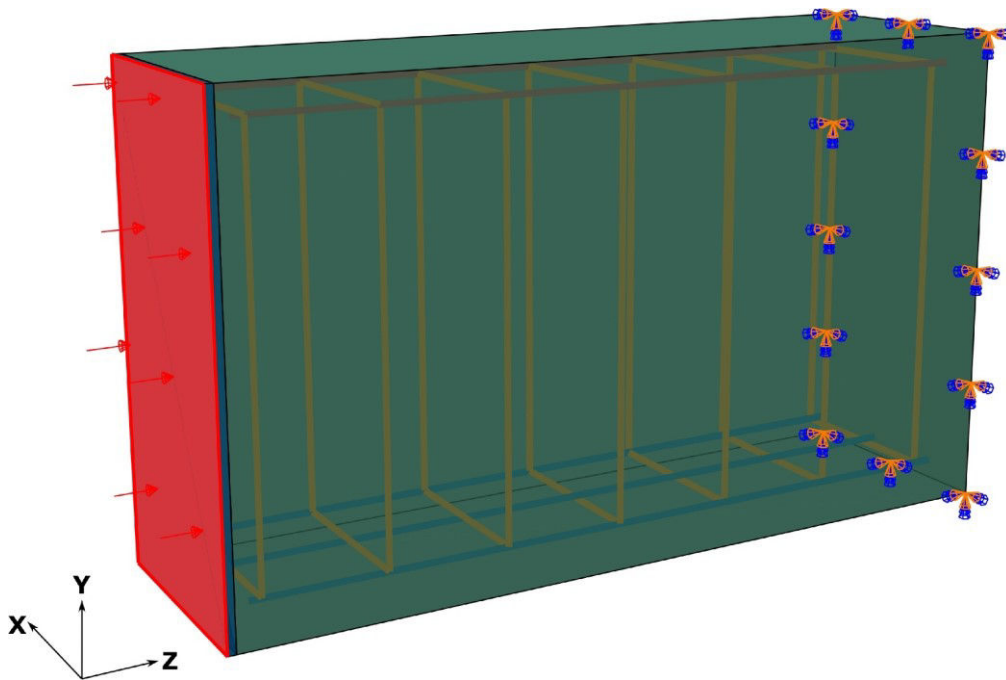


Figure E-3 Abaqus capture of the unit length beam subjected to axial loading.

A first static analysis is run to study the axial behavior of the RC beam an increasing axial pressure of maximum  $\sigma_{33} = 4 \times 10^7 \text{ N/m}^2$  is applied as shown in Figure E-3. A 1 cm thick steel plate is used to uniformly distribute the pressure in the beam cross-section.

Considering that the beam has unit length, the calculated axial displacement corresponds to the axial strain. The constitutive relationship is obtained in terms of generalized stresses and strains ( $N, \epsilon_{zz}$ ) and imposed to nodes of a 1-D beam model, after verification of the elastic relationship  $N = \sigma_{zz} A = EA \epsilon_{zz}$ .

The model using beam elements, subjected to the same boundary conditions is compared with the 3-D model, and the verification of the obtained response of the 1-D beam element is shown in Figure E-4.

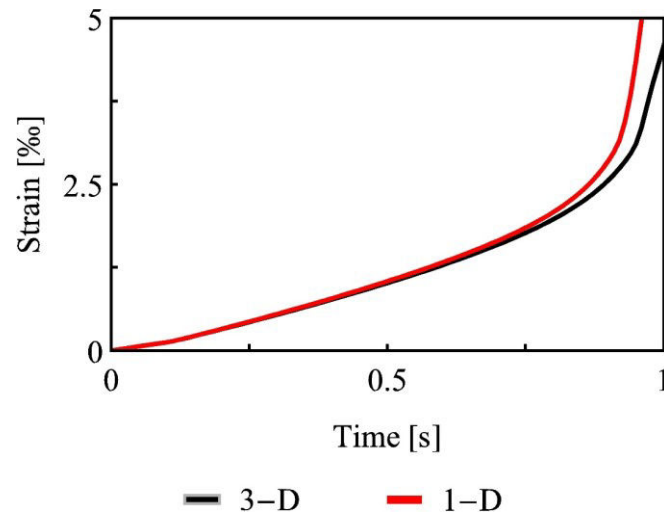


Figure E-4 Strain time history under axial loading: comparison between 1-D and 3-D beam modeling.

## Bending moment 1

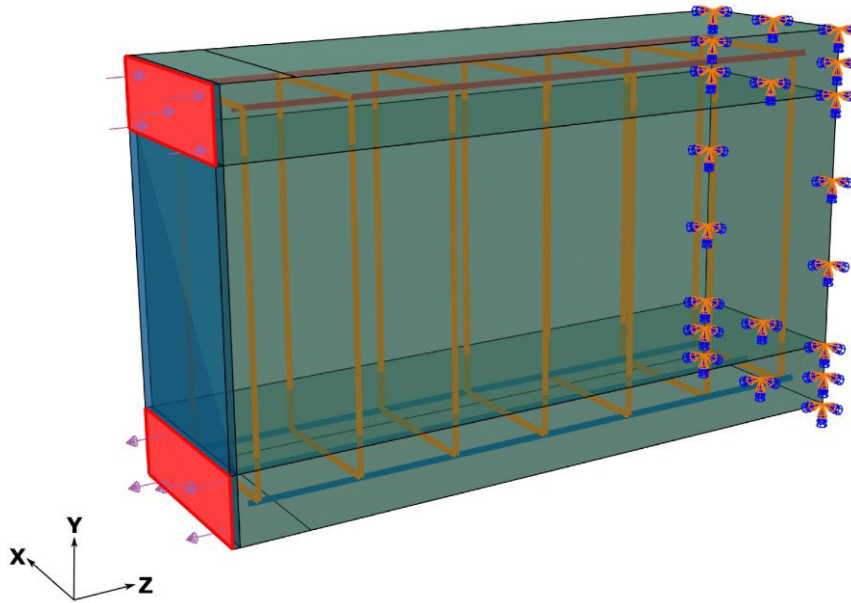


Figure E- 5 Abaqus capture of the unit length beam subjected to bending moment in x-direction.

A static analysis is undertaken to obtain the constitutive law in terms of generalized stress and strain ( $M_x, K_x$ ). An increasing axial pressure of maximum  $\sigma_{33} = 4 \times 10^7 \text{ N/m}^2$  is applied in a band of 10 cm as shown in Figure E- 5. A 1 cm thick steel plate is used to uniformly distribute the pressure in the beam cross-section. Considering the unit length of the beam, the axial displacement  $u_{zz}$  calculated, at the top and bottom, at the free edges of the beam is used to evaluate the curvature  $K_{xx} = (u_{zz\text{-top}} - u_{zz\text{-bot}})/2/(h/2)$ .

The constitutive relationship is obtained in terms of generalized stresses and strains ( $M_x, K_x$ ) and imposed to the nodes of a 1-D beam model, after verification of the elastic relationship  $M_x/K_x = EI_x$  where  $E$  is the Young modulus,  $I_x$  is the moment of inertia around the  $x$ -axis and  $M_x = \sigma_{33}eb(h - e) \Delta t$ . The parameters  $e, b$  and  $h$  are defined in Figure E- 6 and  $\Delta t$  is the time increment.

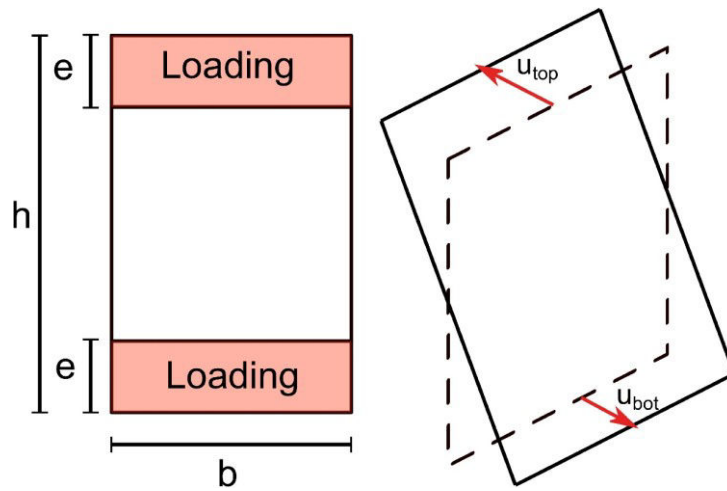


Figure E- 6 Diagram of the beam section (left) and of the deformed section after the application of the bending moment in x-direction (right).

The model using beam elements, subjected to the same boundary conditions is compared with the 3-D model, and the verification of the obtained response of the 1-D beam element is shown in Figure E- 7.

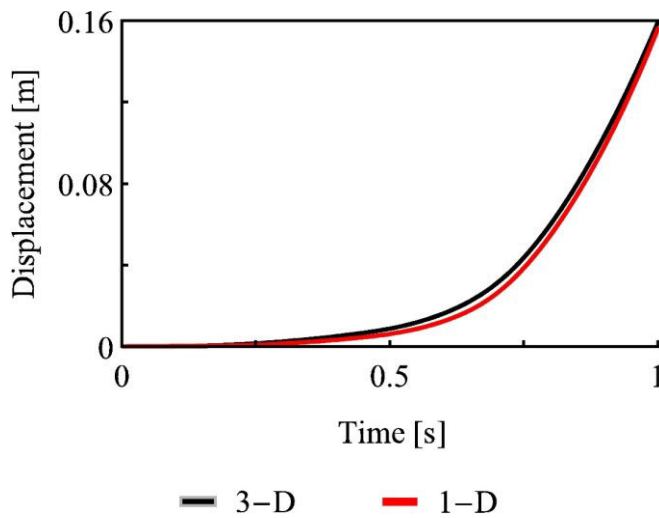


Figure E- 7 Displacement time history, comparison between 1-D and 3-D analysis in bending moment loading in direction x.

## Bending moment 2

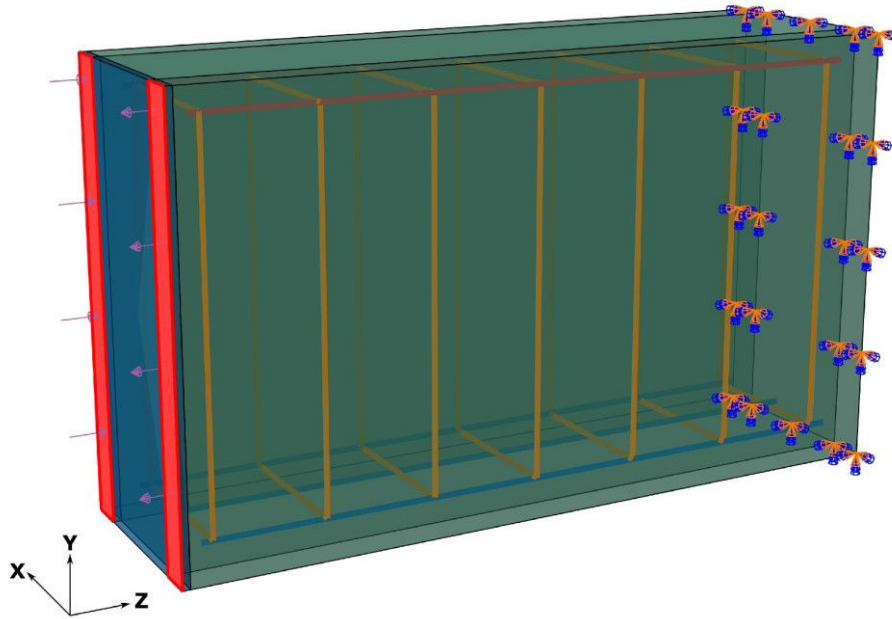


Figure E- 8 Abaqus capture of the unit length beam subjected to bending moment in y-direction.

A static analysis is undertaken to obtain the constitutive law in terms of generalized stress and strain ( $M_y, K_y$ ). An increasing axial pressure of maximum  $\sigma_{33} = 2 \times 10^7 \text{ N/m}^2$  is applied in a band of 5 cm as shown in Figure E- 8. A 1 cm thick steel plate is used to uniformly distribute the pressure in the beam cross-section. Considering the unit length of the beam, the axial displacement  $u_{zz}$  calculated, at the top and bottom, at the free edges of the beam is used to evaluate the curvature  $K_{yy} = (u_{zz\text{-left}} - u_{zz\text{-right}})/2/(b/2)$ , the parameters  $b$ ,  $u_{zz\text{-left}}$  and  $u_{zz\text{-right}}$  are defined in Figure E- 9.

The constitutive relationship is obtained in terms of generalized stresses and strains ( $M_y, K_y$ ) and imposed to the nodes of a 1-D beam model, after verification of the elastic relationship  $M_y/K_y = EI_y$  where  $E$  is the Young modulus,  $I_y$  is the moment of inertia around the  $y$ -axis and  $M_y = \sigma_{33}eh(b - e) \Delta t$ . The parameters  $e$ ,  $b$  and  $h$  are defined in Figure E- 9 and  $\Delta t$  is the time increment.

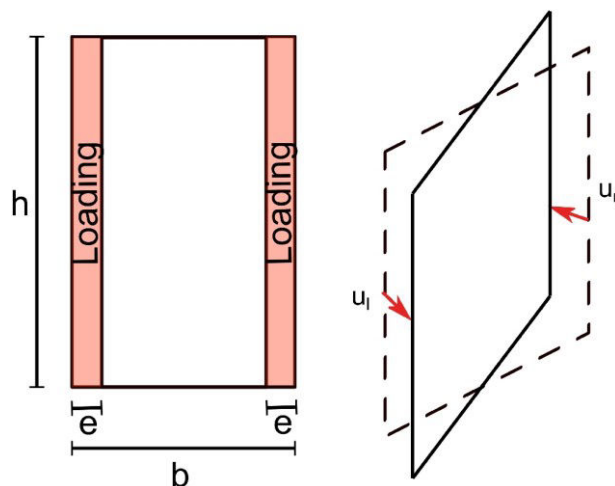


Figure E- 9 Diagram of the beam section (left) and of the deformed section after the application of the bending moment in y-direction (right).

The model using beam elements, subjected to the same boundary conditions is compared with the 3-D model, and the verification of the obtained response of the 1-D beam element is shown in Figure E- 10.

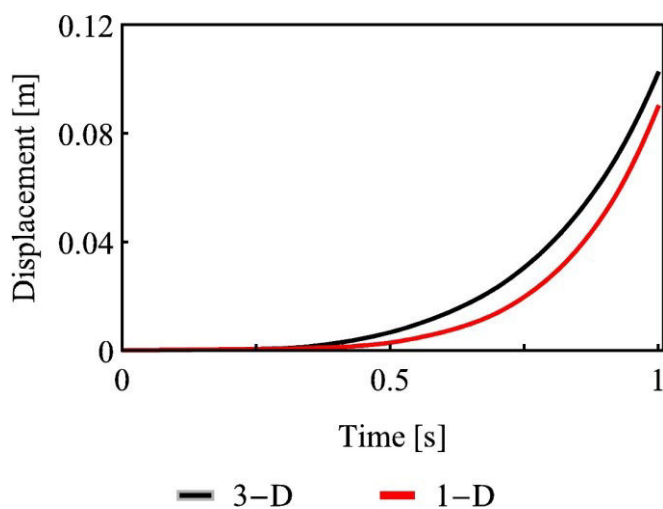


Figure E- 10 Displacement time history, comparison between 1-D and 3-D analysis in bending moment loading in direction y.

### Section definition and RC material definition in Abaqus

After creating the Abaqus and completing the geometry the mesh the steps of analysis the field and history outputs, the loadings and the boundary conditions and creating the job, it is

mandatory to create sets in module Part for each group of beams and columns that have the same steel reinforcement and beam or column section, together.

The material and property are not to be defined. From module Job, Job Manager click on write input. Open the .inp file as text file and add the following text for each defined **SET**.

**\*Beam General Section, elset=SET, section=NONLINEAR GENERAL**

**A, I11, I12, I22, J,  $\Gamma_0$ ,  $\Gamma_W$**

**A** : Area, **I11** : Moment of inertia for bending about the 1-axis, **I12** : Moment of inertia for cross bending, **I22** : Moment of inertia for bending about the 2-axis, **J** : Torsional constant,  **$\Gamma_0$**  : Sectorial moment **OPTIONAL** needed in Abaqus/Standard when the section is associated with open-section beam elements,  **$\Gamma_W$**  : Warping constant **OPTIONAL** needed in Abaqus/Standard when the section is associated with open-section beam elements

**$x_{1c}$ ,  $x_{2c}$ ,  $e_c$**

**$x_{1c}$**  : Local  $x_1$ -coordinate of centroid,  $x_{1c}$ . The default is 0.,  **$x_{2c}$**  : Local  $x_2$ -coordinate of centroid,  $x_{2c}$ . The default is 0,  **$e_c$**  : Thickness of segment ending at this point, The default is -1.

**$x_{1s}$ ,  $x_{2s}$ ,  $e_s$**

**$x_{1s}$**  : Local  $x_1$ -coordinate of shear center,  $x_{1s}$ . The default is 0.,  **$x_{2s}$**  : Local  $x_2$ -coordinate of shear center,  $x_{2s}$ . The default is 0. ,  **$e_s$**  : Thickness of segment ending at this point, The default is -1. **THIS LINE IS OPTIONAL**

**\*AXIAL**

0,0

...

0,  **$\epsilon_{cu}$**

*Insert Tabular ( $N, \epsilon_{zz}$ ) of the centroid of the beam section. The axial behavior tabular starting with 0,0 and ending 0,  $\epsilon_{cu}$  corresponding to the ultimate point*

**\*M1**

0,0

...

0,  **$k_{xu}$**

*Insert Tabular ( $M_x, K_x$ ). The Moment curvature tabular in direction 1 starting 0,0 and ending 0,  $k_{xu}$  corresponding to the ultimate point*

\*M2

0,0

...

0,  $k_{yu}$

*Insert Tabular ( $M_y, K_y$ ). The Moment curvature tabular in direction 1 starting 0,0 and ending 0,  $k_{yu}$  corresponding to the ultimate point*

\*TORQUE

...

add the torque tabular starting 0,0

\*Damping, alpha=**xxx**, beta=**xxx**

*Corresponding to Reighley damping*

\*Transverse Shear

**$\chi_{23}, \chi_{13}$** ,

*Corresponding to shear correction factor in Timoshenko beam elements*

Refer to Abaqus manual for more information and beam general section options 26.3.7 Using a general beam section to define the section behavior

Example of the general beam section definition in the input file

```
*Beam General Section, elset=_I1, section=NONLINEAR GENERAL
```

```
0.18, 0.00135, 0., 0.0054, 0.0037098
```

```
0.,0.,-1.
```

```
*AXIAL
```

```
0,0
```

```
436170.6,9.02396E-005
```

```
...
7879644,0.0208312
0,0.021
*M1
0,0
42000,0.0002786545
...
600000,0.41798
0,0.42
*M2
0,0
25500,0.000705863333333333
...
150000,0.268775666666667
0,0.27
*TORQUE
0,0
10643750000,0.0037098
*Damping, alpha=0.471756, beta=0.00529881
*Transverse Shear
2.007e+09, 2.007e+09,
```

Defining the nonlinear behavior of the concrete in Abaqus

## Appendix A - Nonlinear behavior of RC

**Edit Material** [X]

Name: Concrete

Description:

**Material Behaviors**

Density  
Elastic  
Concrete Damaged Plasticity

General Mechanical Thermal Electrical/Magnetic Other

**Density**

Distribution: Uniform

Use temperature-dependent data

Number of field variables: 0

**Data**

	Mass Density
1	2400

OK Cancel

**Edit Material** [X]

Name: Concrete

Description:

**Material Behaviors**

Density  
Elastic  
Concrete Damaged Plasticity

General Mechanical Thermal Electrical/Magnetic Other

**Elastic**

Type: Isotropic Suboptions

Use temperature-dependent data

Number of field variables: 0

Moduli time scale (for viscoelasticity): Long-term

No compression  
 No tension

**Data**

	Young's Modulus	Poisson's Ratio
1	25545000000	0.2

OK Cancel

**Edit Material**

Name: Concrete

Description:

Material Behaviors

Density

Elastic

**Concrete Damaged Plasticity**

General Mechanical Thermal Electrical/Magnetic Other

Concrete Damaged Plasticity

Plasticity Compressive Behavior Tensile Behavior

Use temperature-dependent data

Number of field variables: 0

Data

	Dilation Angle	Eccentricity	fb0/fc0	K	Viscosity Parameter
1	55	0	1.16	0.67	0.001

OK Cancel

**Edit Material**

Name: Concrete

Description:

Material Behaviors

Density

Elastic

**Concrete Damaged Plasticity**

General Mechanical Thermal Electrical/Magnetic Other

Concrete Damaged Plasticity

Plasticity Compressive Behavior Tensile Behavior

Use strain-rate-dependent data

Use temperature-dependent data

Number of field variables: 0

Data

	Yield Stress	Inelastic Strain
1	2554500	0
2	4978000	0.0001
3	7270500	0.0002
4	9432000	0.0003
5	11462500	0.0004
6	13362000	0.0005
7	15130500	0.0006
8	16768000	0.0007

OK Cancel

**Edit Material**

Name: Concrete

Description:

Material Behaviors

Density

Elastic

**Concrete Damaged Plasticity**

General Mechanical Thermal Electrical/Magnetic Other

Concrete Damaged Plasticity

Plasticity Compressive Behavior Tensile Behavior

Type: Strain

Use strain-rate-dependent data

Use temperature-dependent data

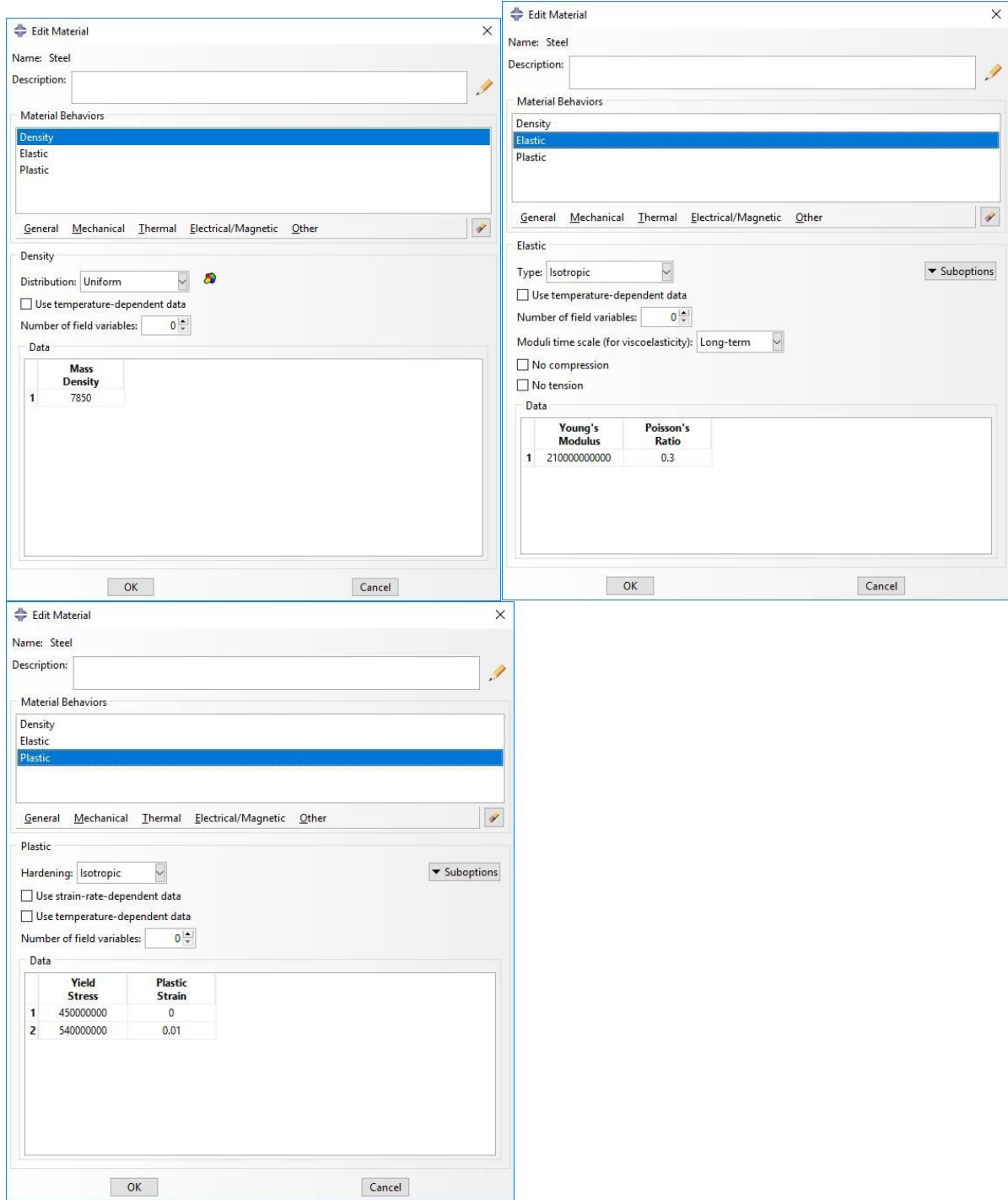
Number of field variables: 0

Data

	Yield Stress	Cracking Strain
1	3334453.1	0
2	0	0.005

OK Cancel

## Defining the nonlinear behavior of the steel in Abaqus

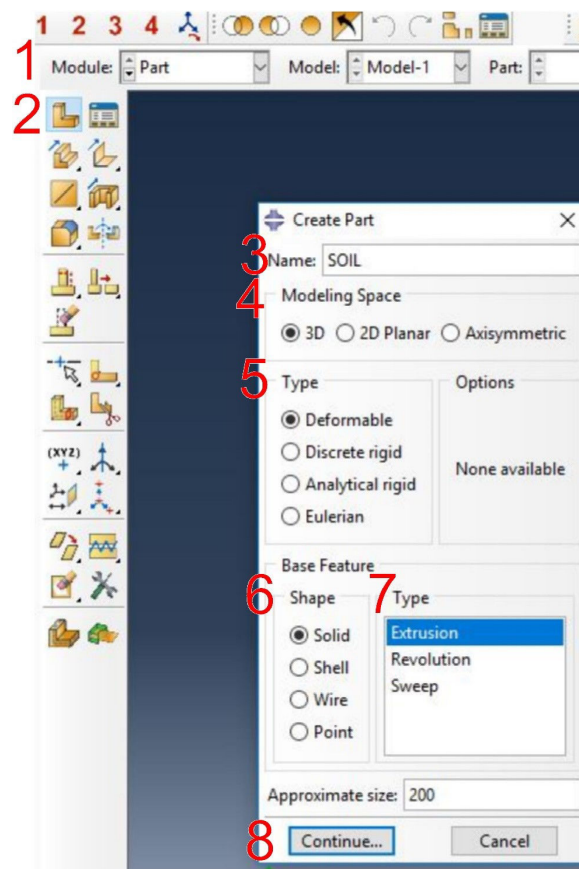




## Appendix B - 1D-3C model for SSI analysis

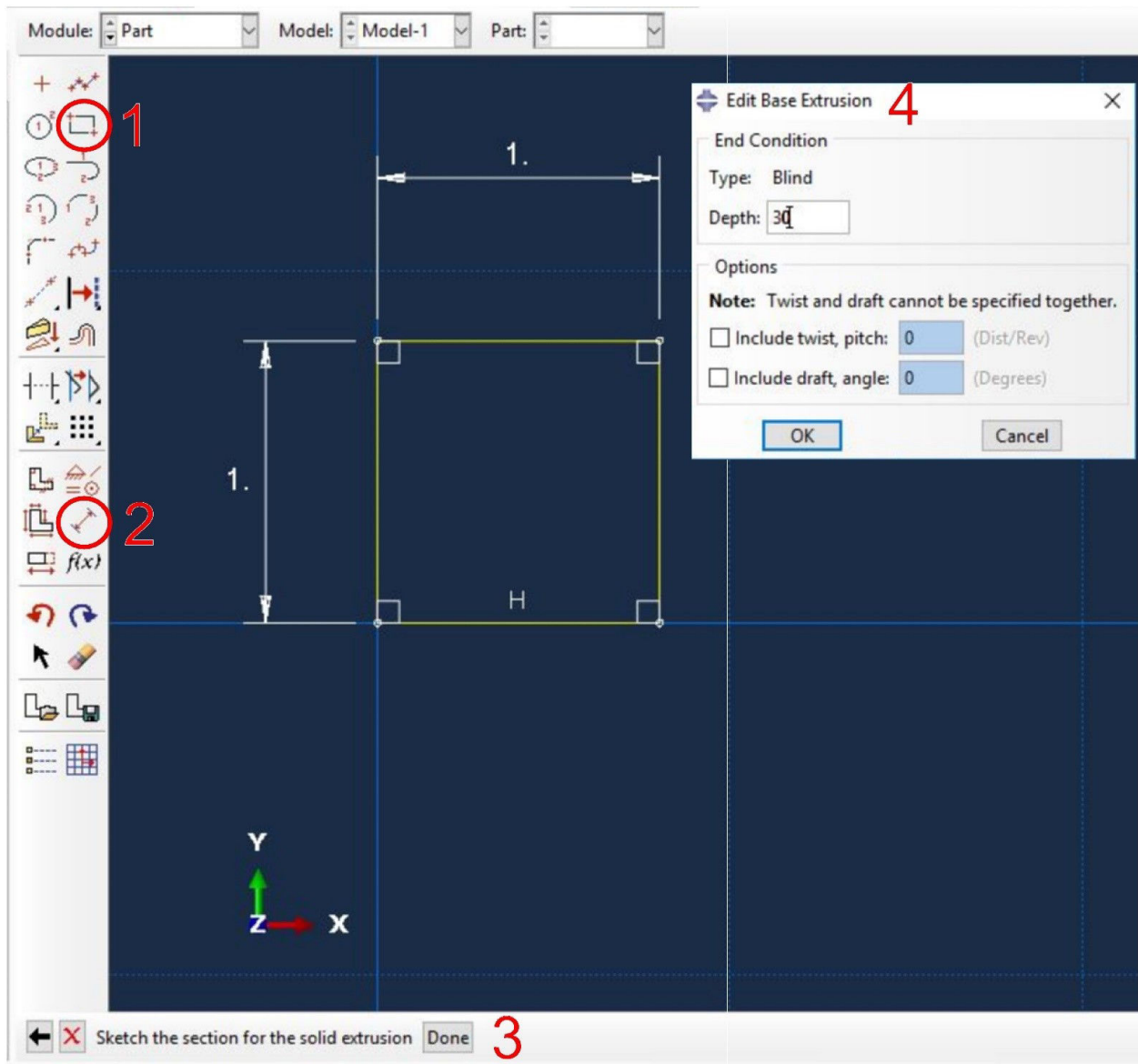
This guide is intended for users who will exercise research or engineering in earthquake design. A step-by-step procedure is described to model the 1-D soil model of linear behavior introduced in 0 for SSI analysis.

### 1-D soil model

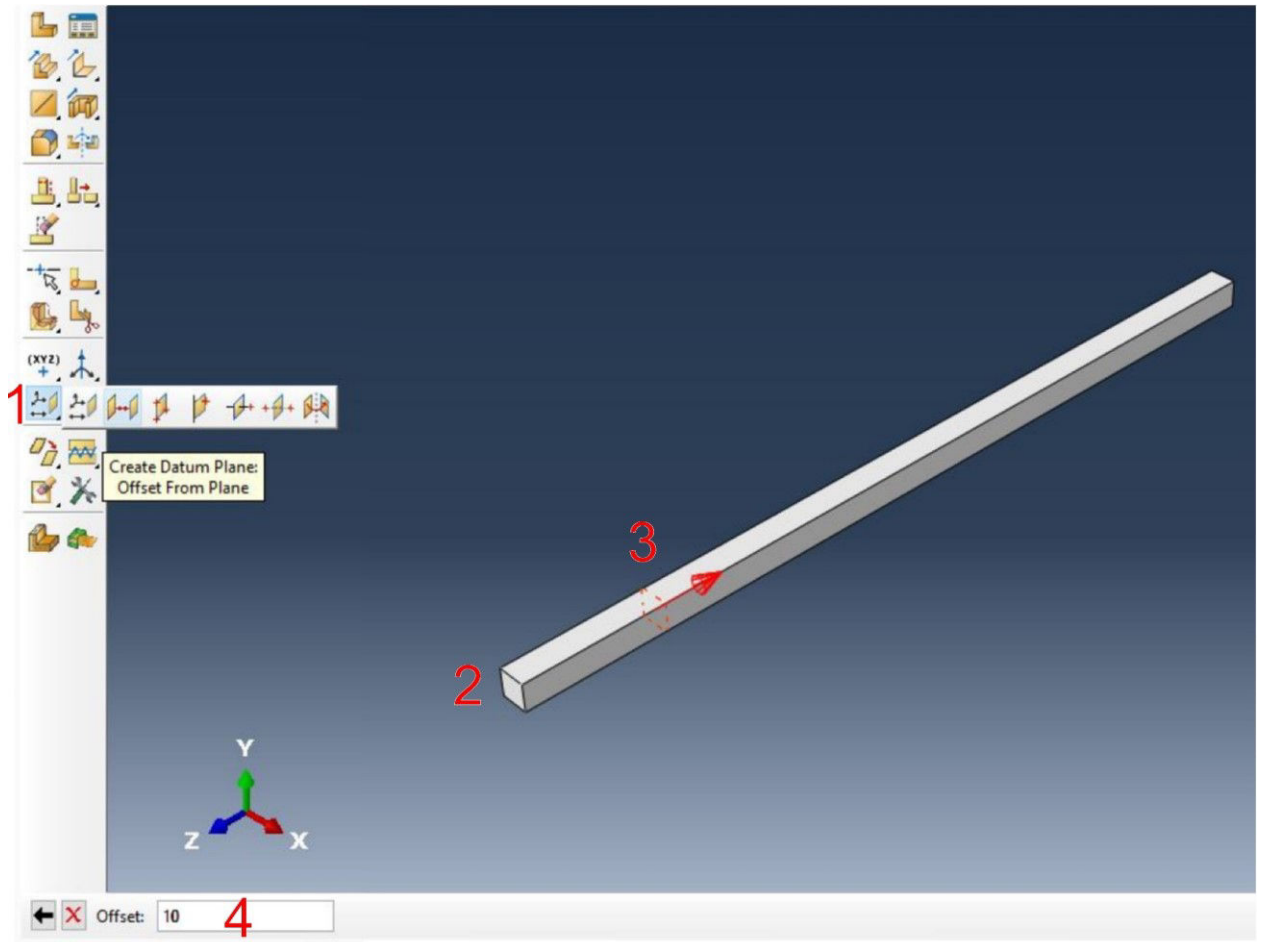


1. Choose the module **Part**
2. Click on the icon **Create Part**
3. Choose a **Name** for your part
4. Select the **Modeling space** → **3D**
5. Select the **Type** → **Deformable**
6. Select the **Base Feature** → **Shape** → **Solid**
7. Select the **Base Feature** → **Type** → **Extrusion**

## 8. Continue

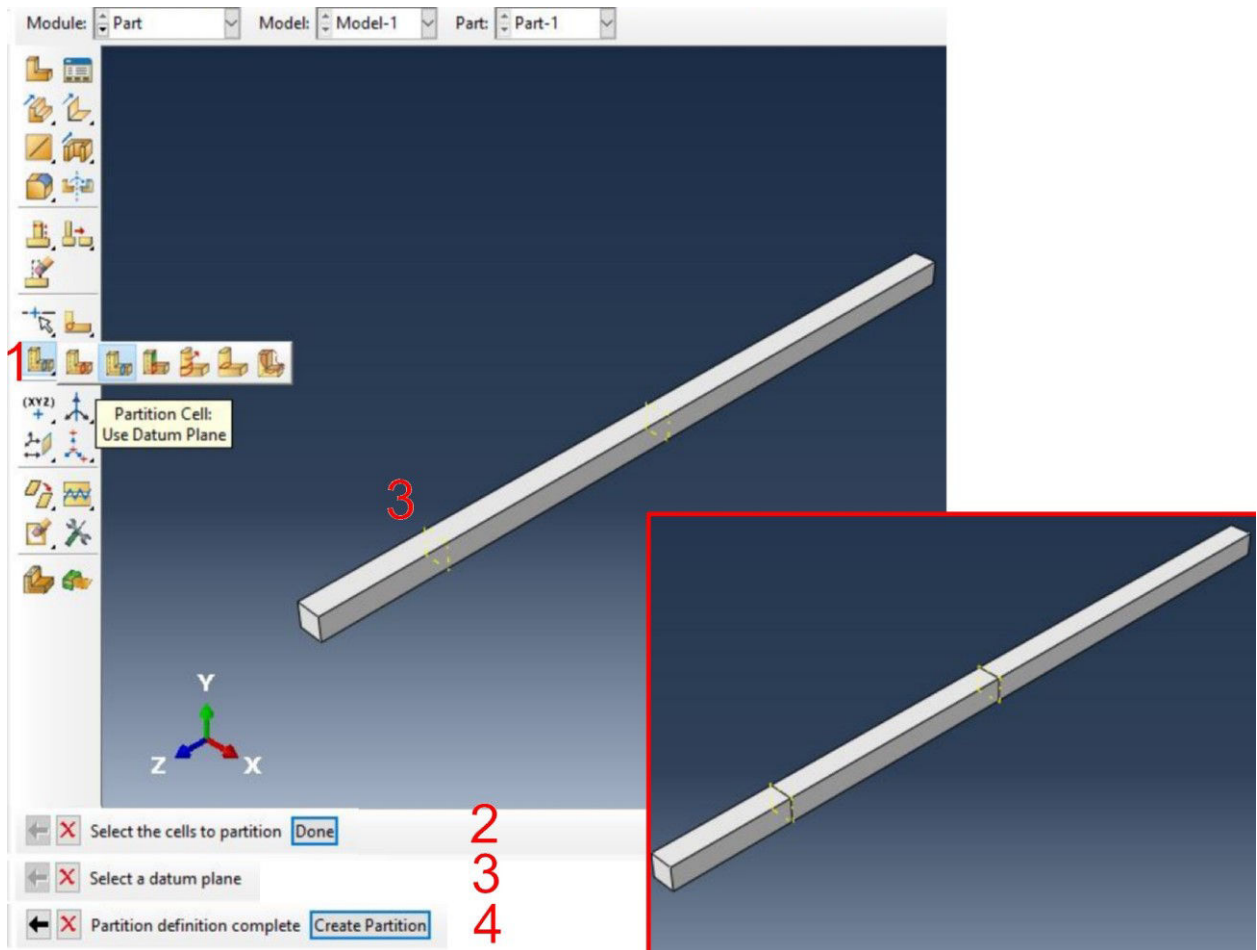


1. Click on the icon **Create Lines: Rectangle** → Draw a rectangle
2. Click on the icon **Add Dimension** → Correct the dimension of the rectangle to  **$1 \times 1 \text{ m}^2$**
3. Click on **Done**
4. Write the **Depth** in the new dialog → **30 m**  
**OK**



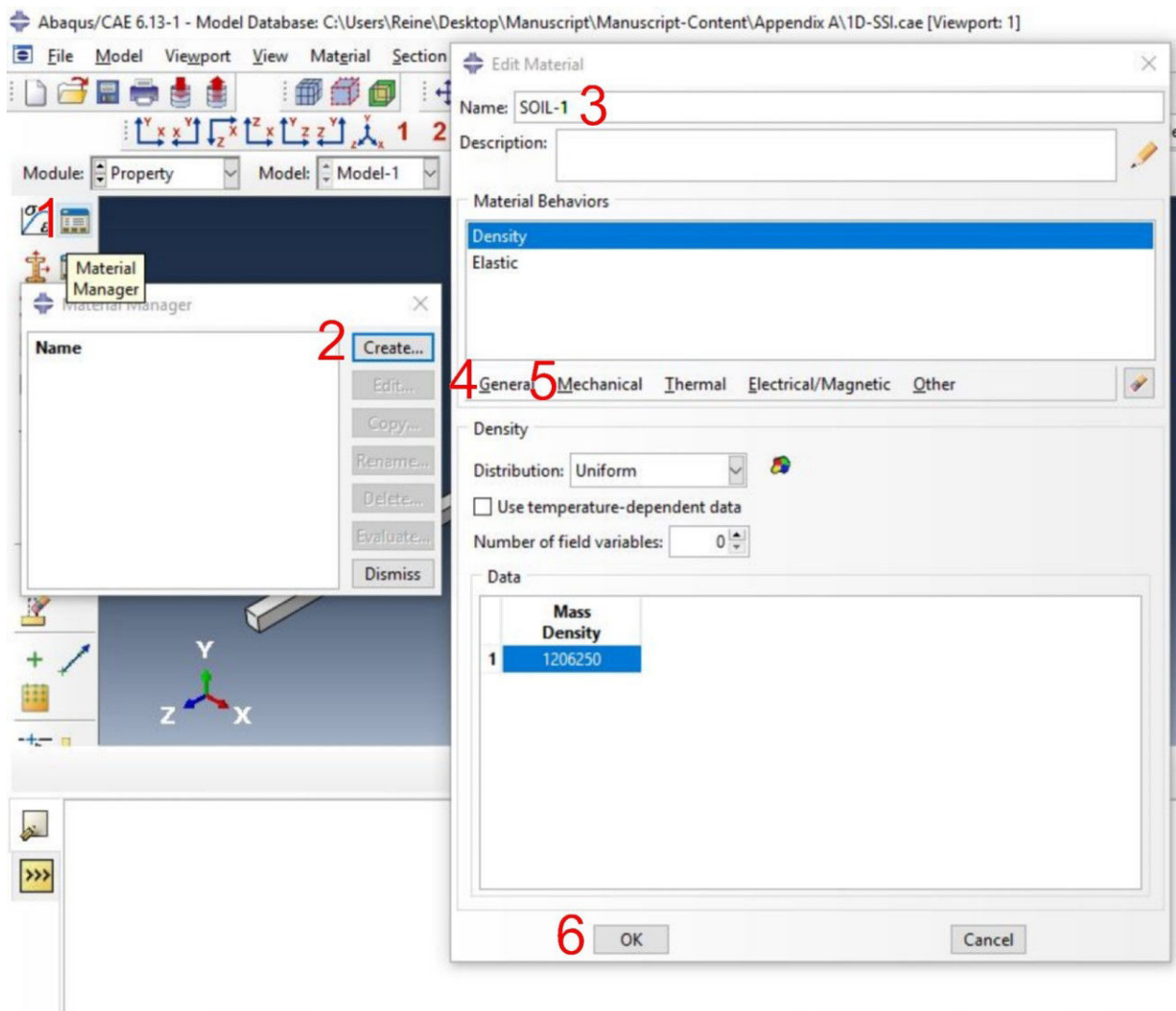
1. Click on the icon **Create Datum Plane: Offset From Plane**
2. Click on the **plane** you want to offset from
3. Choose the **direction** of offset
4. Write the **Offset distance** in the new dialog → **5 m**
5. **Press Enter**

**Repeat this step in order to have planes in the intersection of layers**



1. Click on the icon **Partition Cell: Use Datum Plane**
2. Select the **cell(s)** to partition, for the first partition this step is omitted
3. Select the **datum plane** to define the cutting plane
4. Click on **Create Partition**

**Repeat this step in order to partition all the layers**



Choose the module **Property**

1. Click on the icon **Material Manager**
2. Click on the icon **Create**
3. Choose a **Name** for your material
4. Select from the catalogue **General** → **Density**, enter the density of the material.

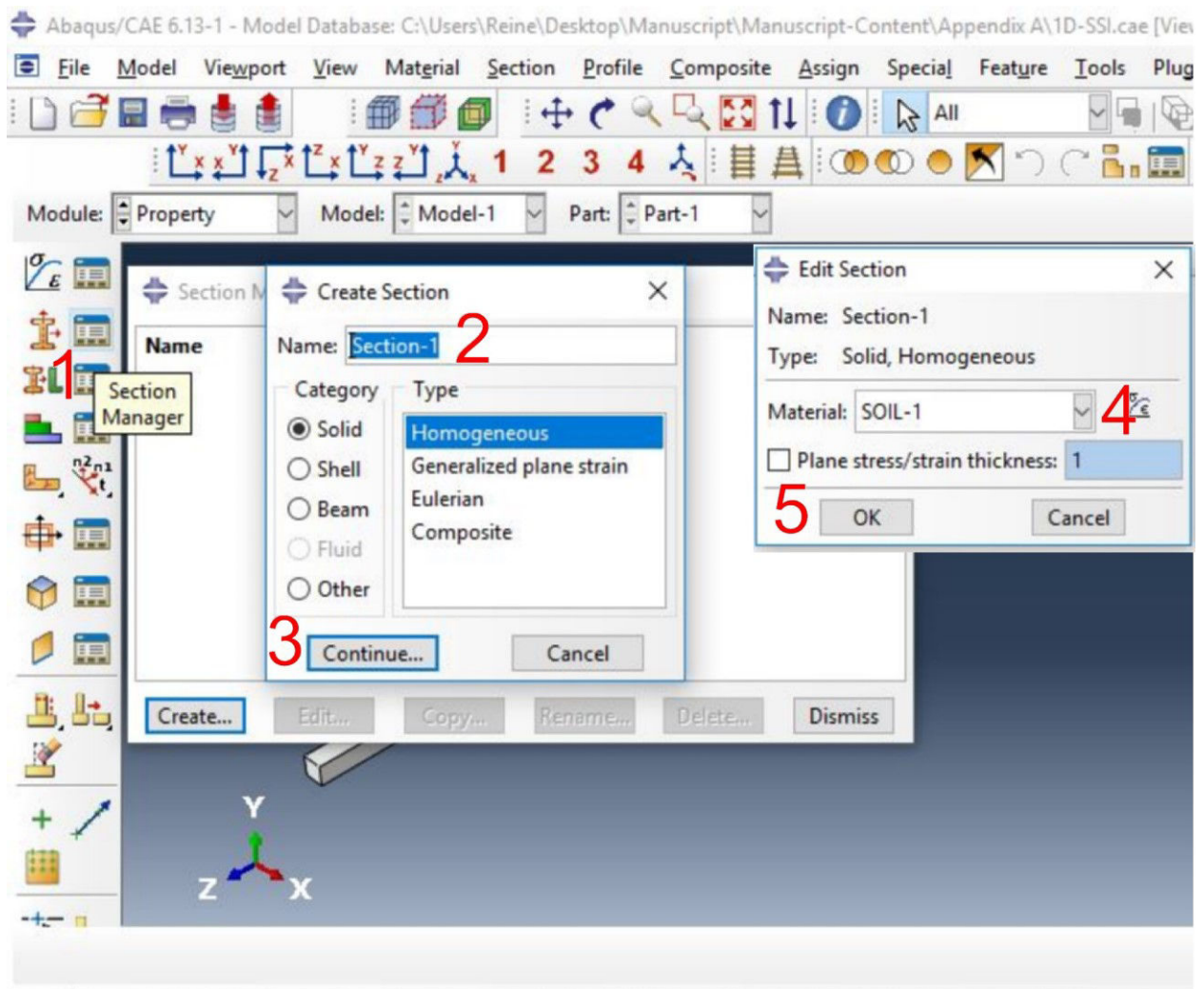
PS: Don't forget to multiply the density by the area

5. Select from the catalogue **Mechanical** → **Elasticity**, enter the Young modulus and the poisson ratio of the material.

PS: Don't forget to multiply the Young modulus by the area

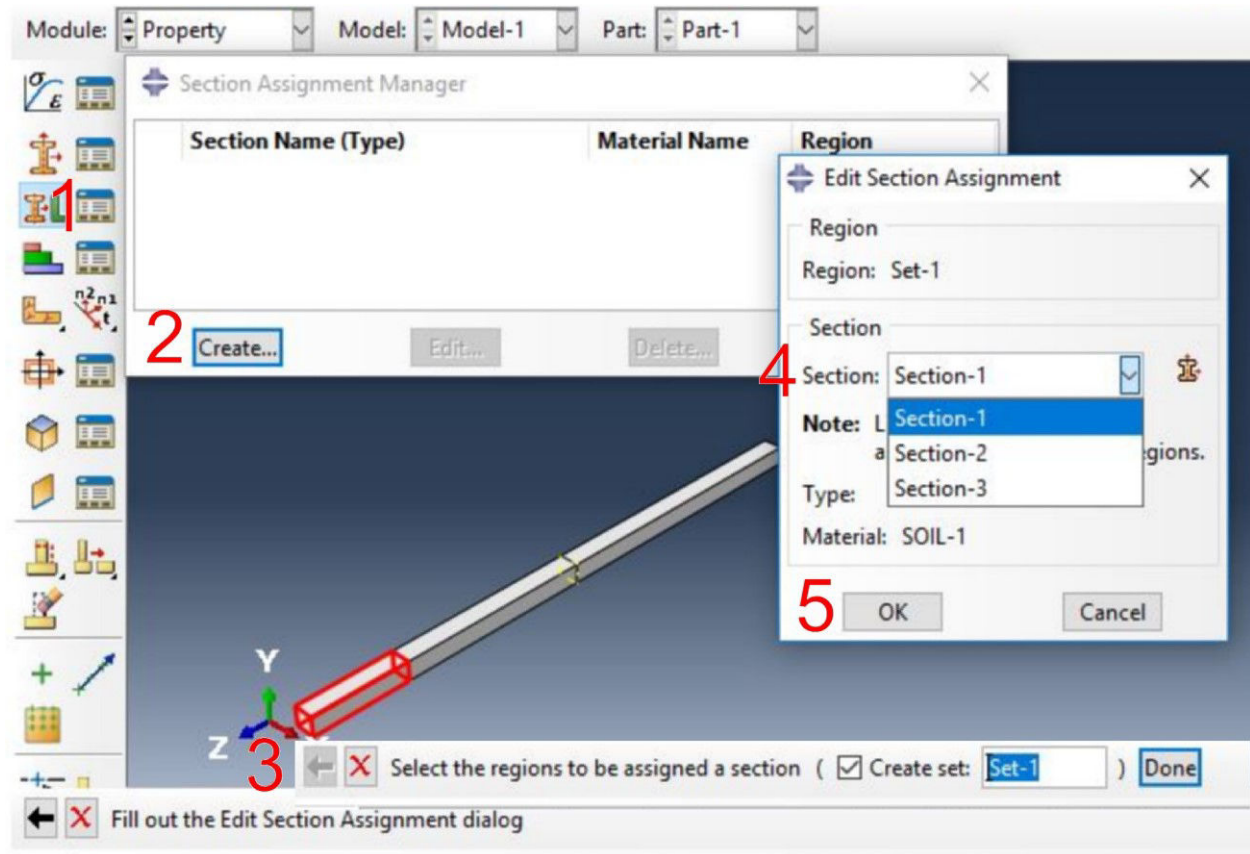
6. Click **OK**

**Repeat this step in order to have a material for each layer**



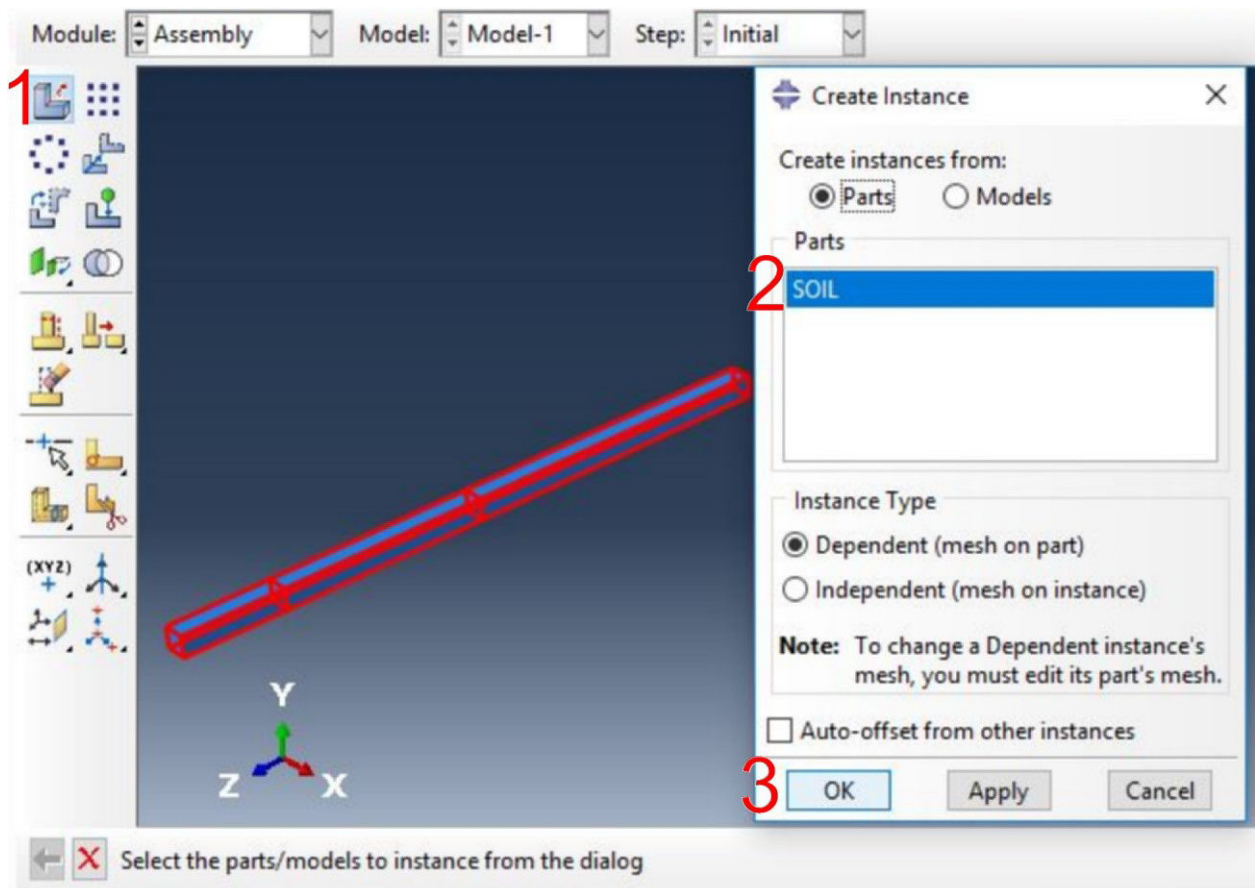
1. Click on the icon **Section Manager**
2. Click on the icon **Create** → Choose a **Name** for your section
  - Select **Solid** from **Category**
  - Select **Homogeneous** from **Type**
3. **Continue**
4. Select the material from the catalogue → **Soil-1**
5. Click **OK**

**Repeat this step in order to have a section for each material**



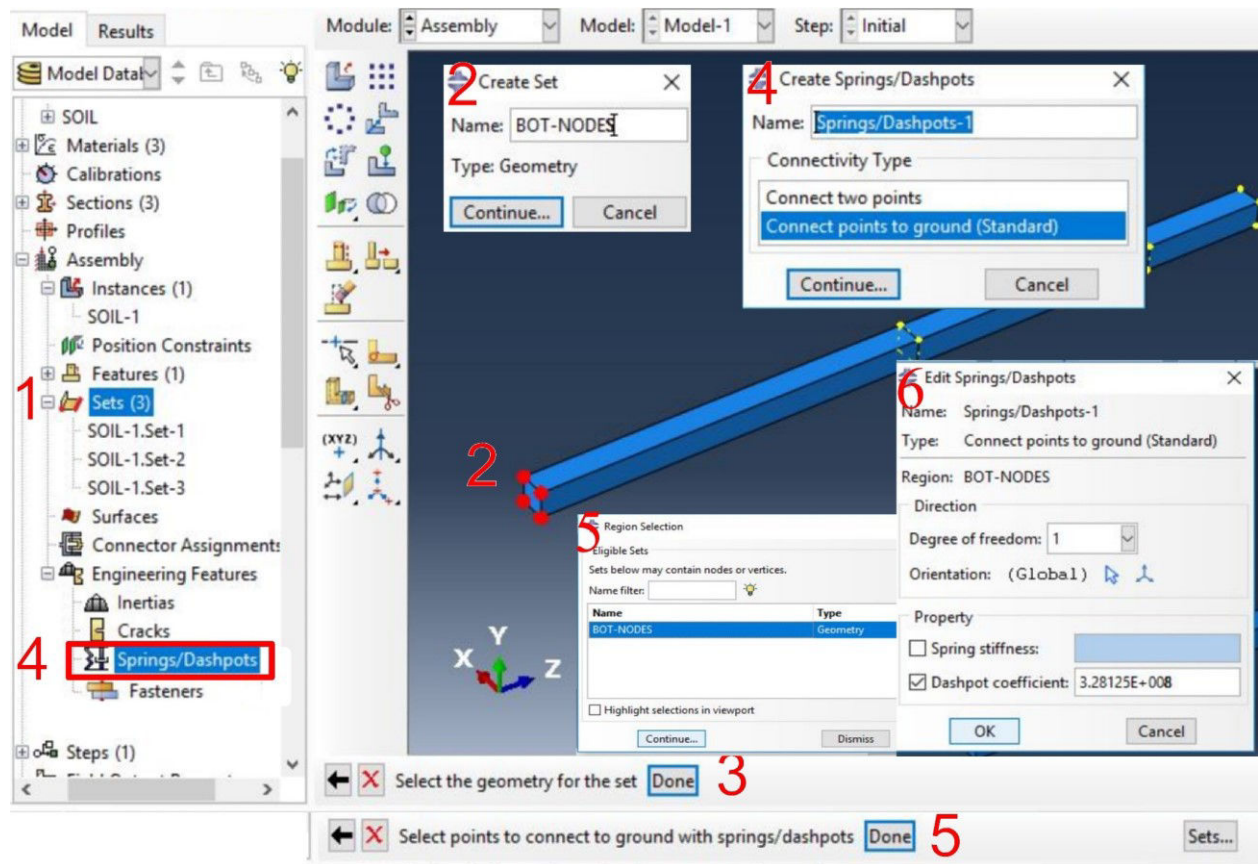
1. Click on the icon **Section Assignment Manager**
2. Click on the icon **Create**
3. Select the **Regions** to be assigned a section and a **Name** for this region  
Click **Done**
4. Select the Section from the catalogue → **Section-1**
5. Click **OK**

**Repeat this step in order to assign a section for each layer**



Choose the module **Assembly**

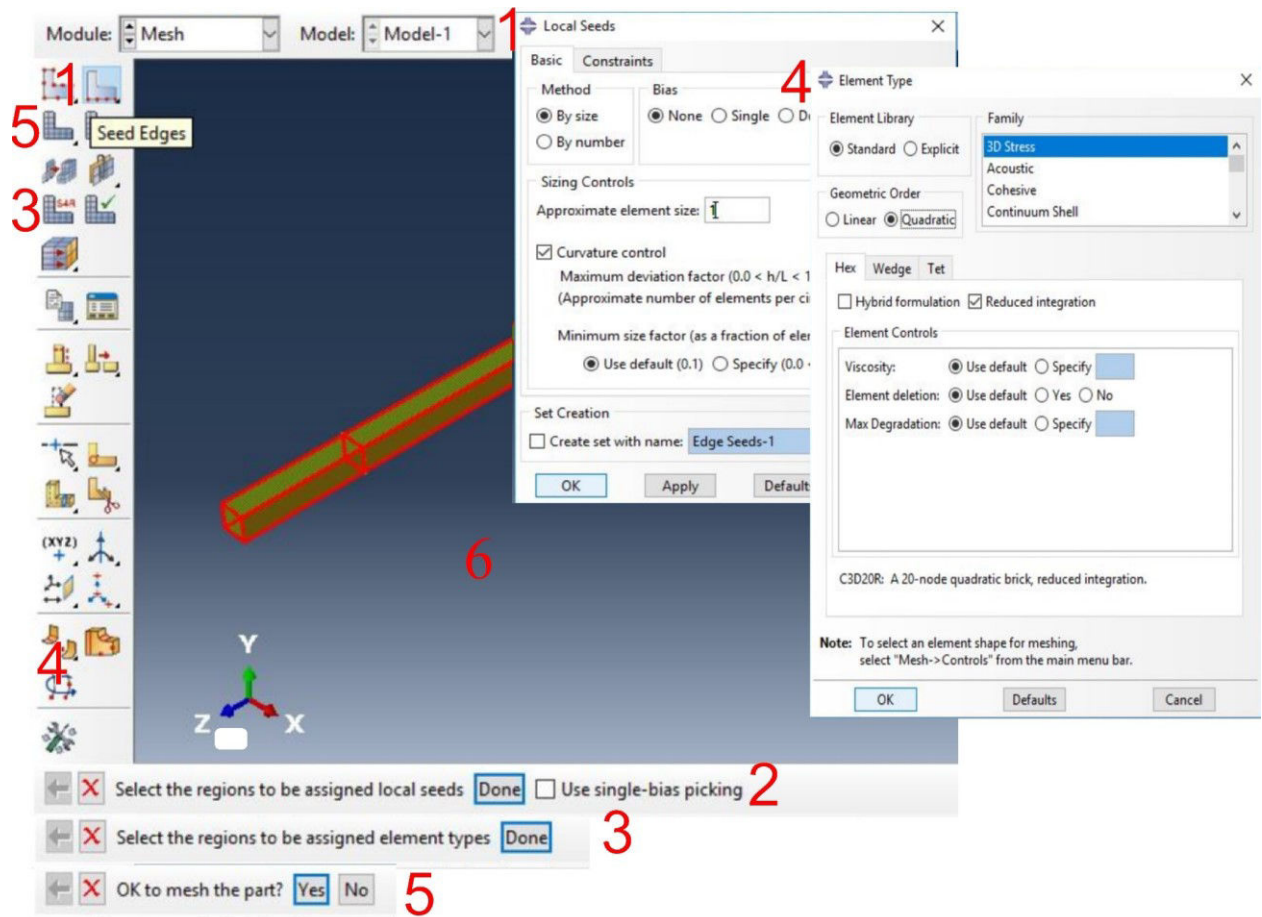
1. Click on the icon **Create Instance**
2. Choose the **SOIL Part** from the list of Parts
3. Click **OK**



1. Double click on **Sets**
2. **Name** the Set → Continue → Select all bottom geometric nodes
3. Click on **Done**
4. Double click on the icon **Springs/Dahpots** → Name → **Select Connect points to ground**
5. Select points from the **Sets** catalogue → Select all bottom nodes → Continue → Done
6. Select the degree of freedom **1** → **disable Spring stiffness** → **Enable Dashpot coefficient** → Enter the value of **damping** → **OK**

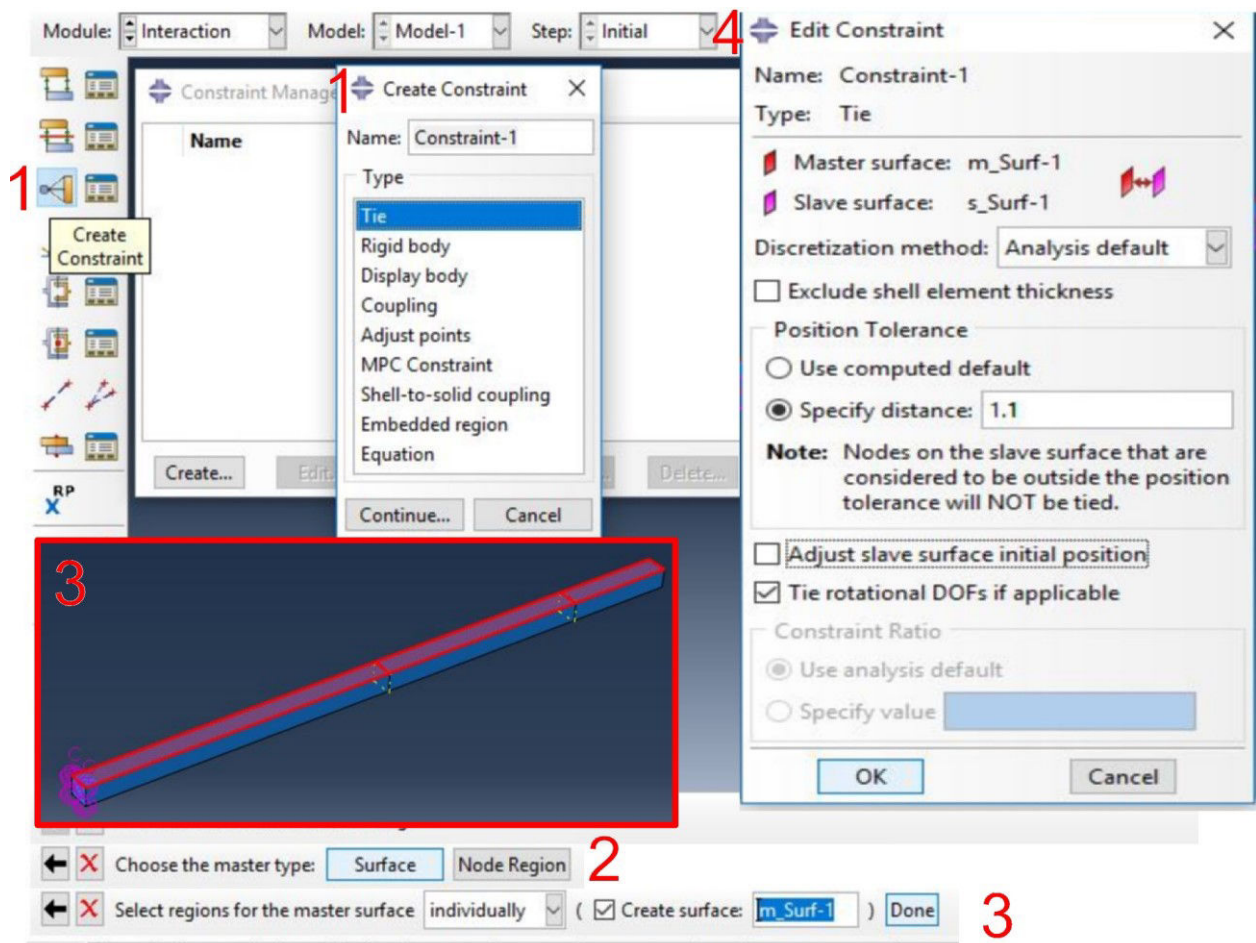
PS. Don't forget to divide by the number of bottom nodes

**Repeat this step for the degrees of freedom 2 and 3**



Choose the module **Mesh**

1. Click on the icon **Seed Edges** → Meshed **By size** → Approximate element size **1** → **OK**
2. **Done**
3. Click on the icon **Assign Element Types** → Select the region to mesh → **Done**
4. From Family select **3D Stress** → from Geometric Order enable **Quadratic** → **OK**
5. Click on **YES**

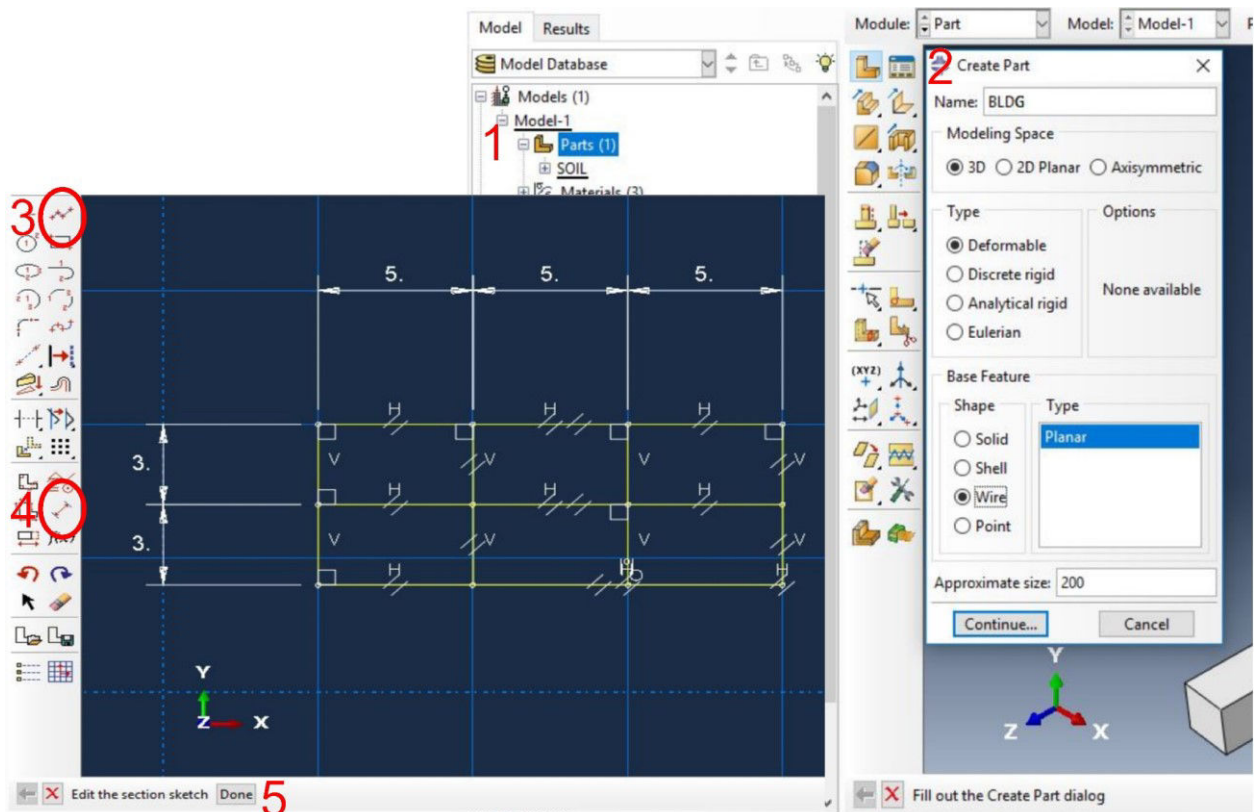


Choose the module **Interaction**

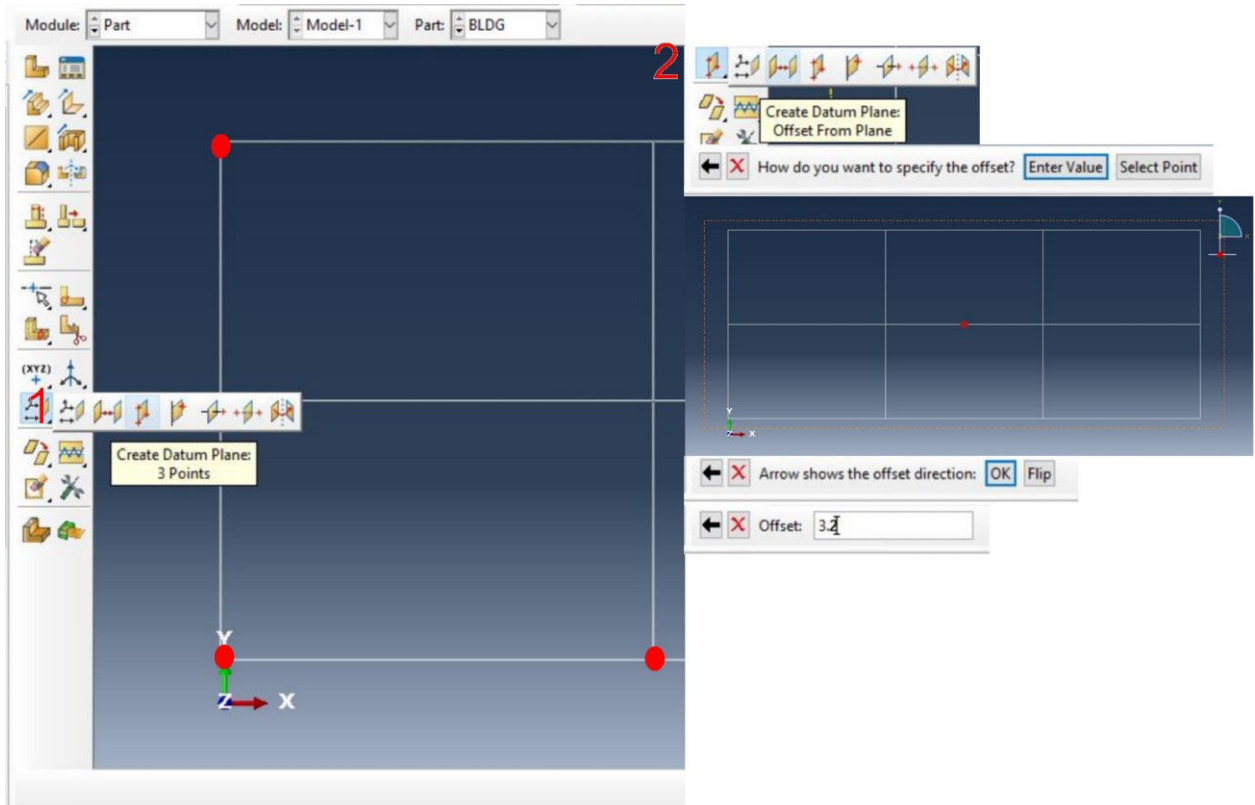
1. Click on the icon **Create Constraint** → Select **Tie** → **Continue**
2. Choose the master type **Surface**
3. Select a lateral surface of the column → Then choose the slave type **Surface** → Select the opposite lateral surface of the column
4. Specify distance **1.1** → **disable** Adjust slave surface initial position → **OK**

**Repeat this step for the other two opposite lateral surfaces**

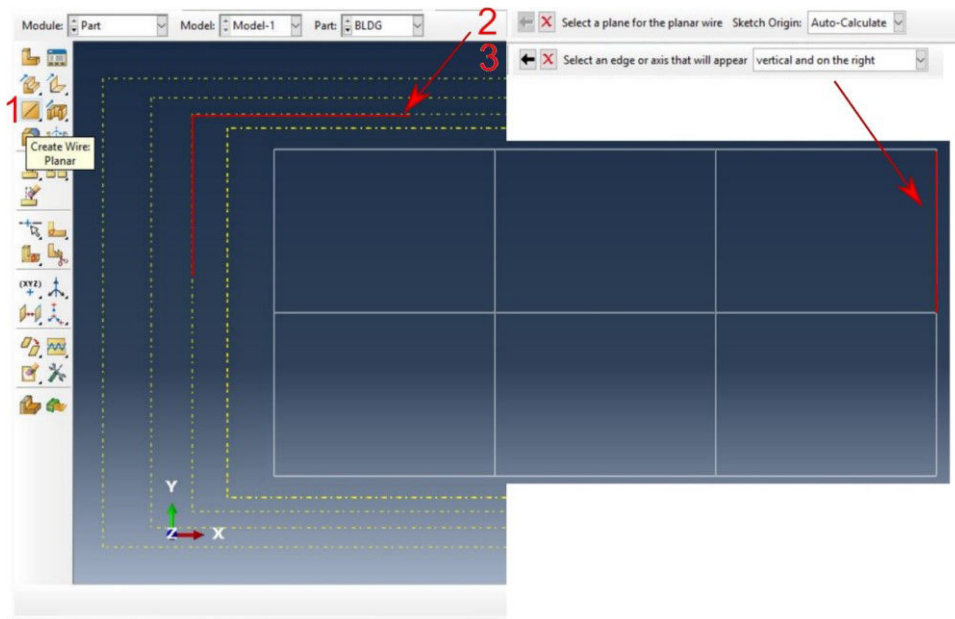
## 3-D building model



1. Double click on **Parts**
2. Choose a **Name** for your part  
Select the **Modeling space** → **3D**  
Select the **Type** → **Deformable**  
Select the **Base Feature** → **Shape** → **Wire**
3. **Sketch** the floor plan of the building as shown in the picture
4. Adjust the dimensions  
**Continue**

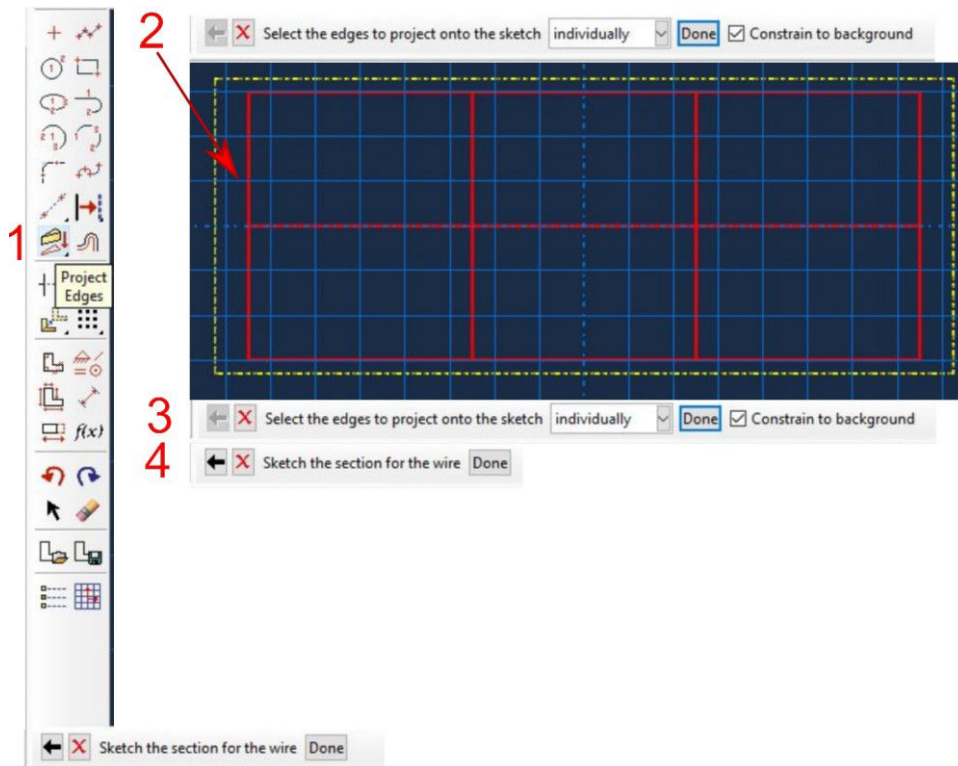


1. Click on the icon **Create Datum Plane: 3 Points** and create the plane using the selecting red points as shown
2. Click on the icon **Create Datum Plane: Offset From Plane**  
Select the **plane** you want to offset from  
Choose the **direction** of offset  
Write the **Offset distance** in the new dialog → **3.2 m**
3. **Press Enter**  
**Repeat this step in order to have a plane for each level**



1. Click on the icon **Create Wire Planar**
2. Select a **plane** on which you want to sketch a planar wire
3. Select an **edge** that will appear on the write of the screen

### Following

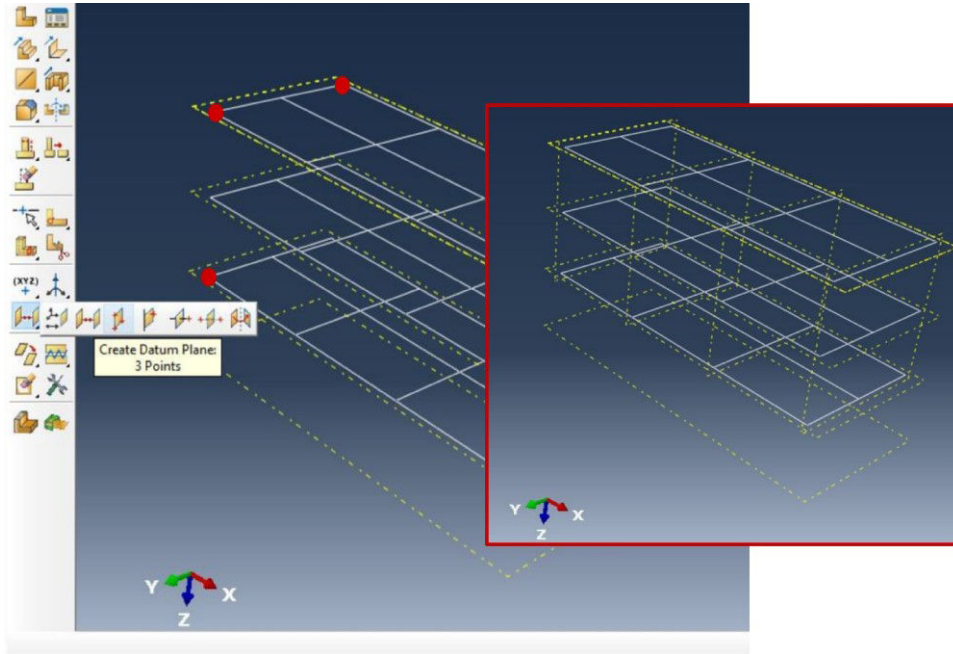


1. Click on the icon **Project Edges**
2. Select the **edges** to project onto the sketch → **Done**

3. **Done**

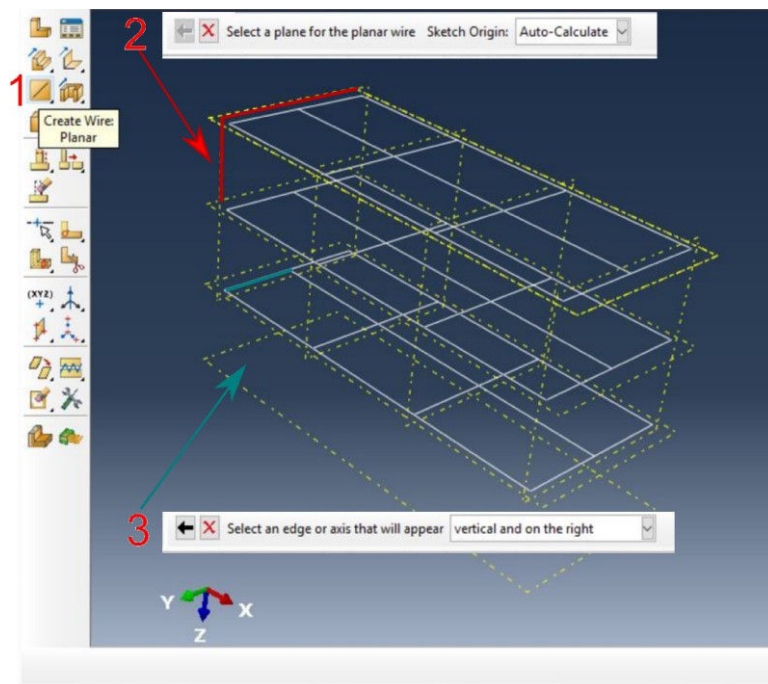
4. **Done**

**Repeat this step in order to have the plan wire for each floor**

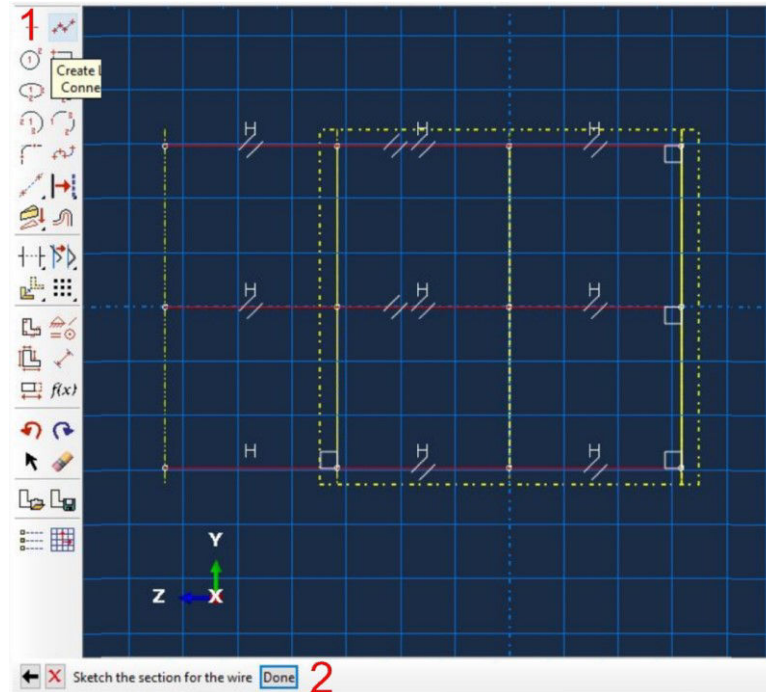


Click on the icon **Create Datum Plane: 3 Points** and create the plane using the selecting red points as shown

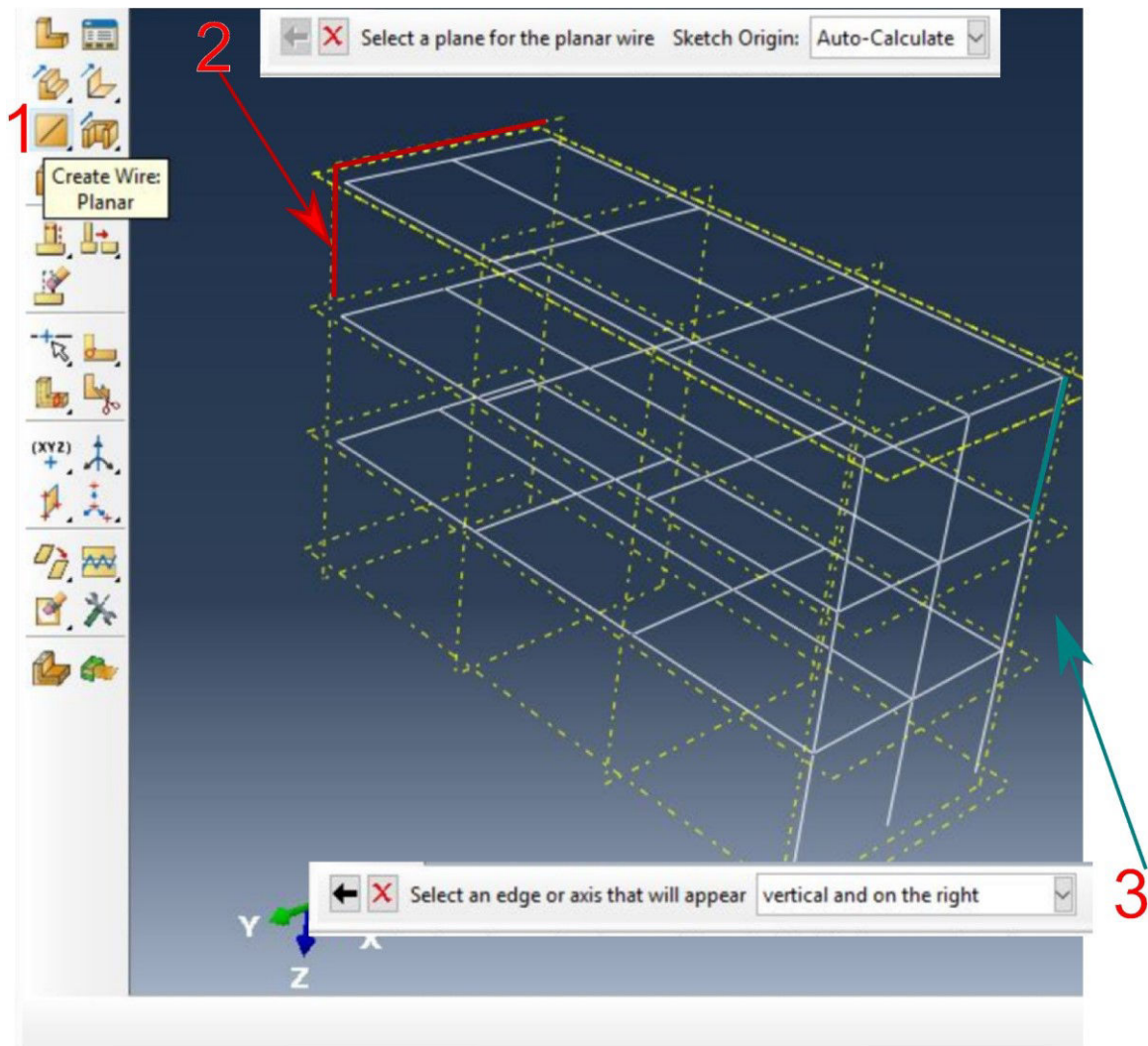
**Repeat this step in order to have datum plans as shown**



1. Click on the icon **Create Wire Planar**
2. Select a **plane** on which you want to sketch a planar wire
3. Select an **edge** that will appear on the wire of the screen

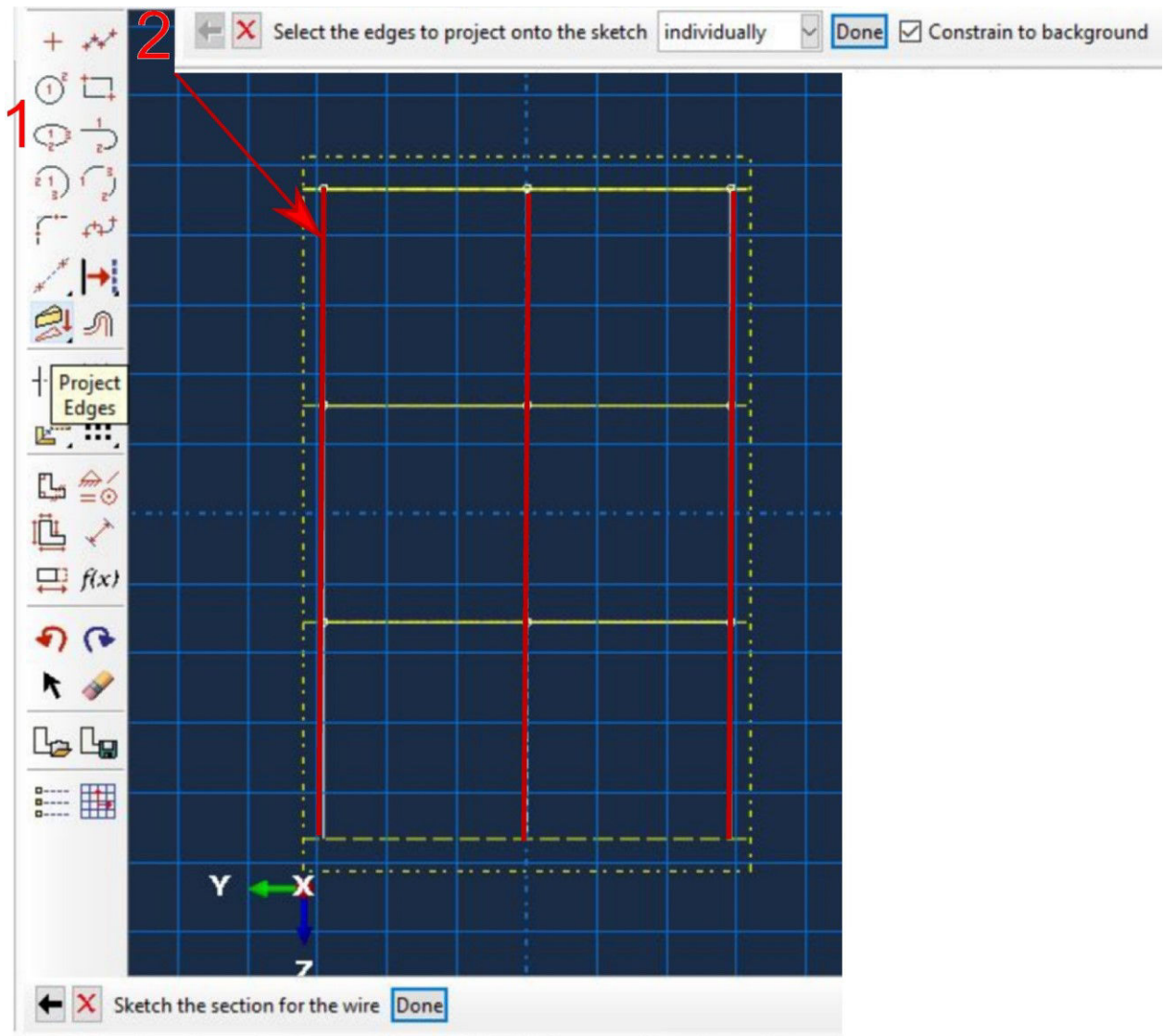


1. Click on the icon **Create Wire**  
Sketch **wire** to create the column as shown
2. **Done**



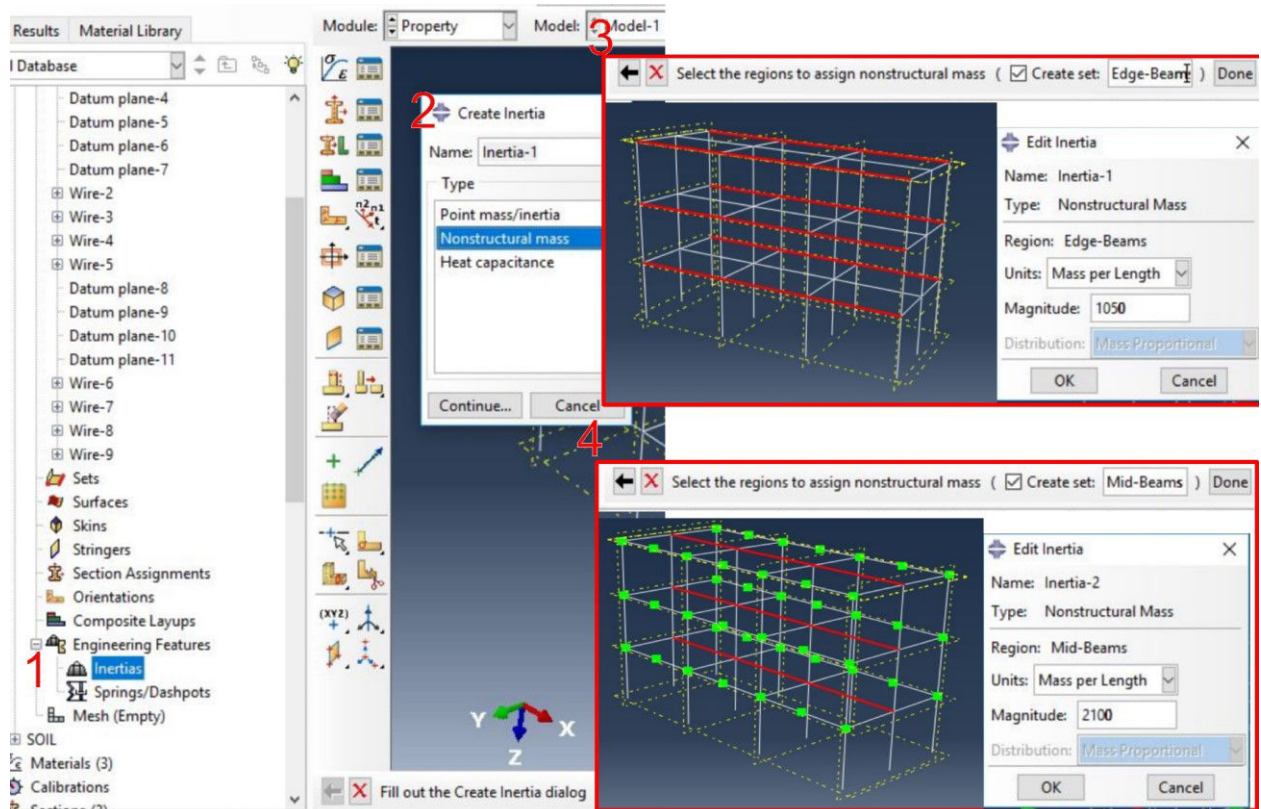
1. Click on the icon **Create Wire Planar**
2. Select a **plane** on which you want to sketch a planar wire
3. Select an **edge** that will appear on the wire of the screen

**Following**

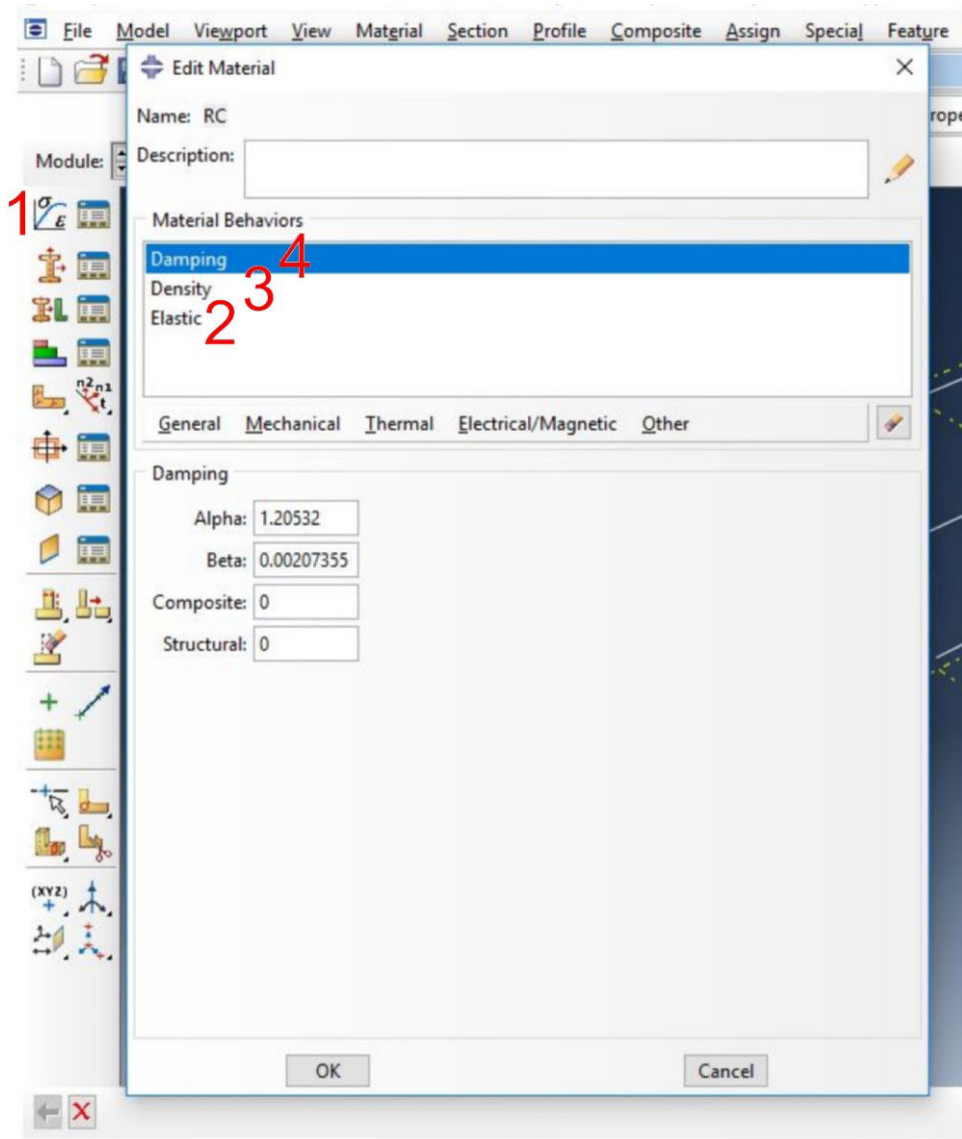


1. Click on the icon **Project Edges**
2. Select the **edges** to project onto the sketch → **Done**
3. **Done**
4. **Done**

**Repeat this step in order to have the plan wire for all y-z datum plans**

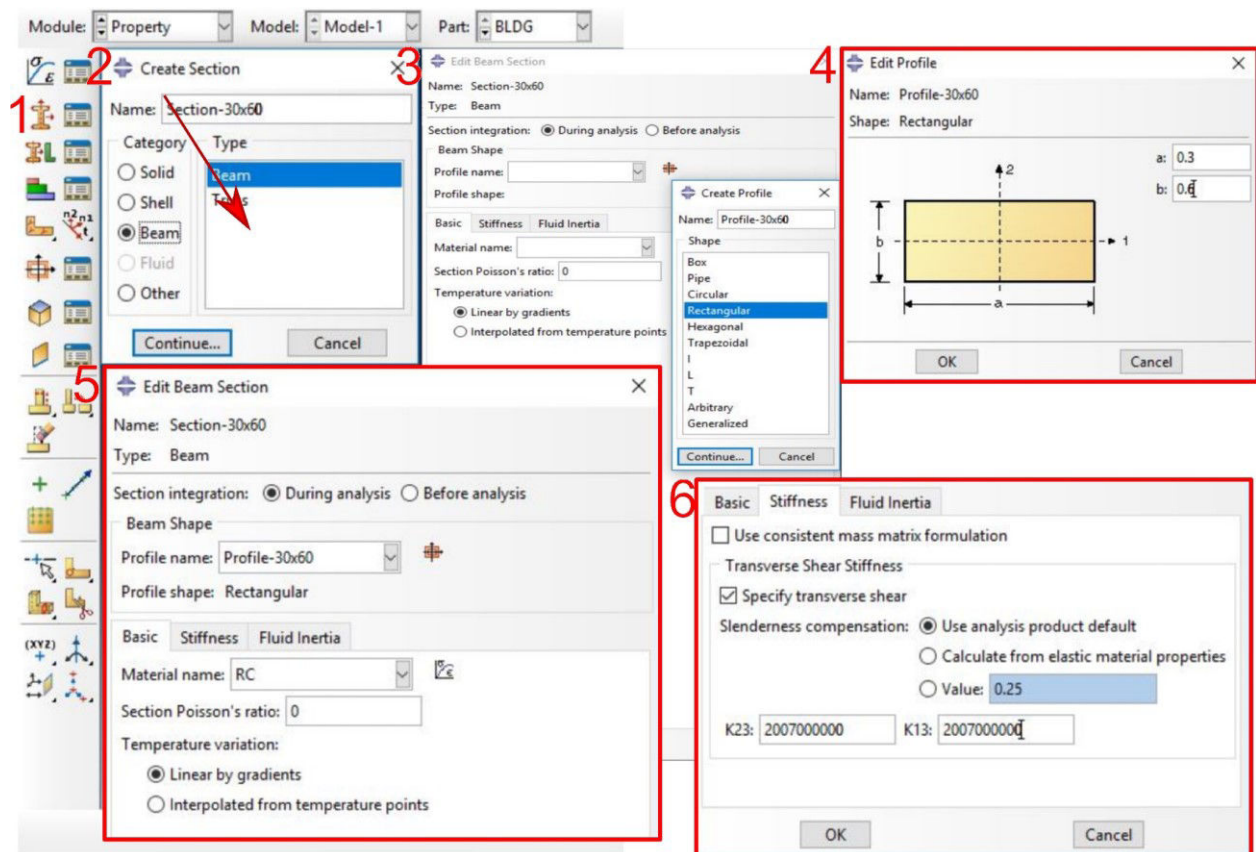


1. Double click on the icon **Inertias** → Name → **Nonstructural mass**
2. Select the region to assign nonstructural mass → Select **Edge Beams** → From Units select **Mass per Length**, from **Magnitude** input **1050** → **OK**
3. Select the region to assign nonstructural mass → Select **Middle Beams** → From Units select **Mass per Length**, from **Magnitude** input **2100** → **OK**



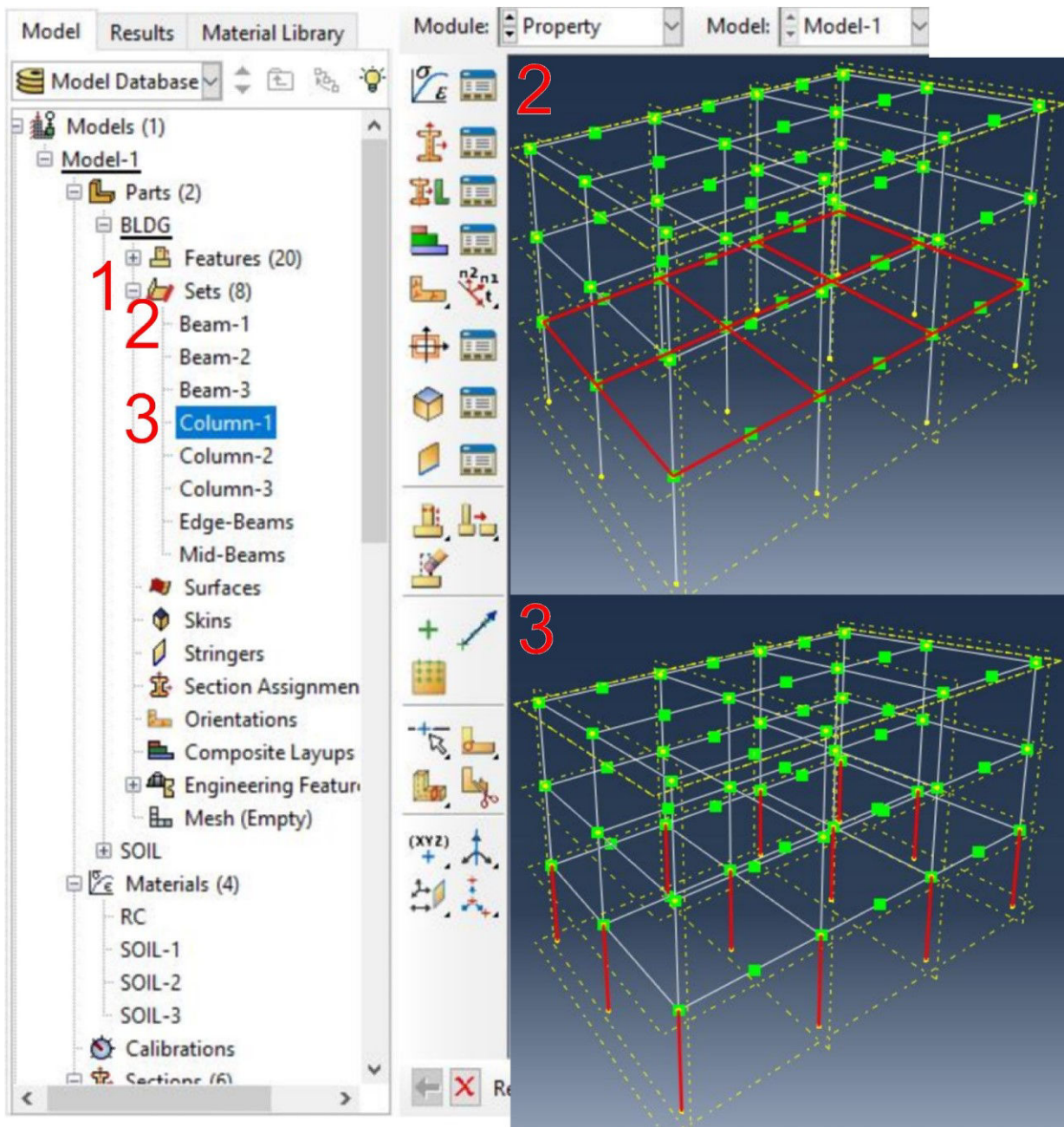
Choose the module **Property**

1. Click on the icon **Create Material** → Choose a **Name** for your material
2. Select from the catalogue **Mechanical** → **Damping**, enter the damping coefficients.
3. Select from the catalogue **General** → **Density**, enter the density of the material.
4. Select from the catalogue **Mechanical** → **Elasticity**, enter the Young modulus and the poison ratio of the material.
5. Click **OK**



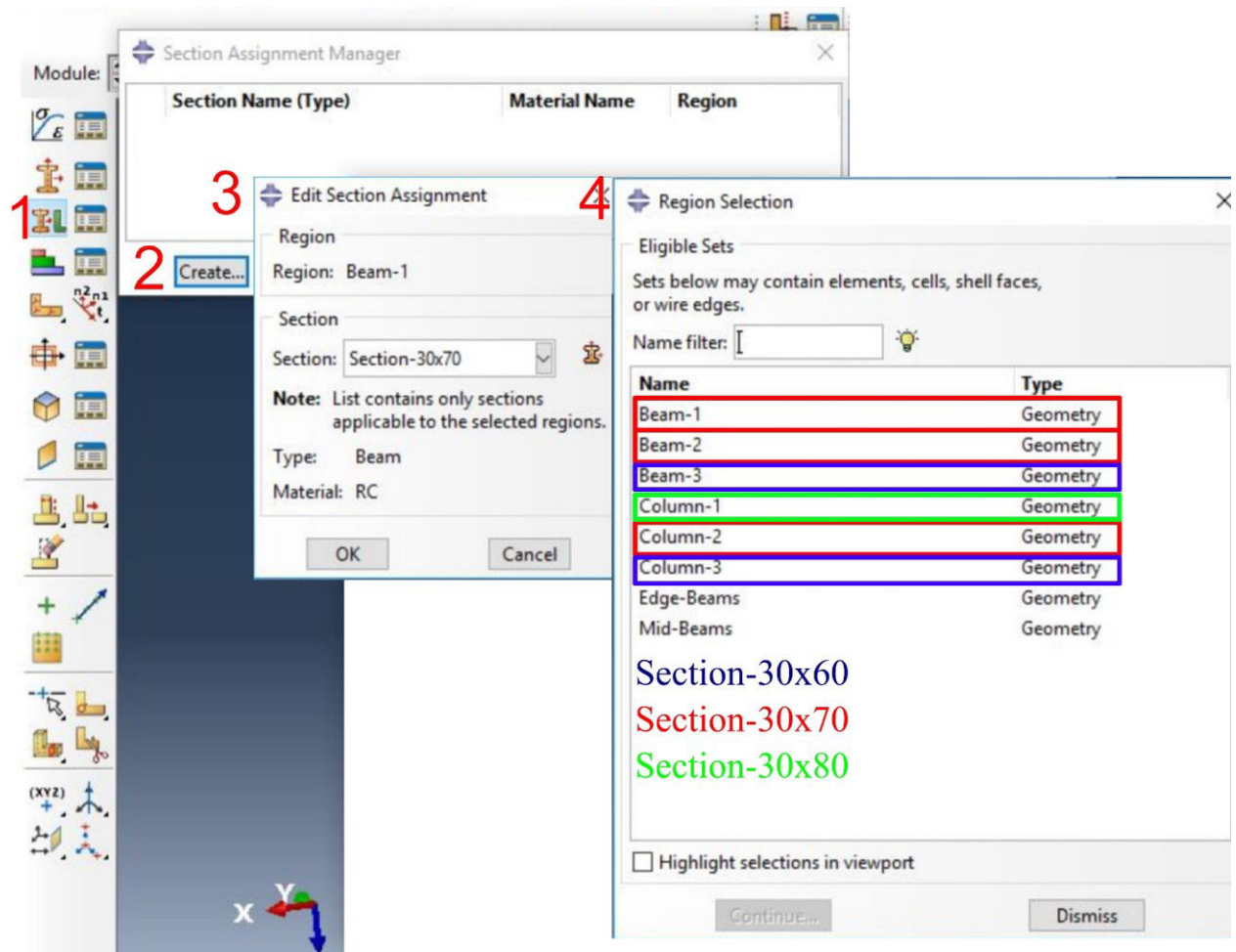
1. Click on the icon **Create Section**
2. Choose a **Name** for your section → Select **Beam** from **Category** → Select **Beam** from **Type** → **Continue**
3. Click on the icon **Create Beam Profile** → Choose a **Name** for your Profile → Select **Rectangular** from **Shape** → **Continue**
4. Input **a** and **b**
5. Choose the material from **Basic** → **Material Name**
6. Enable **Specify transverse shear** from **Stiffness** → input **K23** and **K13** → **OK**

**Repeat this step in order to create a section for beam and column section type**



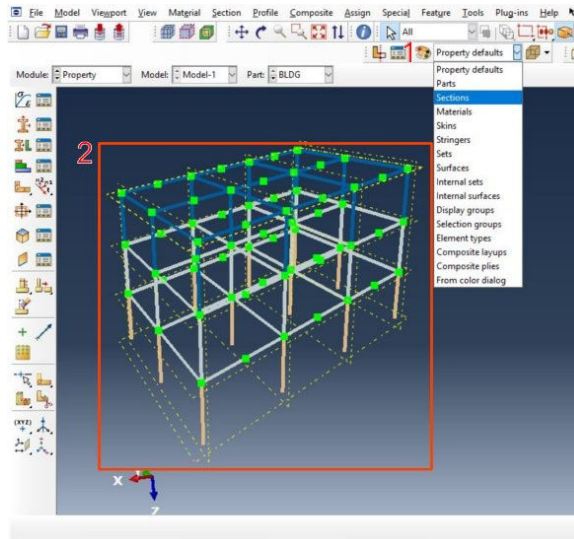
1. Double Click on the icon Sets
2. Create Sets for all the beams on the same level
3. Create Sets for all the columns on the same level

As shown in the Figure

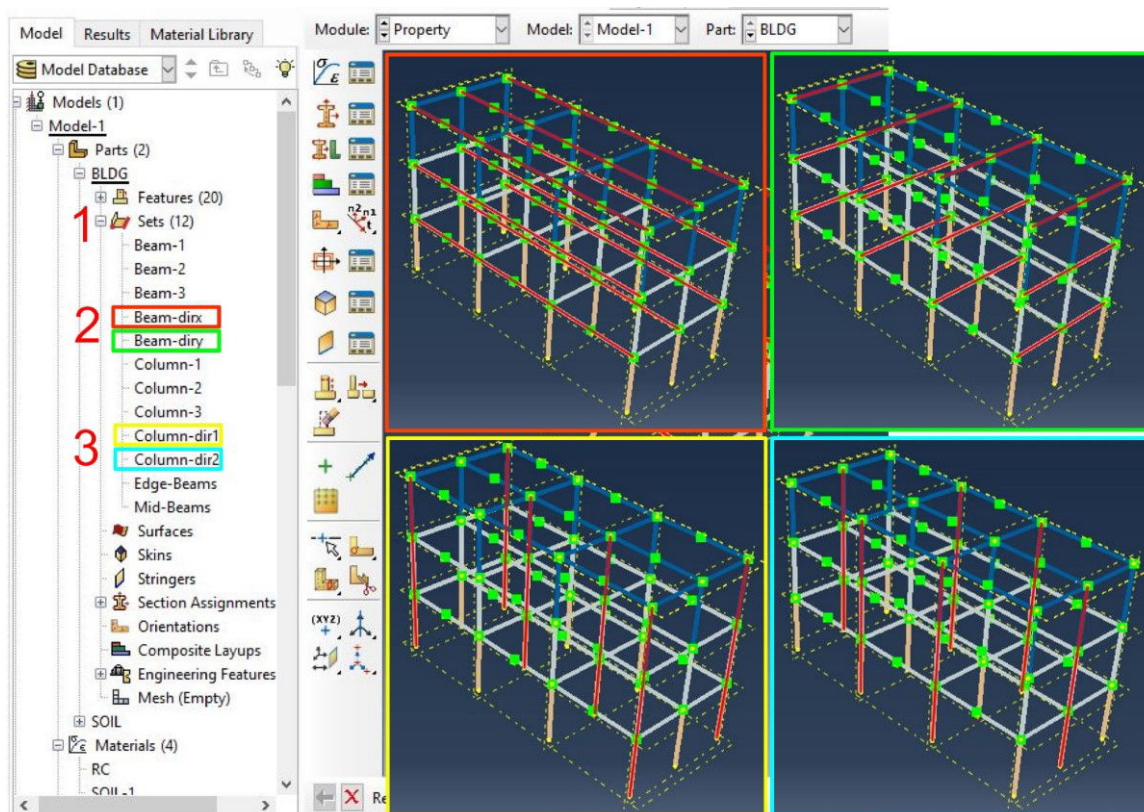


1. Click on the icon **Assign Section**
2. Click on the icon **Create** → Choose a **Region** from sets  
 → Select a section from **Section**

**Repeat this step in order to have a section for all columns and beams as shown in the Figure**

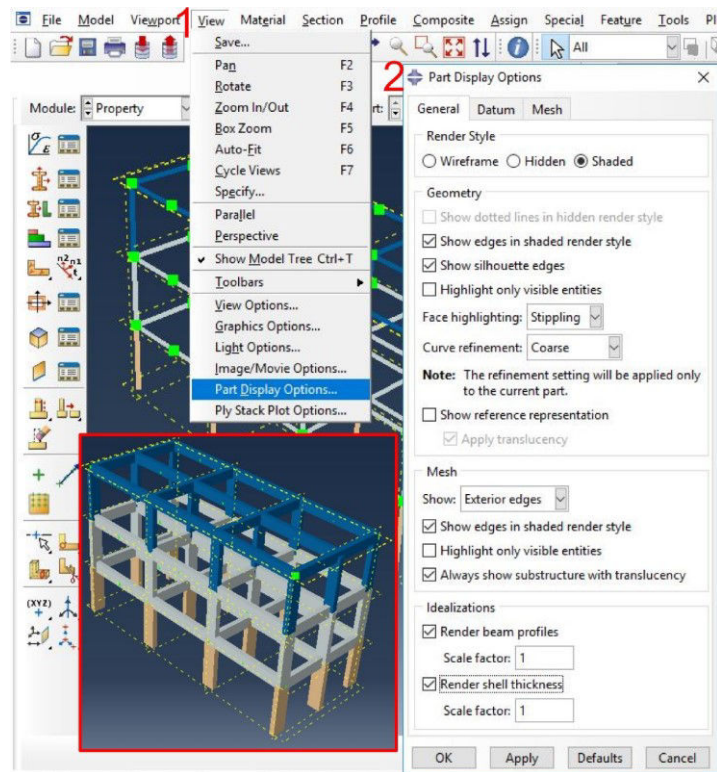


**1. From Property default choose Sections**

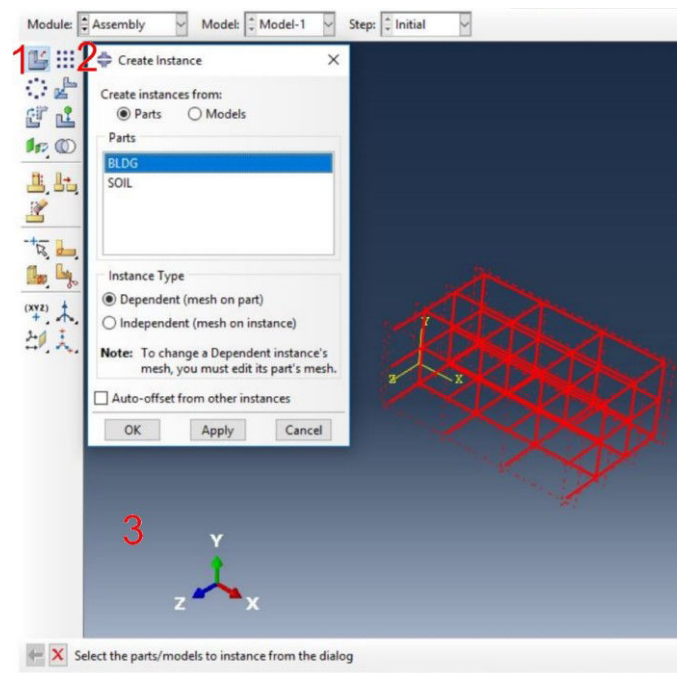


**1. Double Click on the icon Sets**

2. Create sets for beams in the direction x-z → beams in the direction y-z → columns as shown in the yellow square → columns as shown in the aqua blue square



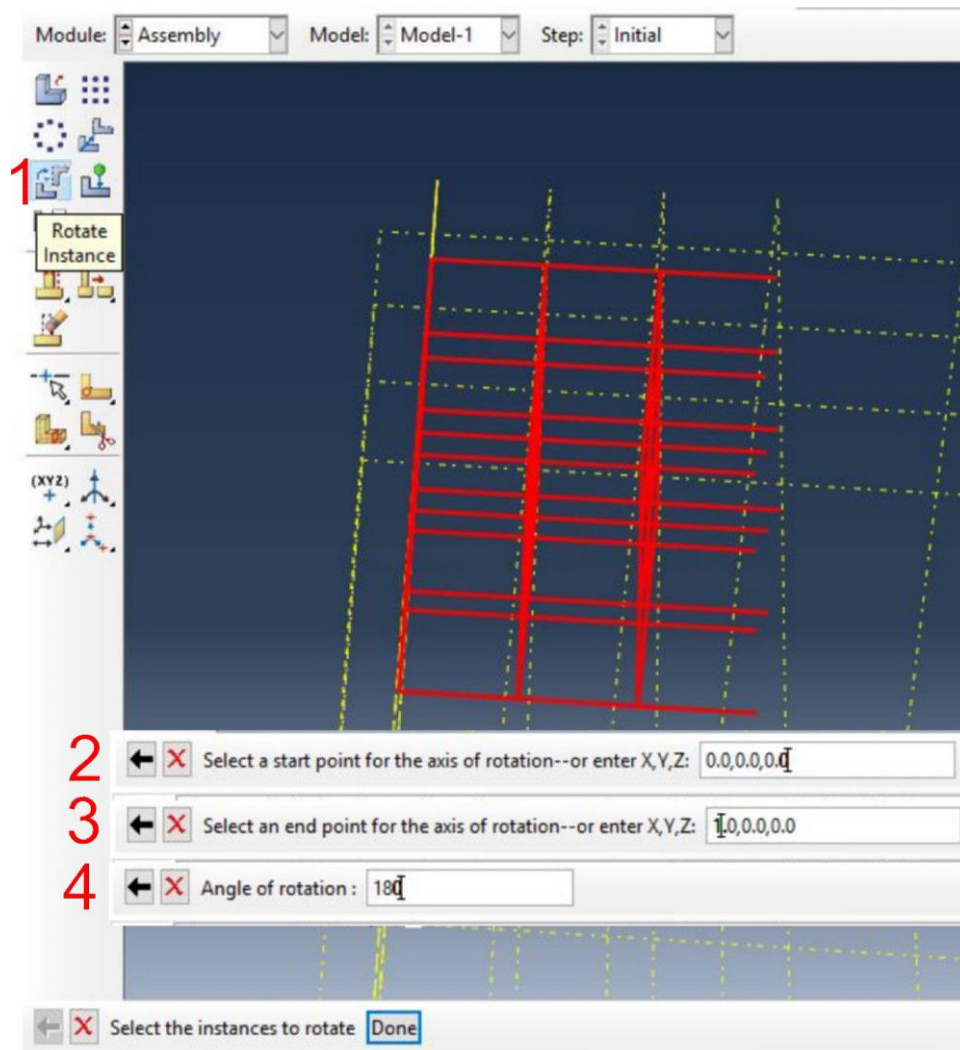
1. Select from **View** → **Part Display Options**
2. Enable → Render beam profiles  
→ Render shell thickness



Choose the module **Assembly**

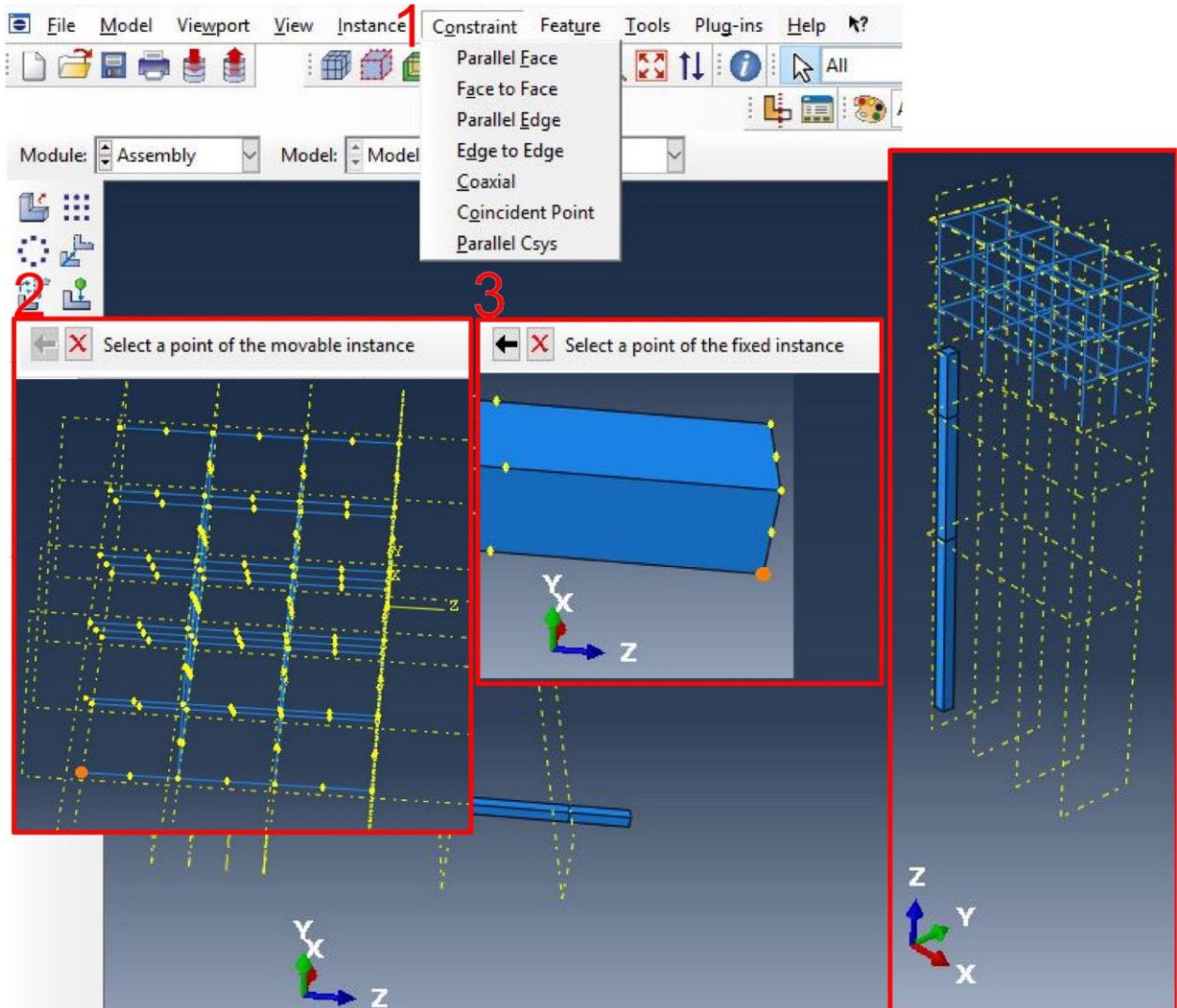
1. Click on the icon **Create Instance**

2. Choose the **Building Part** from the list of Parts
3. Click **OK**

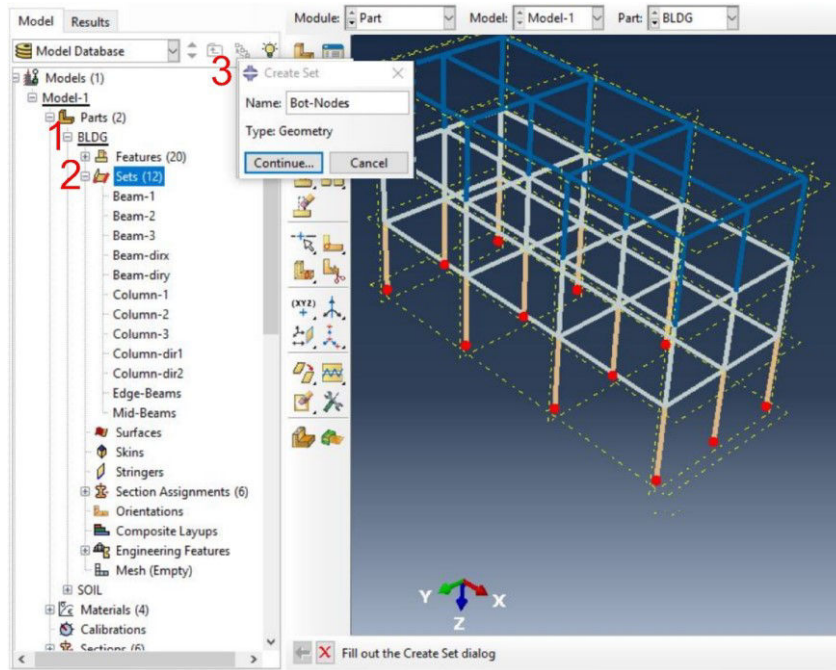


1. Click on the icon **Rotate Instance** → Select the building part → **Done**
2. Select a **start point** for the axis of rotation (**0, 0, 0**)
3. Select an **end point** for the axis of rotation (**1, 0, 0**)
4. Input **Angle of rotation 180**

**Press Enter → OK**

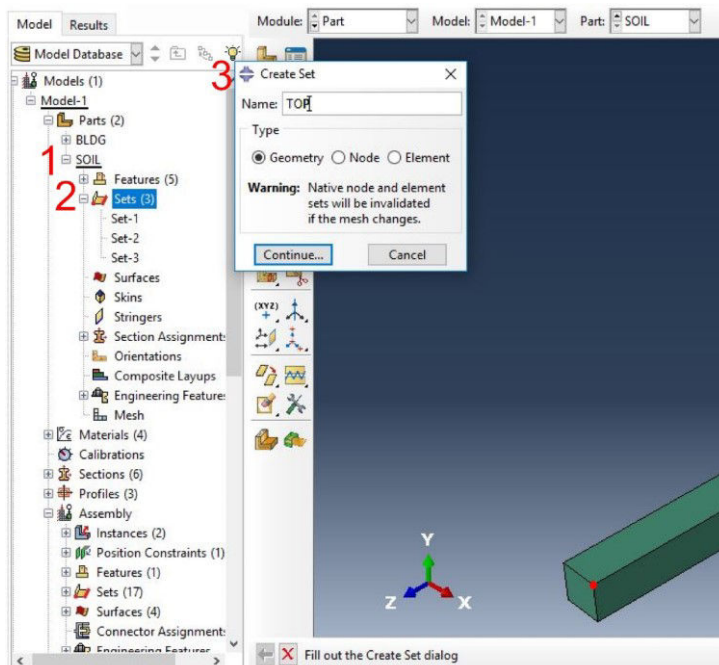


1. Select from **Constraint** → **Coincident Point**
2. Select a point of the movable instance
3. Select a point of the fixed instance



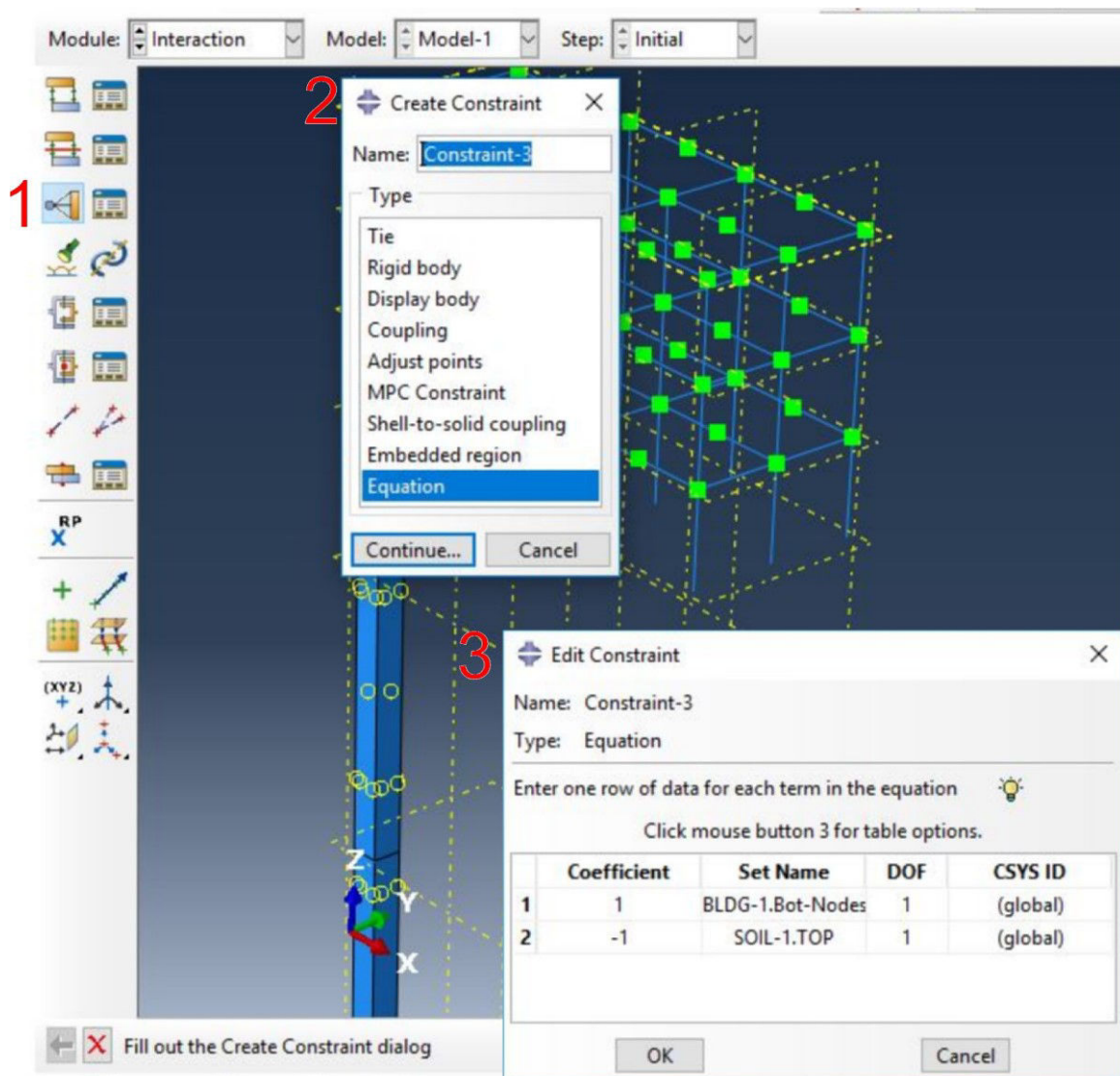
Choose the module **Part**

1. From **building part**
2. Double click on **Sets**
3. Create **Geometry** set for all Bottom nodes of the building → **Continue**



1. From **soil part**
2. Double click on **Sets**

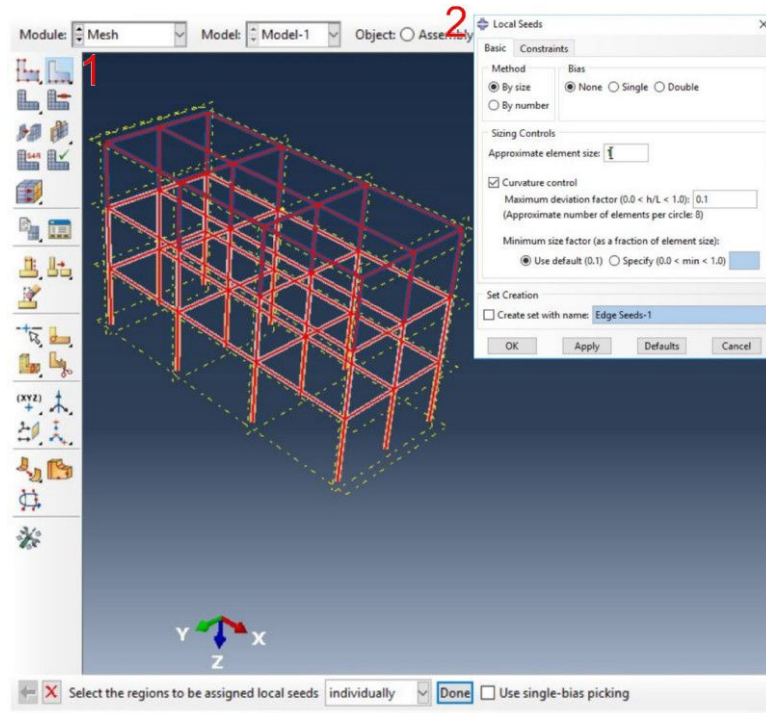
3. Create **Geometry** set for one top node of the soil → **Continue**



Choose the module **Interaction**

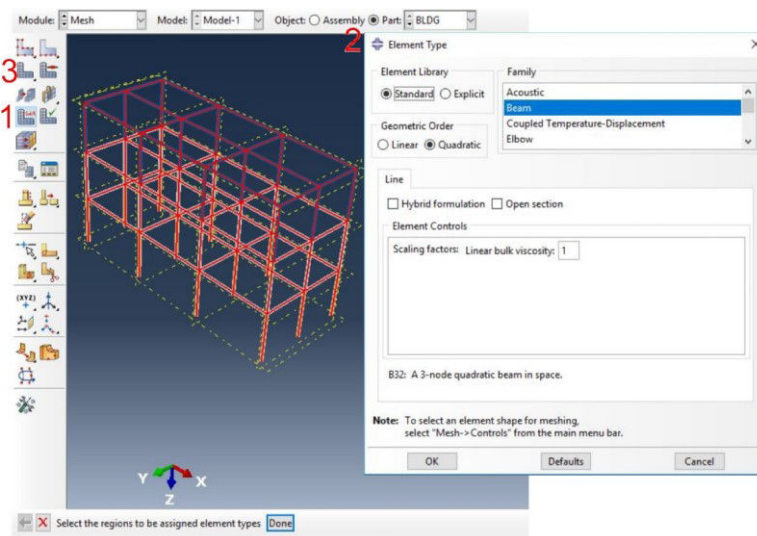
1. Click on the icon **Create Constraint**
2. Select **Equation**
3. Input in table following this Figure

**Repeat this step in order to have a constraint for DOF 1, 2 and 3**



Choose the module **Mesh**

1. Click on the icon **Seed Edges** → Meshed **By size** → Approximate element size **1** → **OK**
2. **Done**

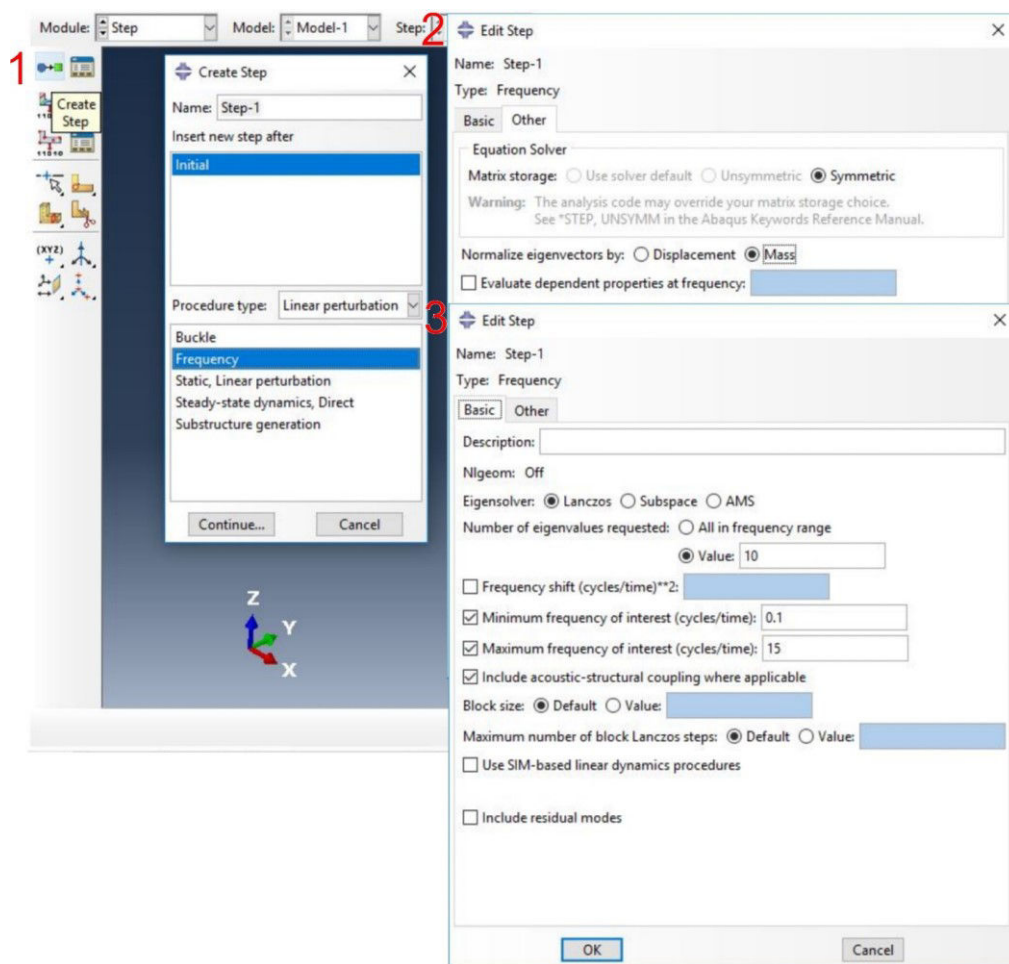


1. Click on the icon **Assign Element Types** → Select the region to mesh → **Done**
2. From Family select **Beam** → from Geometric Order enable **Quadratic** → **OK**
3. Click on the icon **Mesh Part**
- 4.

## Calculation procedure

### Combination of static and dynamic response

The static and dynamic response of the structure can be superposed only in the case considering a linear elastic system. In the case of inelastic systems, the dynamic response of the structure must consider the stresses and strains existing in the structure due to its static response. In the presented work, dry soil is adopted, and static response of the system is negligible compared to the dynamic one. Hence the static response is not considered, only dynamic response of the structure is calculated.



Choose the module **Step**

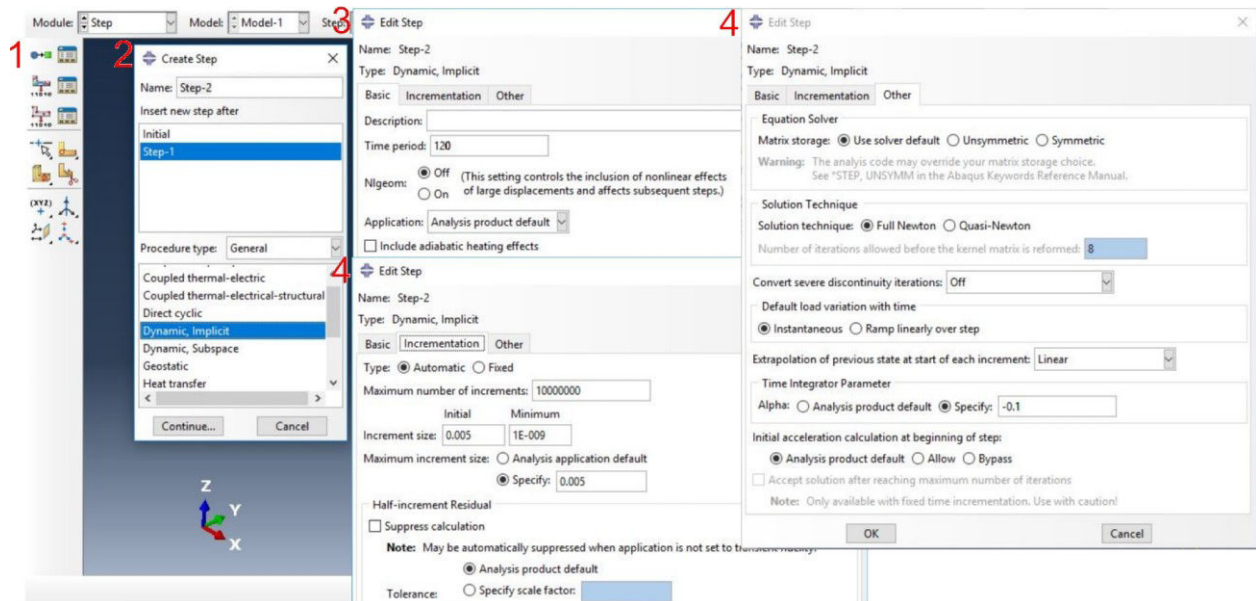
1. Click on the icon **Create Step**

From **Procedure Type** → select **Linear perturbation** → select **Frequency** → **Continue**

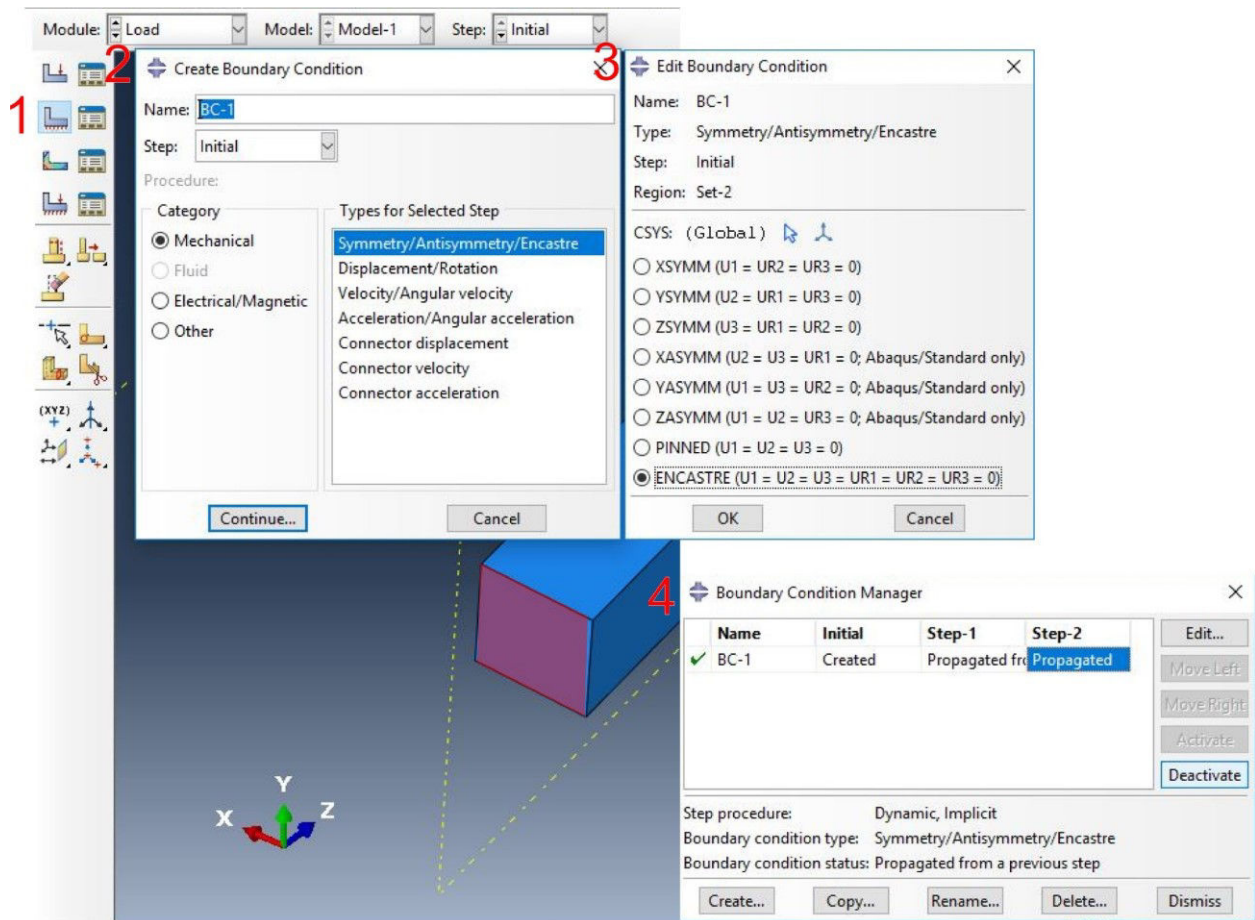
- From **Other** enable **Mass**
- From **Basic** enable **value** → **10**

Enable **Minimum frequency** → **0.1**

Enable **Maximum frequency** → **15** → **OK**



- Click on the icon **Create Step**
- From **Procedure Type** → select **General** → select **Dynamic Implicit** → **Continue**
- From **Basic** → **Time period** → input **10**
- From **Incrementation** → enable **Automatic** →  
 For **Maximum number of increments** input **10**  
 For **Increment size** → **Initial** input **0.005** → **Minimum** input **1E - 009**
- From **Other** → **Convert severe discontinuity iterations** → **OFF**  
 → **Extrapolation of previous state at start of each increment** → **Linear**  
 → **Time Integrator Parameter** → **Alpha** → enable **Specify** → **-0.1**



Choose the module **Load**

1. Click on the icon **Create Boundary Condition**

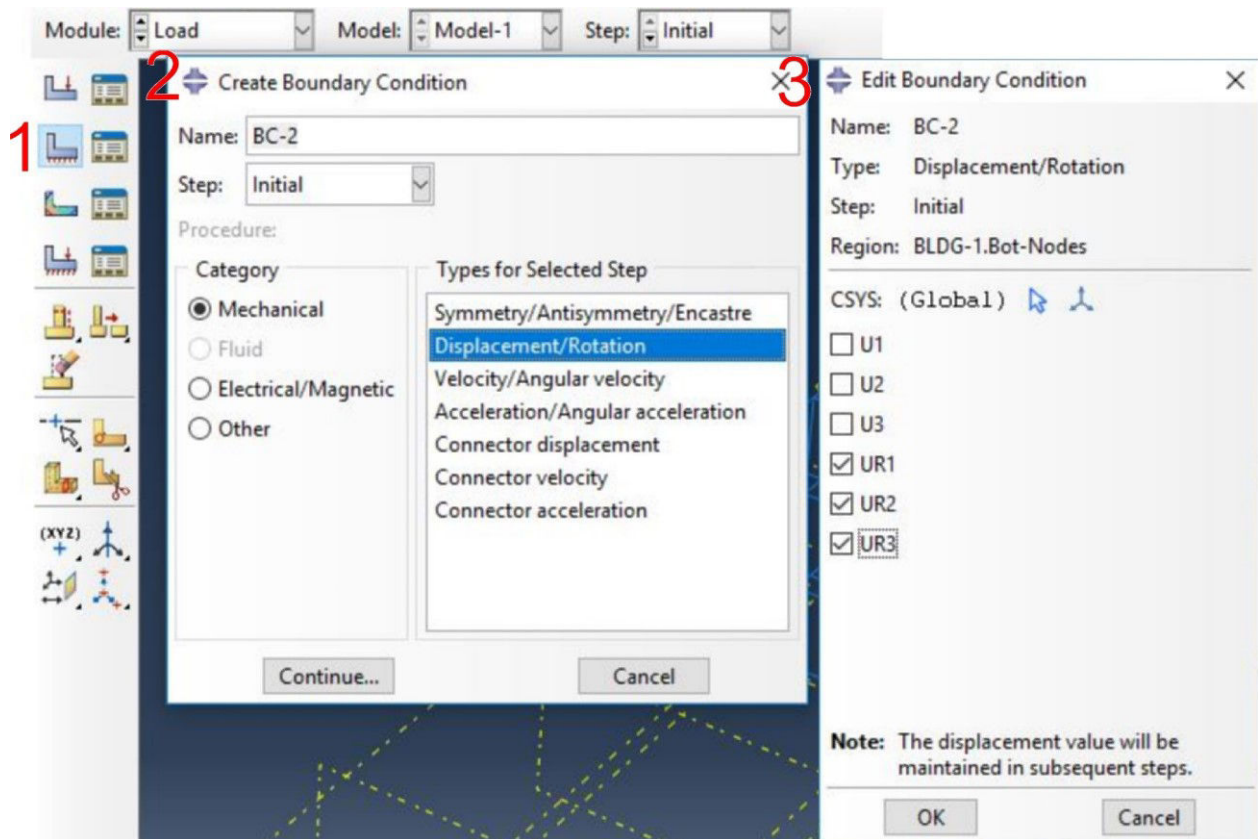
2. From **Step** → select **Initial**

From **Category** → select **Mechanical**

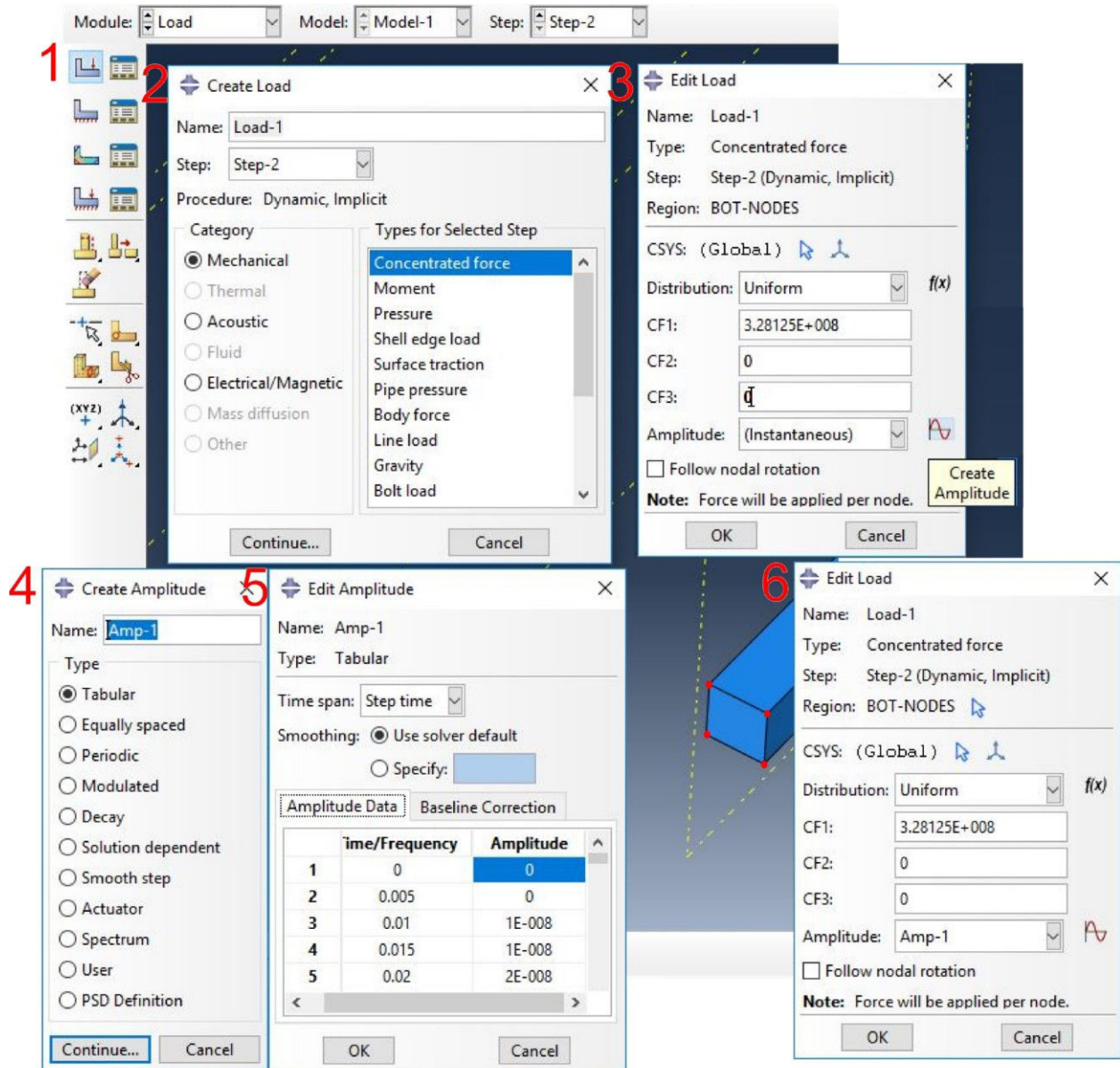
From **Types for selected step** → select **Symetry/Antisymmetry/Encastre** → **Continue**

3. Select the bottom face of the soil → Enable **Encastre** → **OK**

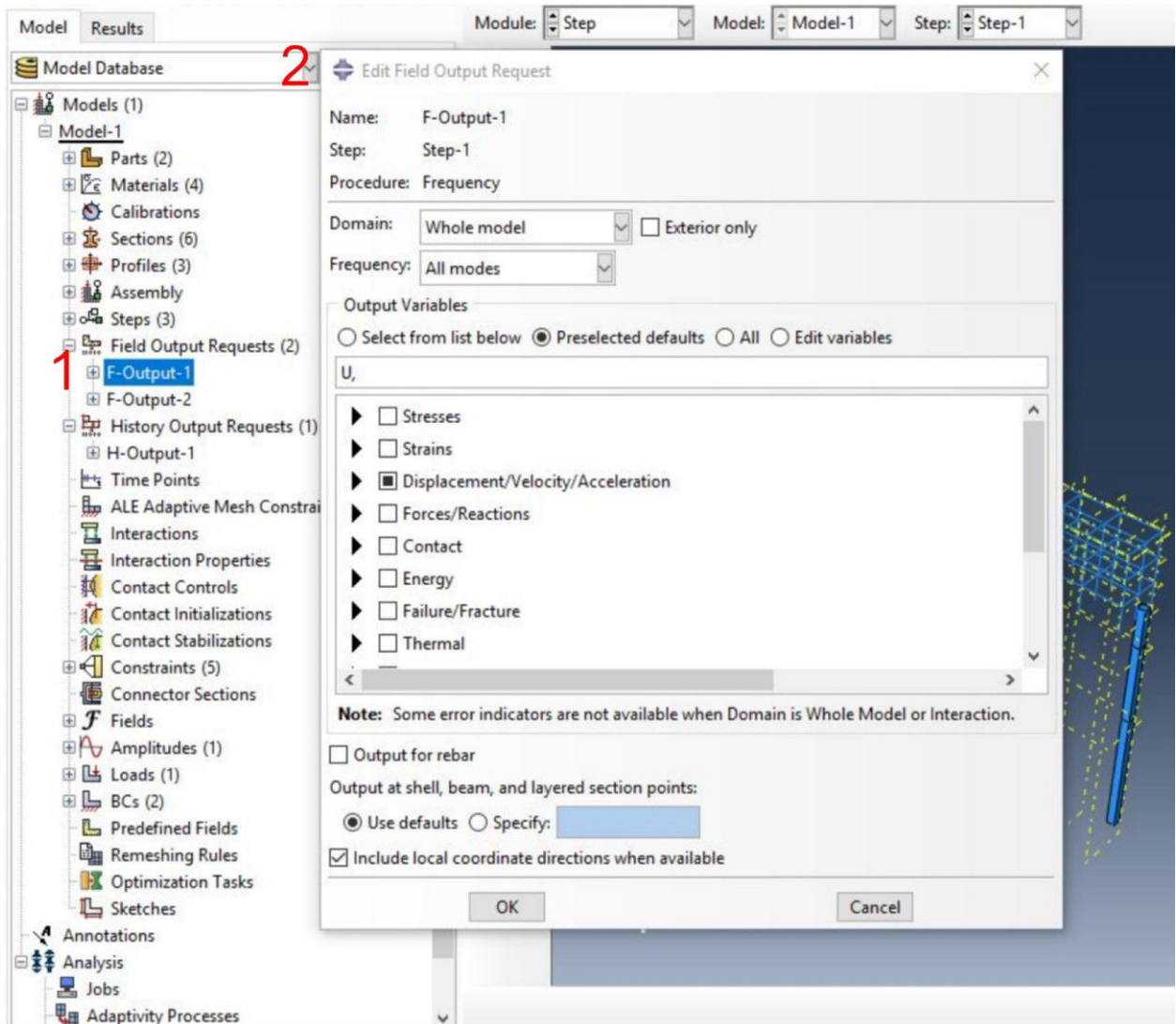
4. Select **Ptopagated** in **Step-2** and **Deactivate**



1. Click on the icon **Create Boundary Condition**
2. From **Step** → select **Initial**  
 From **Category** → select **Mechanical**  
 From **Types for selected step** → select **Displacement/Rotation** → **Continue**
3. Select from sets all building bottom nodes → Enable **UR1**, **UR2** and **UR3** → **OK**



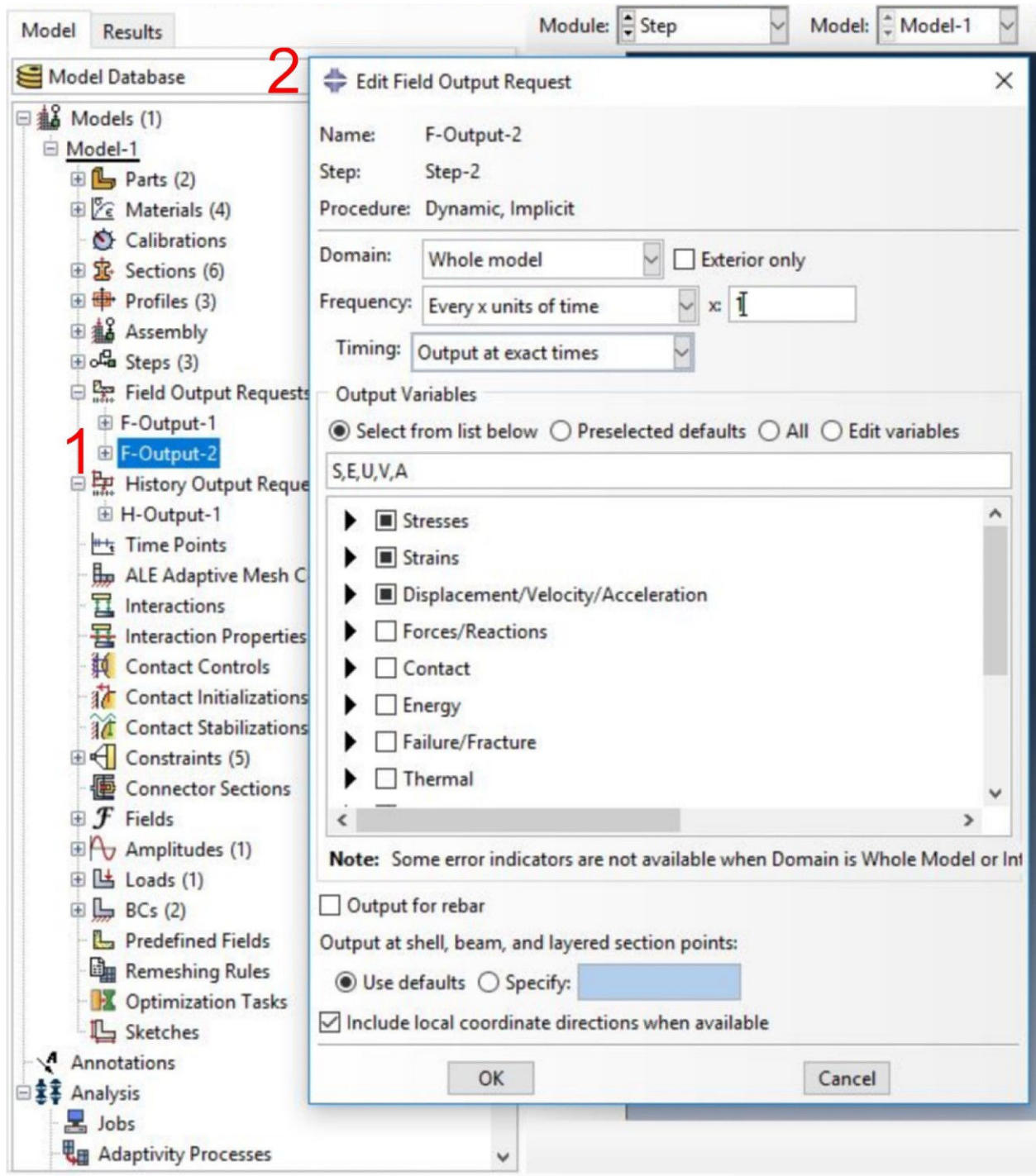
1. Click on the icon **Create Load**
2. From **Step** → select **Step-2**  
From **Category** → select **Mechanical**  
From **Types for selected step** → select **Concentrated Force** → **Continue**
3. Select the bottom nodes of the soil → Input **CF1 = 3.28125E + 008** and **CF2 = CF3 = 0** → Select **Create Amplitude**
4. Select **Tabular** → **Continue**
5. Enter tabular of the signal → **OK**
6. **OK**



1. Double Click on the icon **F-Output-1**

2. **Domain** → Whole model

Select **U** from **Displacement/Velocity/Acceleration** → **OK**



1. Double Click on the icon **F-Output-2**

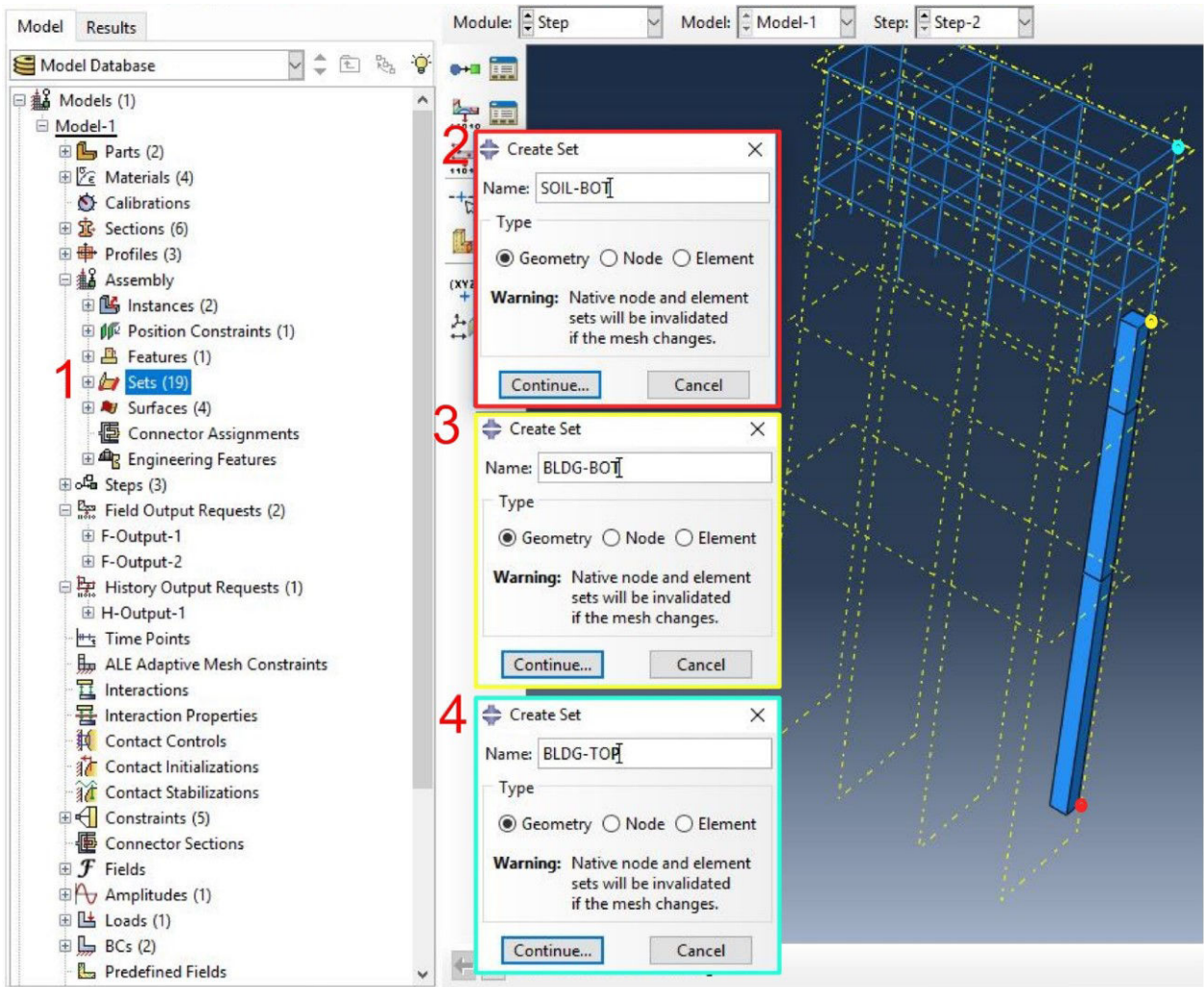
2. **Domain** → Whole model

**Frequency** → every x unit of time →  $x = 1$

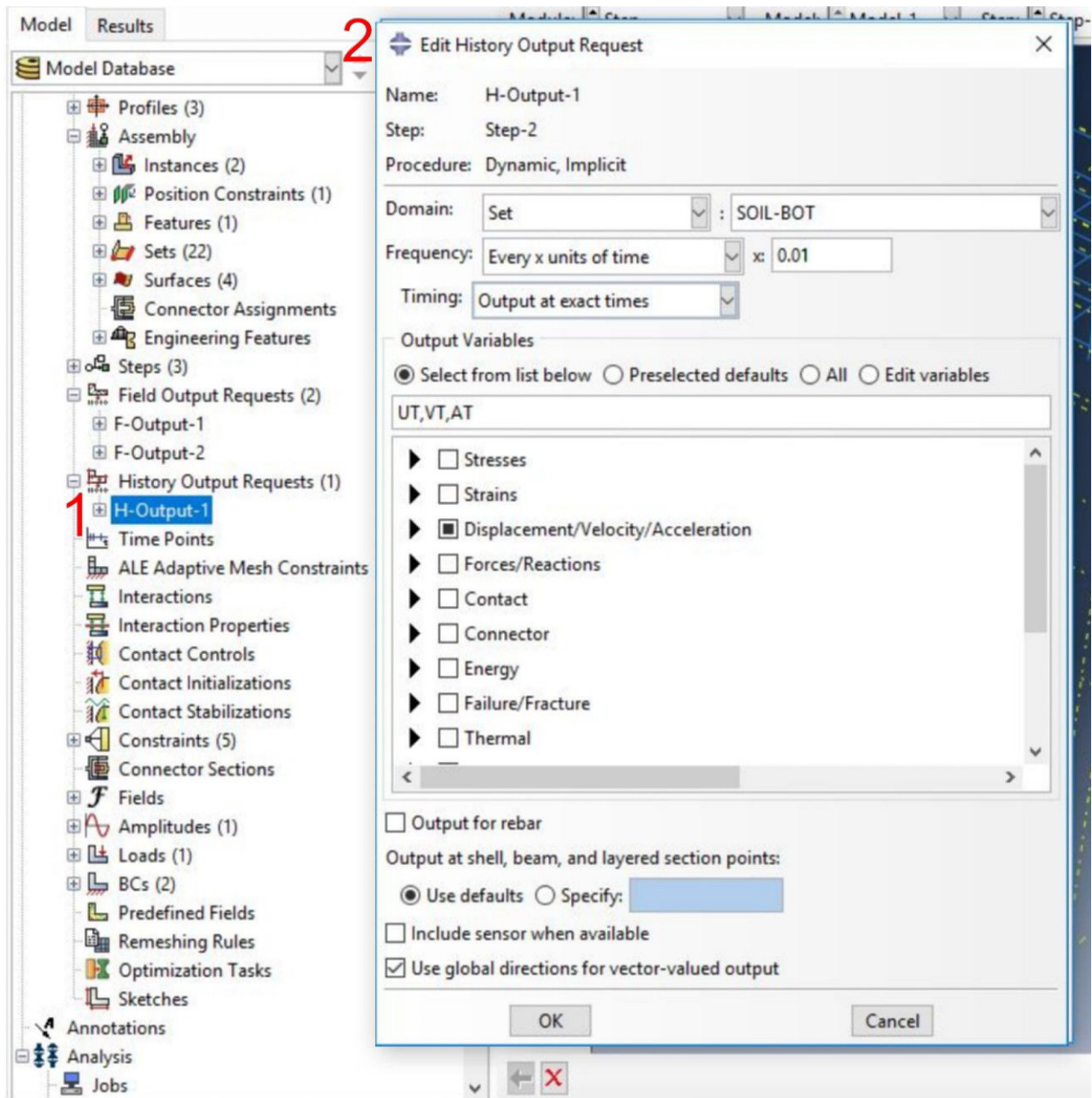
Select **U,V** and **A** from **Displacement/Velocity/Acceleration**

Select **S** from **Stress**

Select **E** from **strain** → **OK**



1. Double Click on the icon **Set from Assembly**
2. Name the set → enable **Geometry** → **Continue** → select a bottom node of the soil → **Done**
3. Repeat steps 1 and 2 only this time select a bottom node of the building
4. Repeat steps 1 and 2 only this time select a top node of the building



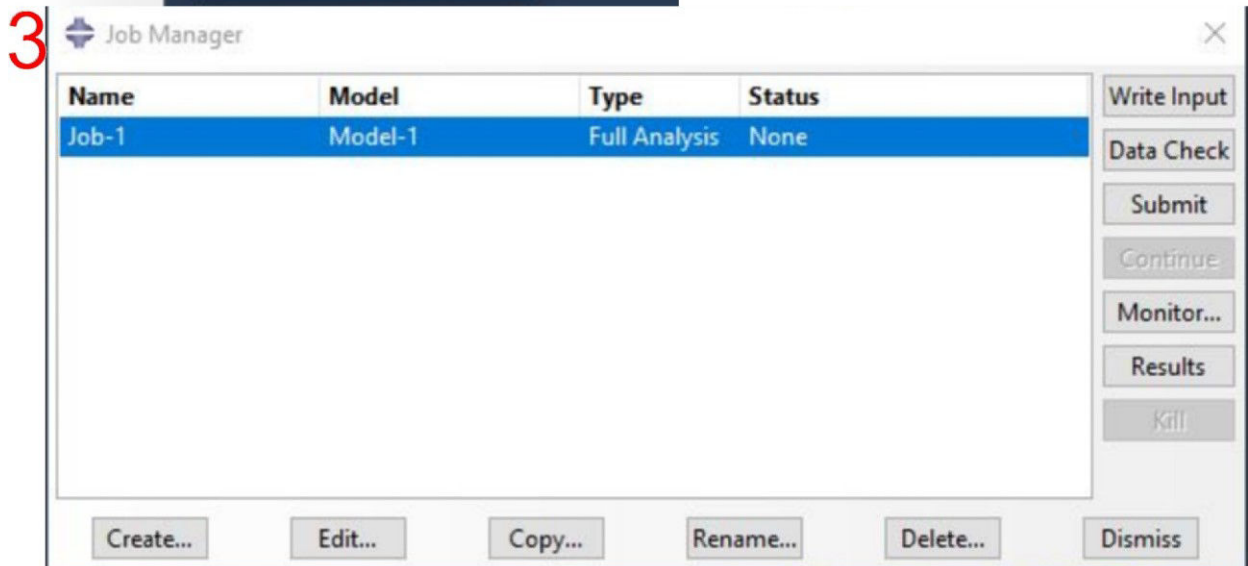
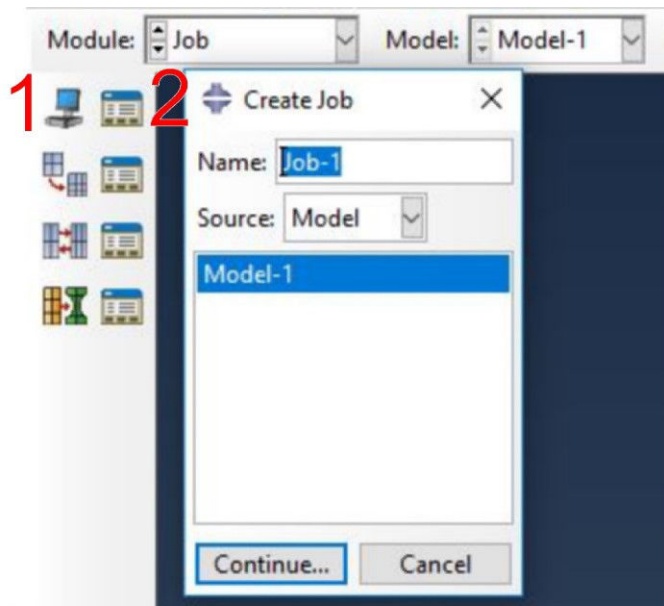
1. Double Click on the icon **History Output Requests**

2. **Domain** → Set → soil bottom node set

**Frequency** → every x unit of time → x = 0.01

Select **UT,VT** and **AT** from **Displacement/Velocity/Acceleration** → **OK**

**Repeat this step for building bottom node set and building top node set**



Choose the module **Job**

1. Click on the icon **Create Job**
2. Select **Model-1** → **Continue**
3. **Submit**

## Appendix C - Soil behavior calibration

The fundamental concepts of plasticity theories are sufficiently general, to be developed in Abaqus for a wide range of materials successfully.

### Equation proof

A yield surface, to determine if the material responds elastically at a certain state of stress, is needed.

Tests on soils provide the backbone curve for a half cycle shear stress-strain.

But Abaqus asks for stress-strain data obtained from the first half cycle of a unidirectional tension or compression experiment.

To obtain yield axial stress-strain curve from yield shear stress-strain curve  $\sigma_0$  and  $\varepsilon_0$  are calculated as follow

$$\sigma(\varepsilon) = \sqrt{3} \tau(\gamma) \quad (\text{B- 1})$$

$$\varepsilon = \sqrt{3} \gamma G_0/E_0 \quad (\text{B- 2})$$

Proof:

Von Mises Criteria

$$\sigma_0 = 1/\sqrt{2} \sqrt{(\sigma_{11} - \sigma_{22})^2 + (\sigma_{11} - \sigma_{33})^2 + (\sigma_{22} - \sigma_{33})^2 + 6 (\tau_{12}^2 + \tau_{13}^2 + \tau_{23}^2)} \quad (\text{B- 3})$$

Where  $\sigma_0$  is the yield stress, then for uniaxial cases

$$\sigma_0 = 1/\sqrt{2} \sqrt{2\sigma_{11}^2 + 6 \tau_{13}^2} \quad (\text{B- 4})$$

$$\sigma_0 = \sqrt{\sigma_{11}^2 + 3 \tau_{13}^2} \quad (\text{B- 5})$$

That can be written as an ellipse equation

$$\sigma_{11}^2 + 3\tau_{13}^2 = \sigma_0^2 \quad (\text{B- 6})$$

Or

$$\sigma_{11}^2/\sigma_0^2 + \tau_{13}^2/(\sigma_0/\sqrt{3})^2 = 1 \quad (\text{B- 7})$$

The ratio between the big axe and the small axe would be

$$2\sigma_{\text{yield}}/2\tau_{\text{yield}} = \sigma_{\text{yield}}/\tau_{\text{yield}} = \sigma_0/(\sigma_0/\sqrt{3}) = \sqrt{3} \quad (\text{B- 8})$$

Hence

$$\sigma_0 = \sqrt{3}\tau_0 \quad (\text{B- 9})$$

Then we can determine  $\varepsilon$  as following

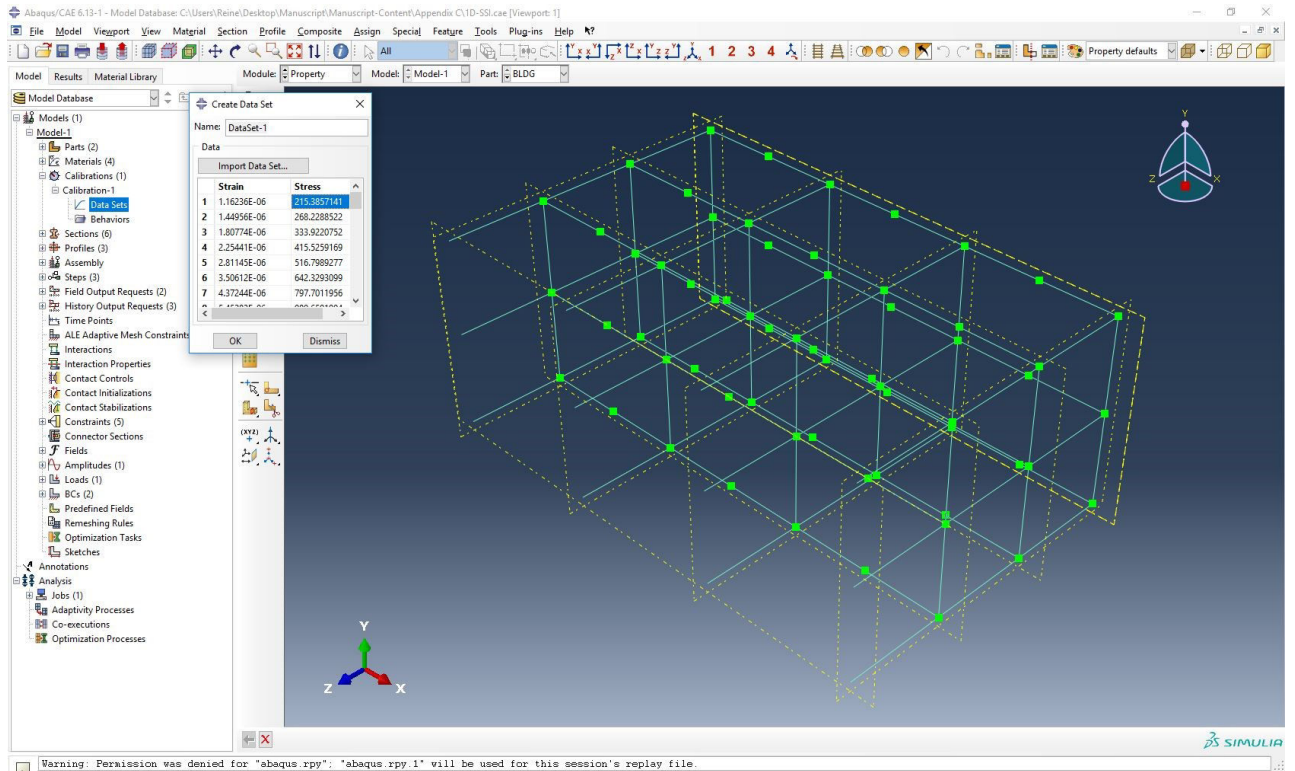
$$\begin{aligned} \sigma(\varepsilon) &= \sqrt{3} \tau(\gamma) \\ E \varepsilon &= \sqrt{3} G \gamma \\ E/E_0 E_0 \varepsilon &= \sqrt{3} G/G_0 G_0 \gamma \\ \frac{E}{E_0} E_0 \varepsilon &= \sqrt{3} \frac{G}{G_0} G_0 \gamma \\ \varepsilon &= \sqrt{3} G_0/E_0 \gamma \end{aligned} \quad (\text{B- 10})$$

## Calibration

Once  $\sigma(\varepsilon)$  and  $\varepsilon$  data are calculated, the calibration experiment should be performed at a strain range,  $\Delta\varepsilon$  that corresponds to the strain range anticipated in the analysis because the material model does not predict different isotropic hardening behavior at different strain ranges. For that reason, i suggest taking the minimum  $\Delta\varepsilon$  accepted by Abaqus.

Two possible ways to enter data; by importing a .txt file or by entering data manually. For this step, total strain must be provided.

## Appendix C - Soil behavior calibration



**Abaqus/CAE Usage:** Property module: calibration → **Data Set:**

$\sigma(\epsilon)$ ,  $\epsilon$

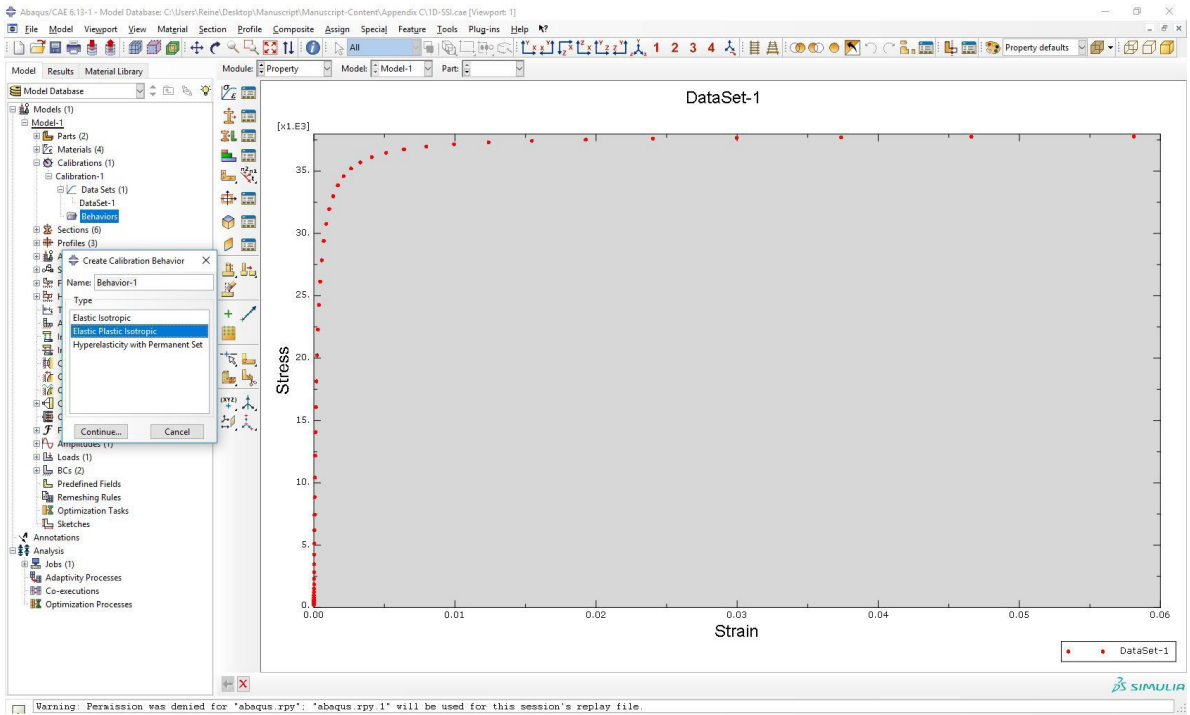
PS: For SSI analysis you need to multiply the stress by the area chosen for the analysis in order to have the correct dynamic equation

**In Abaqus/CAE Usage:** Property module: calibration → **Edit Behavior:**

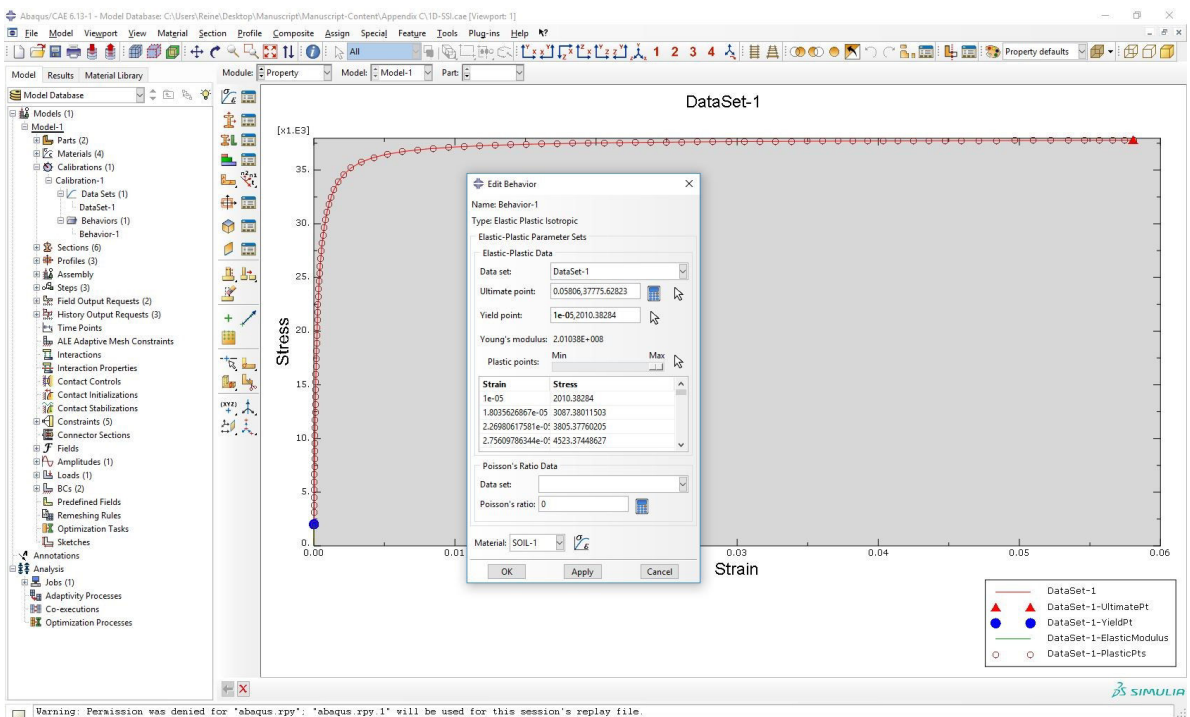
Three behavior types are available:

- Elastic Isotropic
- Elastic Plastic Isotropic
- Hyperelasticity with Permanent Set

For our analysis, Elastic Plastic Isotropic is chosen.



In the Editor, you need:



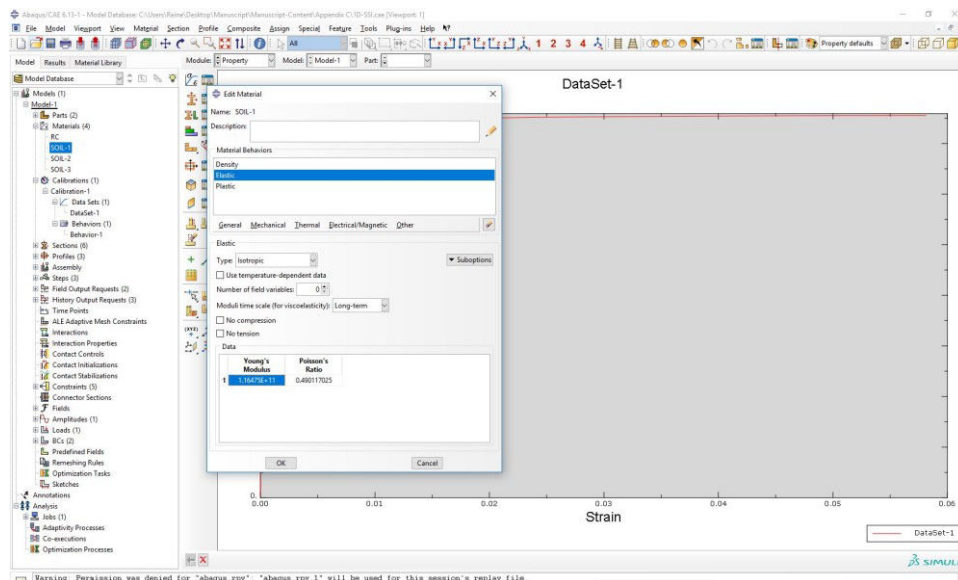
- First: To indicate the data set
- Second: To Calculate or to choose an Ultimate point.

I recommend choosing the calculator tool, it indicates the last point you have given in your set data. You can always enter manually the point coordinates simply by writing them in the text bar or providing it with the set data.

- Third: To pick a yield point. When you pick a yield point the young's modulus is calculated, simply by calculating the slope. This way you can verify if the yield point you have picked corresponds to your soil. To help doing this procedure, I strongly recommend to switch plastic points to max and to use the text bar to increment manually the abscissa (or strain). By pressing ENTER Abaqus will calculate the ordinate (or stress). This procedure takes few minutes, yes, it is by trial and error. The purpose is, to estimate a Young's modulus as close as possible from the real Young's modulus and to have the second point in the table with an ordinate or stress greater than  $E/\epsilon_e$ , where  $\epsilon_e$  is the elastic strain or abscissa of the first point in the table.
  - Fourth: To enter the Poisson's ratio, in this analysis it is entered as a constant value by typing the value in the text bar
- Now, you create a material by clicking on the button next to Material, you name it, and you click on OK.

## Elasticity definition

The Abaqus plasticity models also need an elasticity definition to deal with the recoverable part of the strain. In Abaqus the elasticity is defined by including linear elastic behavior



Go to

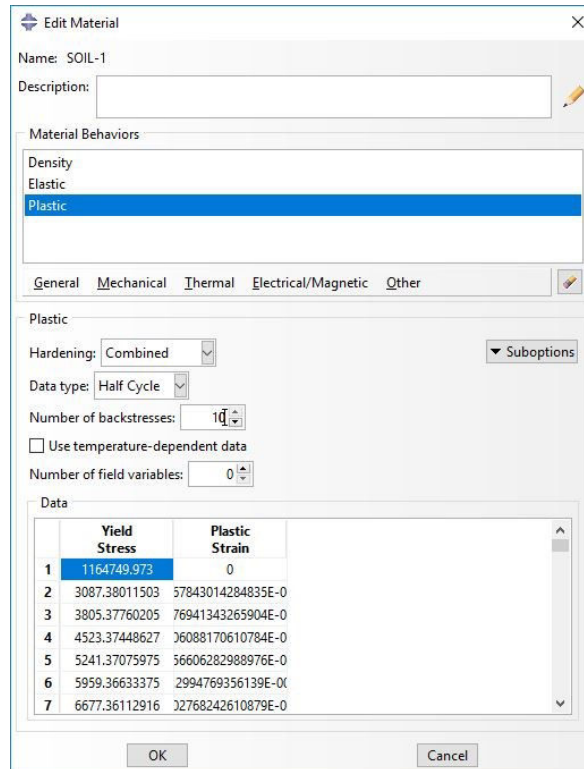
**Abaqus/CAE Usage:** Property module: material

You will find in your editor: **Elastic** and **Plastic** properties

Click on **Elastic** correct the Young's Modulus if needed

## Plasticity definition

Adjusting the Plastic behavior according to your material



Click on **Plastic** correct the first Yield Stress by  $E/\epsilon_e$  if needed. For this analysis:

Hardening → Combined

Data type → Half Cycle

Number of backstresses → 10

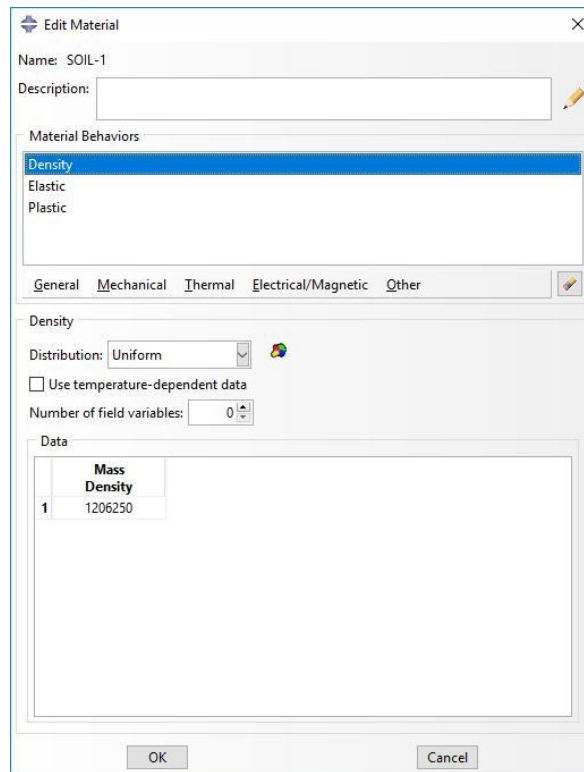
Use temperature-dependent data → disabled

Number of field variables → 0

## Density definition

Do not forget to enter your material's Density

## Appendix C - Soil behavior calibration



**Abaqus/CAE Usage:** Property module: material editor: **General**→**Density**:

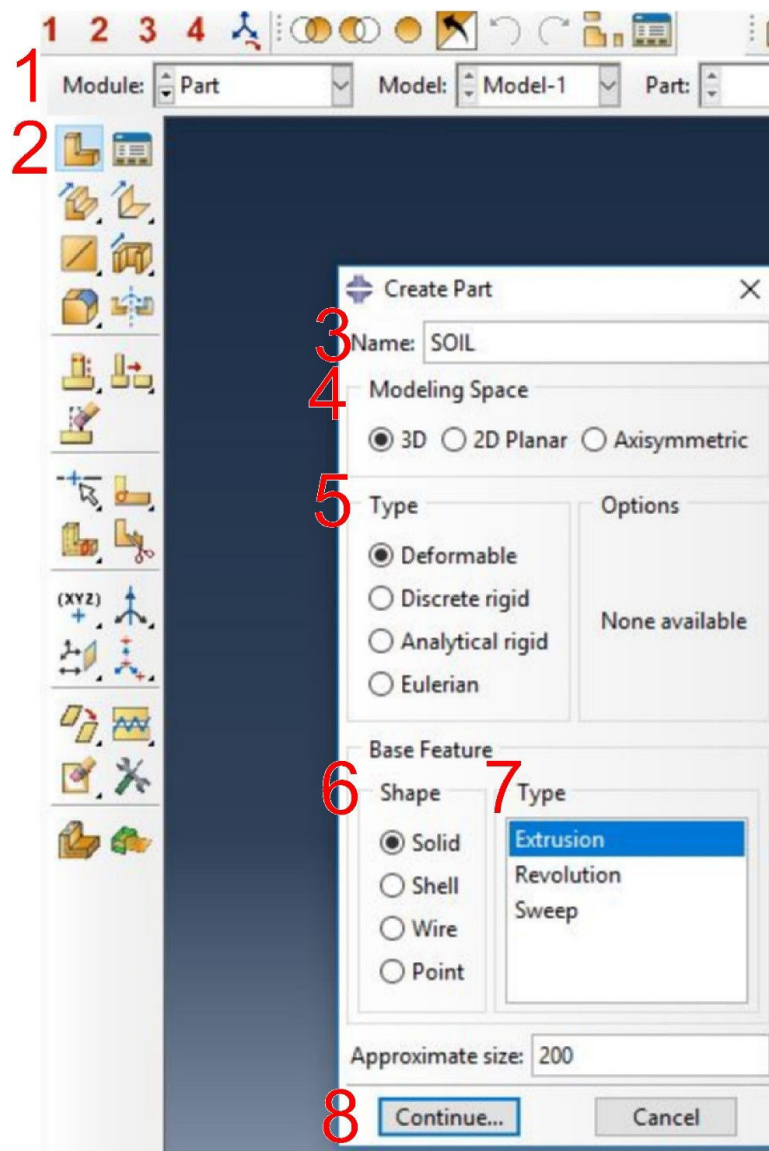
$\rho$



## Appendix D - Guide for 1DT-3C model for SSI and SSSI in Abaqus

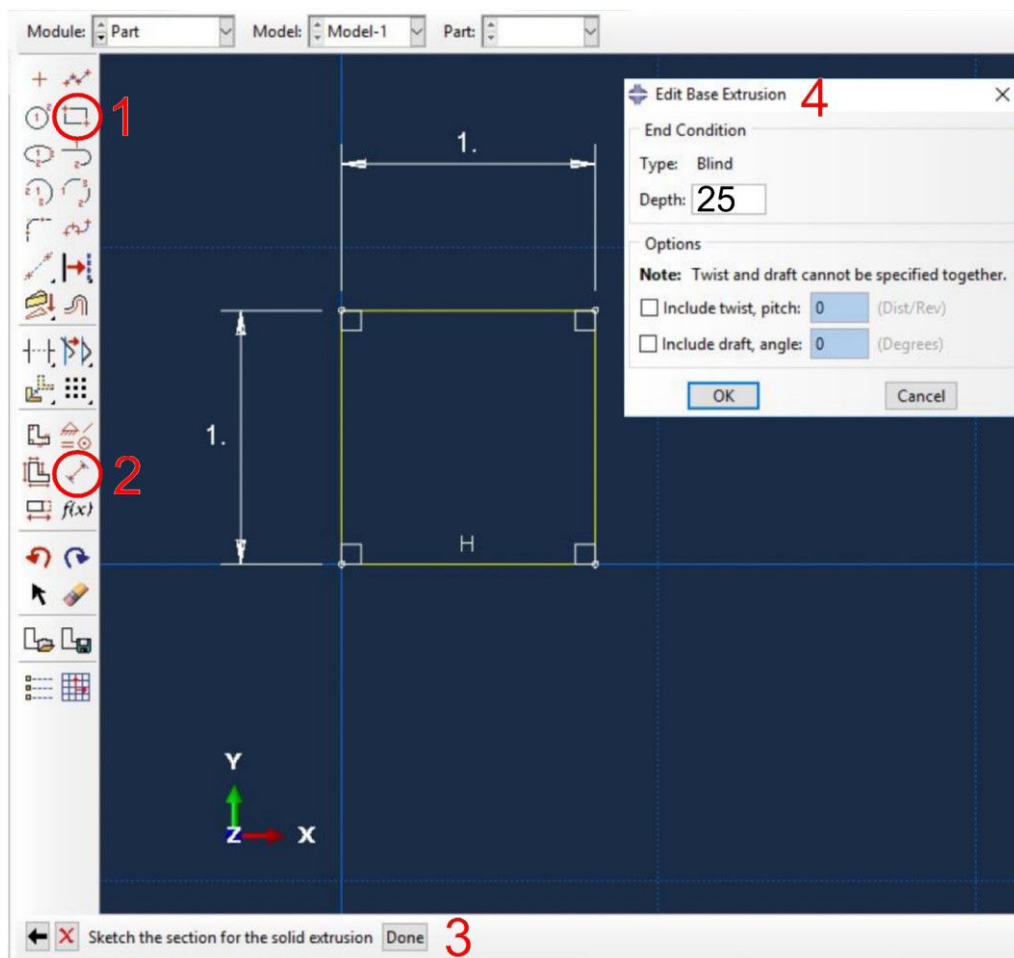
This guide is intended for users who will exercise research or engineering in earthquake design. A step-by-step procedure is described to model the 1DT soil model of nonlinear behavior introduced in Chapter 3 - for SSI analysis.

### 1DT soil model



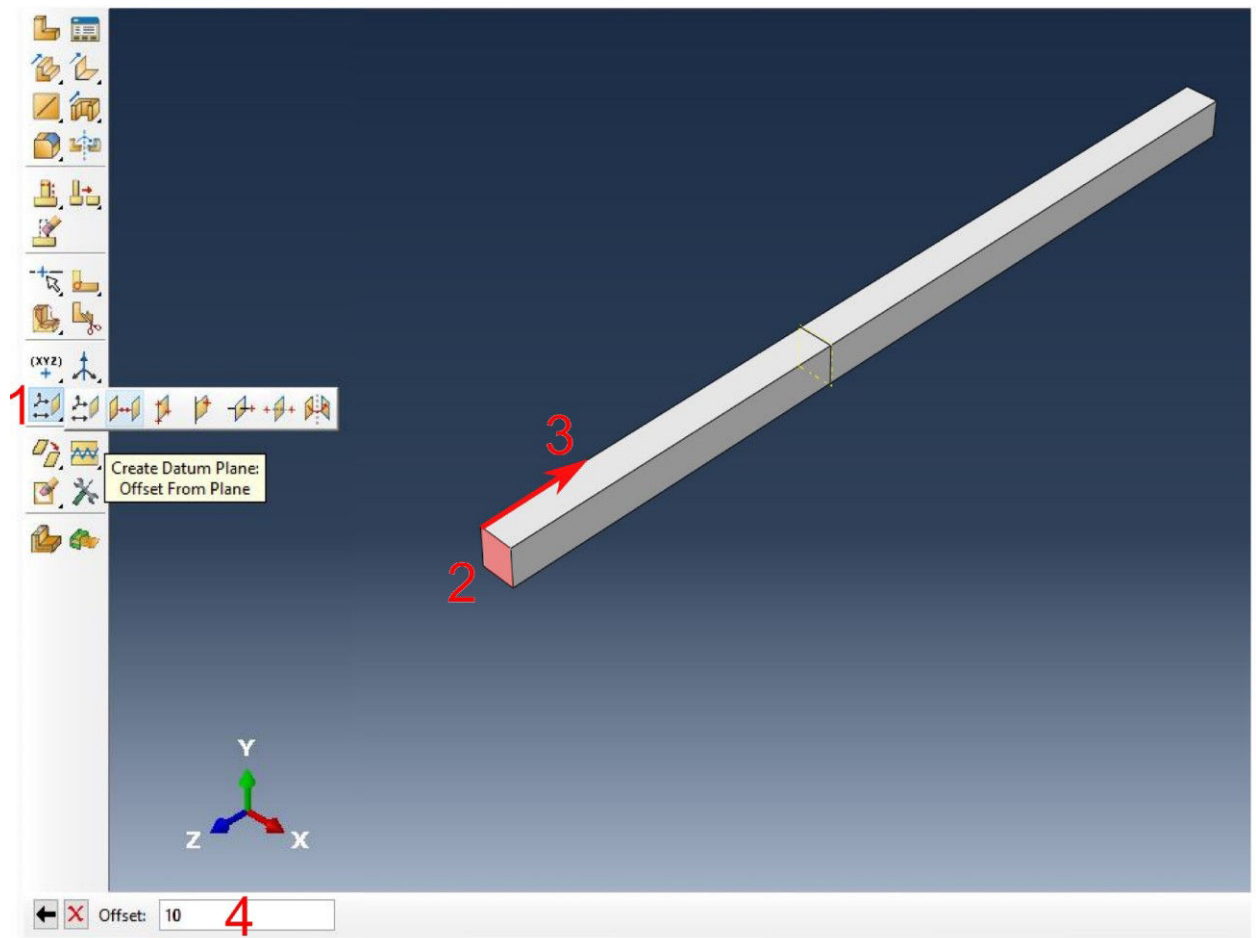
1. Choose the module **Part**
2. Click on the icon **Create Part**

3. Choose a **Name** for your part
4. Select the **Modeling** space → **3D**
5. Select the **Type** → **Deformable**
6. Select the **Base Feature** → **Shape** → **Solid**
7. Select the **Base Feature** → **Type** → **Extrusion**
8. **Continue**



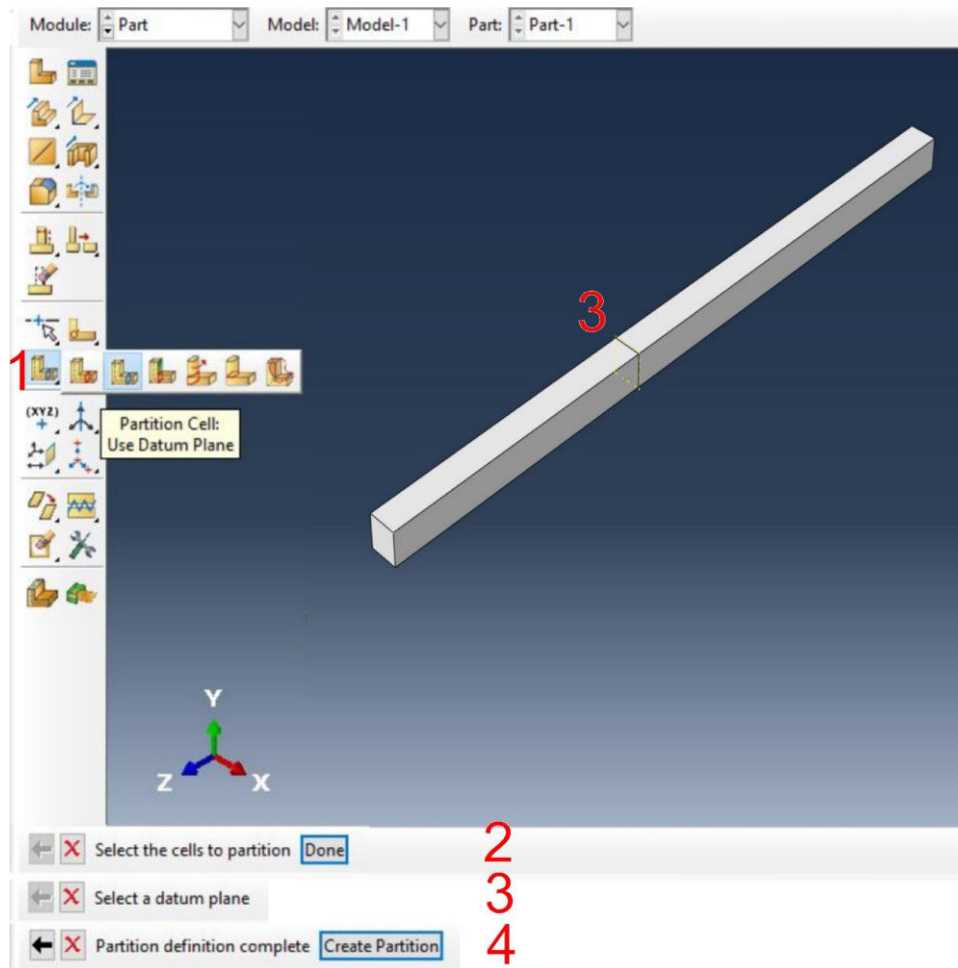
1. Click on the icon **Create Lines: Rectangle** → Draw a rectangle
2. Click on the icon **Add Dimension** → Correct the dimension of the rectangle to  **$1 \times 1 \text{ m}^2$**
3. Click on **Done**
4. Write the **Depth** in the new dialog → **30 m**

**OK**



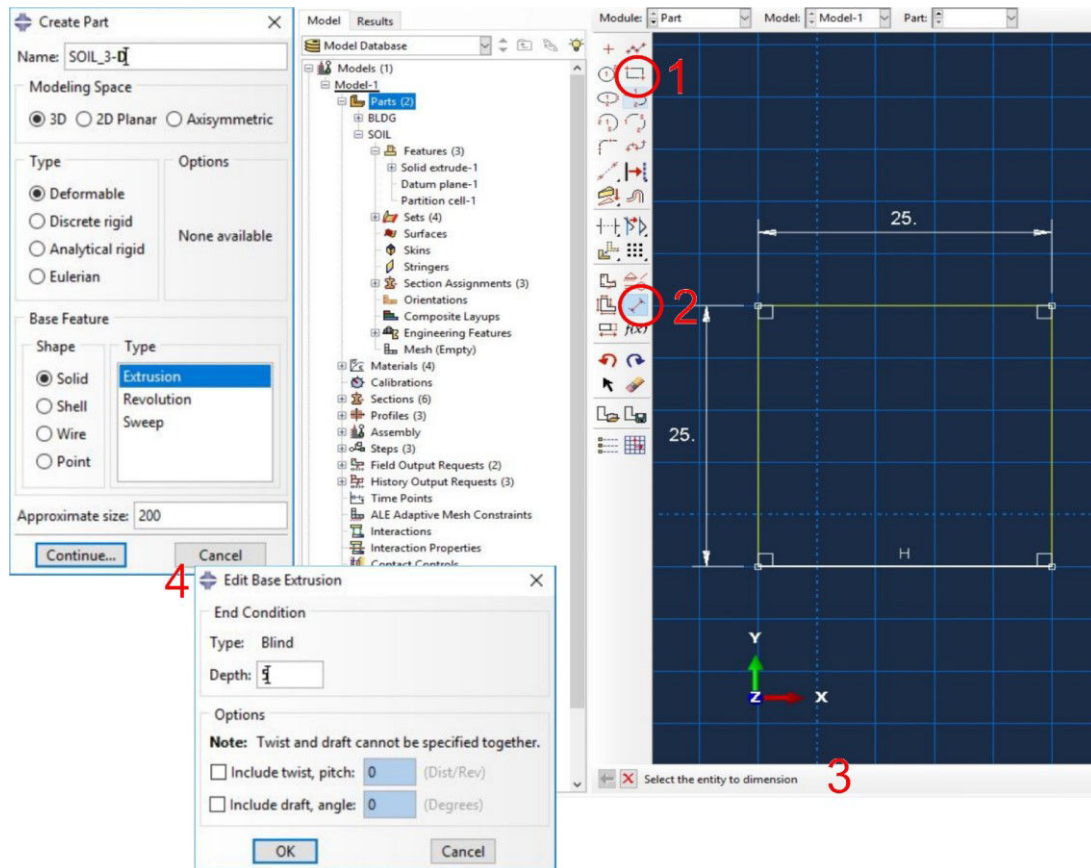
1. Click on the icon **Create Datum Plane: Offset From Plane**
2. Click on the **plane** you want to offset from
3. Choose the **direction** of offset
4. Write the **Offset distance** in the new dialog → **10 m**
5. **Press Enter**

**Repeat this step in order to have planes in the intersection of layers**



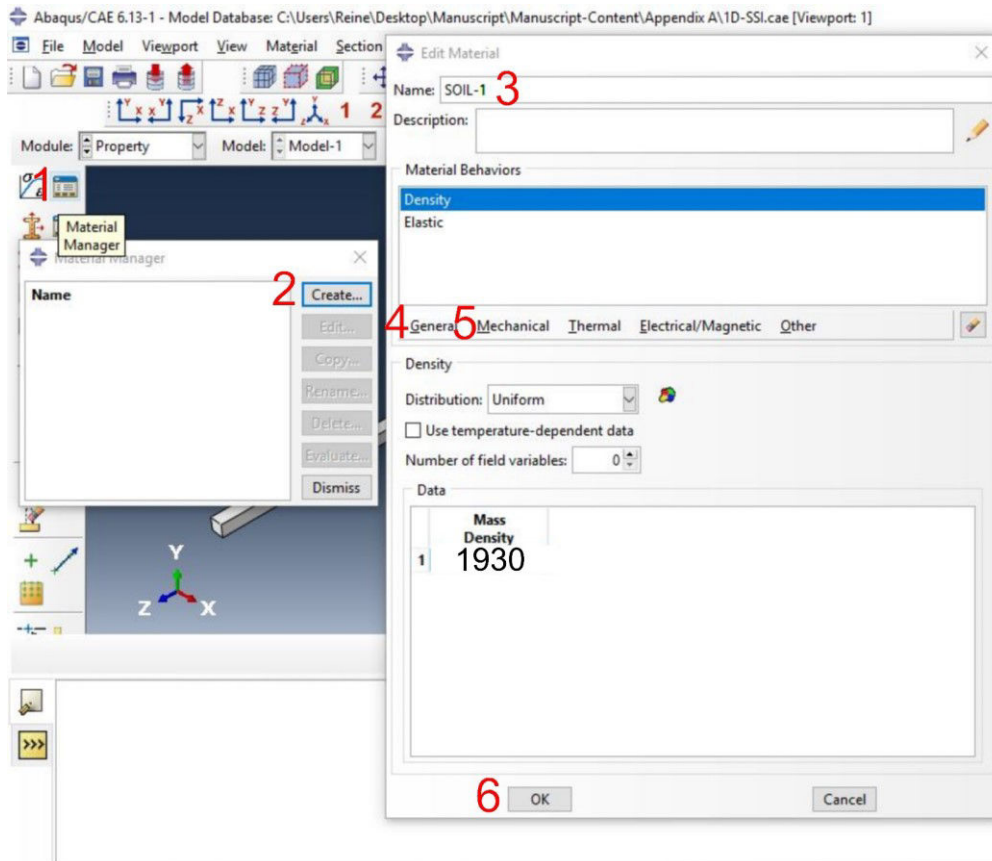
1. Click on the icon **Partition Cell: Use Datum Plane**
2. Select the **cell(s)** to partition, for the first partition this step is omitted
3. Select the **datum plane** to define the cutting plane
4. Click on **Create Partition**

**Repeat this step in order to partition all the layers**



Create new Part

1. Click on the icon **Create Lines: Rectangle** → Draw a rectangle
  2. Click on the icon **Add Dimension** → Correct the dimension of the rectangle to **25 × 25 m<sup>2</sup>**
  3. Click on **Done**
  4. Write the **Depth** in the new dialog → **5 m**
- OK**



Choose the module **Property**

1. Click on the icon **Material Manager**
2. Click on the icon **Create**
3. Choose a **Name** for your material
4. Select from the catalogue **General** → **Density**, enter the density of the material.

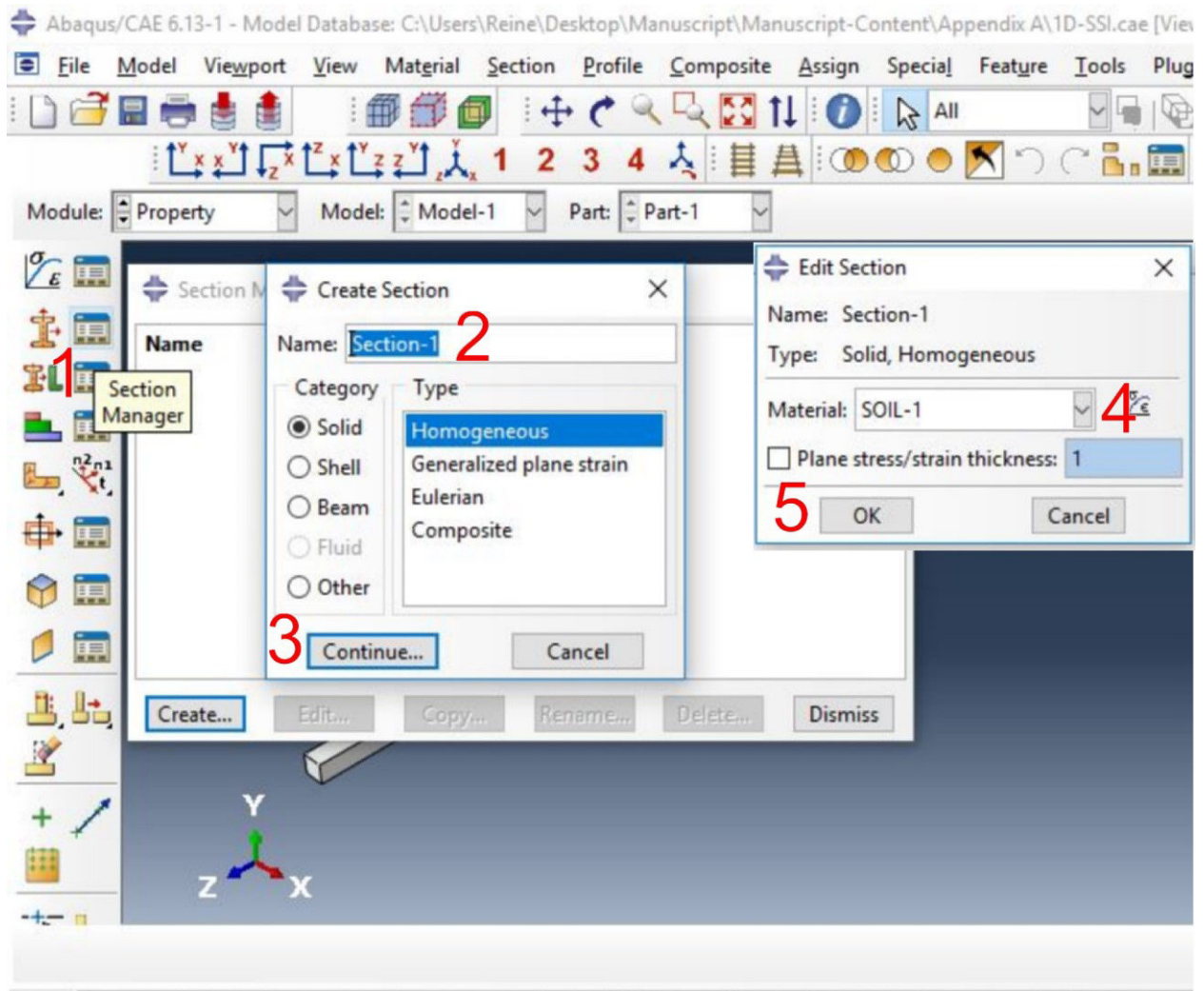
PS: Don't forget to multiply the density by the area

5. Select from the catalogue **Mechanical** → **Elasticity**, enter the Young modulus and the poison ratio of the material.

PS: Don't forget to multiply the Young modulus by the area only for the soil modeled in 1-D

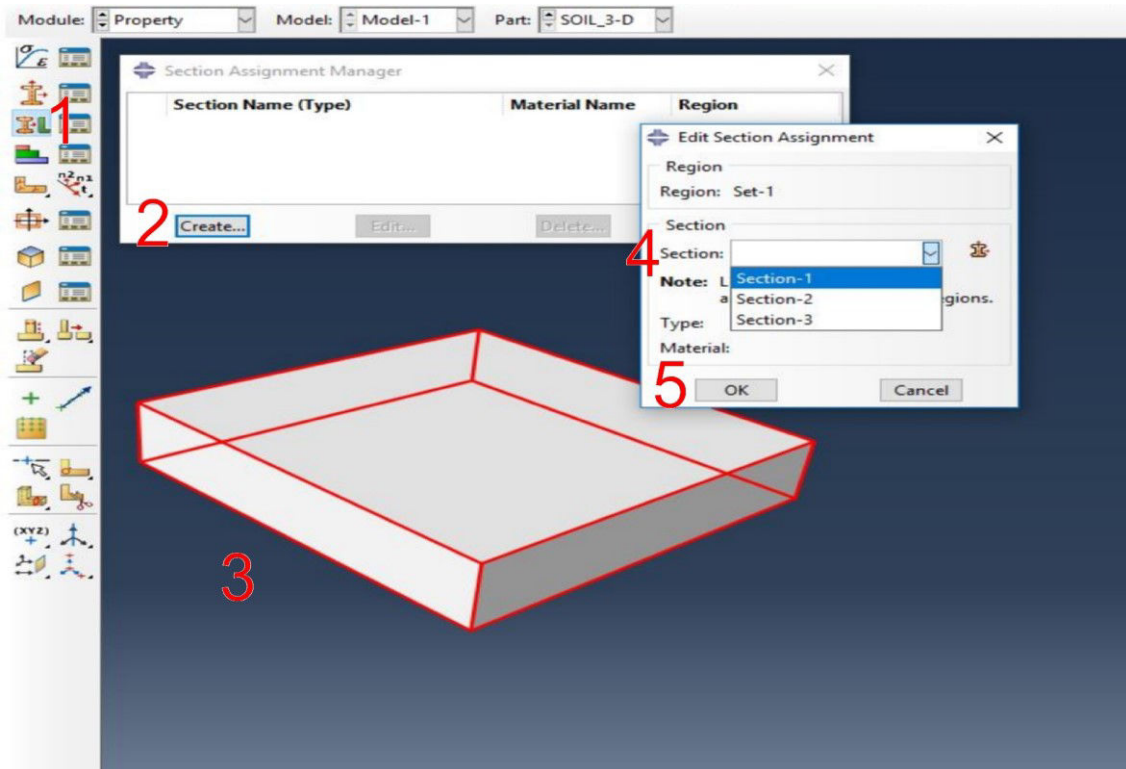
6. Click **OK**

**Repeat this step in order to have a material for each layer**



6. Click on the icon **Section Manager**
7. Click on the icon **Create** → Choose a **Name** for your section
  - Select **Solid** from **Category**
  - Select **Homogeneous** from **Type**
8. **Continue**
9. Select the material from the catalogue → **Soil-1**
10. Click **OK**

**Repeat this step in order to have a section for each material**



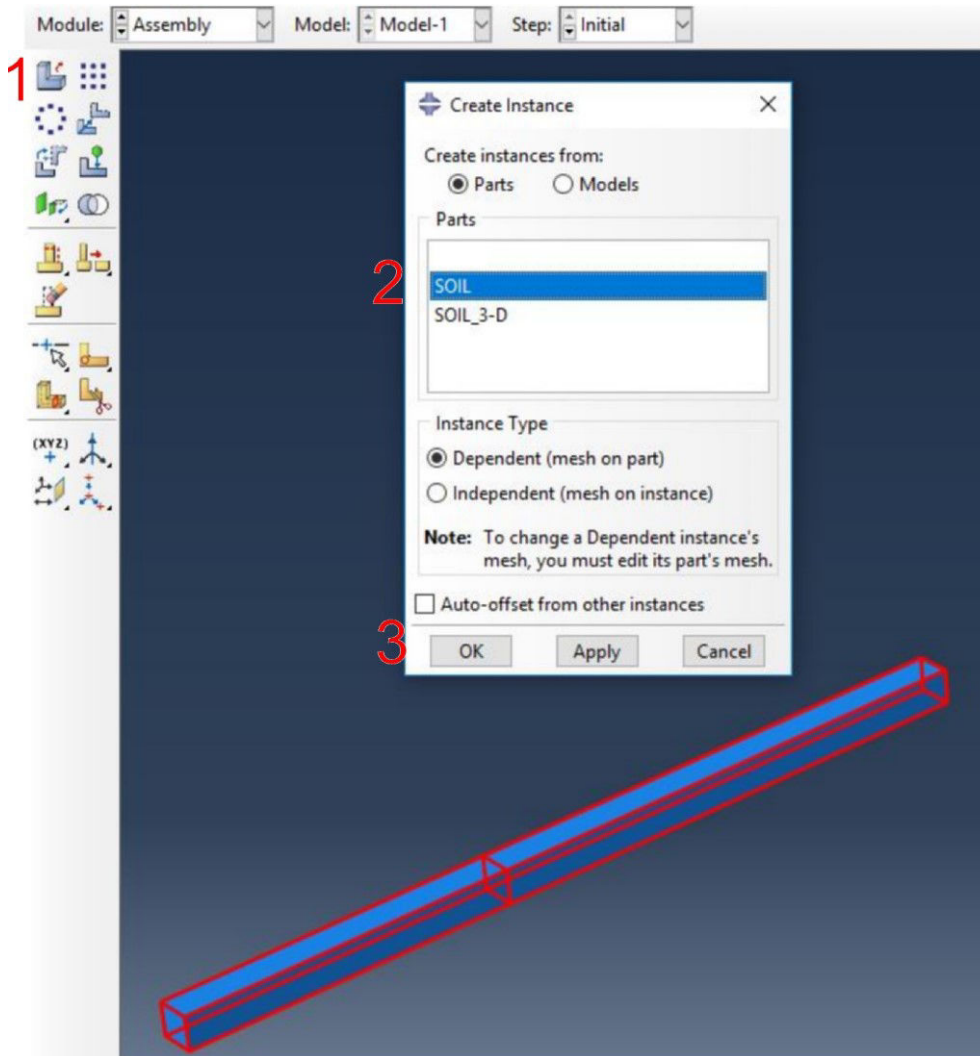
### For each Part

1. Click on the icon **Section Assignment Manager**
2. Click on the icon **Create**
3. Select the **Regions** to be assigned a section and a **Name** for this region

Click **Done**

4. Select the Section from the catalogue → **Section-1**
5. Click **OK**

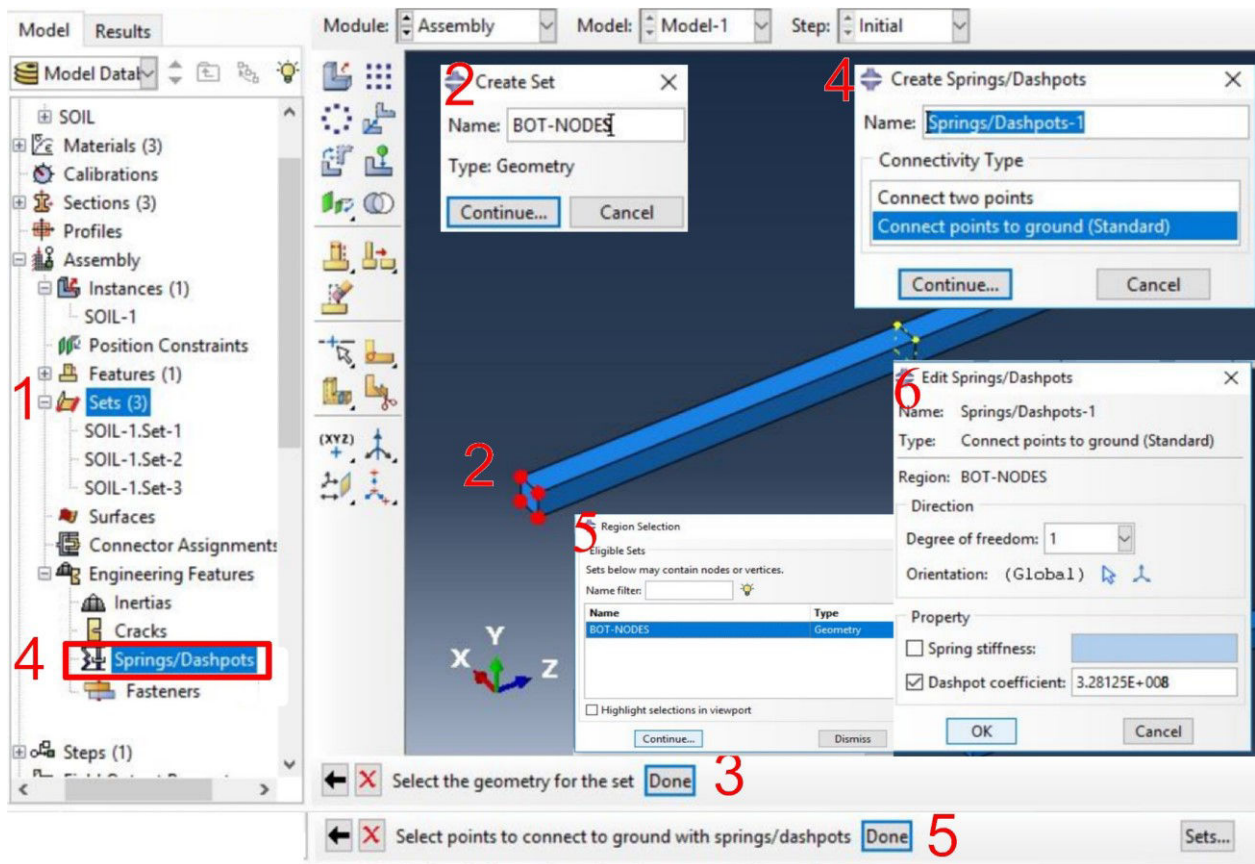
**Repeat this step in order to assign a section for each layer**



Choose the module **Assembly**

1. Click on the icon **Create Instance**
2. Choose the **SOIL Part** from the list of Parts
3. Click **OK**

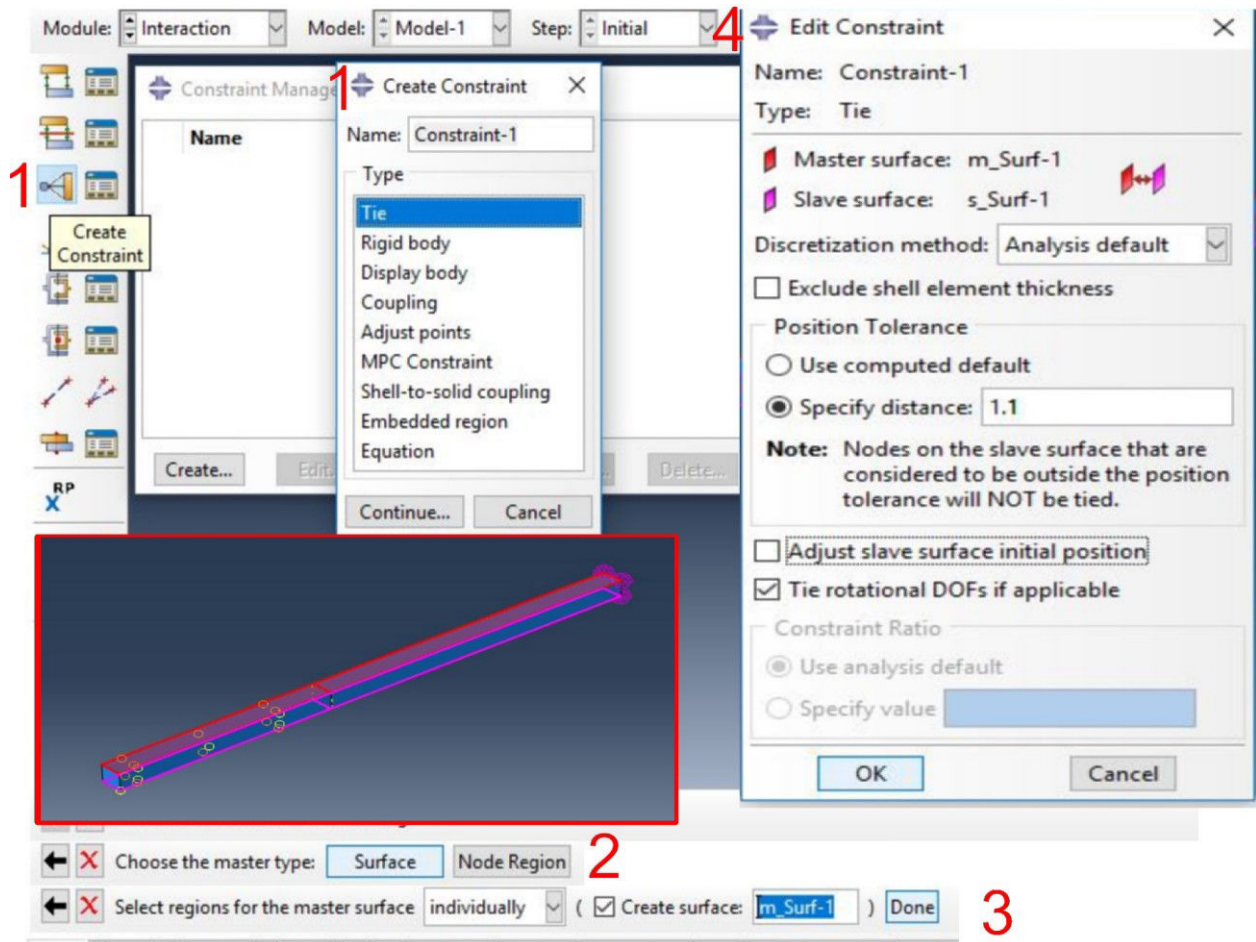
**Repeat this step for the part of 3-D soil**



1. Double click on **Sets**
2. **Name** the Set → Continue → Select all bottom geometric nodes
3. Click on **Done**
4. Double click on the icon **Springs/Dahpots** → Name → **Select Connect points to ground**
5. Select points from the **Sets** catalogue → Select all bottom nodes → Continue → Done
6. Select the degree of freedom **1** → **disable Spring stiffness** → **Enable Dashpot coefficient** → Enter the value of **damping** → **OK**

PS. Don't forget to divide by the number of bottom nodes

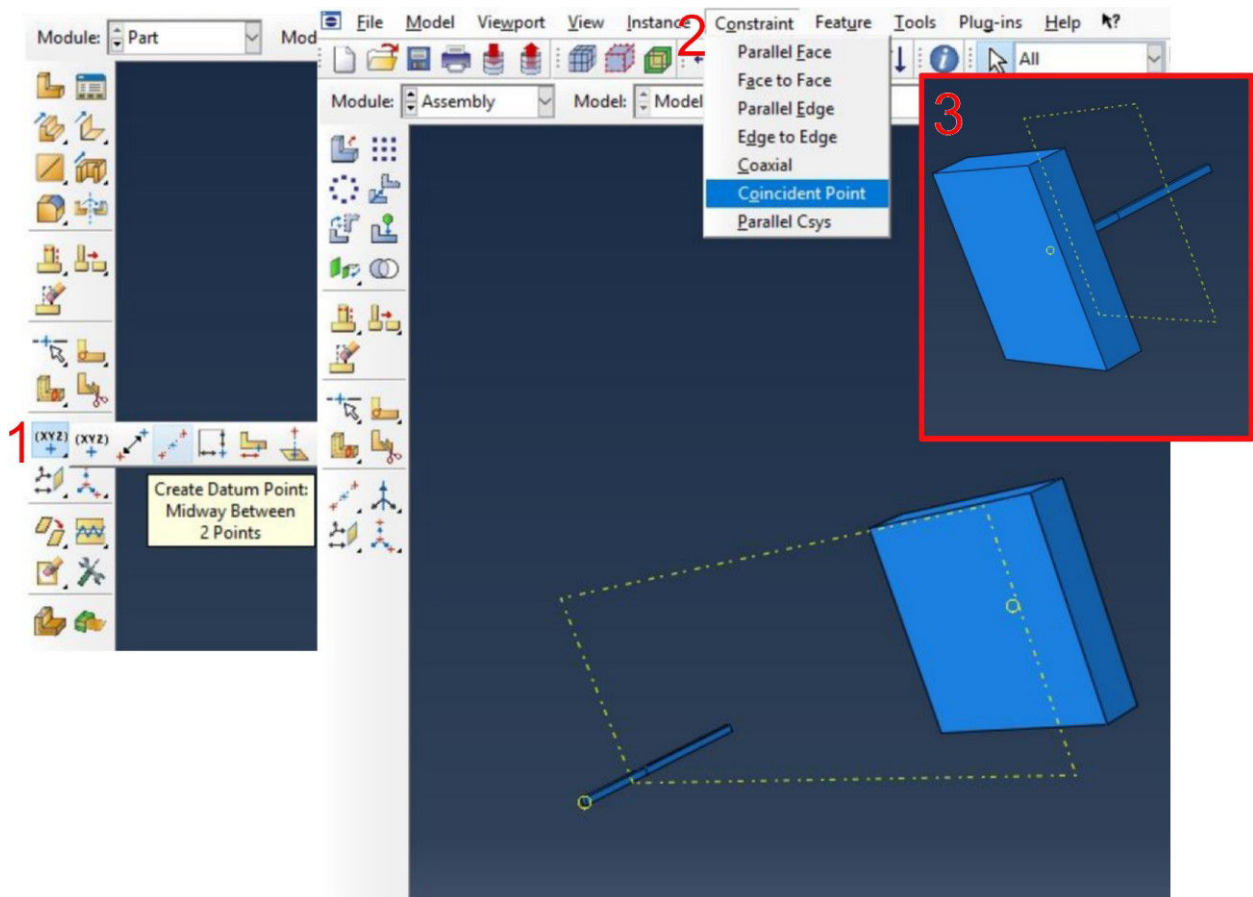
**Repeat this step for the degrees of freedom 2 and 3**



Choose the module **Interaction**

1. Click on the icon **Create Constraint** → Select **Tie** → **Continue**
2. Choose the master type **Surface**
3. Select a lateral surface of the column → Then choose the slave type **Surface** → Select the opposite lateral surface of the column
4. Specify distance **1.1** → **disable** Adjust slave surface initial position → **OK**

**Repeat this step for the other two opposite lateral surfaces and for the 3-D soil** but the distance this time would be **25.1**



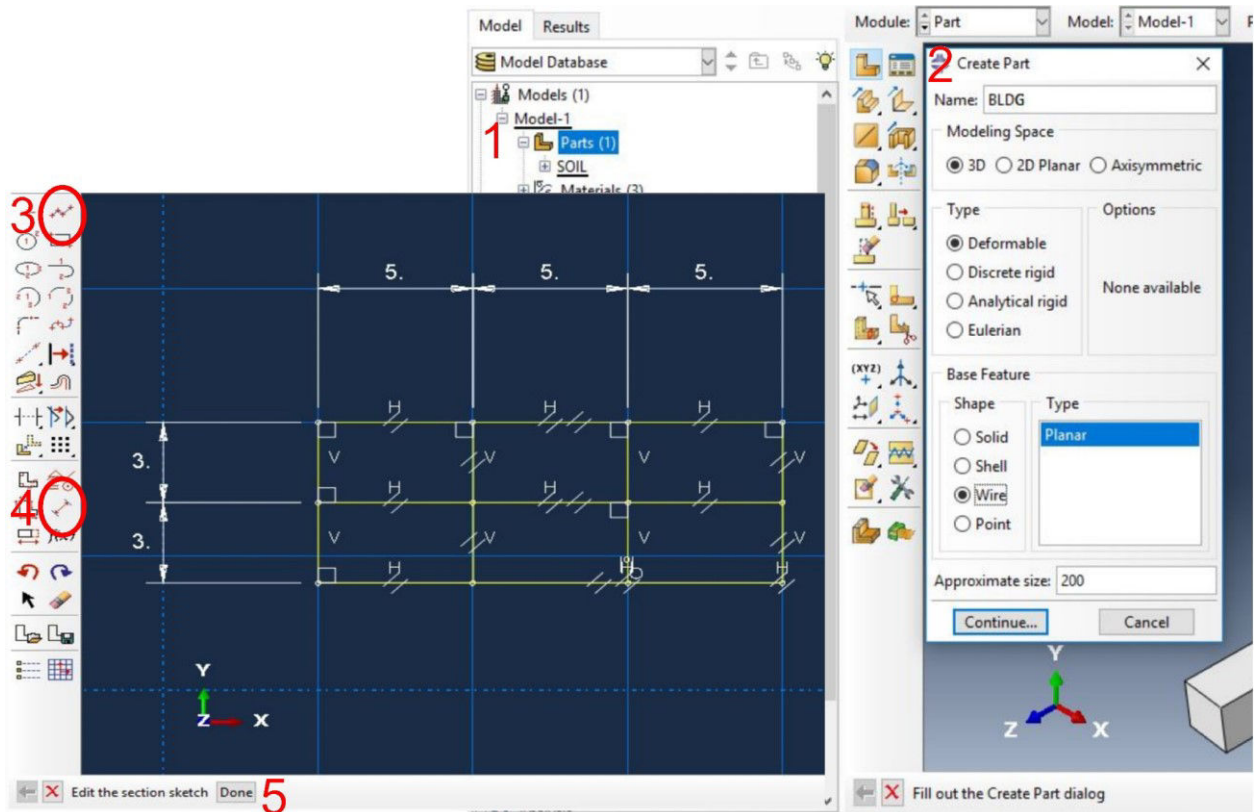
In Module **Part** create datum plane at the mid-top of the 1-D soil and at the mid-bottom of the 3-D soil

1. Click on the icon **Create Datum Point : Midway Between 2 Points** → Select **two points**

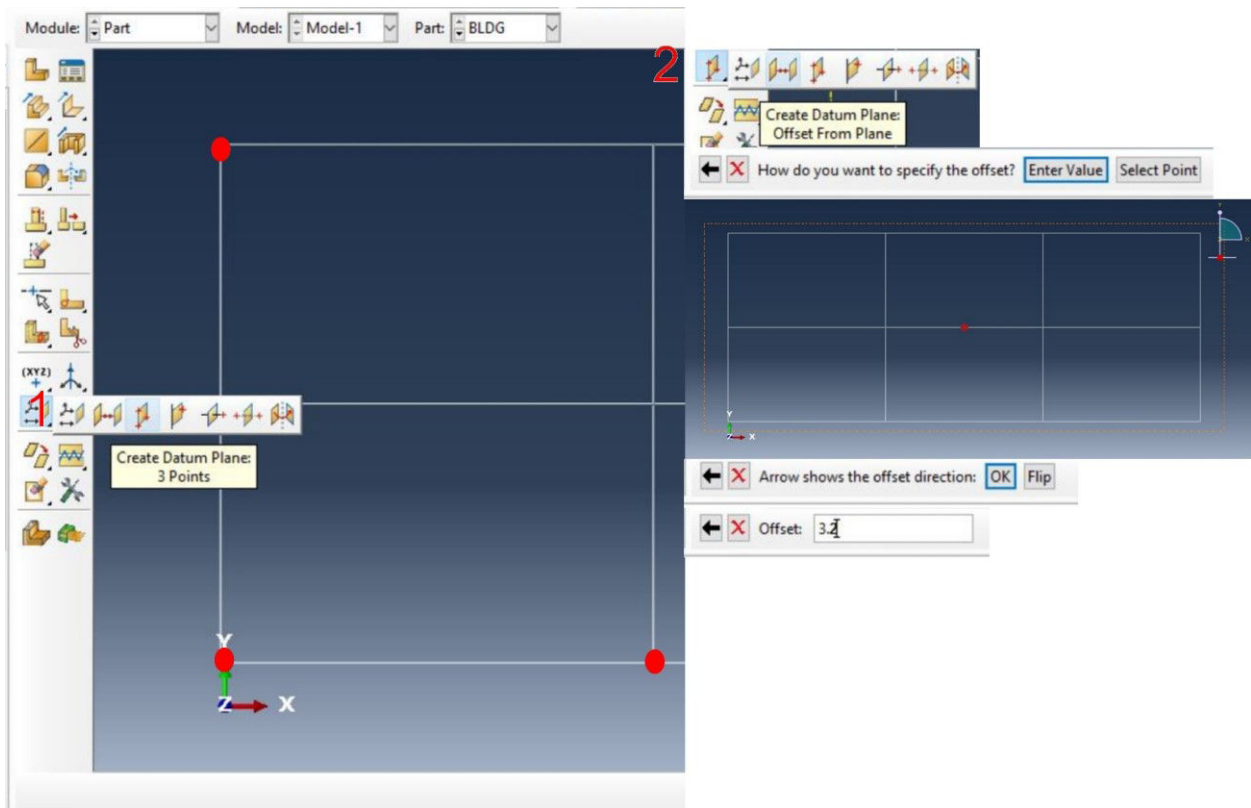
In Module **Assembly**

2. Select **Coincidence Point** from **constraint** → Select the datum points created earlier
3. Both parts will be joined

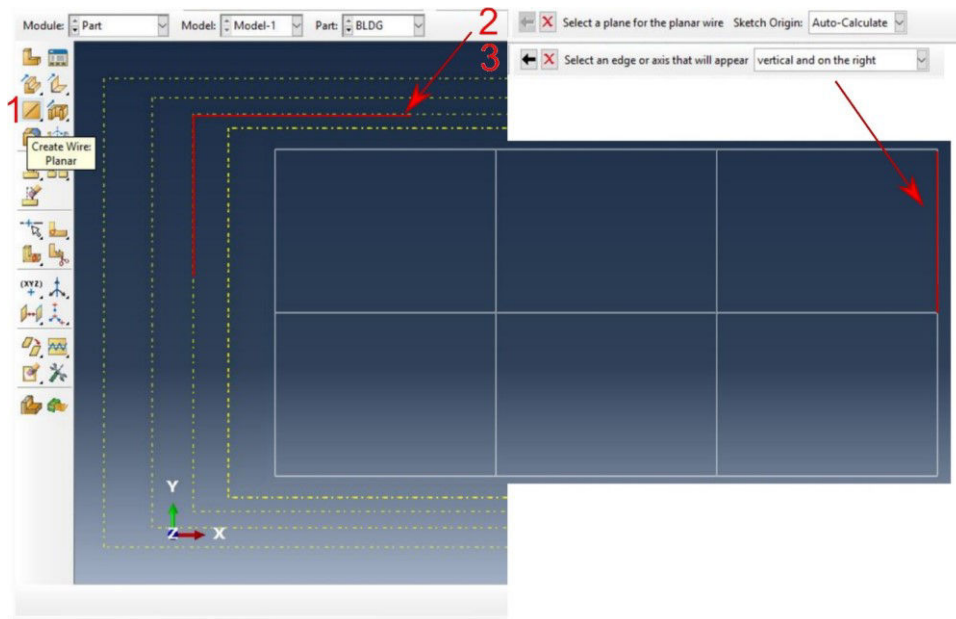
### 3-D building model



1. Double click on **Parts**
2. Choose a **Name** for your part  
Select the **Modeling space** → **3D**  
Select the **Type** → **Deformable**  
Select the **Base Feature** → **Shape** → **Wire**
3. **Sketch** the floor plan of the building as shown in the picture
4. Adjust the dimensions  
**Continue**

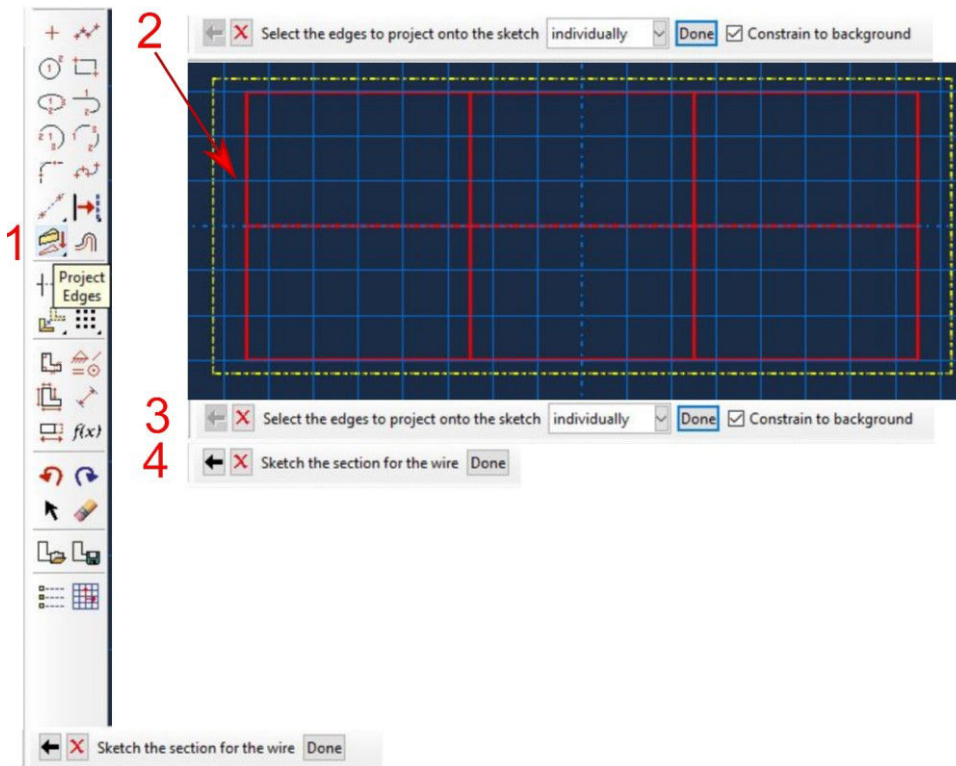


1. Click on the icon **Create Datum Plane: 3 Points** and create the plane using the selecting red points as shown
2. Click on the icon **Create Datum Plane: Offset From Plane**  
 Select the **plane** you want to offset from  
 Choose the **direction** of offset  
 Write the **Offset distance** in the new dialog → **3.2 m**
3. **Press Enter**  
**Repeat this step in order to have a plane for each level**



1. Click on the icon **Create Wire Planar**
2. Select a **plane** on which you want to sketch a planar wire
3. Select an **edge** that will appear on the write of the screen

**Following**

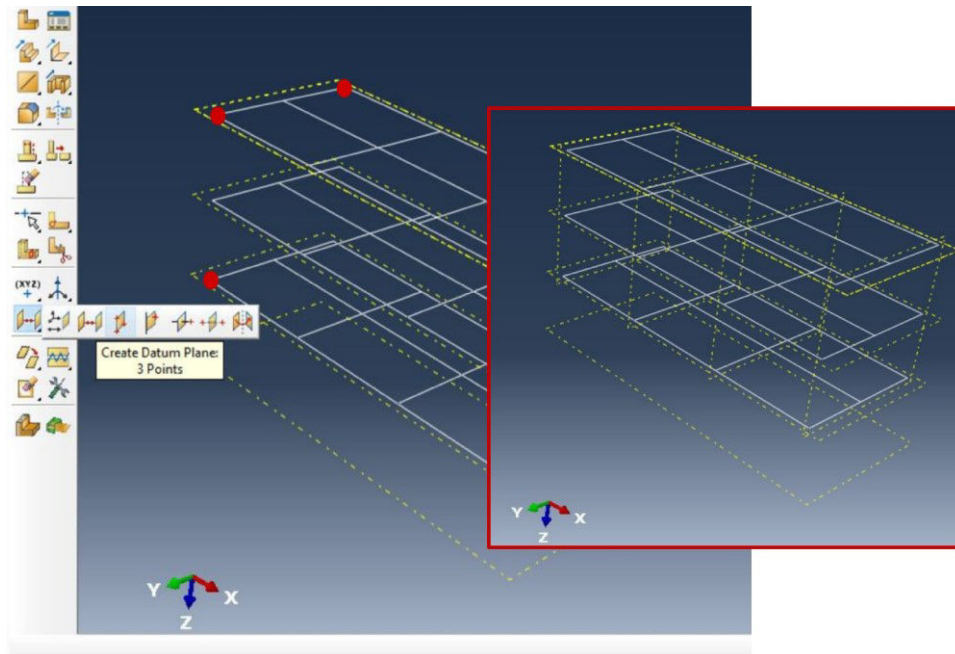


1. Click on the icon **Project Edges**
2. Select the **edges** to project onto the sketch → **Done**

3. **Done**

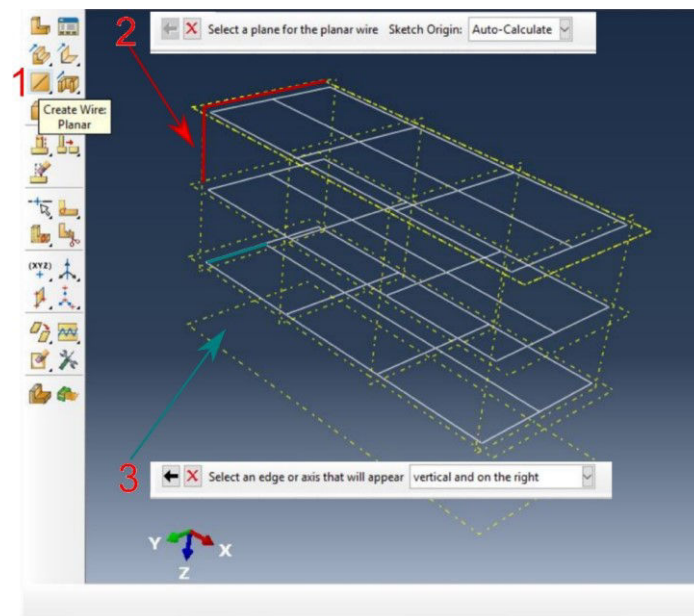
4. **Done**

**Repeat this step in order to have the plan wire for each floor**



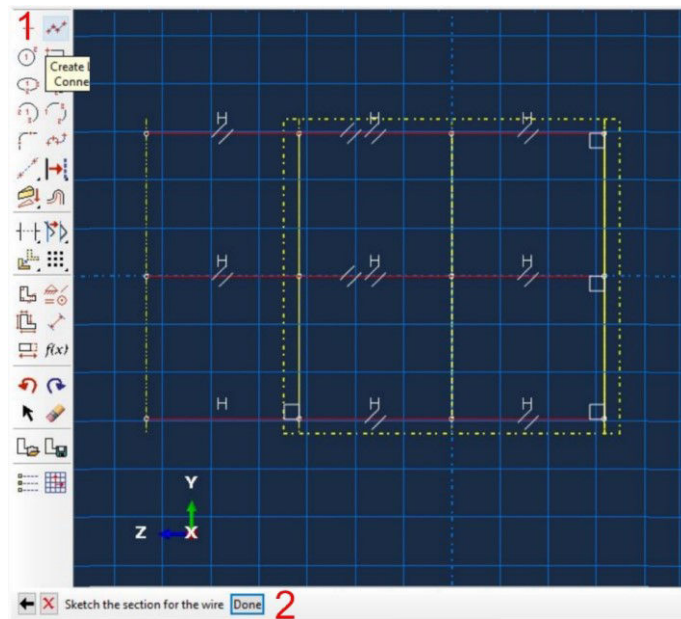
Click on the icon **Create Datum Plane: 3 Points** and create the plane using the selecting red points as shown

**Repeat this step in order to have datum plans as shown**

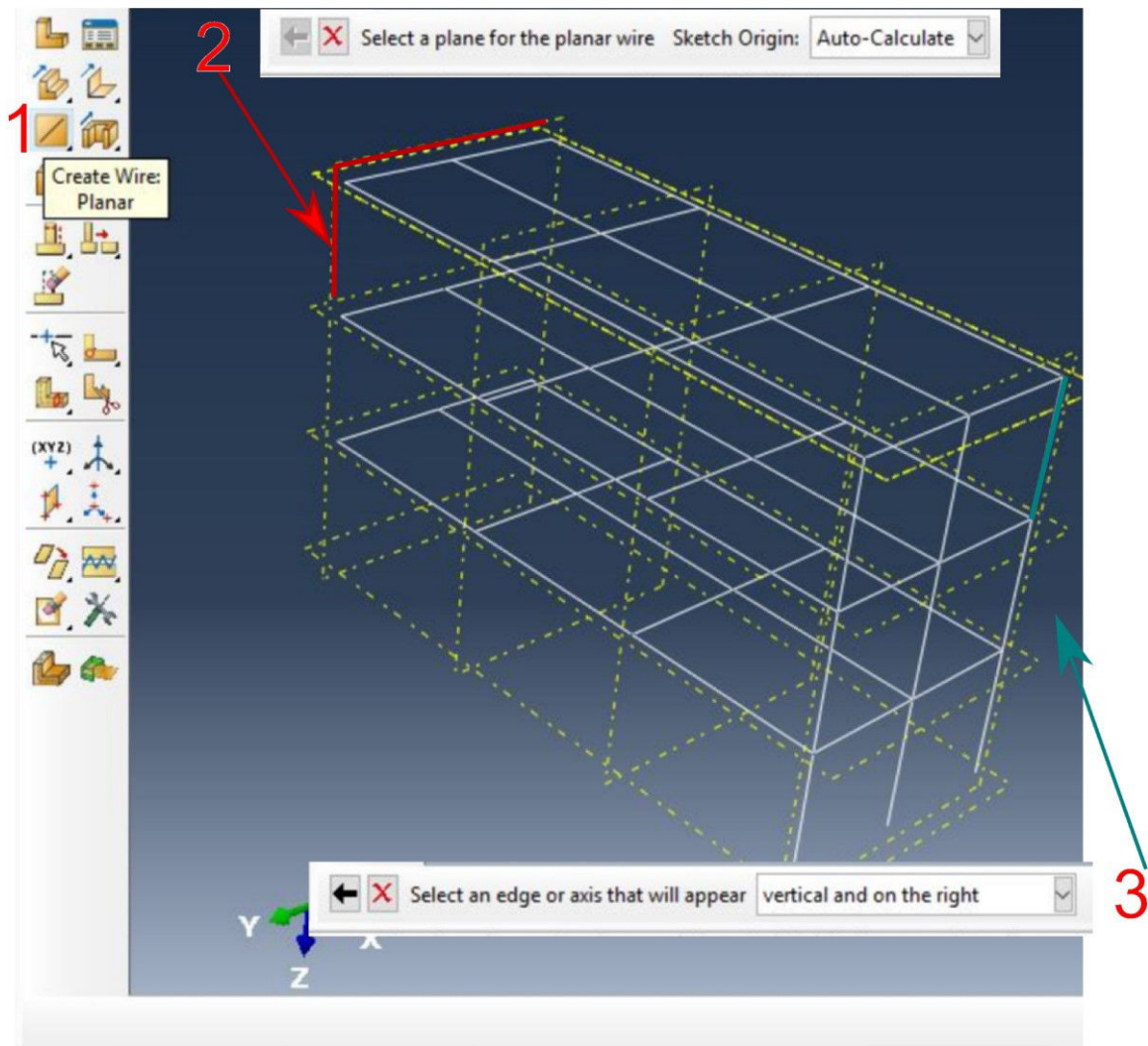


1. Click on the icon **Create Wire Planar**

2. Select a **plane** on which you want to sketch a planar wire
3. Select an **edge** that will appear on the wire of the screen

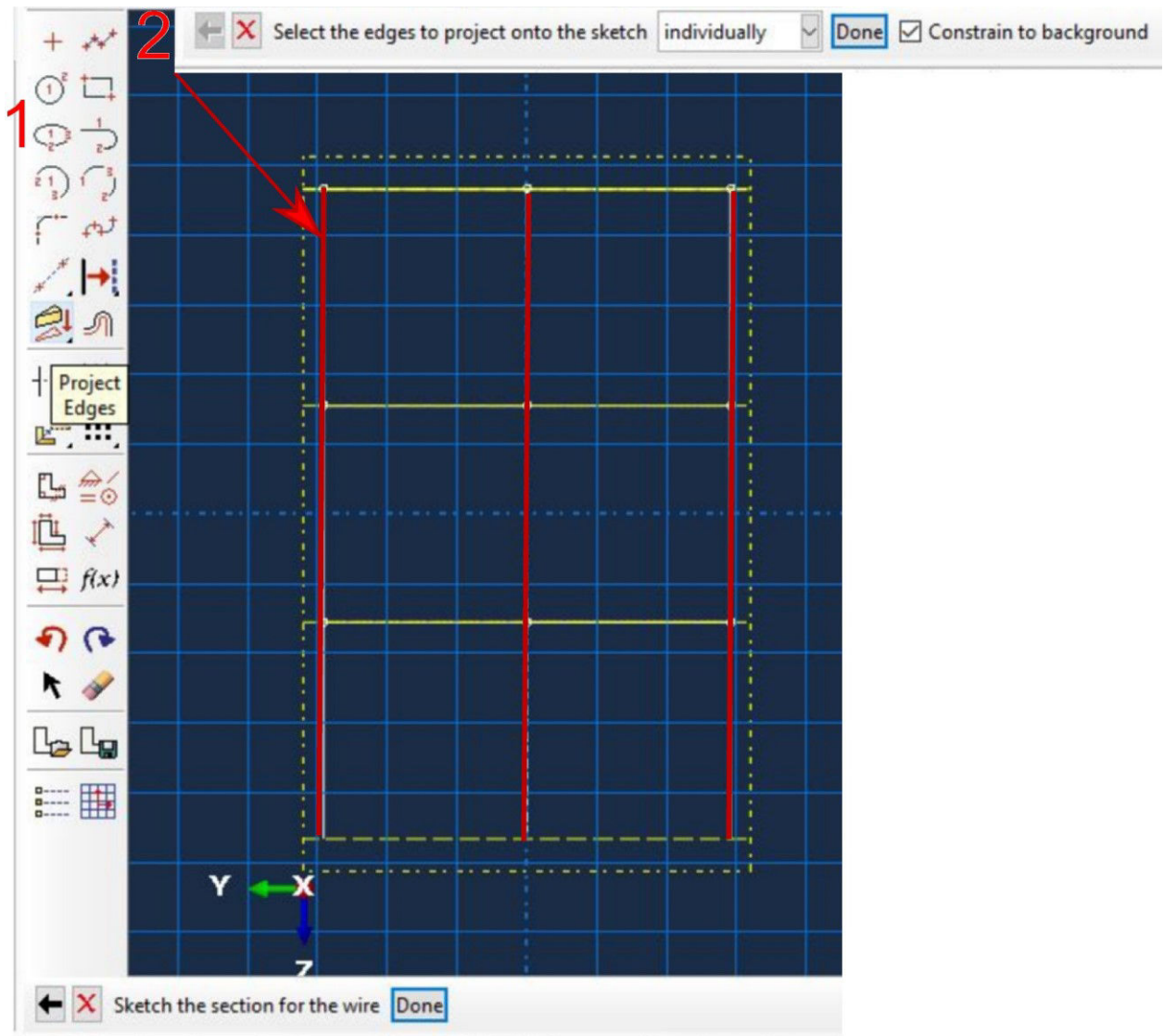


1. Click on the icon **Create Wire**  
Sketch **wire** to create the column as shown
2. **Done**



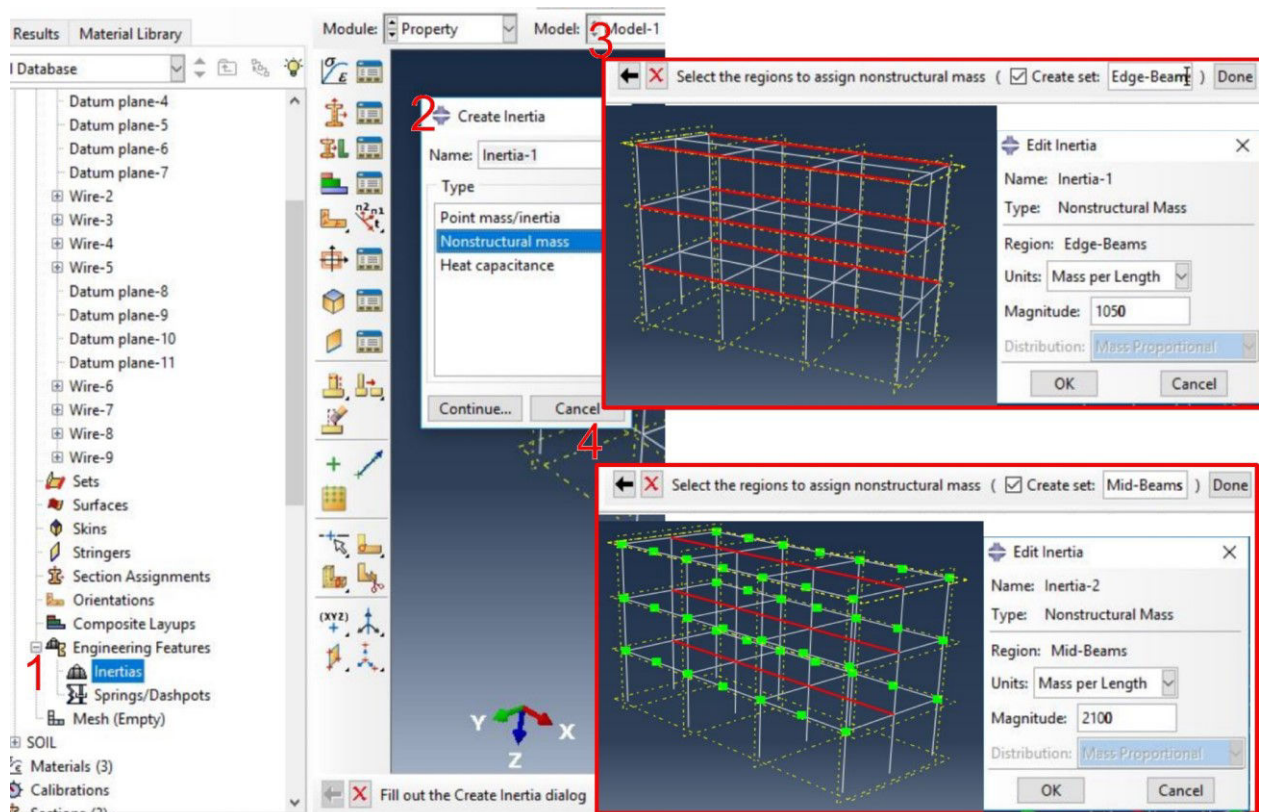
1. Click on the icon **Create Wire Planar**
2. Select a **plane** on which you want to sketch a planar wire
3. Select an **edge** that will appear on the wire of the screen

**Following**

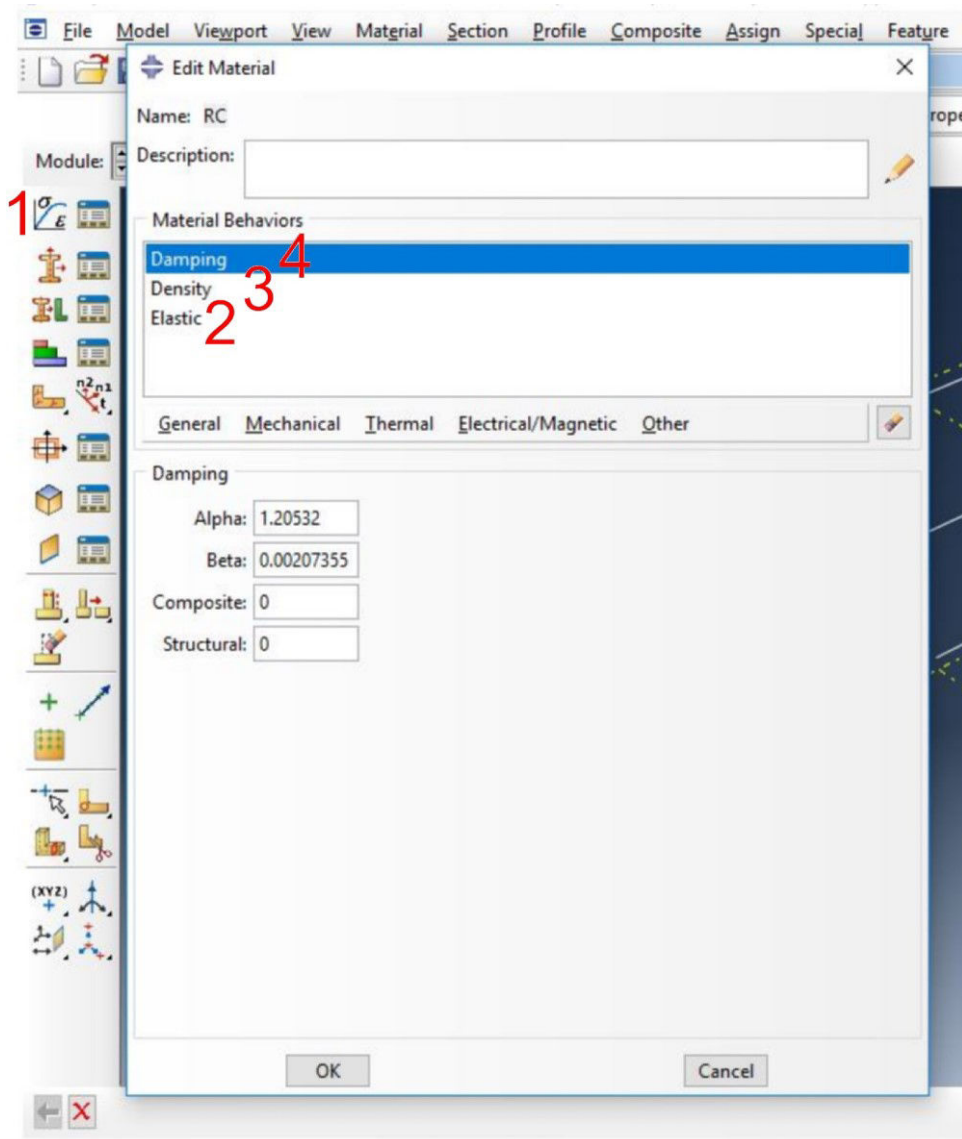


1. Click on the icon **Project Edges**
2. Select the **edges** to project onto the sketch → **Done**
3. **Done**
4. **Done**

**Repeat this step in order to have the plan wire for all y-z datum plans**

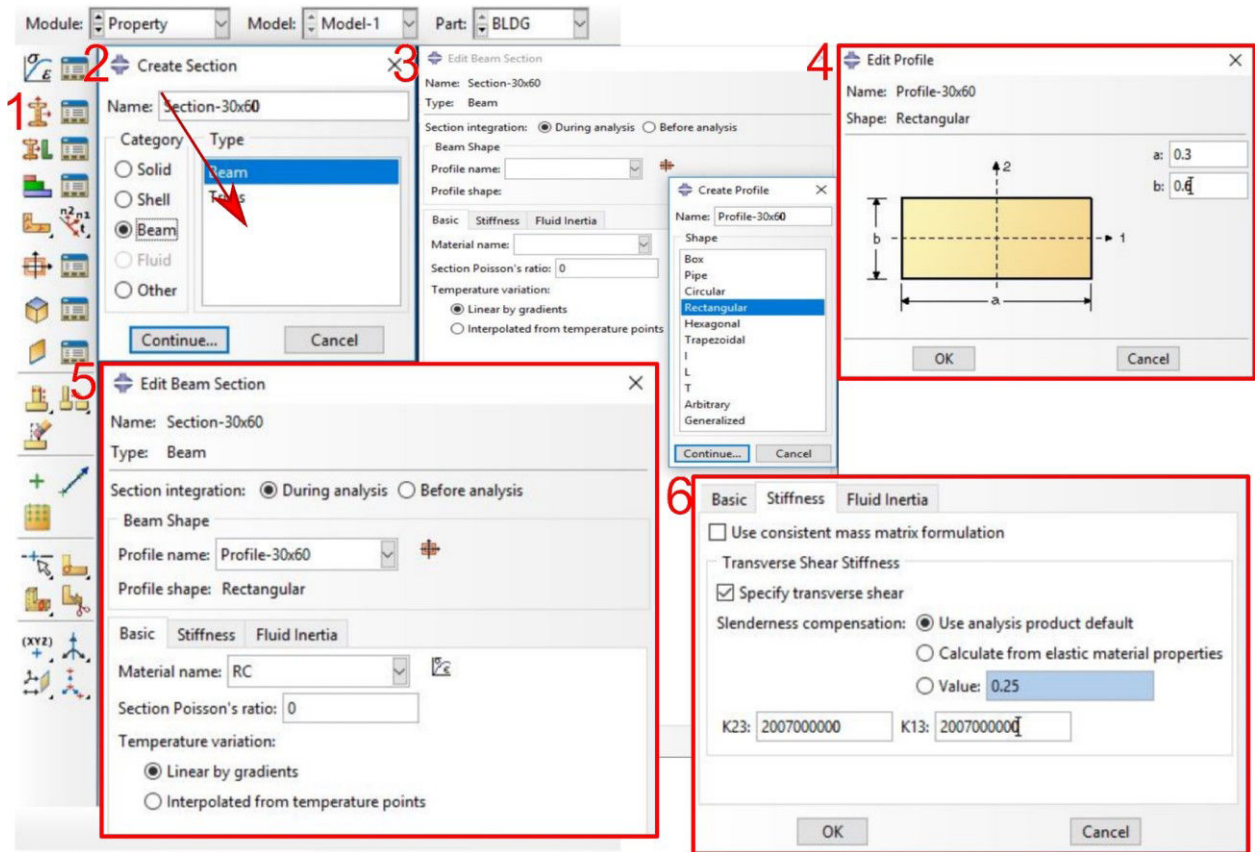


1. Double click on the icon **Inertias** → Name → **Nonstructural mass**
2. Select the region to assign nonstructural mass → Select **Edge Beams** → From Units select **Mass per Length**, from **Magnitude** input **1050** → **OK**
3. Select the region to assign nonstructural mass → Select **Middle Beams** → From Units select **Mass per Length**, from **Magnitude** input **2100** → **OK**



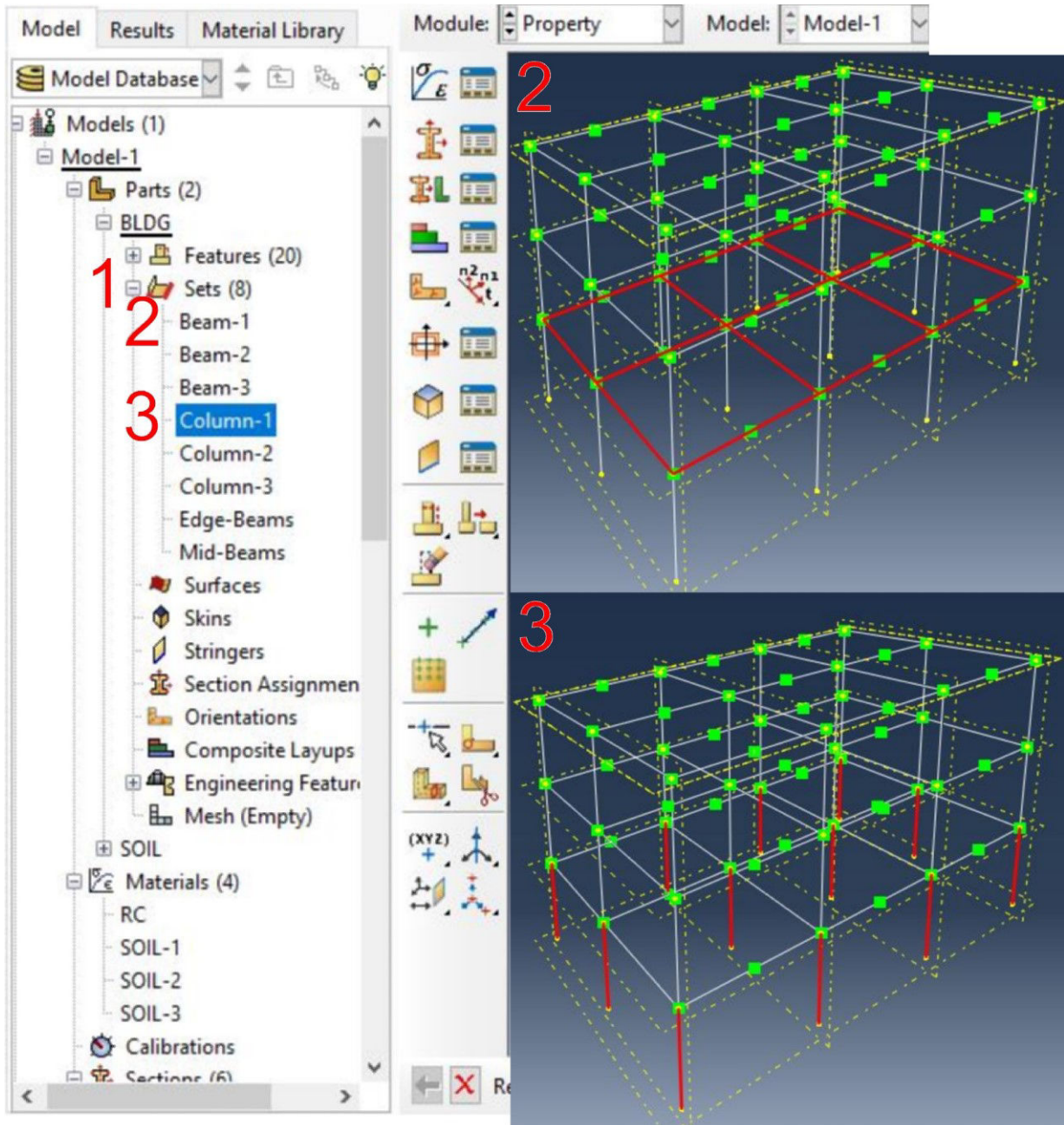
Choose the module **Property**

1. Click on the icon **Create Material** → Choose a **Name** for your material
2. Select from the catalogue **Mechanical** → **Damping**, enter the damping coefficients.
3. Select from the catalogue **General** → **Density**, enter the density of the material.
4. Select from the catalogue **Mechanical** → **Elasticity**, enter the Young modulus and the poison ratio of the material.
5. Click **OK**



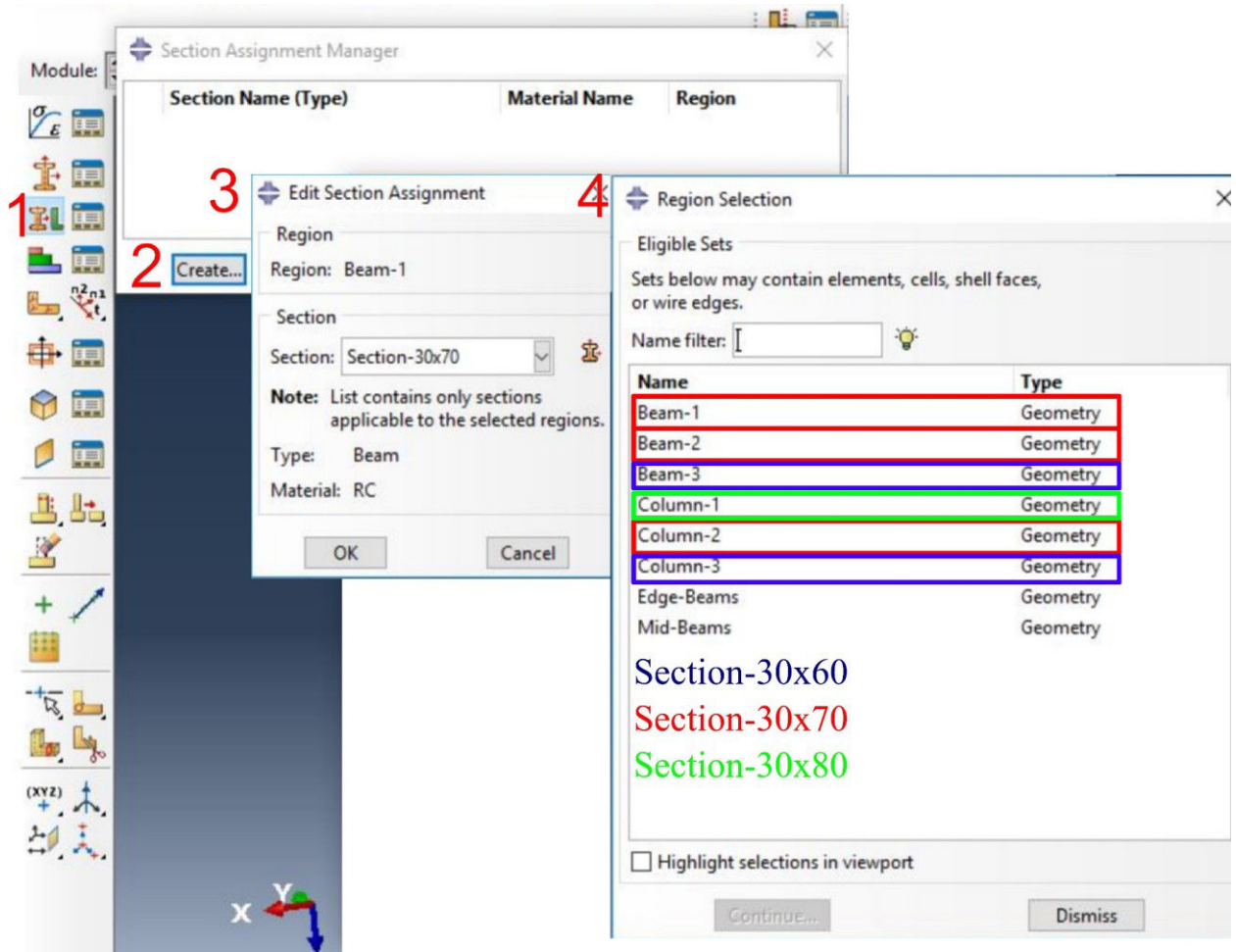
1. Click on the icon **Create Section**
2. Choose a **Name** for your section → Select **Beam** from **Category** → Select **Beam** from **Type** → **Continue**
3. Click on the icon **Create Beam Profile** → Choose a **Name** for your Profile → Select **Rectangular** from **Shape** → **Continue**
4. Input **a** and **b**
5. Choose the material from **Basic** → **Material Name**
6. Enable **Specify transverse shear** from **Stiffness** → input **K23** and **K13** → **OK**

**Repeat this step in order to create a section for beam and column section type**



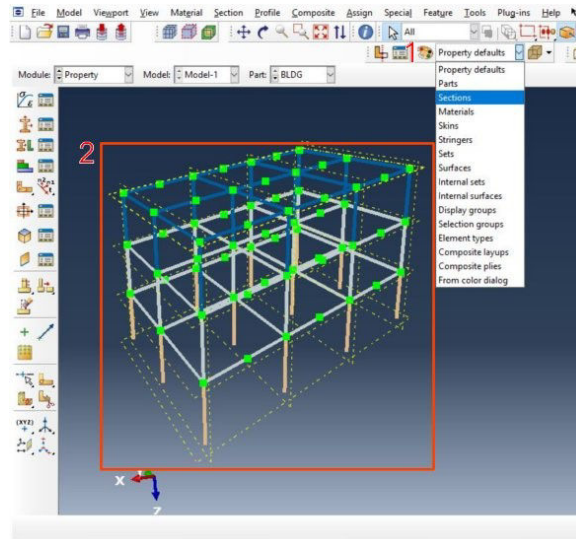
1. Double Click on the icon Sets
2. Create Sets for all the beams on the same level
3. Create Sets for all the columns on the same level

As shown in the Figure

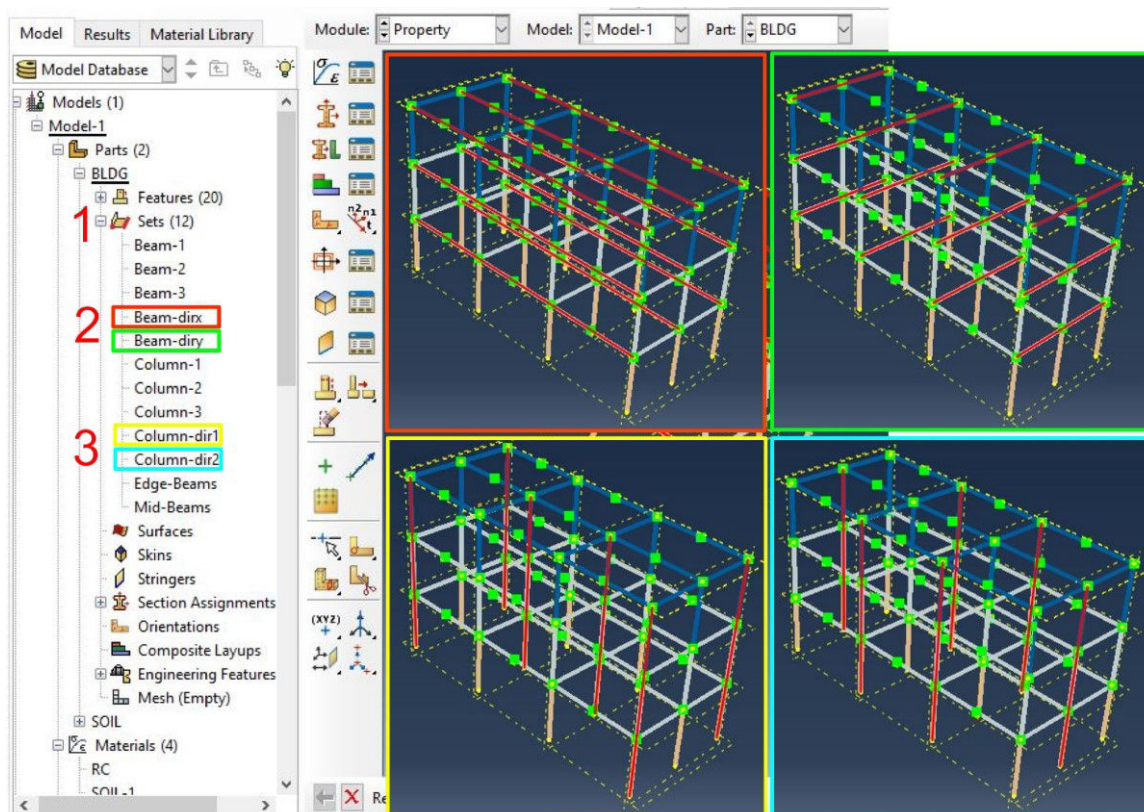


1. Click on the icon **Assign Section**
2. Click on the icon **Create** → Choose a **Region** from sets  
 → Select a section from **Section**

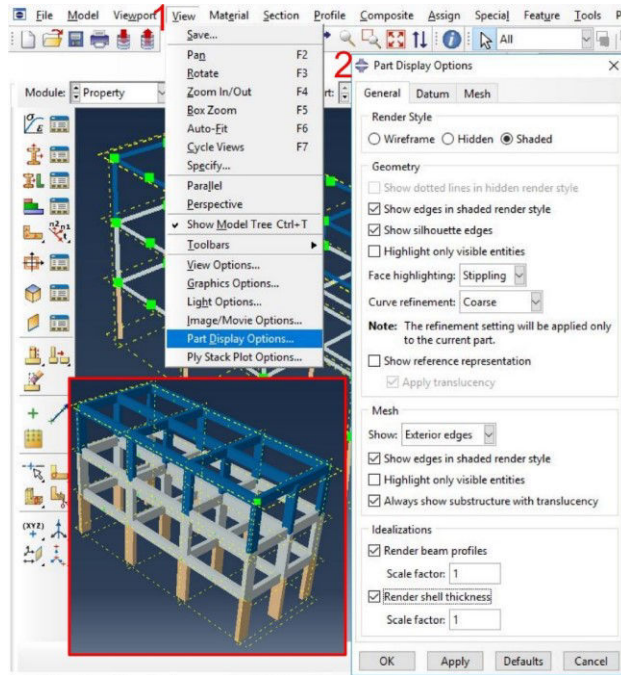
**Repeat this step in order to have a section for all columns and beams as shown in the Figure**



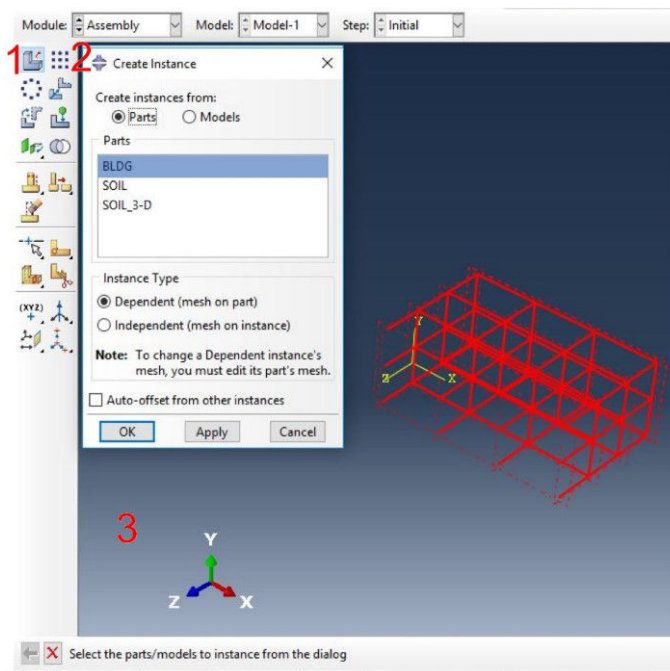
**2. From Property default choose Sections**



1. Double Click on the icon Sets
2. Create sets for beams in the direction x-z → beams in the direction y-z → columns as shown in the yellow square → columns as shown in the aqua blue square



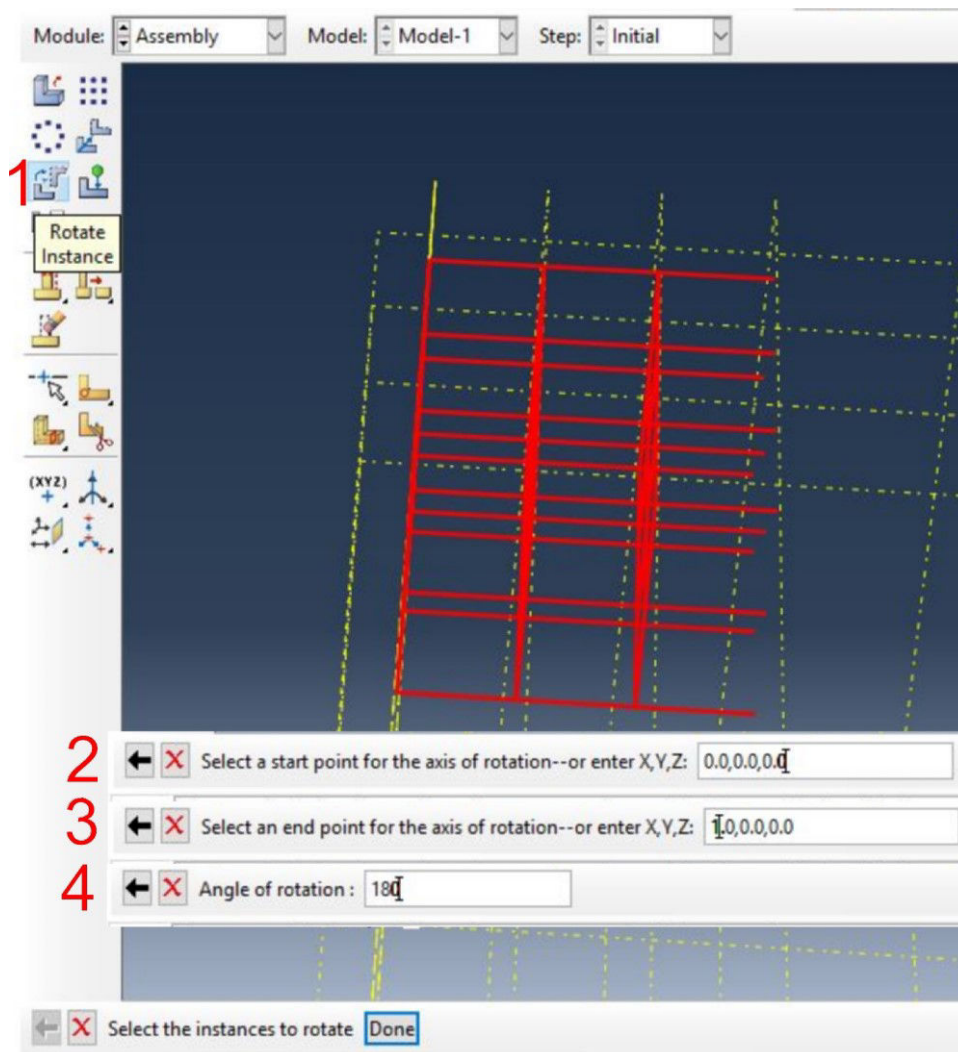
1. Select from **View** → **Part Display Options**
2. Enable → Render beam profiles  
→ Render shell thickness



Choose the module **Assembly**

1. Click on the icon **Create Instance**
2. Choose the **Building Part** from the list of Parts

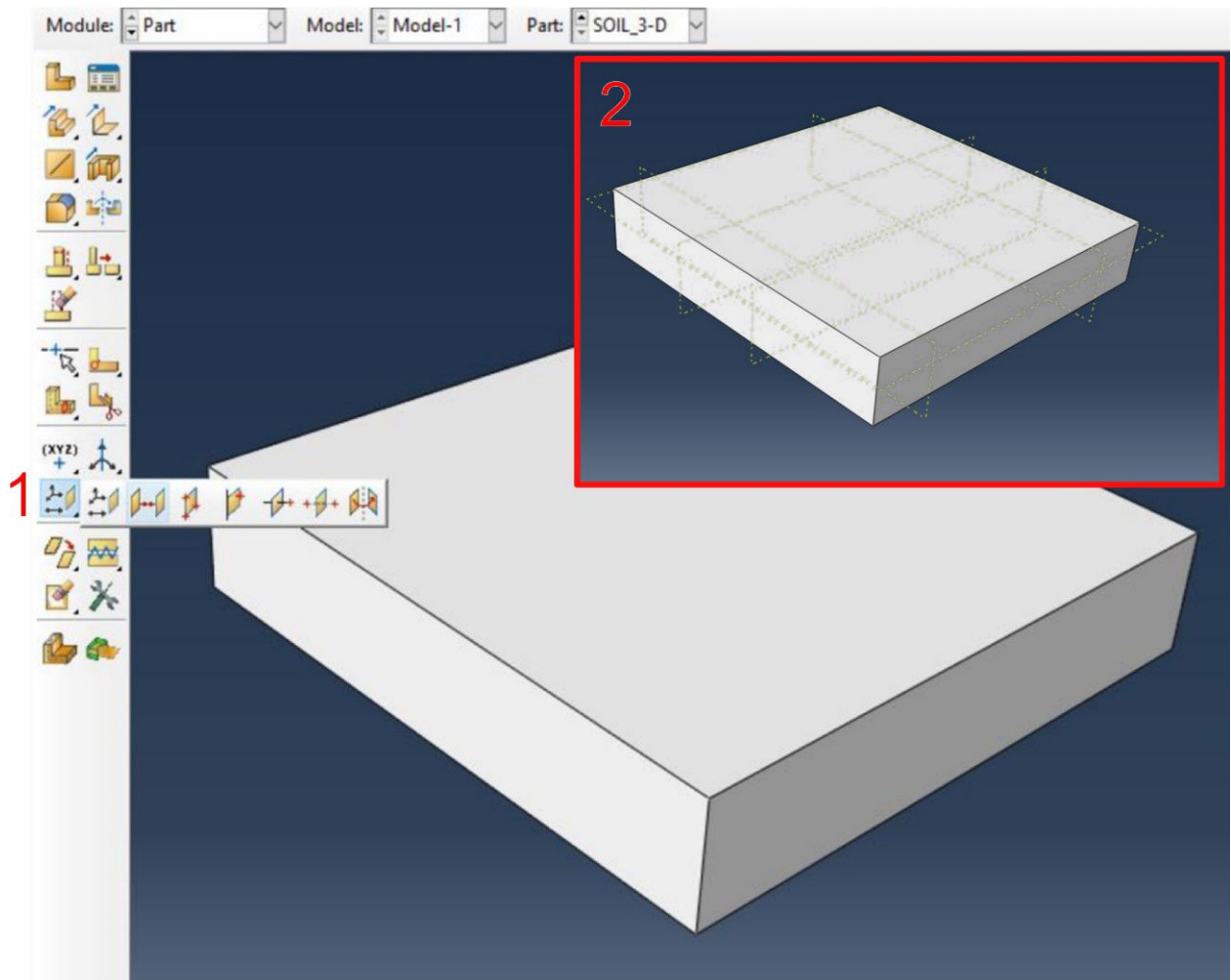
3. Click **OK**



1. Click on the icon **Rotate Instance** → Select the building part → **Done**
2. Select a **start point** for the axis of rotation (**0, 0, 0**)
3. Select an **end point** for the axis of rotation (**1, 0, 0**)
4. Input **Angle of rotation 180**

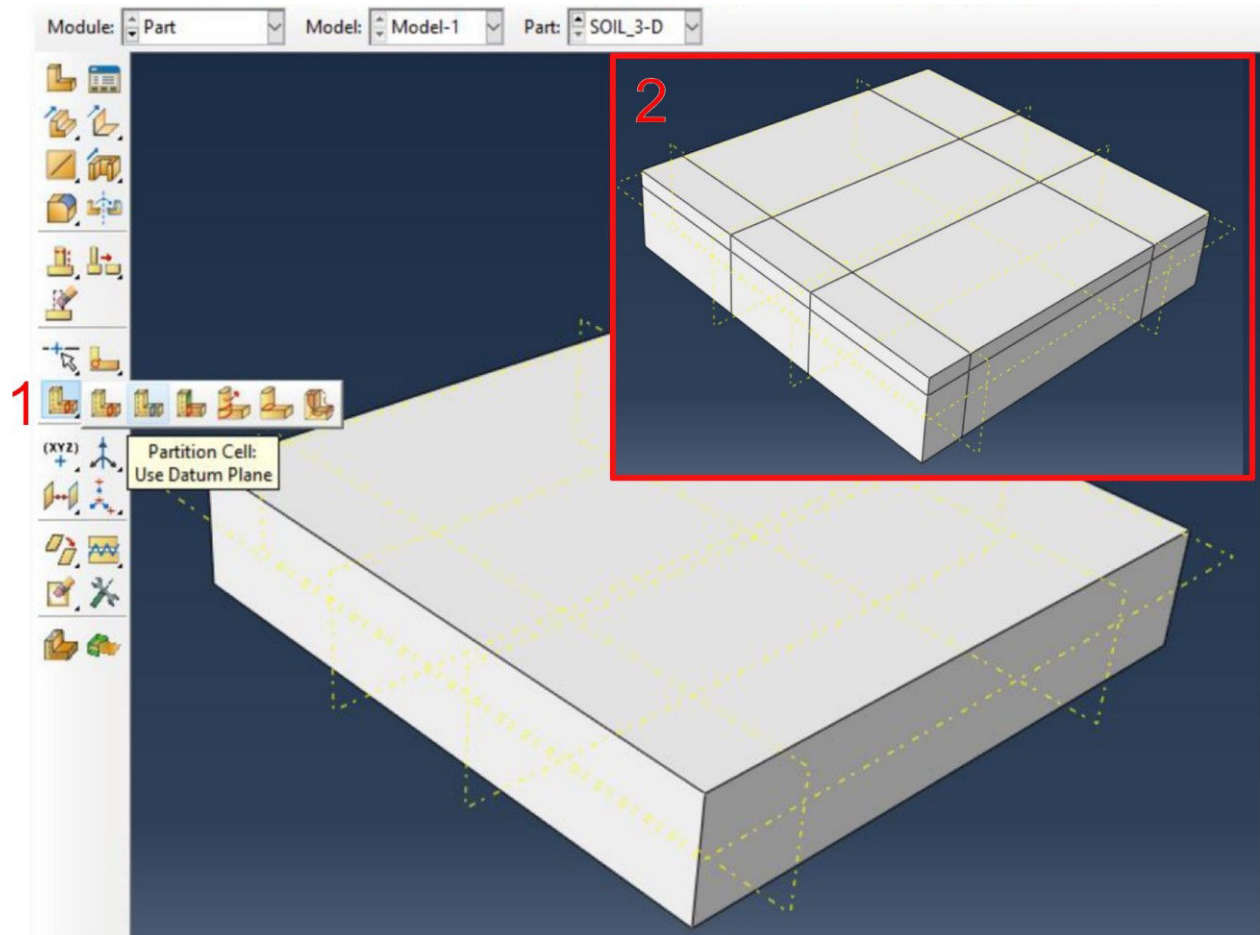
**Press Enter → OK**

### 3-D foundation

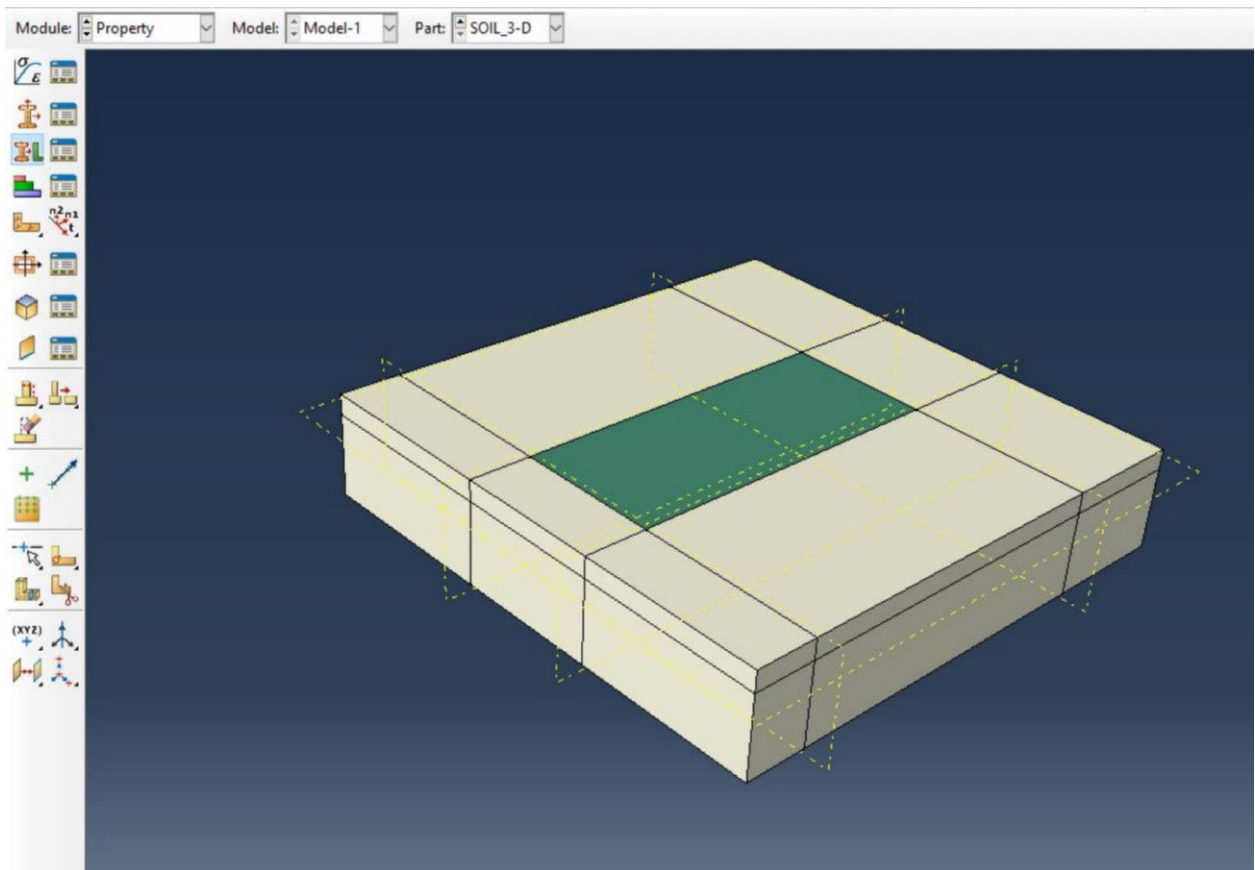


Choose the module **Part** → 3-D Soil Part

1. Click on the icon **Create Datum Plane : Offset from Plane**
2. Create planes to form the edge surfaces of the foundation



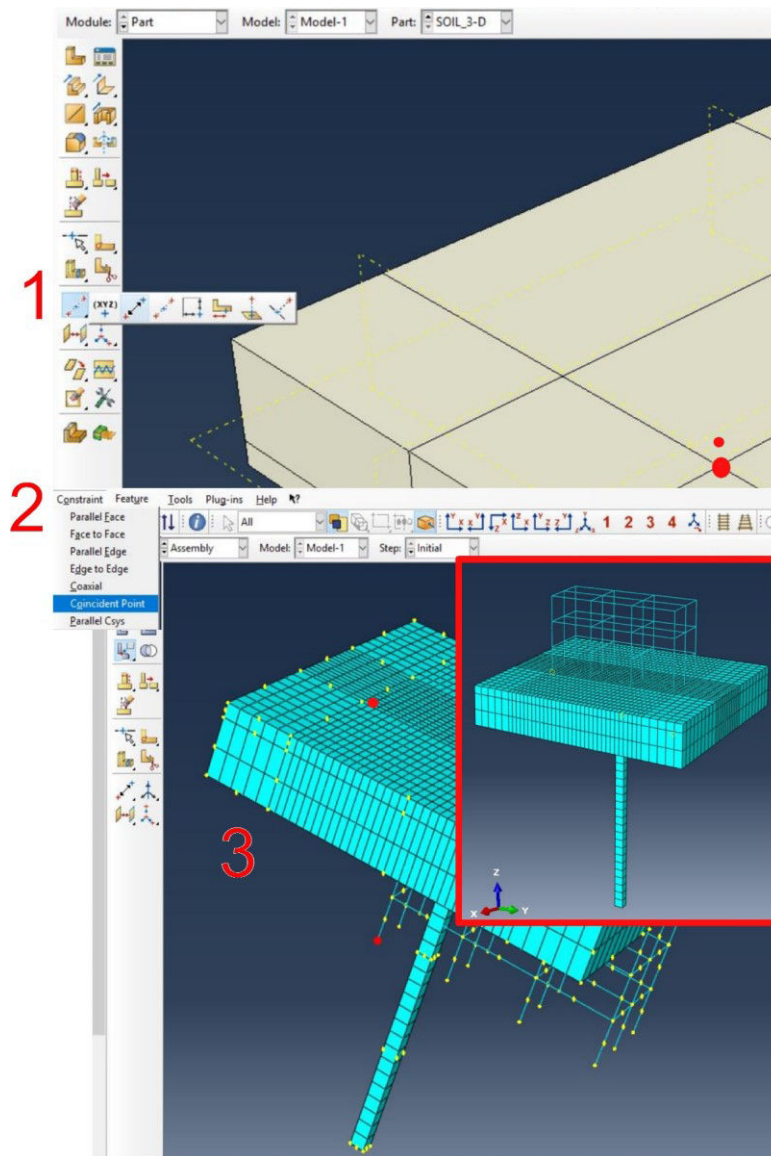
1. Click on the icon **Partition cell : Use Datum Plane**
2. Partition the 3-D soil domain to cut the shape of the embedded foundation



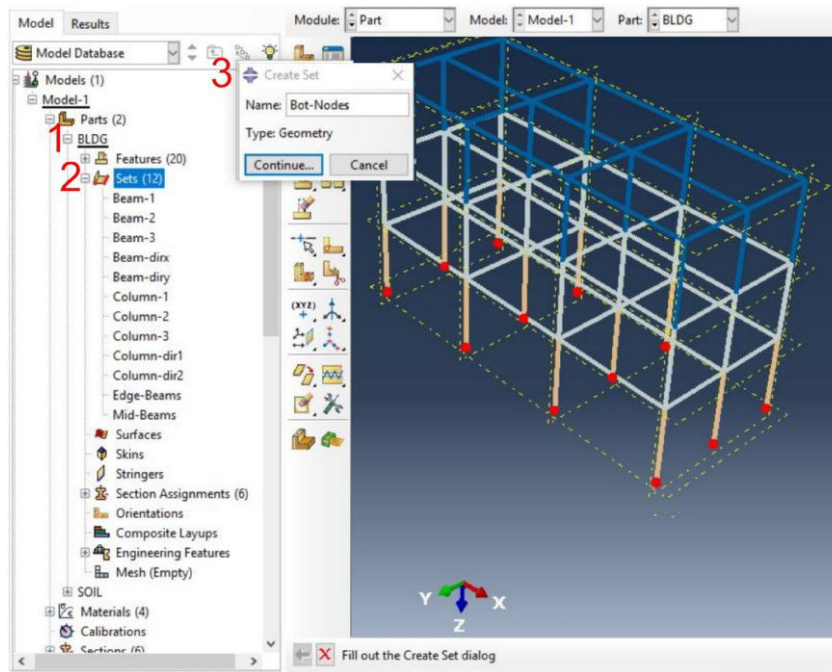
Choose the module **Property** → 3-D Soil Part

1. Click on the icon **Section Manager**
2. Click on the icon **Create** → Choose a **Name** for your section
  - Select **Solid** from **Category**
  - Select **Homogeneous** from **Type**
3. **Continue**
4. Select the material from the catalogue → **Reinforced concrete** for the foundation  
And **Soil-1** for the soil

## Calculation procedure

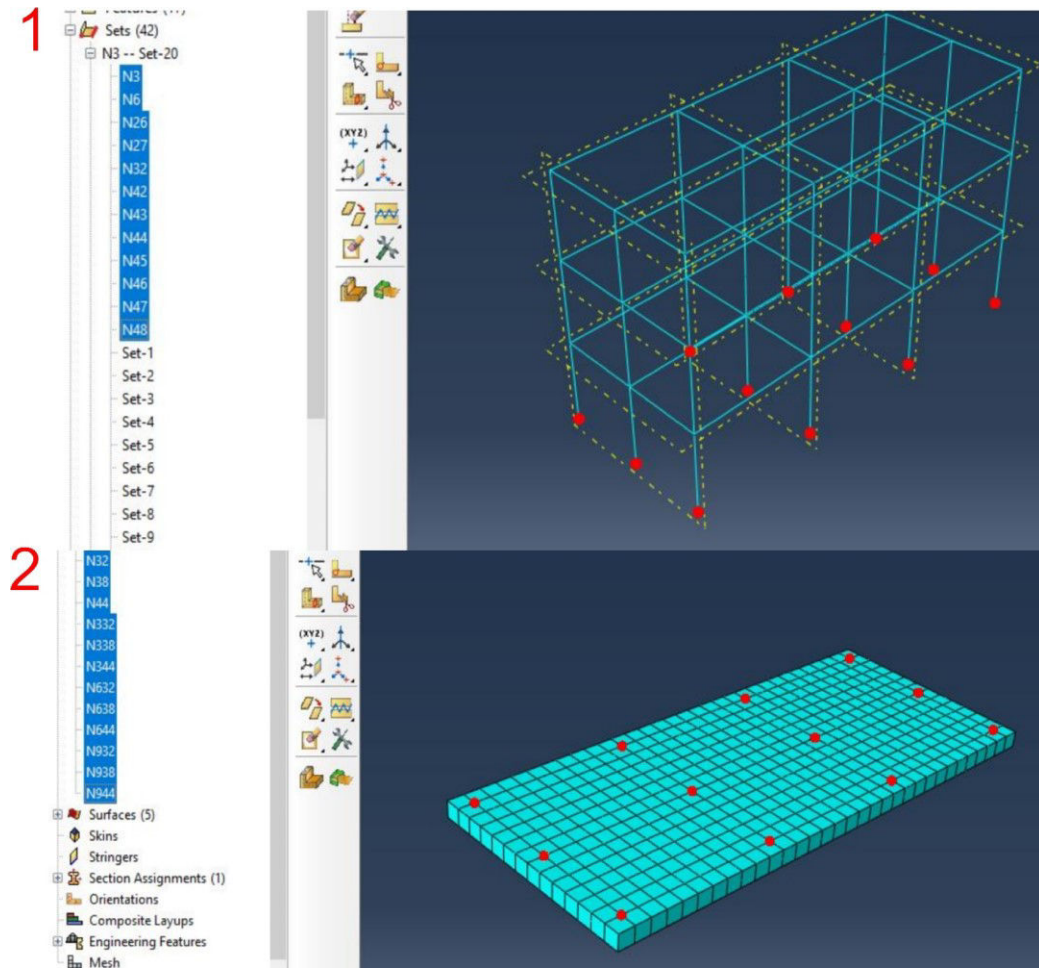


1. In Module **Part** create datum point offset from the edge of the foundation by (0.5,0.5,0) to the inside of the foundation
2. In Module **Assembly**  
Select from **Constraint** → **Coincident Point**  
Select a point of the movable instance  
Select a point of the fixed instance



Choose the module **Part**

1. From **building part**
2. Double click on **Sets**
3. Create **Geometry** set for all Bottom nodes of the building → **Continue**



Choose the module **Part**

**1. From building part**

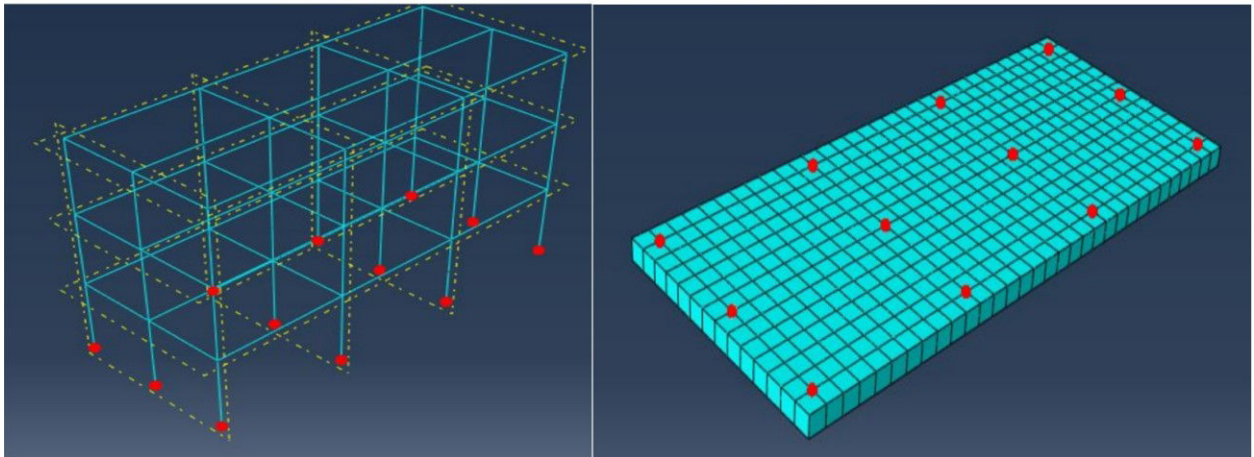
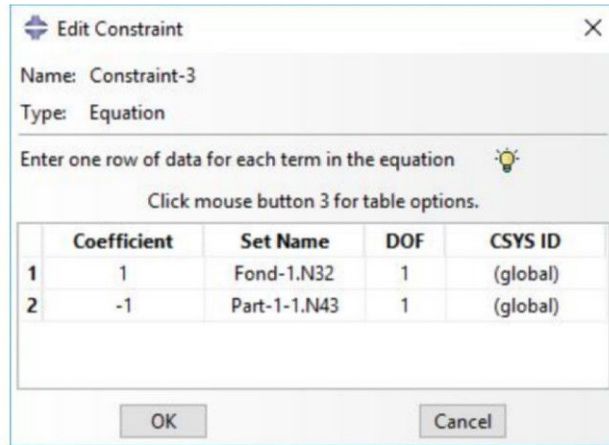
Double click on **Sets**

Create **Geometry** set for very Bottom node of the building → **Continue**

**2. From 3-D soil part**

Double click on **Sets**

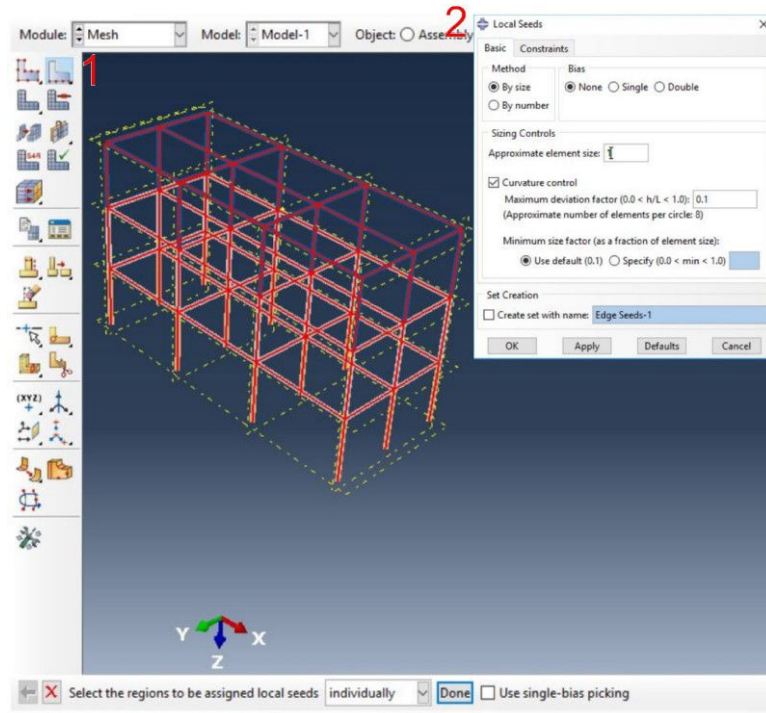
Create **Geometry** set for very Top node of the foundation that coincides with the first node of the building columns → **Continue**



**This step needs to be done for each bottom node set from the part building and its coincident node set from the foundation in the part 3-D soil**

1. Click on the icon **Create Constraint**
2. Select **Equation**
3. Input in table following this Figure

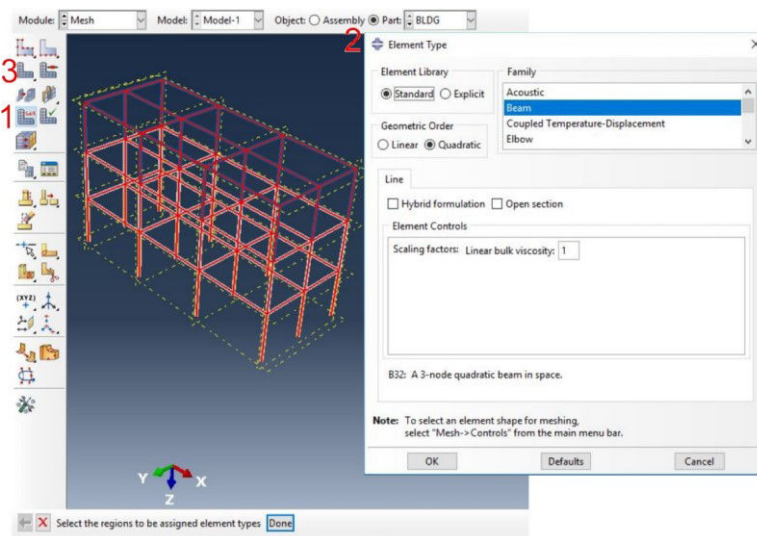
**Repeat this step in order to have a constraint for DOF 1, 2 and 3**



Choose the module **Mesh**

3. Click on the icon **Seed Edges** → Meshed **By size** → Approximate element size **1** → **OK**

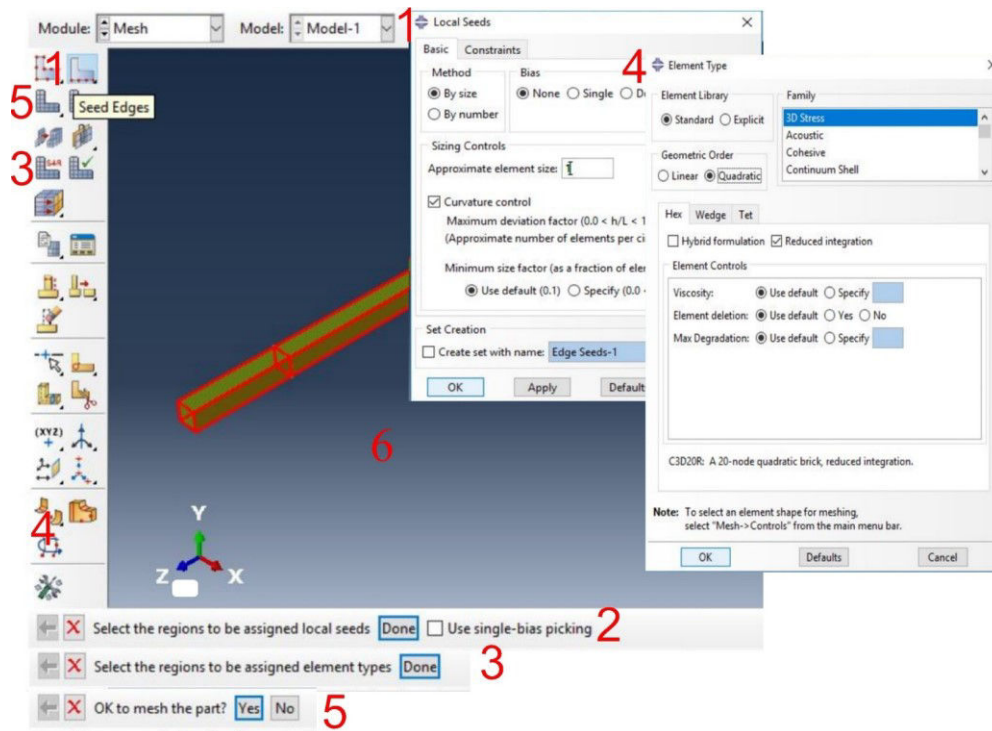
4. **Done**



5. Click on the icon **Assign Element Types** → Select the region to mesh → **Done**

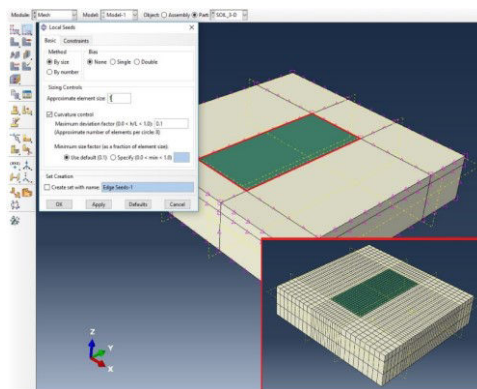
6. From Family select **Beam** → from Geometric Order enable **Quadratic** → **OK**

7. Click on the icon **Mesh Part**



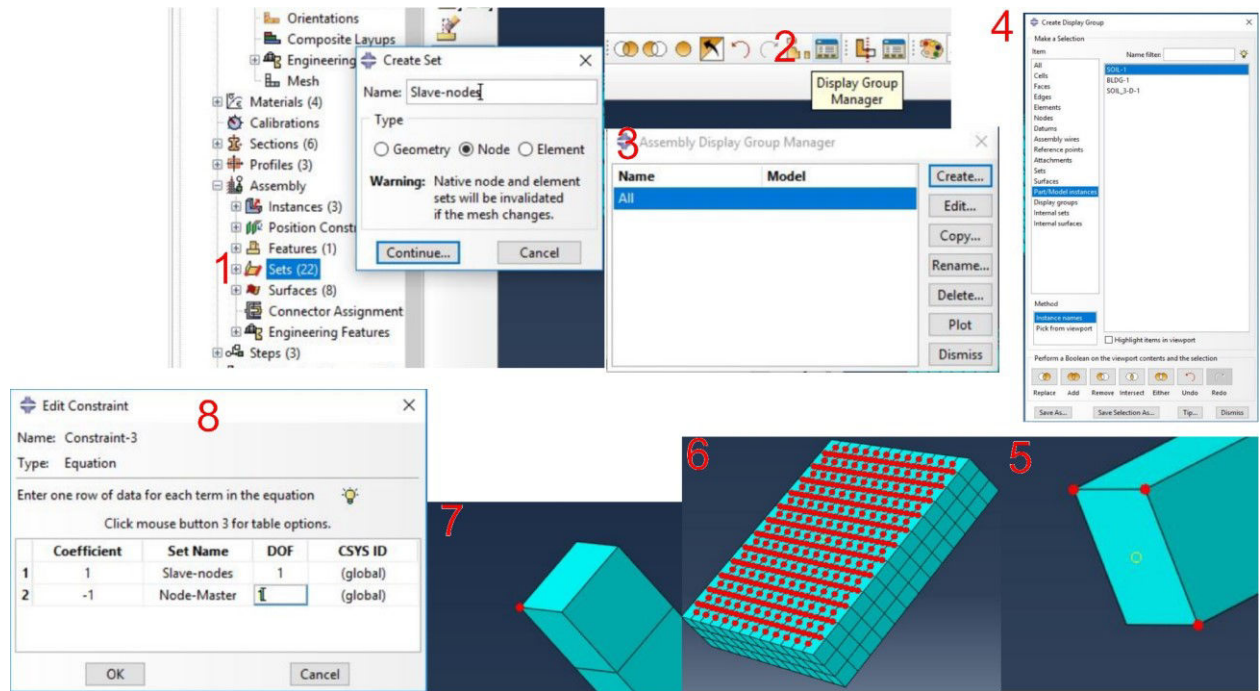
Choose the module **Mesh**

1. Click on the icon **Seed Edges** → Meshed **By size** → Approximate element size **1** → **OK**
2. **Done**
3. Click on the icon **Assign Element Types** → Select the region to mesh → **Done**
4. From Family select **3D Stress** → from Geometric Order enable **Quadratic** → **OK**
5. Click on **YES**



**Repeat this step for the part of Foundation** Approximate element size **0.5**

**Repeat this step for the part of 3-D soil** Approximate element size **2**

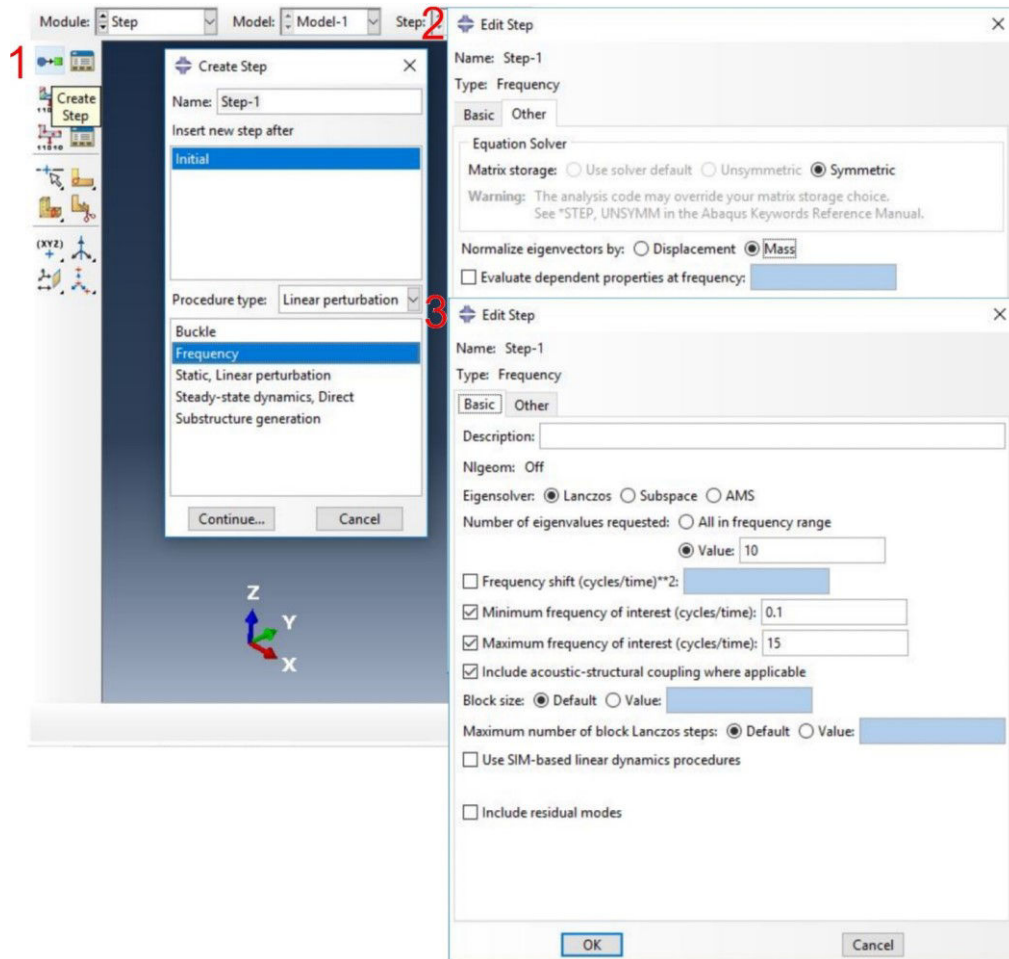


1. Double click on the icon **Sets: Slave-nodes** → Select all nodes in the bottom of the 3-D soil without edge nodes (as shown in 6) and all node at the top of the 1-D soil except one (as shown in 5) in order to do that follow the steps
2. Click on **Display Group Manager**
3. Click on **Create**
4. From **Item** select **Part/Model instances** → Select 1-D Soil → from Perform a boolean on the viewport contents and the selection click **Replace**
5. Select the top 3 nodes
6. Repeat 4 for the 3-D soil → Select all the bottom nodes except nodes at the edges
7. Repeat from 1 to create Node-Master and select the top node not selected before from the 1-D soil part
8. Create a Constraint Equation as following for the Dof 1,2 and 3

### Combination of static and dynamic response

The static and dynamic response of the structure can be superposed only in the case considering a linear elastic system. In the case of inelastic systems, the dynamic response of the structure

must consider the stresses and strains existing in the structure due to its static response. In the presented work, dry soil is adopted, and static response of the system is negligible compared to the dynamic one. Hence the static response is not considered, only dynamic response of the structure is calculated.



Choose the module **Step**

1. Click on the icon **Create Step**

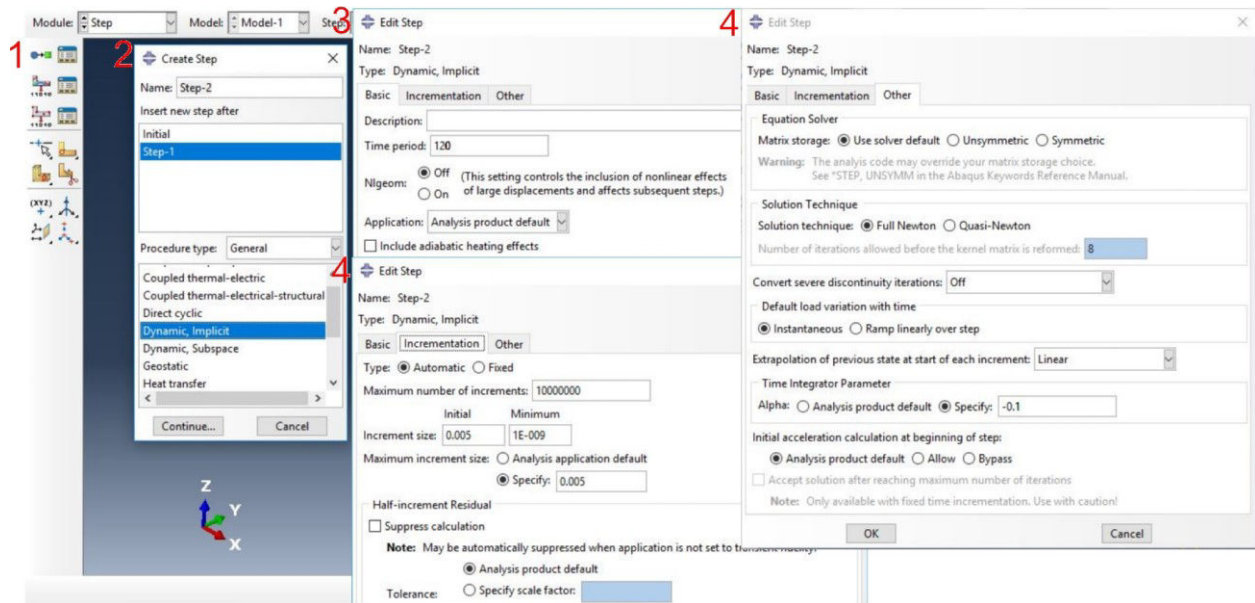
From **Procedure Type** → select **Linear perturbation** → select **Frequency** → **Continue**

2. From **Other** enable **Mass**

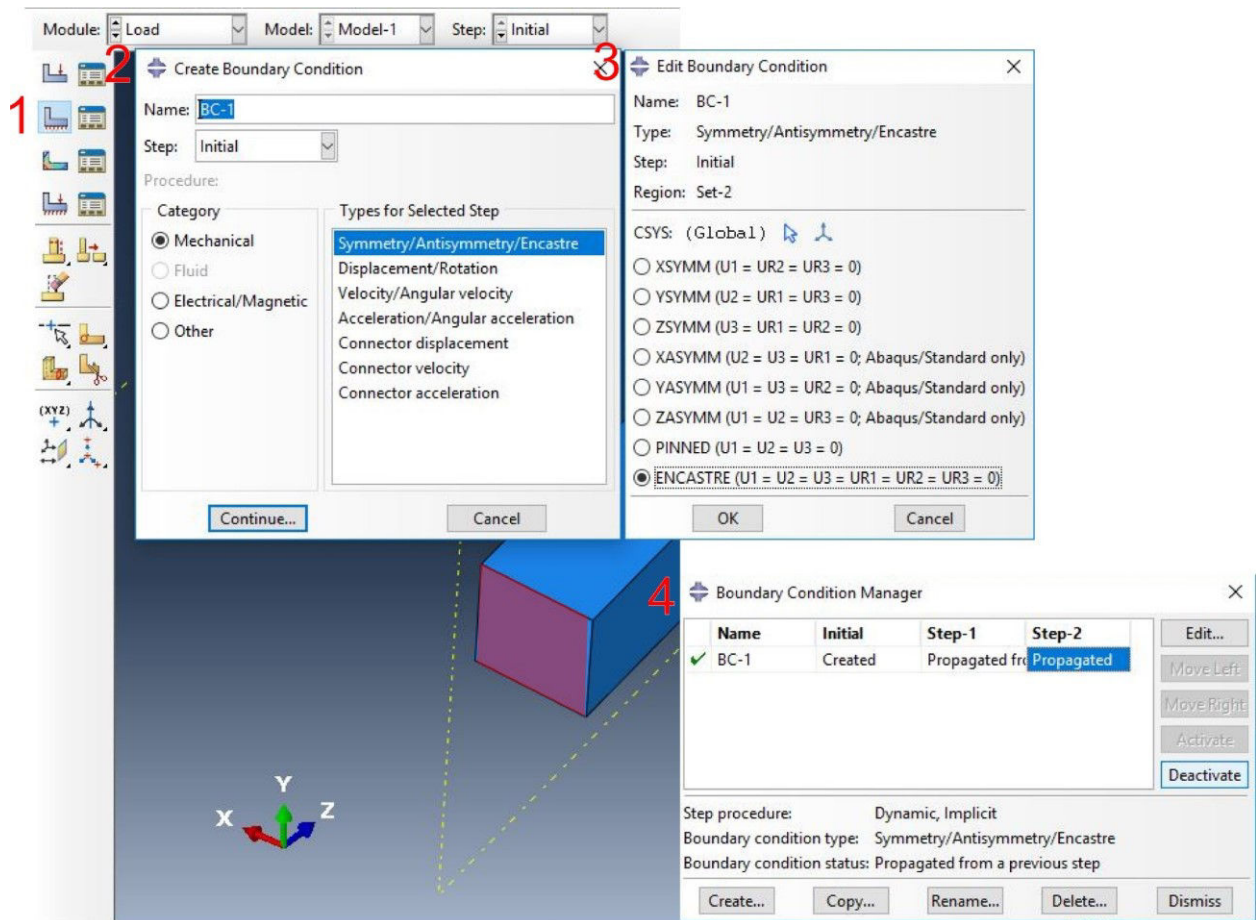
3. From **Basic** enable **value** → **10**

Enable **Minimum frequency** → **0.1**

Enable **Maximum frequency** → **15** → **OK**



1. Click on the icon **Create Step**
2. From **Procedure Type** → select **General** → select **Dynamic Implicit** → **Continue**
3. From **Basic** → **Time period** → input **10**
4. From **Incrementation** → enable **Automatic** →  
 For **Maximum number of increments** input **10**  
 For **Increment size** → **Initial** input **0.005** → **Minimum** input **1E - 009**
5. From **Other** → **Convert severe discontinuity iterations** → **OFF**  
 → **Extrapolation of previous state at start of each increment** → **Linear**  
 → **Time Integrator Parameter** → **Alpha** → enable **Specify** → **-0.1**



Choose the module **Load**

1. Click on the icon **Create Boundary Condition**

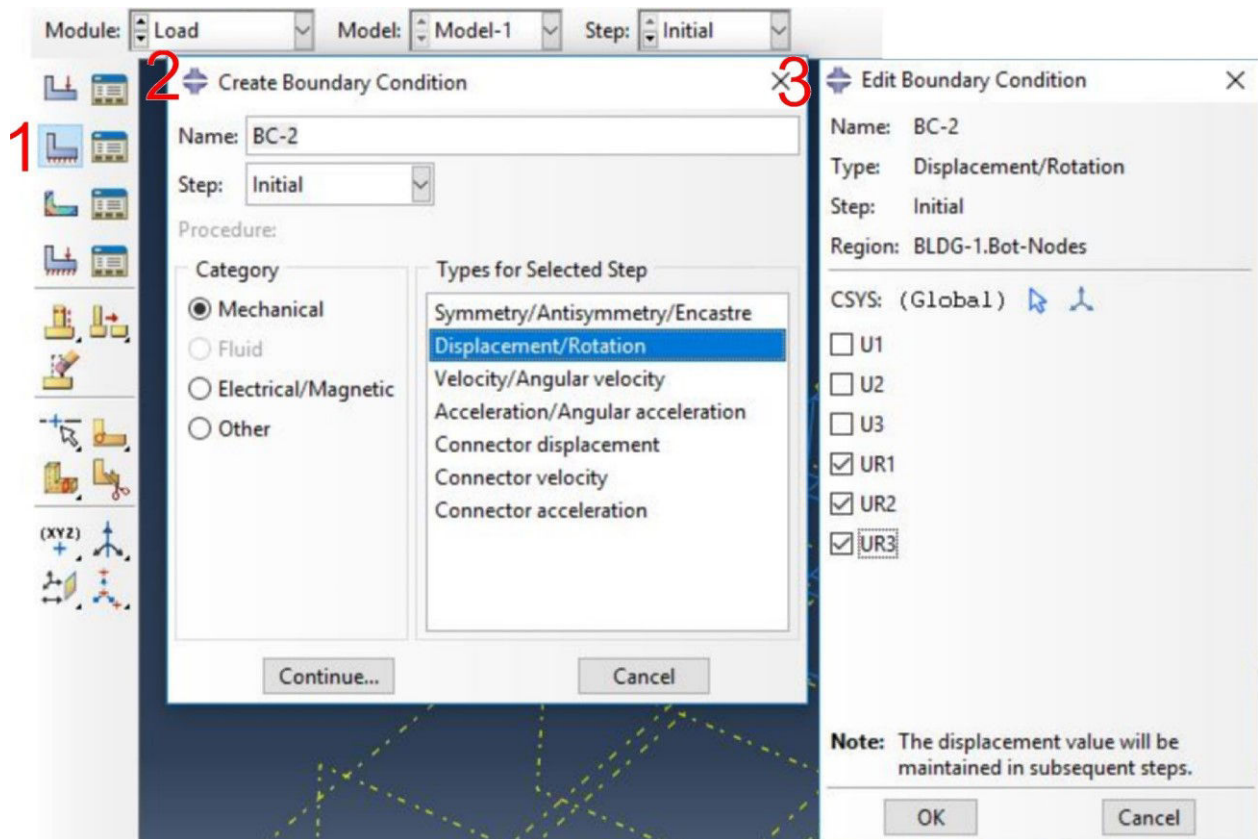
2. From **Step** → select **Initial**

From **Category** → select **Mechanical**

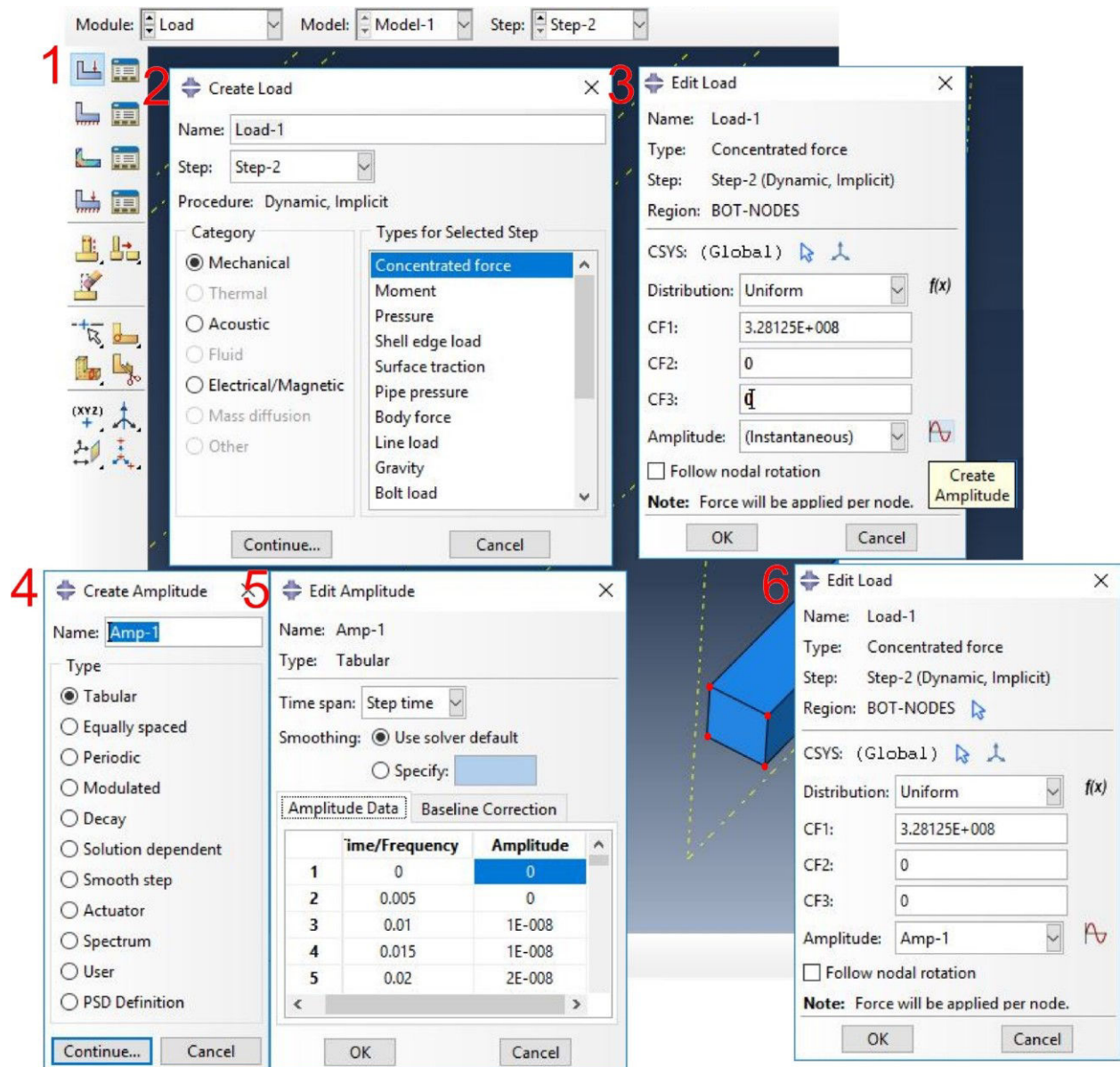
From **Types for selected step** → select **Symetry/Antisymmetry/Encastre** → **Continue**

3. Select the bottom face of the soil → Enable **Encastre** → **OK**

4. Select **Ptopagated** in **Step-2** and **Deactivate**



1. Click on the icon **Create Boundary Condition**
2. From **Step** → select **Initial**  
From **Category** → select **Mechanical**  
From **Types for selected step** → select **Displacement/Rotation** → **Continue**
3. Select from sets all building bottom nodes → Enable **UR1**, **UR2** and **UR3** → **OK**



1. Click on the icon **Create Load**

2. From **Step** → select **Step-2**

From **Category** → select **Mechanical**

From **Types for selected step** → select **Concentrated Force** → **Continue**

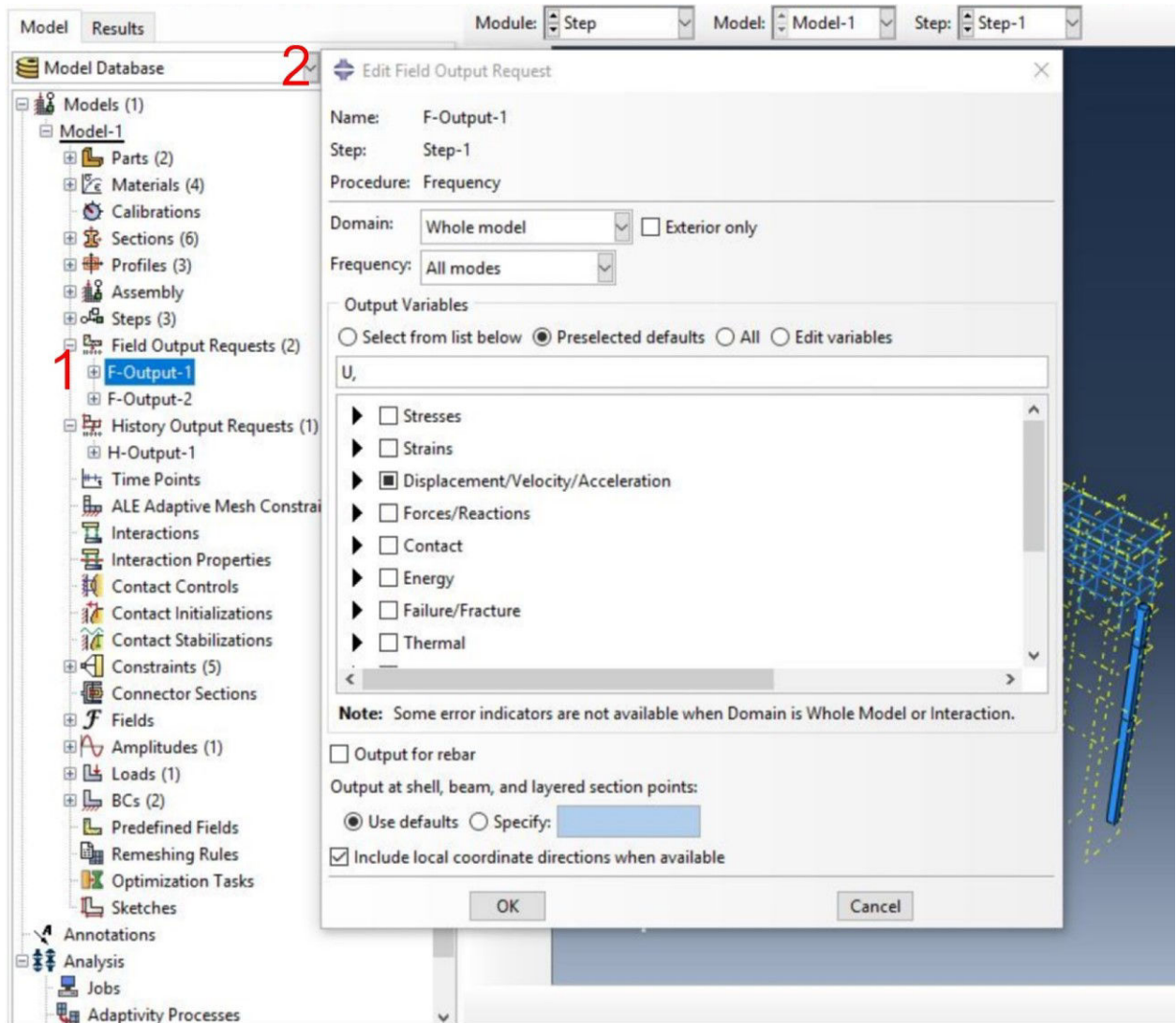
3. Select the bottom nodes of the soil → Input **CF1 = 3.28125E + 008** and

**CF2 = CF3 = 0** → Select **Create Amplitude**

4. Select **Tabular** → **Continue**

1. Enter tabular of the signal → **OK**

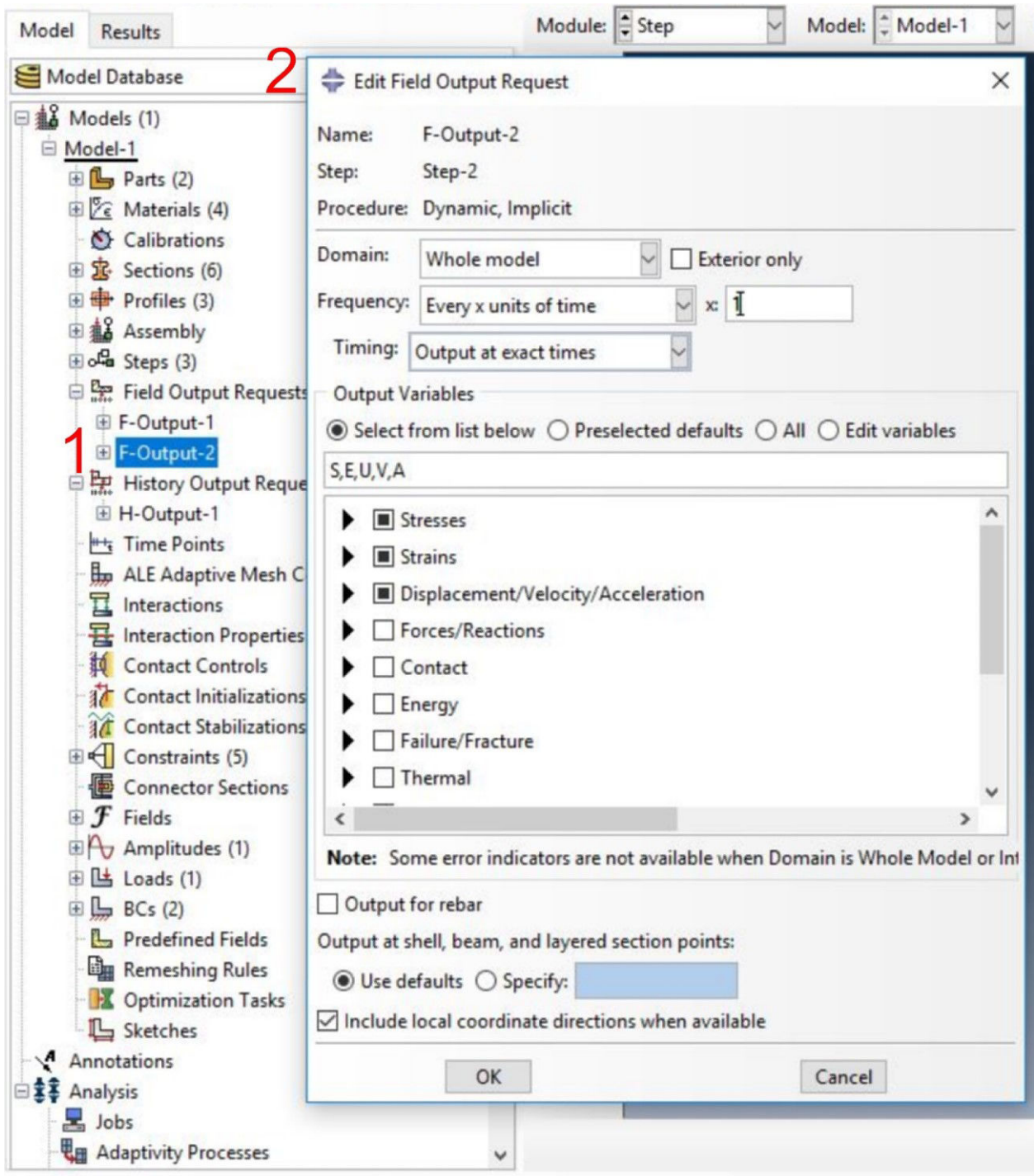
2. **OK**



1. Double Click on the icon **F-Output-1**

2. **Domain** → Whole model

Select **U** from **Displacement/Velocity/Acceleration** → **OK**



1. Double Click on the icon **F-Output-2**

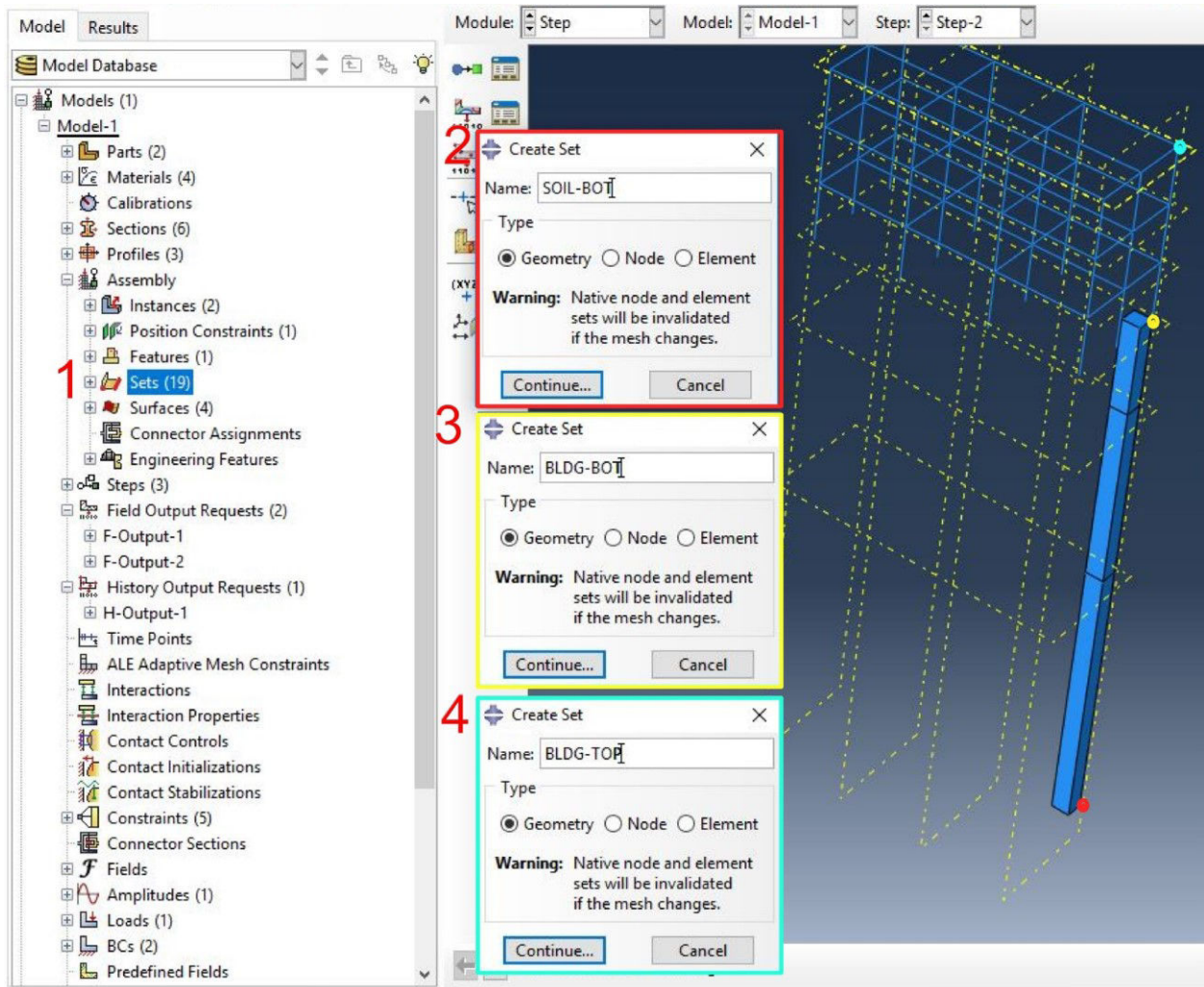
2. **Domain** → Whole model

**Frequency** → every x unit of time →  $x = 1$

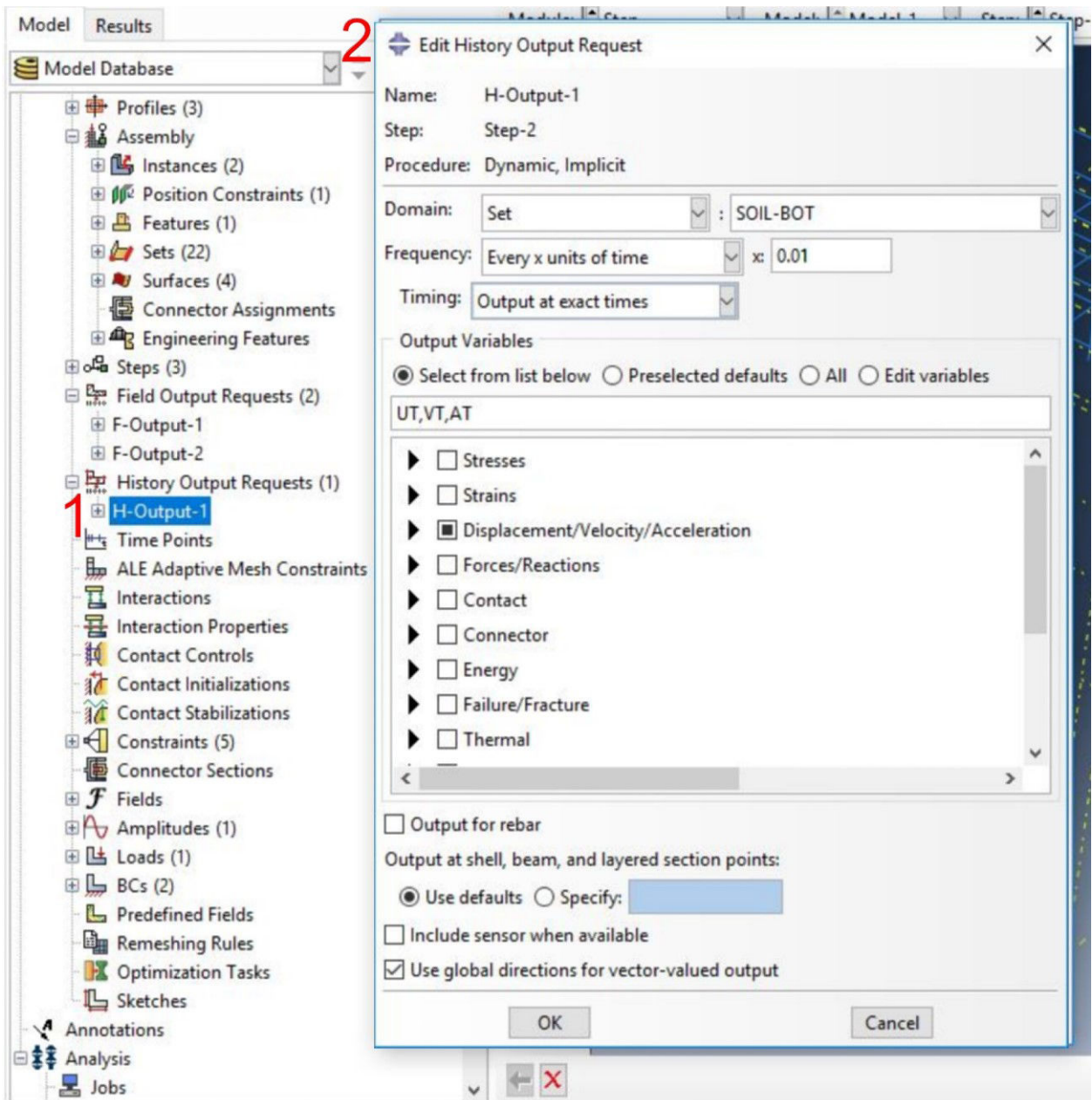
Select **U, V** and **A** from **Displacement/Velocity/Acceleration**

Select **S** from **Stress**

Select **E** from **strain** → **OK**



1. Double Click on the icon **Set from Assembly**
2. Name the set → enable **Geometry** → **Continue** → select a bottom node of the soil → **Done**
3. Repeat steps 1 and 2 only this time select a bottom node of the building
4. Repeat steps 1 and 2 only this time select a top node of the building



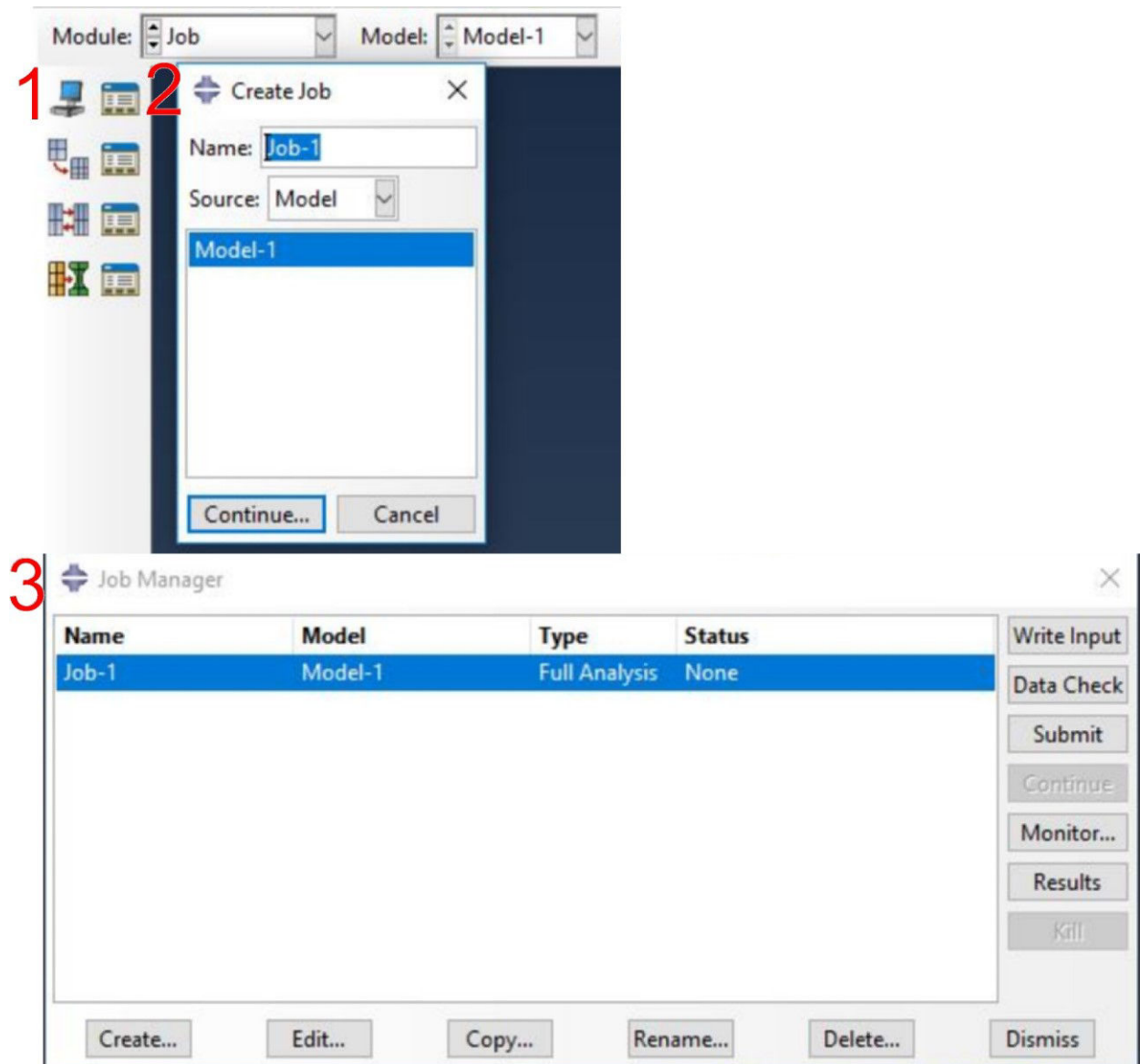
1. Double Click on the icon **History Output Requests**

2. **Domain** → Set → soil bottom node set

**Frequency** → every x unit of time → x = 0.01

Select **UT,VT** and **AT** from **Displacement/Velocity/Acceleration** → **OK**

**Repeat this step for building bottom node set and building top node set**



Choose the module **Job**

1. Click on the icon **Create Job**
2. Select **Model-1** → **Continue**
3. **Submit**



## **Author's publications**

### **International journals**

Fares R., Santisi d'Avila M. P., Deschamps A. (2018 accepted) Soil-Structure Interaction analysis using a 1DT-3C wave propagation model.

Fares R., Santisi d'Avila M. P., Deschamps A. (2018 under review) Towards a seismic design of reinforced concrete buildings taking into account site effects and interaction between soil and structures.

### **International conferences**

Fares R., Santisi d'Avila M. P., Deschamps A. (2018) Response spectrum considering soil-structure interaction for buildings with shallow foundation. *16th European Conference on Earthquake Engineering, Thessaloniki, Greece.*

Fares R., Santisi d'Avila M. P., Deschamps A. (2017) Advantages and detriments of 1-directional 3-component wave propagation approach for soil-structure interaction modeling. *10th International Conference on Structural Dynamic, Rome, Italy.*

